VNiVERSiDAD D SALAMANCA

CAMPUS DE EXCELENCIA INTERNACIONAL

FACVLTAD DE CiENCiAS QVíMiCAS

DEPARTAMENTO DE iNGENiERíA QVíMiCA Y TEXTiL

Study of instability and breakup of high viscous capillary jets to produce monodisperse size-controlled microparticles

María Cristina Rodríguez Rivero

Salamanca, 2014

VNiVERSiDAD DE SALAMANCA

FACVLTAD DE CiENCiAS QVíMiCAS

DEPARTAMENTO DE iNGENiERíA QVíMiCA Y TEXTiL

Study of instability and breakup of high viscous capillary jets to produce monodisperse size-controlled microparticles

Memoria para optar a grado de Doctor por la Universidad de Salamanca

realizada por

María Cristina Rodríguez Rivero

Salamanca, 2014

El Dr. D. Miguel Ángel Galán Serrano, Catedrático de Universidad en el Departamento de Ingeniería Química y Textil de la Universidad de Salamanca y la Dra. Dña. Eva M. Martín del Valle, Profesora Titular de Universidad en el Departamento de Ingeniería Química y Textil de la Universidad de Salamanca

Informan:

Que la memoria titulada "Study of instability and breakup of high viscous capillary jets to produce monodisperse size-controlled microparticles" que para optar al Grado de Doctor en Ingeniería Química, Programa de Doctorado de "Reactividad y Tecnología Químicas", presenta María Cristina Rodríguez Rivero, ha sido realizada bajo nuestra dirección en el Departamento de Ingeniería Química y Textil de la Universidad de Salamanca.

Considerando que constituye un trabajo de tesis, se autoriza su presentación ante la Comisión de Tercer Ciclo de la Universidad de Salamanca.

Y para que así conste, a los efectos oportunos, se firma la presente en Salamanca a 21 de Mayo de 2014.

Fdo: D. Miguel Ángel Galán Serrano **Fdo: Dña. Eva M. Martín del Valle**

Agradecimientos

A mis tutores de tesis, los Doctores Eva Martín del Valle y Miguel Ángel Galán Serrano, por darme la oportunidad de desarrollar este trabajo, por lo que le han aportado y por la cara más cercana que no queda reflejada en este escrito.

A mis compañeros y amigos del Departamento y la Facultad, en especial a Antonio, Jesús, Jose, Milena, Montaña y Pepe y las recientes incorporaciones, Álvaro y Loreto. A Belén, Manolo y María. A Audelino y Chema. A Jesús *QF* por las conversaciones y los pinchos compartidos y a Mariano por los momentos dentro y fuera de la Facultad.

A los Doctores Loic Hilliou y Carlos Gracia por la ayuda prestada. Al Dr. Paulo Augusto por su simpatía desde Béjar.

A mis compañeros de estancia en Londres, en particular a Alister y Yasuhide, y al profesorado al que tuve la oportunidad de conocer, mención especial a los profesores Salvador Navarro, Denis Doorly y Paul Luckham.

A Pedro *Zamora*, a Dácil, Dani, Guaya y Raquel; a Emma y Nando, Marga y Xulia, por su amistad durante tantos años.

A mi familia, siempre cerca a pesar de la distancia, y a Fernando, por formar parte de mi familia y por años cargados de anécdotas.

Gracias a todos los que lean estos agradecimientos porque en mayor o menor medida han compartido esta experiencia conmigo.

Al firmamento y a Gran Canaria, siempre reconforta abstraerse por momentos al paraíso.

“Nobody ever figures out what life is all about, and it doesn't matter.

Explore the world. Nearly everything is really interesting if you go into it deeply enough...”

Richard Feynman

TABLE OF CONTENTS

FIGURES

GENERAL NOMENCLATURE

A: amplitude of the surface disturbance (m)

d: diameter (referred to jet, nozzle or droplet diameter) (m)

D: characteristic diameter (m)

f: frequency of the disturbance (s^{-1})

k: wavenumber (m^{-1})

Q: volumetric flow rate (m^3/s)

V: liquid velocity (m/s)

SMD: Sauter mean diameter

Greek symbols

ρ: density of the liquid (Kg/m^3)

σ: surface tension (N/m)

η: dynamic viscosity (Pa·s)

λ: wavelength of the surface disturbance (m)

λ_C: relaxation time under steady shear flow (s)

τ: relaxation time under dynamic shear flow (s)

λ_{ext}: relaxation time under uniaxial extensional flow (s)

ω: growth rate (s^{-1})

Ω: Dimensionless growth rate

Subscripts

j: jet

n: nozzle

opt: optimal conditions

l: liquid

a: air

RESUMEN EN ESPAÑOL.

RESUMEN EN ESPAÑOL

I. INTRODUCCIÓN

Este trabajo se incluye dentro de un proyecto que tiene por objetivo la liberación de principios activos encapsulados en partículas micrométricas para su empleo en terapias biomédicas.

Se consideran micropartículas aquellas de tamaño inferior a 1 mm. Éstas pueden presentar diferente estructura y morfología, siendo la más característica la forma esférica, y están formadas normalmente por un núcleo interno rodeado por una membrana diferenciada, recibiendo también para este caso el nombre de microcápsula.

Se encuentran en gran variedad de aplicaciones. Entre las más comunes se encuentran las tecnologías de impresión por tinta (inkjet printing), la inyección de combustible en motores, los aerosoles en agricultura, el diseño de detergentes y productos de alimentación, etc. (Dubey et al. 2009).

Además de las aplicaciones mencionadas, el interés en el uso de estos sistemas en la industria farmacéutica y las terapias biomédicas se ha incrementado en las últimas décadas, ya que proporcionan una protección eficaz del material inmovilizado contra degradación física, química o biológica y permiten el control de la liberación del principio activo contenido.

Asimismo son más fáciles de implantar en comparación con otros dispositivos de mayor tamaño y, con un control adecuado de los materiales, producen menos necrosis celular y fibrosis inespecífica (Zimmermann et al. 2008).

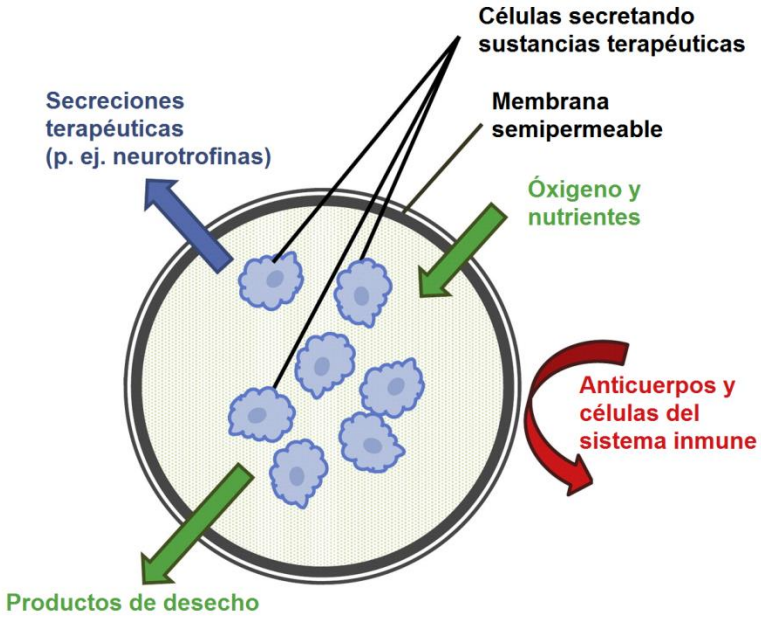

Figura I: Esquema de un sistema de encapsulación de células - base de terapias contra el rechazo inmune - (Zanin et al. 2012).

II. MOTIVACIÓN

Cuando la aplicación para la que se diseñan las micropartículas tiene relación con el campo biomédico las características de mayor importancia son la estabilidad mecánica, tamaño, forma, homogeneidad y biocompatibilidad de las mismas.

Entre los materiales biocompatibles más usados los polímeros de origen natural presentan grandes ventajas respecto a otros compuestos (Rathore et al. 2013).

Sin embargo, las disoluciones poliméricas de baja viscosidad producen carencias en la estabilidad mecánica de las partículas (Zimmermann et al. 2008), por lo que el empleo de polímeros de media/alta viscosidad se convierte en requisito casi indispensable para la formación de las microcápsulas.

Respecto al control del tamaño y la forma de las partículas se ha comprobado que el trasplante de microcápsulas de tamaños heterogéneos o de forma irregular se relaciona con una mayor probabilidad de rechazo temprano de los injertos que las contienen (Zhang et al. 2001), por lo que debe conseguirse un control de los mismos. Por otro lado, un

control adecuado de estos parámetros permite lograr un proceso de administración controlada y una adecuada predicción de comportamiento - tasas de liberación o cantidad de células por cápsula -.

Por estas razones el presente estudio se fundamenta en la necesidad de desarrollar, caracterizar y analizar una técnica que permita obtener microcápsulas con altas prestaciones mecánicas a partir de polímeros biocompatibles de media/alta viscosidad para su uso en el campo biomédico.

III. OBJETIVOS

Como se ha indicado con anterioridad el objetivo de este trabajo ha sido el desarrollo de una nueva técnica para producir microcápsulas de tamaños que van desde 300 hasta 600 micrómetros a partir de polímeros de viscosidad media-alta para su empleo en el campo biomédico.

La nueva técnica se basa en la combinación de un sistema de vibración de boquilla junto con un sistema de presurización, produciendo chorros capilares estables que evolucionan y rompen de forma controlada por inestabilidad laminar.

Como objetivos más específicos dentro de este plan general se pueden establecer los siguientes:

- Configurar una nueva técnica que permita el desarrollo de inestabilidades laminares en chorros poliméricos de viscosidad media-alta.

- Generar las curvas de comportamiento, lo que permitirá estudiar el efecto de diferentes parámetros tales como viscosidad, tensión superficial, caudal, etc. y obtener un conjunto de ecuaciones semiempíricas que predigan el tamaño de partícula en una primera aproximación.

De los estudios previos se manifiesta la importancia de realizar un estudio más profundo de la reología del polímero, que permita abordar un enfoque físico de la inestabilidad más completo.

- Investigar la naturaleza reológica de las disoluciones poliméricas utilizadas.

- Obtener una relación de dispersión de la inestabilidad del chorro de forma que el proceso de formación de microgotas (previas a las micropartículas) pueda ser descrito con precisión a partir de un modelo basado en el análisis matemático.

Con el fin de predecir comportamientos que no puedan ser obtenidos fácilmente bajo las condiciones experimentales actuales se realiza un estudio del sistema empleando técnicas de dinámica de fluidos computacional (CFD).

- Realizar simulaciones computacionales de flujos multifásicos con el objetivo de proporcionar una base sólida para un posible escalado del sistema tras la comparación entre simulaciones y resultados experimentales.

IV. POLÍMERO Y SISTEMA EXPERIMENTAL

De entre los materiales para la formación de microcápsulas los hidrogeles de polímeros naturales o sintéticos son ampliamente usados por a su alto contenido en agua, su estructura matricial tridimensional y su naturaleza hidrófila. Esto los hace adecuados para interactuar con otros fluidos y tejidos. De entre los hidrogeles más empleados están los alginatos (Tun et al. 1996).

Los alginatos son sales del ácido algínico, polisacáridos lineales solubles en agua obtenidos a partir de algas pardas. Están compuestos por dos unidades monoméricas: β-D ácido manurónico (M) y α-L-gulurónico (G) que se agrupan en diferentes bloques. Una de las propiedades más importantes de los alginatos es su capacidad para gelificar, lo que se conoce como reacción de gelificación iónica, con cationes polivalentes y convertirse así insoluble en agua. Durante el proceso de gelificación los cationes polivalentes sustituyen a los iones monovalentes asociados a los grupos carboxilo. Este modelo se conoce como modelo de "caja de huevos" (Figura II).

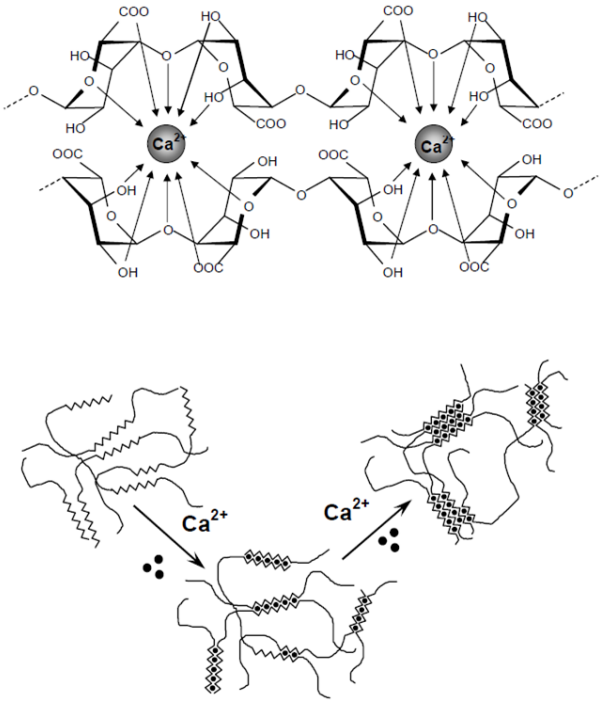

Figura II: Proceso de gelificación iónica. (a) Modelo "caja de huevos". (b) Asociación de cadenas (Zimmermann et al. 2008).

Como se indicó anteriormente la tecnología desarrollada consiste en un dispositivo que combina un sistema de alta presión y un sistema de boquilla con vibración inducida (Figura III).

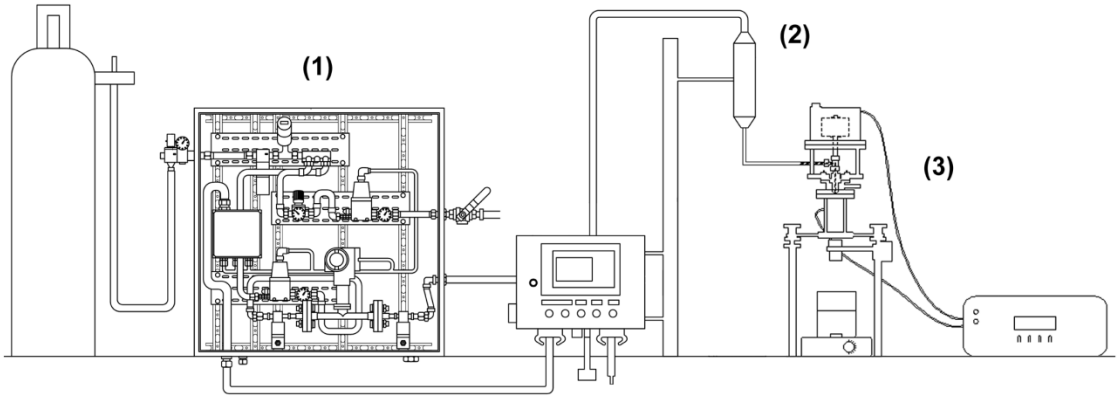

Figura III: Sistema de producción de micropartículas desarrollado. (1) Sistema neumático (2) Tanque presurizado (3) Subsistema de generación de perturbación controlada.

El proceso consiste en la formación de gotas a partir del chorro generado desde la boquilla y su posterior gelificación en un baño de cloruro de bario (2% en peso). Las gotas se estabilizan con los iones Ba^{2+} para generar una membrana sólida semipermeable (Figura IV).

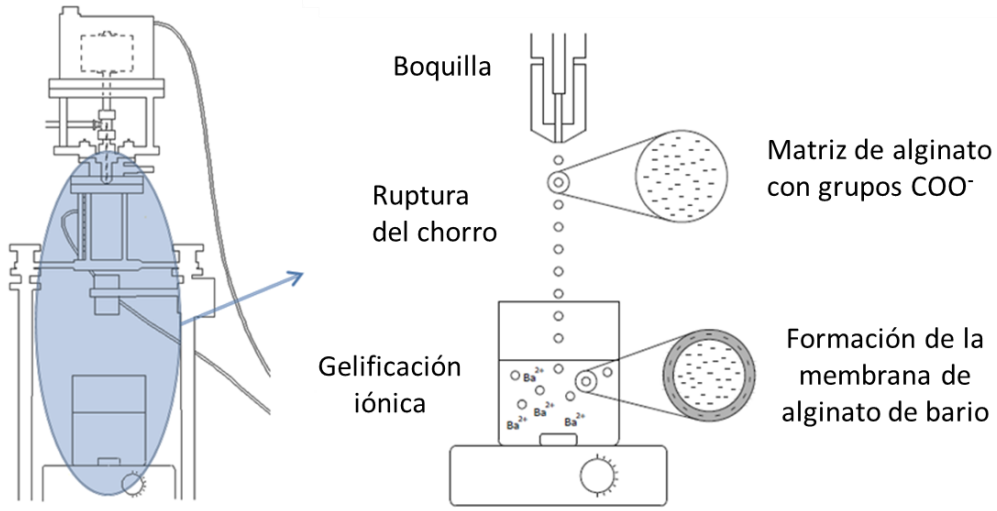

Figura IV: Proceso de formación de gota y gelificación en cloruro de bario.

V. Inestabilidades en chorros fluidos

Cuando un líquido pasa a través de una boquilla, el chorro que se forma sufre variaciones a lo largo de su caída. Estos cambios se deben a perturbaciones en el sistema de suministro del fluido - cambios en su velocidad o presión - así como por fluctuaciones en las propiedades del líquido tales como la temperatura, la viscosidad, o la tensión superficial (Ashgriz and Yarin 2011).

Como resultado, existe un choque entre fuerzas disruptivas y cohesivas en el chorro, lo que da lugar al crecimiento de oscilaciones en la interfase entre líquido y medio circundante, cambiando así su perfil geométrico.

La relación entre dichas fuerzas dará lugar al incremento de las oscilaciones hasta su ruptura o a la estabilización del mismo.

Para clasificar estos procesos de desestabilización y ruptura se definen diferentes regímenes. La clasificación más usada se realiza de acuerdo a una serie de factores como son la gravedad, la inercia, la tensión superficial y las fuerzas de viscosidad.

Un esquema de esta clasificación se muestra en la Figura V.

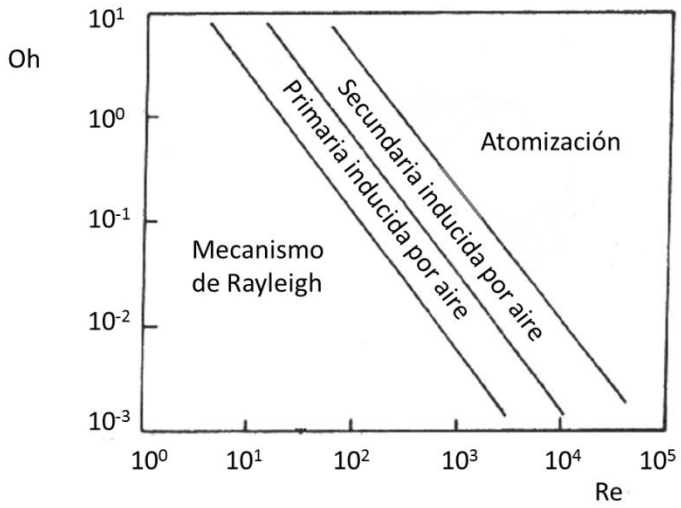

Figure V: Clasificación de los modos de desintegración de chorros fluidos descritos por Reitz (Reitz and Bracco 1986).

La mayor parte de los experimentos recogidos en este trabajo se realizaron utilizando una boquilla circular con un diámetro de 150 micrómetros, que se traduce en un chorro cilíndrico de dimensiones similares.

Tomando, a partir de los valores propios del polímero y del proceso, una densidad de 1000 kg/m^3, una tensión superficial de 0.076 N/m, una viscosidad de 1,5 Pa·s y una velocidad media del chorro de 5 m/s se obtienen los siguientes valores de los números adimensionales de Ohnesorge, Reynolds y Weber:

$$Oh = \frac{\eta}{\sqrt{\rho \cdot \sigma \cdot D}} = \frac{1.5}{\sqrt{1000 \cdot 0.076 \cdot 150 \cdot 10^{-6}}} = 14.05 \qquad \text{(I)}$$

$$\mathrm{Re} = \frac{\rho \cdot v \cdot D}{\eta} = \frac{1000 \cdot 5 \cdot 150 \cdot 10^{-6}}{1.5} = 0.5 \qquad \text{(II)}$$

$$We = \frac{\rho \cdot v^2 \cdot D}{\sigma} = \frac{1000 \cdot 5^2 \cdot 150 \cdot 10^{-6}}{0.076} = 49.34 \qquad \text{(III)}$$

que se corresponden con el primer mecanismo recogido en la Figura V o mecanismo de Rayleigh.

Este tipo de régimen se caracteriza por el crecimiento de oscilaciones con simetría axial en la superficie del chorro y por un tamaño de gota que excede el diámetro del mismo.

Los autores Savart (Savart 1833) y Plateau (Plateau 1873) estudiaron este tipo de desestabilización y concluyeron que la inestabilidad se producía a causa de la tensión superficial en la interfase del chorro y el medio circundante. Años más tarde Rayleigh (Rayleigh 1879) dio una explicación numérica del fenómeno y desde entonces se ha convertido en un problema clásico de la dinámica de fluidos.

VI. CURVAS DE COMPORTAMIENTO

El dispositivo experimental está diseñado para funcionar bajo diferentes condiciones de caudal y viscosidad (tabla I).

Dada la versatilidad del mismo se pueden generar curvas de comportamiento en un amplio intervalo, lo que es de gran interés para obtener información sobre el sistema objeto de estudio y así obtener ecuaciones de predicción de comportamientos.

Tabla I: Condiciones generales de experimentación

Parámetro	Intervalo de valores
Viscosidad del alginato	450-2620 mPa·s
Caudal del alginato	5-9 mL/min
Tensión superficial	0.076 N/m
Densidad	1000 kg/m^3

La frecuencia aplicada en cada caso en este primer estudio se calcula a partir de la expresión de Weber (IV) para el cálculo de longitud de onda óptima. Ésta recoge parámetros físico-químicos básicos de la disolución y el chorro (Weber 1931).

$$\lambda_{opt} = \pi \cdot \sqrt{2} \cdot d \left(1 + \frac{3\eta}{\sqrt{\rho\sigma \cdot d}} \right)^{1/2} \qquad \text{(IV)}$$

$$f_{opt} = \frac{v}{\lambda_{opt}} \qquad \text{(V)}$$

La figura VI representa el tamaño de micropartícula (medido como diámetro medio de Sauter –SMD-) como función del caudal para varias viscosidades.

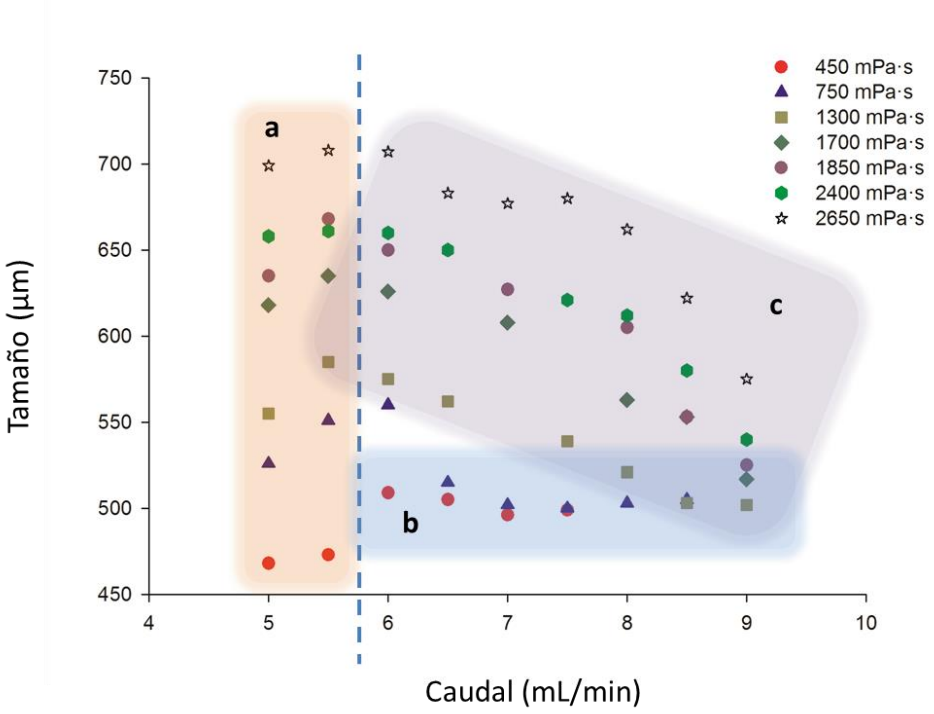

Figura VI: Efecto de la viscosidad y caudal en el tamaño de micropartícula. Curvas de comportamiento y clasificación de diferentes comportamientos.

A partir de las curvas se observan ciertos patrones que han sido enmarcados en la figura y se describen a continuación:

De forma general el tamaño de partícula aumenta al aumentar la viscosidad para todos los casos.

Sin embargo el efecto del caudal presenta comportamientos distintos:

- Para caudales inferiores a 6 mL/min, el tamaño de partícula aumenta con la velocidad de flujo.
- Para caudales superiores a 6 mL/ min y disoluciones con viscosidades por debajo de 0.80 Pa·s el tamaño permanece constante.
- Para caudales superiores a 6 mL/min y disoluciones con viscosidades por encima de 0.80 Pa·s el tamaño disminuye con un aumento del caudal.

De entre todos, el último comportamiento descrito resulta el de mayor interés para este estudio, ya que recoge el intervalo de viscosidades y caudales que se pretenden abarcar con esta técnica.

Tras el estudio inicial y la determinación de las variables de mayor influencia en el proceso – viscosidad y caudal hasta el momento - el objetivo es obtener una serie de ecuaciones semiempíricas que permitan predecir el tamaño final de micropartícula.

No se ha encontrado en la bibliografía un enfoque semiempírico para este proceso, aunque este tipo de análisis es frecuente en los procesos de atomización. Por ello, se realizó un estudio comparativo entre un proceso de atomización descrito por la teoría de onda (Mansour and Chigier 1995) y el proceso aquí desarrollado con el fin de evaluar el posible uso de esta teoría y sus ecuaciones semiempíricas derivadas.

El resultado de esta comparación sugiere que ambos mecanismos de ruptura presentan diversas similitudes. Así pues, a partir del mecanismo de onda y el análisis realizado por los autores Mansour y Chigier (Mansour and Chigier 1995), se seleccionan una serie de ecuaciones semiempíricas para la atomización de fluidos no newtonianos que pueden ser de aplicación al sistema objeto de estudio – la desestabilización de chorros de alginato mediante vibración controlada -. Las ecuaciones obtenidas, ajustadas a partir de datos experimentales, son las siguientes:

$$\frac{SMD}{D} = 11.58 \cdot We^{-0.341} + 0.211 \cdot Oh^{0.682} \qquad \text{(VI)}$$

$$\frac{SMD}{D} = 3.30 \cdot \left(\frac{Oh^2}{We} \right)^{0.151} \qquad \text{(VII)}$$

Tras un segundo conjunto de experimentos de verificación se tiene que la primera de las expresiones muestra un mejor ajuste a los datos y sugiere que la predicción es fiable en las condiciones empleadas.

Por ello, de este primer estudio, se puede concluir por un lado que el mecanismo de onda, aceptado para la atomización de líquidos no newtonianos, quizás también puede aplicarse al nuevo sistema desarrollado.

Por otro lado, tras analizar el efecto del caudal, surgen cuestiones sobre el comportamiento del fluido ante los efectos combinados del flujo en cizalla y extensional que se dan en el proceso, lo que dio lugar posteriormente a un estudio reológico del sistema.

A su vez debe tenerse en cuenta que el efecto de la frecuencia aplicada se debe analizar en mayor detalle y con la ayuda de imágenes de la evolución y ruptura del chorro, como se realizó con posterioridad.

VII. COMPORTAMIENTO REOLÓGICO

La mayor parte de los polímeros se comportan como fluidos no newtonianos, mostrando en la mayoría de los casos viscoelasticidad (Muller and Davidson 1994). Un número creciente de autores ha llegado a la conclusión de que existen diferencias sustanciales entre la ruptura de fluidos viscoelásticos y newtonianos, por lo que la reología del alginato ayudará a determinar la evolución de la inestabilidad (Middleman 1965; Goldin et al. 1969; Bousfield et al. 1986; Christanti and Walker 2001; Yarin 1993).

Para ello se realiza la caracterización reológica de las muestras mediante la determinación de la viscosidad intrínseca [η] y sus propiedades en cizalla simple y en tracción uniaxial.

[η] se puede definir, para un determinado soluto en un disolvente dado, como la facilidad de una molécula aislada del soluto de incrementar la viscosidad del disolvente.

A partir de la determinación de [η] se observa, para concentraciones bajas, un comportamiento marcado por la fuerza iónica de las disoluciones dado el carácter polielectrolito del compuesto. Sin embargo, a concentraciones elevadas, la interacción de las cadenas enmascara el efecto del polielectrolito y el comportamiento pasa a ser el de un polímero neutro en disolución (Hilliou et al. 2009; Dobrynin et al. 1995). Esta naturaleza se infiere también a partir de otras medidas reológicas como se describirá a lo largo de este trabajo.

Una vez determinado el carácter polielectrolito-neutro de la disolución, se realiza la caracterización mediante cizalla simple a través de curvas de flujo y ensayos de cizalla oscilatorios de pequeña amplitud o SAOS.

Por encima de un valor de cizalla, conocido como tasa de cizalla crítica $\dot{\gamma}^*$, los datos de las curvas de flujo (figura VII) muestran una viscosidad dependiente de dicha velocidad de cizalla. A partir del valor de $\dot{\gamma}^*$se obtiene un tiempo característico conocido como tiempo de relajación de la muestra definido por $\lambda_c = 1/\dot{\gamma}^*$

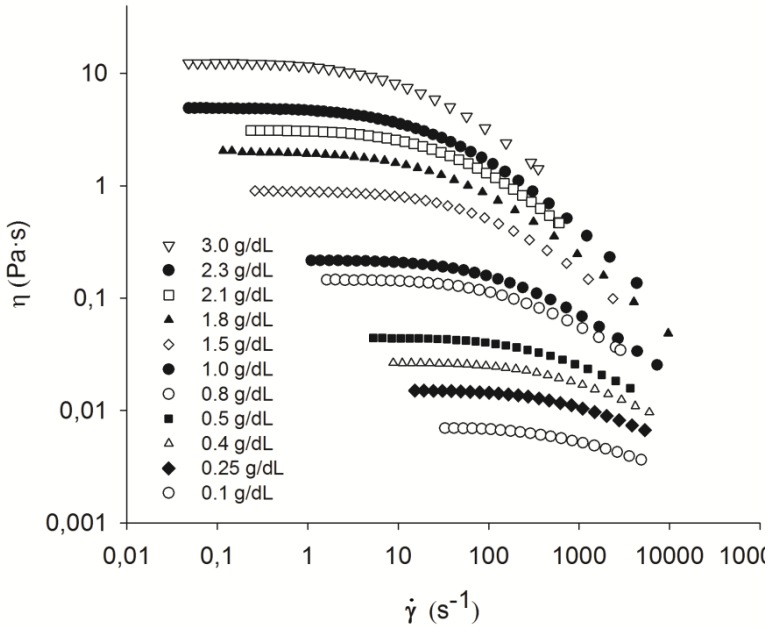

Figura VII: Efecto de la velocidad de cizalla en la viscosidad aparente para diferentes concentraciones.

A partir de ensayos dinámicos (oscilatorios de baja amplitud o SAOS) también se puede obtener un tiempo de relajación τ, generalmente a partir de la frecuencia del punto de corte entre los módulos de elasticidad del polímero G' (storage modulus) y rozamiento viscoso G'' (loss modulus). Sin embargo, en el presente trabajo y debido a problemas inerciales en el reómetro, este punto de corte resulta difícil de determinar. Por ello τ se ha obtenido a partir de las pendientes de dichos módulos G' y G'' en las zonas de baja frecuencia (regiones terminales).

La dependencia de τ respecto a la concentración (figura insertada en VIII) coincide con el exponente encontrado para la dependencia de λ_c con la concentración, lo que indica la consistencia de los experimentos.

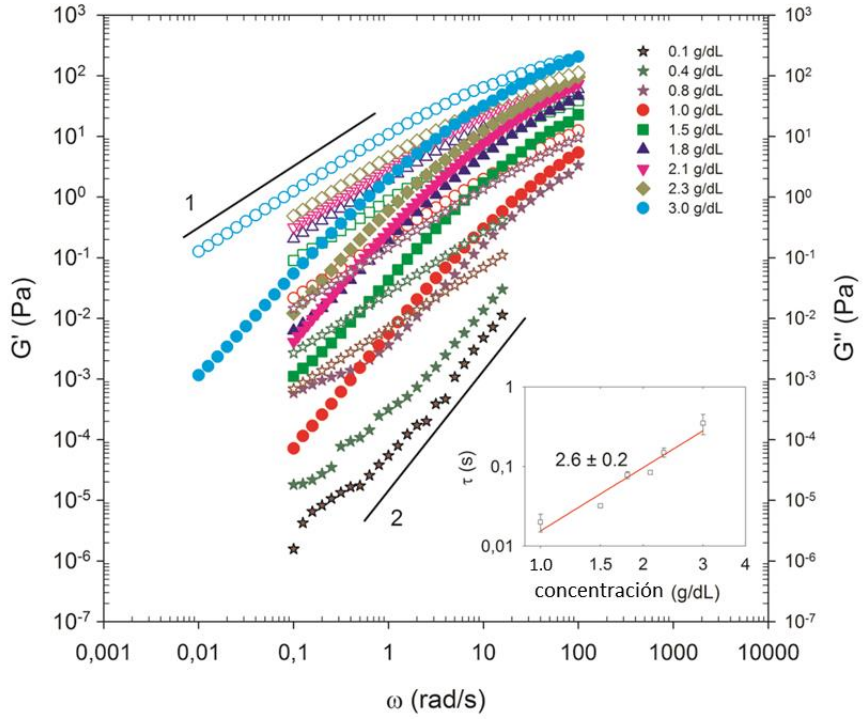

Figura VIII: Efecto de la frecuencia angular en los módulos G' y G''. Efecto de la concentración en los tiempos de relajación.

Para el estudio del comportamiento del alginato en flujo uniaxial, se utilizó un reómetro extensional de rotura capilar– CaBER - (Entov and Hinch 1997).

El cálculo de los números adimensionales elastocapilar y de Deborah (considerando los dos valores de tiempo de relajación - λ_c y τ -) sugieren dos posibles comportamiento: por un lado, los efectos viscosos podrían superar a los efectos elásticos a tiempos cortos (Clasen et al. 2012; Haward et al. 2012; Clasen 2010) y por otro lado, como se propone para sistemas diluidos (Clasen et al. 2012; Vadillo et al. 2012) los valores sugieren un proceso controlado enteramente por efectos elásticos.

Ambos casos han sido estudiados mediante la aplicación de las expresiones que rigen los diferentes comportamientos (Anna and McKinley 2001). Tras el estudio se concluye que el cálculo directo del tiempo de relajación mediante esta técnica no es sencillo. Sin embargo, el análisis que describe el comportamiento elástico como predominante en casi todo el intervalo temporal ajusta mejor los datos y será considerado como válido de cara a análisis posteriores (Figura IX).

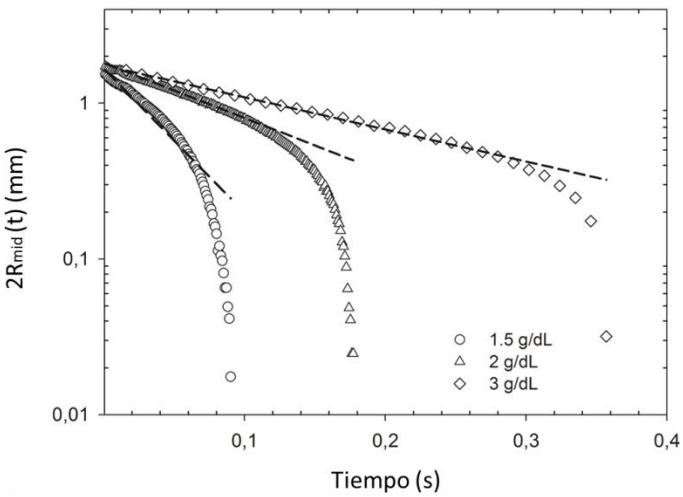

Figura IX: Evolución del proceso de contracción de filamento como función del tiempo Ajuste de la expresión que describe comportamiento elástico.

La comparación entre los valores de viscosidad aparente bajo cizalla y los valores de viscosidad extensional aparente se muestran en la Figura X, en la que se observa también una disminución de la viscosidad extensional aparente con la tasa de variación extensional.

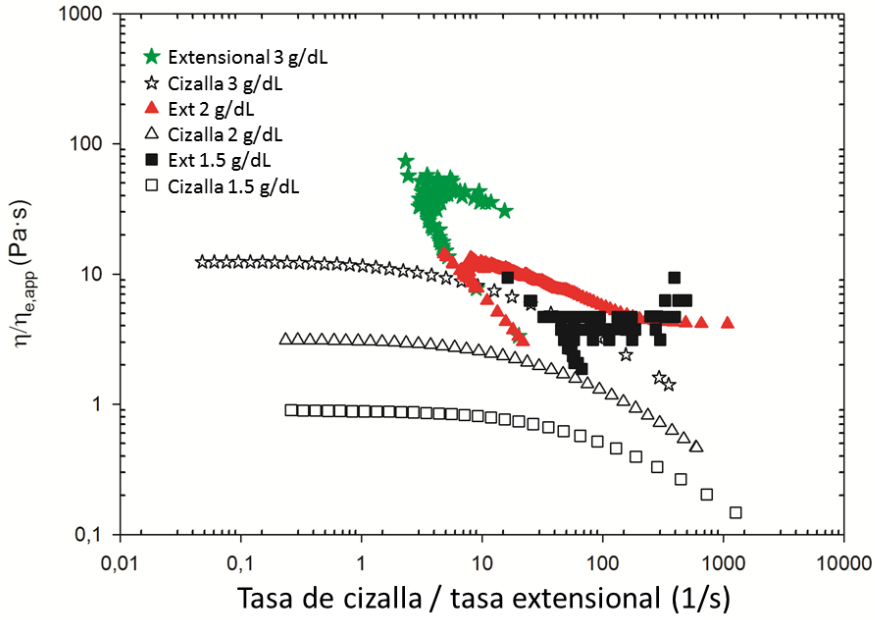

Figura X: Viscosidad extensional aparente y viscosidad de cizalla como función de las tasas de variación de cizalla y extensional.

A partir del estudio extensional también se obtiene el valor de tiempo de relajación del polímero, λ_{ext}, bajo la influencia de un campo de flujo extensional. En la tabla II se recogen los diferentes tiempos de relajación medidos para tres concentraciones de polímero.

Tabla II: Valores de viscosidad a esfuerzo de cizalla cero y tiempos de relajación medidos mediante las diferentes técnicas descritas.

c (g/dL)	η_0 (Pa·s)	$\lambda_{c,cizalla}$(s)	τ_{SAOS}(s)	λ_{ext} (s)
1.5	0.911	$7.66 \cdot 10^{-3}$	0.032	0.0157
2.0	2.744	0.0175	0.080	0.0410
3.0	12.70	0.0481	0.350	0.0703

VIII. ESTUDIO DE INESTABILIDAD LINEAL

Mediante una cámara de alta velocidad se realizaron grabaciones de la evolución de los chorros poliméricos en diferentes condiciones de operación. Las disoluciones de alginato describieron patrones como los mostrados en la figura XI donde se pueden apreciar poco después de la salida de la boquilla, para los casos en los que se impone vibración, el desarrollo de ondas periódicas, de marcado carácter sinusoidal con simetría axial.

Aguas abajo el patrón se convierte en una estructura de gotas en cadena –BOAS-, típica de fluidos viscoelásticos (Clasen et al. 2006a).

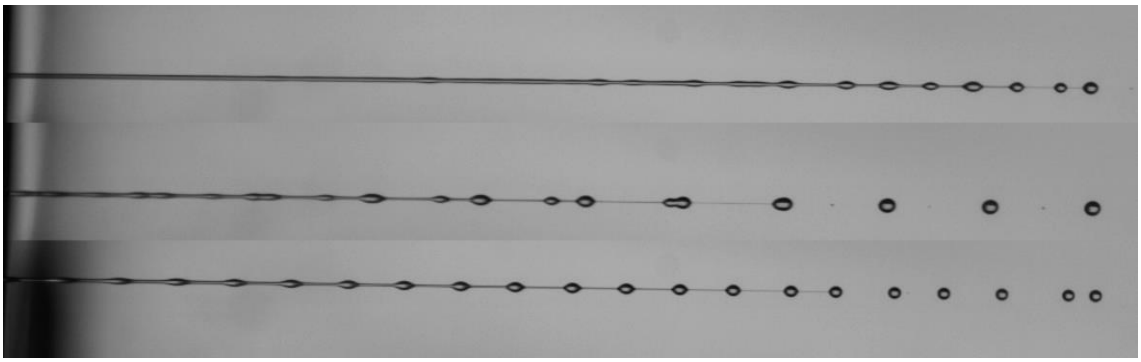

Figura XI: Formación de gota a partir de una disolución de alginato sódico 1.3 g/dL a un caudal de 5 mL/min aplicando desde arriba hacia abajo: 0, 800 y 1650 Hz.

Las imágenes asimismo proporcionan información acerca de ciertos comportamientos que coinciden con el primer análisis realizado sobre el efecto de la viscosidad y caudal y también sobre el efecto de la frecuencia de la vibración externa aplicada.

Un aumento de la viscosidad, para el mismo caudal y frecuencias similares, implica un aumento de la longitud de ruptura y la formación de gotas exhibe efectos no-lineales marcados. Por otra parte un aumento del caudal, manteniendo viscosidad y frecuencia aplicada constantes, implica generalmente un aumento de la longitud de ruptura, siendo un

comportamiento que no se repite en todos los casos y del que resulta complicado inferir conclusiones.

Se ha comprobado también que existe un intervalo amplio de frecuencias que conducen a la ruptura del chorro, aunque no todas ellas conducen a la formación de gotas y microcápsulas homogéneas. En todos los casos se observa un intervalo óptimo y una frecuencia mínima a partir de la cual el chorro no presenta gotas satélite.

Por ello, el principal objetivo del modelo matemático que se lleva a cabo es el de determinar las condiciones óptimas que coincidan con el intervalo de frecuencias óptimo experimental a través de una relación de dispersión, que relacione el número de onda (*k)* y la tasa de crecimiento de las ondas *(Ω)*.

Se realiza así un análisis temporal lineal en base a los resultados observados de la experimentación (crecimiento exponencial con el tiempo de la amplitud de la onda en la interfase), basado en el desarrollo de perturbaciones del tipo:

$$r = r_0 + A_0 e^{(\omega t + ikz)} \qquad \text{(VIII)}$$

Este análisis lleva a una ecuación de dispersión mediante la que se obtiene el número de onda de la perturbación $k = 2\pi/\lambda$ (siendo λ la longitud de onda) que implica un crecimiento más rápido de la inestabilidad para ciertas condiciones particulares.

El comportamiento no newtoniano de las disoluciones requiere de una ecuación constitutiva adecuada para el correcto análisis del sistema. Uno de los modelos viscoelásticos más generales es el modelo corrotacional de Oldroyd-B (Bird et al. 1987), que se incluye en el análisis.

La expresión de dispersión obtenida es la siguiente:

$$\left[Oh\frac{Oh+\bar{t}\cdot El\cdot\Omega}{Oh+El\cdot\Omega}\right]^2\left\{2(ak)^2\left[1-\left(\frac{al}{ak}\right)^2\right]+(ak)^3\left[1+\left(\frac{al}{ak}\right)^2\right]^2\frac{I_0(ak)}{I_1(ak)}-4(ak)^2(al)\frac{I_0(al)}{I_1(al)}\right\}= \qquad \text{(IX)}$$
$$=1-(ak)^2$$

En este modelo están incluidos los valores de viscosidad a cizalla cero η_0, la constante de tiempo t_1 o tiempo de relajación, que puede ser diferente en función del proceso que determine que el polímero se relaje extensionalmente, tangencialmente, etc, y t_2 o tiempo de retardo que también se define como el tiempo que tarda la muestra en recuperar su estado inicial a partir de diferentes consideraciones físicas.

η_0 puede ser obtenido de las curvas de flujo; sin embargo, el tiempo de relajación se ha calculado a partir de distintas medidas bajo diferentes campos externos. Por ello se determinará el tiempo de relajación que mejor describe el proceso mediante comparación entre las curvas de dispersión con los datos experimentales. De acuerdo con diferentes estudios (Pearson 1976) en general los esfuerzos extensionales determinan mejor este tipo de procesos de ruptura.

Por otro lado, la obtención del tiempo de retardo t_2 no resulta sencilla y se recurre a información encontrada en bibliografía acerca de este parámetro (Brenn et al. 2000; Gordon et al. 1973; Kroesser and Middleman 1969).

La relación de dispersión (IX) incluye la tasa de crecimiento adimensional Ω y el número de onda k de forma implícita por lo que ha de resolverse utilizando el método de Newton con la condición impuesta de derivada nula a fin de estimar el valor máximo de la función.

En primer lugar se determina cuál es el tiempo de relajación más adecuado para computar Ω de entre los tres valores diferentes que se han medido. La figura XII muestra el efecto de los diferentes tiempos de relajación en la tasa de crecimiento de una solución de 1.8 g/dL y 6 mL/min y la tabla III compara valores predichos por las curvas de dispersión con los experimentales.

Los resultados sugieren que los datos obtenidos a partir del tiempo de relajación extensional se ajustan mejor a las condiciones experimentales, conclusión que coincide con lo esperado (Pearson 1976). Por lo tanto, el tiempo de relajación extensional λ_{ext} es el que se considerará para el análisis de las curvas de dispersión.

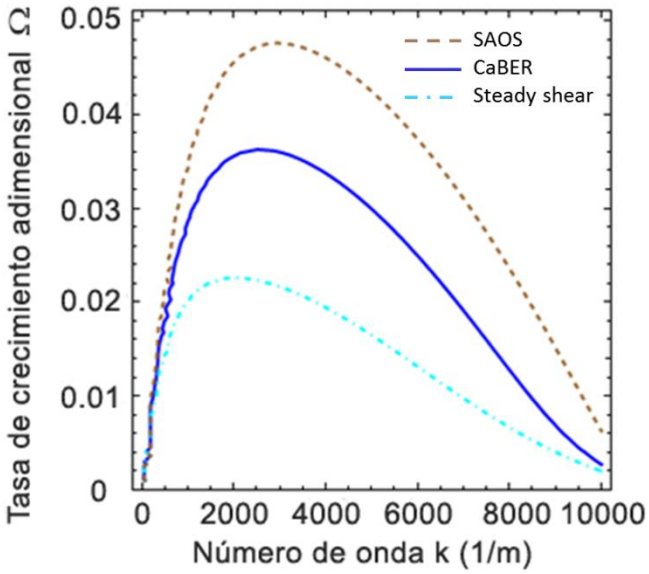

Figura XII: Curvas de dispersión con los diferentes valores de tiempo de relajación.

Tabla III: Valores obtenidos a partir de los distintos tiempos de relajación y comparación con datos experimentales.

	$t_{1,cizalla}$ (s)	$t_{1,CaBER}$ (s)	$t_{1,SAOS}$ (s)
t_1 (s)	0.017	0.033	0.080
k (m^{-1})	2034	2577	2952
Ω	0.023	0.036	0.047
λ (m)	0.0076	0.0024	0.0021
Tamaño teórico (μm)	523	483	462
Frecuencia teórica (s^{-1})	1335	1691	1938
Tamaño experimental (μm)		≈561	
Frecuencia experimental (s^{-1})		1500 - 1800	

Los datos recogidos en la tabla III sugieren que la diferencia entre el tamaño de gota calculado y el tamaño final de micropartícula puede deberse a un hinchamiento de la estructura al solidificar en el baño gelificante (lo que sugiere un estudio al respecto).

Una vez determinado el tiempo de relajación a usar en el estudio, el efecto de la viscosidad puede evaluarse a partir de la expresión (IX).

La figura XIII muestra como un aumento de la viscosidad implica una disminución pronunciada de Ω y k, lo que daría lugar a un retraso de la ruptura y a gotas más grandes. Esto coincide con los resultados experimentales, con una longitud de ruptura y un tamaño de micropartícula mayor.

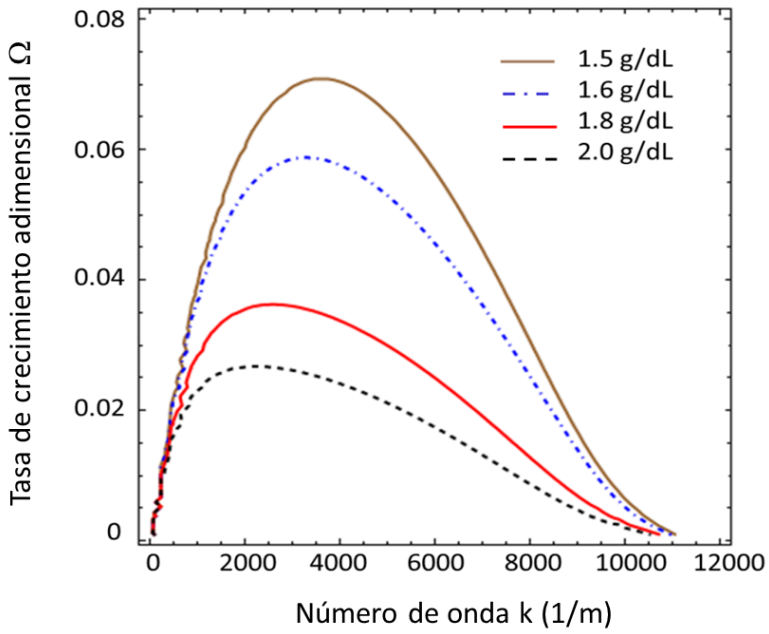

Figura XIII: Curvas de dispersión para diferentes valores de viscosidad.

En la Figura XIV se recogen las curvas de dispersión de Ω frente a k para diferentes caudales manteniendo viscosidad constante.

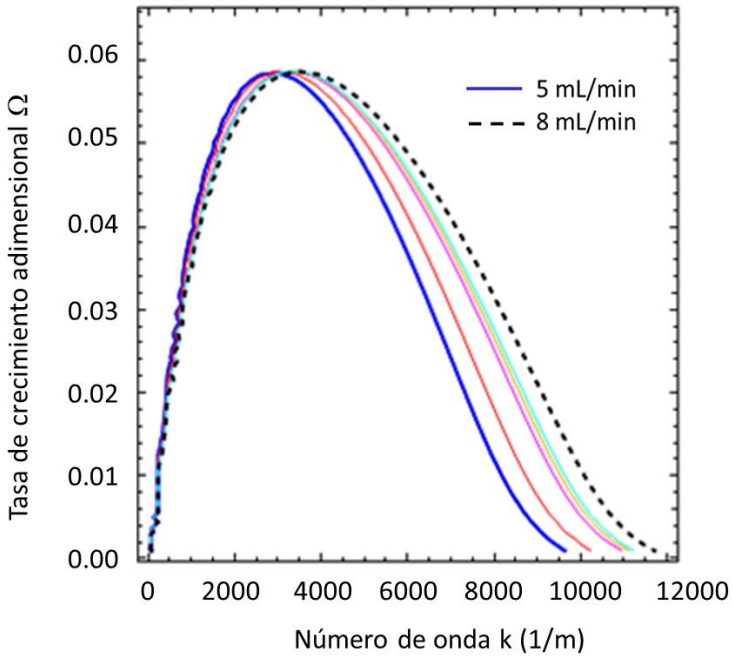

Figura XIV: Curvas de dispersión para diferentes valores de caudal.

A partir de dicha figura se puede observar que el efecto del caudal sobre Ω no es el esperado. Se observa un desplazamiento hacia k más altos cuando el caudal aumenta, tendencia que coincide con las mediciones experimentales. Sin embargo la tasa de crecimiento aumenta con el caudal, lo que implicaría una desestabilización más rápida del chorro.

No obstante, a caudales bajos (5-6.5 mL/min) se ha comprobado de forma experimental que la longitud de ruptura permanece prácticamente constante, aumentando a partir de estos valores con el aumento de caudal.

Por tanto, aunque de forma no muy clara, parece que se da una discrepancia entre la tasa de crecimiento prevista y la longitud de ruptura experimental, lo que motiva la necesidad de un estudio adicional sobre este tema.

IX. REFERENCES

Anna SL, McKinley GH (2001) Elasto-capillary thinning and breakup of model elastic liquids. Journal of Rheology 45 (1):115-138

Ashgriz N, Yarin AL (2011) Capillary Instability of Free Liquid Jets. In: Ashgriz N (ed) Handbook of Atomization and Sprays. Springer.

Bird RB, Armstrong RC, Hassager O (eds) (1987) Dynamics of polymeric liquids: Fluid Mechanics, vol 1. Second edn. John Wiley & Sons.

Bousfield DW, Keunings R, Marrucci G, Denn MM (1986) Nonlinear analysis of the surface tension driven breakup of viscoelastic filaments. Journal of Non-Newtonian Fluid Mechanics 21 (1):79-97. doi: 10.1016/0377-0257(86)80064-7

Brenn G, Liu Z, Durst F (2000) Linear analysis of the temporal instability of axisymmetrical non-Newtonian liquid jets. International Journal of Multiphase Flow 26 (10):1621-1644. doi: 10.1016/s0301-9322(99)00115-9

Clasen C (2010) Capillary breakup extensional rheometry of semi-dilute polymer solutions. Korea-Australia Rheology Journal 22 (4):331-338

Clasen C, Eggers J, Fontelos MA, Li J, McKinley GH (2006a) The beads-on-string structure of viscoelastic threads. Journal of Fluid Mechanics 556:283-308

Clasen C, Phillips PM, Palangetic L, Vermant, Jan (2012) Dispensing of rheologically complex fluids: The map of misery. AIChE Journal 58 (10):3242-3255. doi:10.1002/aic.13704

Christanti Y, Walker LM (2001) Surface tension driven jet break up of strain-hardening polymer solutions. Journal of Non-Newtonian Fluid Mechanics 100 (1-3):9-26. doi: 10.1016/s0377-0257(01)00135-5

Dobrynin AV, Colby RH, Rubinstein M (1995) Scaling theory of polyelectrolyte solutions. Macromolecules 28 (6):1859-1871

Dubey R, Shami TC, Rao KUB (2009) Microencapsulation Technology and Applications. Defence Science Journal 59 (1):82-95

Entov VM, Hinch EJ (1997) Effect of a spectrum of relaxation times on the capillary thinning of a filament of elastic liquid. Journal of Non-Newtonian Fluid Mechanics 72 (1):31-53. doi:http://dx.doi.org/10.1016/S0377-0257(97)00022-0

Goldin M, Yerushalmi J, Pfeffer R, Shinnar R (1969) Breakup of a laminar capillary jet of a viscoelastic fluid. Journal of Fluid Mechanics 38 (04):689-711. doi:10.1017/S0022112069002540

Gordon M, Yerushalmi J, Shinnar R (1973) Instability of Jets of Non-Newtonian Fluids. Transactions of the Society of Rheology 17 (2):303-324

Haward SJ, Sharma V, Butts CP, McKinley GH, Rahatekar SS (2012) Shear and Extensional Rheology of Cellulose/Ionic Liquid Solutions. Biomacromolecules 13 (5):1688-1699. doi:10.1021/bm300407q

Hilliou L, Freitas F, Oliveira R, Reis MAM, Lespineux D, Grandfils C, Alves VD (2009) Solution properties of an exopolysaccharide from a Pseudomonas strain obtained using glycerol as sole carbon source. Carbohydrate Polymers 78 (3):526-532. doi:http://dx.doi.org/10.1016/j.carbpol.2009.05.011

Kroesser FW, Middleman S (1969) Viscoelastic jet stability. AIChE Journal 15 (3):383-386. doi:10.1002/aic.690150316

Mansour A, Chigier N (1995) Air-blast atomization of non-Newtonian liquids. Journal of Non-Newtonian Fluid Mechanics 58:161-194

Middleman S (1965) Stability of a viscoelastic jet. Chemical Engineering Science 20 (12):1037-1040. doi: 10.1016/0009-2509(65)80105-1

Muller FL, Davidson JF (1994) Rheology of Shear Thinning Polymer Solutions. Industrial & Engineering Chemistry Research 33 (10):2364-2367. doi:10.1021/ie00034a016

Pearson JRA (1976) Instability in Non-Newtonian Flow. Annual Review of Fluid Mechanics 8 (1):163-181. doi:10.1146/annurev.fl.08.010176.001115

Plateau J (ed) (1873) Statique expérimentale et théorique des liquides soumis aux seules forces moléculaires. Gauthier-Villars, Paris

Rathore S, Desai PM, Liew CV, Chan LW, Heng PWS (2013) Microencapsulation of microbial cells. Journal of Food Engineering 116 (2):369-381. doi:http://dx.doi.org/10.1016/j.jfoodeng.2012.12.022

Rayleigh L (1879) On the capillary phenomena of jets. Proc R Soc London 29

Reitz RD, Bracco FV (1986) Mechanisms of breakup of round liquids jets. In: Cheremisnoff N (ed) The encyclopedia of Fluid Mechanics. pp 233-249

Savart F (1833) Mémoire sur la constitution des veines liquides lancées par des orifices circulaires en mince paroi. Annali di Chimica 53:337-386

Tun T, Inoue K, Hayashi H, Aung T, Gu YJ, Doi R, Kaji H, Echigo Y, Wang WJ, Setoyama H, Imamura M, Maetani S, Morikawa N, Iwata H, Ikada Y (1996) A newly developed three-layer agarose microcapsule for a promising biohybrid artificial pancreas: Rat to mouse xenotransplantation. Cell Transplantation 5 (5, Supplement 1):S59-S63. doi:http://dx.doi.org/10.1016/0963-6897(96)00042-5

Vadillo DC, Mathues W, Clasen C (2012) Microsecond relaxation processes in shear and extensional flows of weakly elastic polymer solutions. Rheologica Acta 51 (8):755-769

Weber C (1931) Zum Zerfall eines Flüssigkeitsstrahls. Zeit für angewandte Mathematik und Mechanik. 11:136

Yarin AL (1993) Free Liquid Jets and Films: Hydrodynamics and Rheology. New York

Zanin MP, Pettingill LN, Harvey AR, Emerich DF, Thanos CG, Shepherd RK (2012) The development of encapsulated cell technologies as therapies for neurological and sensory diseases. Journal of Controlled Release 160 (1):3-13. doi:http://dx.doi.org/10.1016/j.jconrel.2012.01.021

Zhang WJ, Laue C, Hyder A, Schrezenmeir J (2001) Purity of alginate affects the viability and fibrotic overgrowth of encapsulated porcine islet xenografts. Transplantation Proceedings 33 (7–8):3517-3519. doi:http://dx.doi.org/10.1016/S0041-1345(01)02419-8

Zimmermann U, Cramer H, Jork A, Thürmer F, Zimmermann H, Fuhr G, Hasse C, Rothmund M (2008) Microencapsulation-Based Cell Therapy. In: Biotechnology. Wiley-VCH Verlag GmbH, pp 547-571. doi:10.1002/9783527620937.ch19

CONCLUSIONES EN ESPAÑOL

Como conclusiones generales:

- Se ha desarrollado una nueva tecnología que permite tratar polímeros de alta viscosidad para producir microcápsulas controladas y se ha modelado el efecto de los principales parámetros que afectan al tamaño de micropartícula y a la formación de las gotas precedentes.

- Esta nueva tecnología produce con éxito micropartículas de tamaño controlado en el intervalo de 300 a 600 micrómetros y alta resistencia mecánica para su uso en aplicaciones biomédicas.

A partir de los estudios experimentales y teóricos que se recogen en este trabajo se pueden extraer las siguientes conclusiones particulares:

- Una nueva técnica basada en una tecnología combinada de vibración de boquilla y sistema presurizado logra superar los problemas relacionados con la formación de chorros capilares continuos a partir de disoluciones poliméricas de media/alta viscosidad.

- Esta técnica provoca el desarrollo de inestabilidades laminares en los chorros continuos. Se realiza un primer estudio de la influencia de ciertas variables físico-químicas sobre el tamaño de micropartícula (SMD) mediante curvas de comportamiento. Asimismo se analiza la dependencia del SMD respecto a la viscosidad, caudal y tensión superficial a través de números adimensionales.

- A partir de las curvas de comportamiento, el efecto estabilizador de la viscosidad se verifica de forma clara. Sin embargo el efecto del caudal genera dudas que hacen considerar el estudio de la influencia de los efectos de cizalla y extensional en el sistema.

- A su vez se aborda una primera aproximación para predecir el comportamiento del sistema relacionando el tamaño de partícula con la viscosidad y caudal mediante

expresiones matemáticas de tipo semiempírico. Se evalúa para ello un conjunto de expresiones basadas en la teoría del mecanismo de onda.

- Las expresiones semiempíricas obtenidas predicen de forma adecuada el tamaño de partícula especialmente para viscosidades por encima de 1500 mPa·s. En particular, una de las expresiones propuestas muestra un buen ajuste bajo todas las condiciones ensayadas, lo que demuestra que el mecanismo de onda, aceptado para la atomización de líquidos no-Newtonianos, también puede ser de aplicación al nuevo sistema desarrollado.

- Se determinaron a continuación las propiedades reológicas de las muestras de alginato sódico en disolución bajo los diferentes campos de flujo que afectan al proceso.

- Las disoluciones mostraron comportamiento de polielectrolito para concentraciones bajas con un desplazamiento a comportamiento de polímero neutro para concentraciones más elevadas. Este comportamiento se confirma aplicando las teorías de escala al efecto de la concentración en la viscosidad específica, en los tiempos de relajación a partir de cizalla constante y en los tiempos de relajación a partir de SAOS.

El análisis del comportamiento de las muestras bajo campo extensional se realizó considerando dos enfoques diferentes de los que:

- Una reducción exponencial del filamento seguida de una ruptura lineal final resultó ser el mejor de los regímenes que describe los datos experimentales. Las disoluciones también mostraron "adelgazamiento bajo deformación" *(strain thinning)* de la viscosidad extensional.

- Tras caracterizar la reología del polímero se lleva a cabo un análisis físico más completo de la inestabilidad, con la ayuda de imágenes capturadas mediante cámara de alta velocidad. Estas muestran una estructura de gotas en cadena (BOAS), típica de fluidos viscoelásticos. El intervalo de frecuencias que dan lugar a la ruptura del chorro es amplio pero no todas ellas dan lugar a micropartículas

homogéneas. Se observa un intervalo óptimo para todos los casos y, en general, existe una frecuencia mínima a partir de la que el chorro no presenta gotas satélite. Los fenómenos no lineales de migración, oscilación y fusión de gotas se presentan fuera del intervalo óptimo.

- De la observación experimental se infieren tendencias de comportamiento que muestran cómo un incremento de la viscosidad, manteniendo constante caudal y condiciones de perturbación, aumenta la longitud de ruptura y cómo un aumento de caudal, para las condiciones óptimas de ruptura, también aumenta la longitud de ruptura o la mantiene relativamente constante.

Se propone un análisis temporal lineal para explicar el mecanismo de ruptura laminar polimérica, cuyo principal objetivo consiste en determinar las condiciones óptimas que coincidan con el intervalo experimental de frecuencias óptimo.

- El análisis lineal permitió predecir el intervalo de frecuencias óptimo para lograr muestras homogéneas y reveló los efectos que influyen en mayor medida en el comportamiento del sistema través de una relación de dispersión – que relaciona el número de onda con el crecimiento de las ondas –, por comparación de las curvas de dispersión con los datos experimentales.

- Mediante la evaluación de diferentes magnitudes del tiempo de relajación (obtenidas a partir de medidas bajo distintos campos de flujo) se verificó que los efectos extensionales ejercen una mayor influencia que los efectos de cizalla en el comportamiento del sistema.

- Las curvas de dispersión predicen tasas de crecimiento más cortas con un aumento de la viscosidad y tasas de crecimiento relativamente constantes con un aumento del caudal. Este segundo comportamiento genera, una vez más, ciertas dudas acerca de la valoración del efecto del caudal.

- El enfoque propuesto resulta válido para describir el mecanismo de ruptura de chorros de polímeros viscoelásticos de media y alta viscosidad. La ecuación

constitutiva de viscosidad empleada, Oldroyd-B, resulta apropiada en el intervalo de concentraciones estudiado.

- Tras el estudio físico del sistema se realizaron estudios de Dinámica de Fluidos Computacional (CFD) para definir el método de resolución y las condiciones que permitiesen comparar las soluciones numéricas simuladas con los resultados experimentales y disponer así de una base sólida para un posible escalado del sistema.

- Las tendencias obtenidas mostraron resultados cualitativos interesantes, en concordancia con los patrones observados de los datos experimentales. Sin embargo, el uso de modelos de Newton generalizados no explica la formación de una estructura de gotas en cadena, como la que se observa en las imágenes experimentales.

- El modelo de volumen de fluido (VOF), con el ajuste que se realizó del mismo, trata el seguimiento de la interfase de forma satisfactoria. Los resultados muestran coherencia, lo que lleva a considerar su uso como adecuado para el estudio de inestabilidades capilares laminares.

CHAPTER 1.

INTRODUCTION, MOTIVATION AND OBJECTIVES.

1. INTRODUCTION, MOTIVATION AND OBJECTIVES

1.1. Concept, importance and applications of microencapsulation

The use of microparticles embraces a variety of engineering and industrial applications such as inkjet printing technology, fuel injection, food drying, fine chemical industries, catalytic reactions, self-healing polymers or special fabrics (Dubey et al. 2009).

Microparticles are systems of micrometric size (< 1 mm) that can differ in structure and morphology. In general the term *microsphere* is specifically applied to any microparticle presenting spherical shape. The term *microcapsule* is used when a core is surrounded by a membrane made by a different material or structure than the inner part, or matrix. Figure 1.1 schematically shows different types of microparticles.

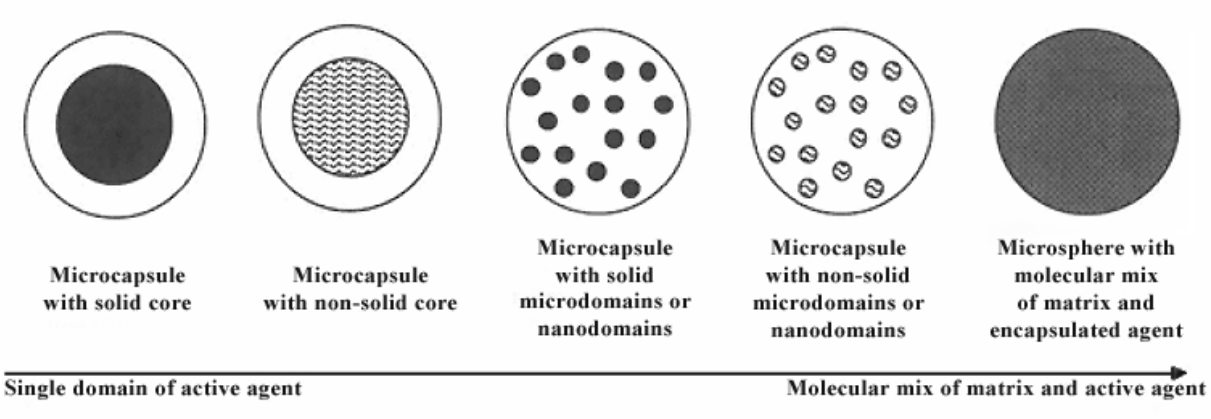

Figure 1.1: Scheme of different types of microparticles (Duane T. Birnbaum and Brannon-Peppas 2003)

Thus, microencapsulation is the process by which an active ingredient is surrounded by a solid coating, obtaining a membrane - core system of micrometric size (< 1 mm). The coating forms a rigid semi-permeable structure.

The main advantages of these microsystems are their small size and high specific surface. Their small size makes easy to target small areas and their higher surface area involves a more efficient mass transfer effect.

In addition to the applications named before, the interest in using these microsystems in medicine and pharmaceutical industries has increased in the last decades. The main reasons are the effective protection that microparticles can provide to the immobilized material and the control of release profiles.

Furthermore, microcapsules offer several advantages over the use of other techniques. They are easier to implant, more resistant to breakage and, when the purity and nature of the coating materials are well controlled, they produce less nonspecific fibrosis, which means less cellular necrosis (Zimmermann et al. 2008). A better explanation of fibrotic overgrowth and its consequences will be explained in next sections. Other advantages will be summarized along this chapter.

These features have led to the use of microcapsules for the entrapment of low molecular weight compounds as proteins and drugs (Ortakci and Sert 2012; de Souza et al. 2013; Voellmy et al. 1977). Hence, several methods that achieve improved drug administration with microcapsules are well established nowadays. They effectively control release rates through sustained release or release under specific conditions and avoid drug concentration peaks. Furthermore, its protective membrane prevents quick enzymatic degradation and loss viability in the gastrointestinal system (Cook et al. 2012).

In addition, new techniques to deliver drugs to specific target tissues or areas are developing fast. This type of release is known as “drug targeting” or “targeting release”. It aims to differentiate between cells and tissues in such a way that microparticles stay constrained in the target place. This avoid systemic toxicity due to a lower drug concentration in healthy, not targeted tissues (Koo et al. 2005; Solaro 2010).

Concerning the mechanisms of release of the core material there are three main different methods (Martín del Valle et al. 2009): mechanical rupture of the capsule wall, dissolution or melting of the wall, and diffusion through the wall. Figure 1.2 illustrates two of them. Less common release mechanisms include slow erosion of the shell and biodegradation.

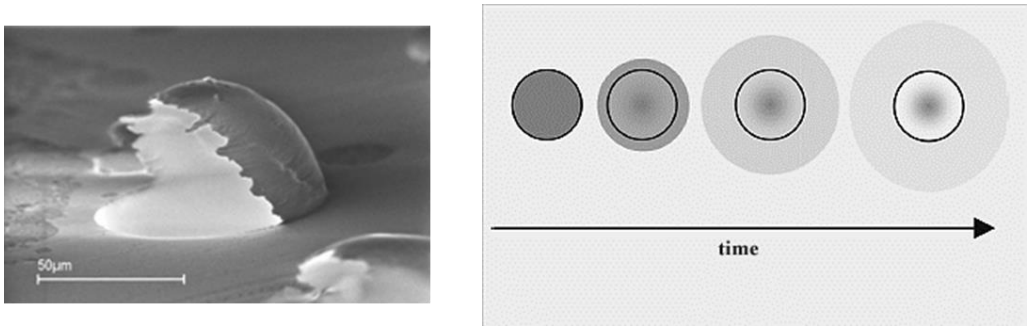

Figure 1.2: Different mechanisms to release the active ingredient: (a) Mechanically ruptured microcapsules in carbonless copy paper (Southwest Research Institute) and (b) Controlled diffusion rate through the membrane (Martín del Valle et al. 2009).

Finally a major effort is being conducted to cell encapsulation therapies. They consist of the entrapment of living cells with a proper semi-permeable membrane. This membrane allows the incoming of nutrients and oxygen and the outgoing of therapeutic factors from the immobilized cells, avoiding immunorejection (Acarregui et al. 2013).

In the past decades much work has focused on this type of transplantation to provide a way to achieve immunoisolation and overcome the use of immunosuppressive drugs (Lanza and Chick 1997). Nowadays the applications extend to many other fields (Zanin et al. 2012; Renggli-Zulliger et al. 1999).

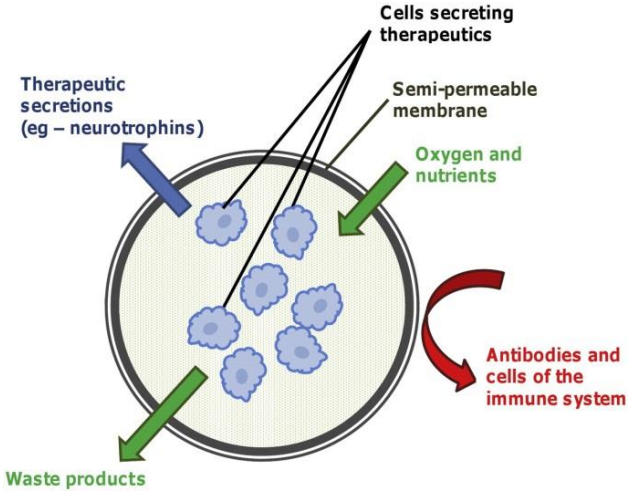

Figure 1.3: Scheme of encapsulated cells and the basis of immunorejection therapies (Zanin et al. 2012).

1.2. History of microencapsulation

One of the first references in the history of microencapsulation refers to a casual observation by chemists Wolfgang Pauli and Peter Rona in 1902. They formed a uniform emulsion under vigorous stirring from neutral salts and warm gelatine solution. This phenomenon was further investigated in the early '20s and recieved the name of *coacervation* (Bungenberg de Jong and Kruyt 1930). Bungenburg pointed out the possibility of using this phenomenon for producing microcapsules for drugs. Although the concept was pretty simple, finding the appropriate conditions was extremely difficult.

In the late '30s Barry Green began to investigate coacervation for the National Cash Register Company, which saw a potential application of this process in their office products. Green developed a method to microencapsulate ink that allowed him to obtain a prototype carbonless copy paper. He improved the technique till industrial scale, resulting in the first patents on this field (Green 1945; The National Cash Register 1963).

In the following years, the microencapsulation found more applications in the field of food - encapsulation of flavours, vitamins, etc. - and agrochemicals - encapsulation of pesticides and fertilizers (Levic et al. 2013; Nazzaro et al. 2012; Bagle et al. 2013). In the mid '50s the pharmaceutical company Smith Kline and French introduced this technology to achieve sustained or prolonged release of drugs. One of the first drugs to be microencapsulated was the aspirin to prevent gastric irritation. The spread of this technique in the pharmaceutical field was very fast.

Concerning cell encapsulation therapies and immunoisolation one of the earliest applications took place when Bisceglie immobilized tumour cells on a polymeric membrane and transplanted them into the abdominal cavity of pigs (Bisceglie 1933). After analysing the survival of the cells he concluded that they were not destroyed by the immune system.

In the 70s extensive research was carried out on transplanted cells for protecting pancreatic islets from immunorejection to treat diabetes (Chick et al. 1975; Lim and Sun 1980). Still nowadays wide research in the microencapsulation of insulin producing cells (islets of Langerhans) is being conducted (Lee et al. 2012b; Kim et al. 2012).

Cell encapsulation therapies are growing fast and find applications to treat a wide variety of diseases. They have been found to be particularly suitable for delivering therapeutics to the central nervous system.

Hence, researchers are studying conditions involving neurodegeneration, such as Alzheimer's and Parkinson's diseases with promising results (Zanin et al. 2012).

Furthermore, their use in cancer therapies is also a leading application. Both encapsulated cells and the encapsulation of antiangiogenic and antitoumoral products have been used and are being investigated for the treatment of tumours (Salmons and Gunzburg 2010; Urbanska et al. 2012).

1.3. Problem definition

As explained before microcapsules offer several advantages over the use of other techniques involving bulk liquids for instance, particularly in bioapplications. The main advantages include its potential use in a wider range of transplantation sites and the removal of invasive surgery for its administration, as their way of implantation is usually by injection. Furthermore, regarding the viability of the graft, not the whole of it is lost if a few of the total microcapsules break.

A possible disadvantage of microcapsules could be their retrieval. However, when this is necessary it is typically performed by lavage and needle aspiration, which offer a less invasive procedure than other techniques (Lanza and Chick 1997; Chaikof 1999). Nevertheless most treatments do not require this step since the use of biocompatible materials is extended.

To date, the main limitations when using microcapsules are fibrotic overgrowth and low stability. The former one involves an excessive production and deposition of extracellular matrix, which forms an extra barrier that prevents the diffusion of oxygen and nutrients and leads to ischemia and subsequent necrosis of the cells in the graft. This can then seriously affect the viability of encapsulated cells (Schrezenmeir et al. 1992). As a

solution, it seems that the use of polymers with high purity or the use of antifibrotic agents can reduce this condition (Zhang et al. 2001; Zhang et al. 2000).

The second limitation - low mechanical stability – involves the need of achieving a minimum stability to reduce ruptures derived from microcapsule handling and mechanical failures due to the administration process, osmotic stress and host movements.

In turn, another requirement in biomedical application is the biocompatibility of the materials and processes. Finding and synthesising biocompatible materials has been positively overcome during the past decades, where polymeric solutions are on top (Rathore et al. 2013).

However, raw polymeric solutions of low viscosity produce a non-reliable mechanical behaviour of the microcapsules. One of the ways to solve this disadvantageous situation is by using high viscosity polymers (Peirone et al. 1998). Nevertheless, there is a lack of techniques to control efficiently high viscosity fluid breakup and size and shape of the microparticles. In addition, polymers show Non-Newtonian behaviour - typically viscoelastic - which makes more complex their analysis.

Furthermore, the control of size and shape is very important because they are crucial for achieving a controlled administration process and a proper analysis and prediction of behaviour, such as release rates and amount of cells per capsule.

It also has a major role since it has been checked that transplant of heterogeneous-sized or irregular-shaped microparticles are related to a higher probability of early failure of the graft (Zimmermann et al. 2008).

Finally, concerning the methodology, many of the processes to produce microparticles use harmful conditions, where the ingredient contained in the matrix can be affected by organic solvents or extreme temperatures. Therefore, it is highly important to find safe methods. Moreover, most applications require thousands of beads to collect the necessary number of cells for a therapeutic dose so the technique must be potentially scaled up.

1.4. Motivation

The motivation of the present work is based on the need to develop, characterize and investigate a technique to produce microparticles that comply with the strict requirements commented before for their use in the biomedical field.

The research group is conducting three different lines on the study of techniques to generate nano- and microcapsules. They are summarized in the following paragraphs.

- Nanocapsules from 200 to 400 nanometres: with ionic gelation and electrostatic complexation. Nanoparticles with low polydispersity index and different superficial features are produced. They are used for drug targeting due to their functionalized surface.

- Microcapsules from 1 to 5 micrometres: with the use of supercritical carbon dioxide as antisolvent in a technique called solution enhanced dispersion by supercritical fluids (SEDS). Particles of drugs such as acetaminophen and tretinoin from powders of about 50 micrometres are micronized to particles between 1-5 micrometres.

Finally, the third line of study is focused on the development of techniques that allow the processing of high viscosity biocompatible fluids so that high stability and reliability of the microcapsules can be achieved. This would allow their use for the production of microsystems with potential applications in biomedicine. Two techniques are being studied:

- Microcapsules from 20 to 100 micrometres: by using a fan jet nozzle that disrupts a laminar jet exiting an orifice by a gas current. The liquid alone comes from an upper nozzle and the air meets and surrounds it before a second orifice downstream, from which they exit together. The distortion of the liquid jet takes place downstream due to gas drag.

- Microparticles from 300 to 600 micrometres: with the use of a vibrating nozzle technique combined with other means, achieving a novel methodology. This method will be detailed along this work.

The main aim lies in the understanding of the physical process and its modelling. Once the process is widely analysed it will be able to predict the behaviour of the system through semiempirical and analytical expressions.

The microcapsules obtained from this technique have been already used as microdevices in the prevention of late postpneumonectomy bronchopleural fistula (LBPF) through an interdisciplinary research project (coded GRS/213/A/08).

This project is led by Dr. José Luis Aranda Alcaide as principal investigator. Other researchers include members of the University Hospital of Salamanca (Dr. Gonzalo Varela Simó from the Thoracic Surgery Department and Dr. M ª Dolores Ludeña from the Section of Pathology), of the Faculty of Veterinary Medicine of the University of León (Dr. Manuel Gonzalo Order, Dr. José Antonio Rodríguez-Altonaga Martinez and Dr. Marta Regueiro Purriños), personnel of the Tissue Bank of the San Francisco Clinic Foundation in León and Dr. Eva Martin del Valle, co-director of this thesis.

Pneumonectomy is a surgical procedure in which an entire lung is removed (pulmonary resection). It is mainly done as lung cancer treatment when the removal of a smaller portion of the lung has been discarded. A bronchopleural fistula (BPF) is a communication between the pleural space and the bronchial tree and, by far, this rare condition is mainly caused by the postoperative complication of pneumonectomy. Thus, it remains one of the most serious complications of pneumonectomy (Hollaus et al. 1997). Its incidence ranged from 0.8 to 15% in recent years (Misthos et al. 2006).

BPFs are classified as early or late fistulas. Early fistulas, those appearing till thirty days after the surgery, are easier to treat through reoperation. However, for late BPF (weeks to years postoperatively) the procedures become more difficult or impossible to perform (Misthos et al. 2006).

Therefore, the primary objective of the project consists of avoiding the appearance of a late bronchopleural fistula postneumonectomy (LBPF). A porcine model is studied, where a coverage for the devascularized bronchial stump is implanted. This coverage is made by a simple biocompatible suturable matrix of alginate that coats a tissue graft - fibrin matrix - with fibroblasts, vascular endothelial growth factor (VEGF) and fibroblast growth factor (bFGF) within the aforementioned microcapsules (De La Puente et al. 2011).

The microcapsules containing bFGF are then adequate in size and resistance to withstand the conditions of biological stress to which they are subjected. They allow, in

turn, a controlled release profile so that the overall release of the tissue graft is dual and maintained over time.

OBJECTIVES

1.5. Objectives

The general aim of this work is the development of a new technique to generate microcapsules of sizes ranging from 300 to 600 micrometres from medium-high viscosity polymers (0.450-2.650 Pa·s).

This technique is part of a larger project with the purpose of finding adequate procedures to produce nano- and microcapsules fulfilling the requirements to be mainly used in therapeutic procedures.

The novel technique will be based in a combined technology of vibrating nozzle and pressurized system. Part of the system has been patented.

The technology tackles the difficulties of converting high viscosity bulk solutions into capillary stable continuous jets that will evolve to a laminar instability, which is a common problem in current techniques.

The specific objectives are:

- To set up a new technique that allows developing laminar instabilities in medium-high viscosity polymeric jets.

In order to obtain a first approach to the physical process a set of previous studies is carried out. The behavioural curves allow studying the effect of different parameters. These parameters can be related to the particle size through mathematical expressions. Therefore, the objective should be:

- To obtain a semiempirical set of equations to predict particle size as a first approach.

After the analysis of the set – up studies it is clear that the rheology of the polymer is of main importance to step further into a more complex analysis. In consequence it is necessary:

- To investigate thoroughly the rheological nature of the solutions used.

Once the polymer is well characterized a more complete physical approach to the analysis of the instability is addressed in order to:

- To obtain a dispersion relation that describes the process accurately from a mathematical analysis. Thus, the behaviour of the main parameters affecting the process can be extensively analysed.

Finally, in order to optimize the number of experiments and predict behaviours that cannot be visualized with the current experimental conditions, CFD techniques are used to study the system. They have the objective to:

- To implement computational modelling of multiphase flows in order to compare with the experimental results and provide a solid base to a possible scale – up.

1.6. Contents of this thesis

The contents of this thesis are presented in a set of chapters. Chapter 2 collects the state of the art concerning different processes of microparticle production, materials of common use and the features of the selected encapsulating polymer for this study.

Chapter 3 refers to materials and methods used during the attainment of this work.

Chapter 4 describes the experimental device developed, the generation of behavioural curves and the semiempirical analysis relating main variables of the process (surface tension, viscosity and flow rate). It also collects literature about the instabilities in jets, namely laminar instabilities.

Chapter 5 deals with the physical study of the system, this is the fluid rheology and the mathematical model that leads to a dispersion relation describing the best conditions to promote a monodisperse controlled droplet (and microcapsule) formation.

Chapter 6 collects computational studies based on two-fluid hydrodynamic analysis performed with the commercial software package Ansys® FLUENT®.

Finally Chapters 7 includes the conclusions and outlooks of the work.

1.7. References

Acarregui A, Orive G, Pedraz JL, Hernández RM (2013) Therapeutic applications of encapsulated cells. Methods in Molecular Biology 1051:349-364

Bagle AV, Jadhav RS, Gite VV, Hundiwale DG, Mahulikar PP (2013) Controlled release study of phenol formaldehyde microcapsules containing neem oil as an insecticide. International Journal of Polymeric Materials and Polymeric Biomaterials 62 (8):421-425

Bisceglie V (1933) Uber die antineoplastische immunitat; heterologe Einpflnzung von Tumoren in Huhner-embryonen. Ztschr Krebsforsch 40:122–140

Bungenberg de Jong HG, Kruyt HR (1930) Koazervation (Entmischung in Kolloidalen Systemen). Koll Zeitsch 50:39-48

Cook MT, Tzortzis G, Charalampopoulos D, Khutoryanskiy VV (2012) Microencapsulation of probiotics for gastrointestinal delivery. Journal of Controlled Release 162 (1):56-67. doi:http://dx.doi.org/10.1016/j.jconrel.2012.06.003

Chaikof EL (1999) Engineering and Material Considerations in Islet Cell Transplantation. Annual Review of Biomedical Engineering 1 (1):103-127. doi:10.1146/annurev.bioeng.1.1.103

Chick W, Like A, Lauris V (1975) Beta cell culture on synthetic capillaries: an artificial endocrine pancreas. Science 187 (4179):847-849. doi:10.1126/science.187.4179.847

De La Puente P, Ludeña D, Fernández A, Aranda JL, Varela G, Iglesias J (2011) Autologous fibrin scaffolds cultured dermal fibroblasts and enriched with encapsulated bFGF for tissue engineering. Journal of Biomedical Materials Research - Part A 99 A (4):648-654. doi:10.1002/jbm.a.33231

de Souza JRR, Feitosa JPA, Ricardo NMPS, Trevisan MTS, de Paula HCB, Ulrich CM, Owen RW (2013) Spray-drying encapsulation of mangiferin using natural polymers. Food Hydrocolloids 33 (1):10-18

Duane T. Birnbaum, Brannon-Peppas L (2003) Microparticle Drug Delivery Systems. Drug Delivery Systems in Cancer Therapy. Humana Press, Totowa, New Jersey

Dubey R, Shami TC, Rao KUB (2009) Microencapsulation Technology and Applications. Defence Science Journal 59 (1):82-95

Green BK (1945) US Patent: 2374862.

Hollaus PH, Lax F, El-Nashef BB, Hauck HH, Lucciarini P, Pridun NS (1997) Natural history of bronchopleural fistula after pneumonectomy: A review of 96 cases. The Annals of Thoracic Surgery 63 (5):1391-1396. doi:http://dx.doi.org/10.1016/S0003-4975(97)00409-8

Kim JY, Kim HW, Bae SJ, Joo DJ, Huh KH, Fang YH, Cho Y, Jeong JH, Kim YS, Lee JI (2012) Hybrid Cellular Spheroids From Hepatocellular Carcinoma and Insulin-Secreting Cell Lines. Transplantation Proceedings 44 (4):1095-1098. doi:http://dx.doi.org/10.1016/j.transproceed.2012.02.016

Koo OM, Rubinstein I, Onyuksel H (2005) Role of nanotechnology in targeted drug delivery and imaging: a concise review. Nanomedicine: Nanotechnology, Biology and Medicine 1 (3):193-212. doi:http://dx.doi.org/10.1016/j.nano.2005.06.004

Lanza RP, Chick WL (1997) Immunoisolation: at a turning point. Immunology Today 18 (3):135-139. doi:http://dx.doi.org/10.1016/S0167-5699(97)01008-6

Lee JI, Kim HW, Kim JY, Bae SJ, Joo DJ, Huh KH, Fang YH, Jeong JH, Kim MS, Kim YS (2012b) Microencapsulation of Pancreatic Islets With Canine Ear Cartilage for Immunoisolation. Transplantation Proceedings 44 (4):1091-1094. doi:http://dx.doi.org/10.1016/j.transproceed.2012.02.015

Levic S, Djordjevic V, Rajic N, Milivojevic M, Bugarski B, Nedovic V (2013) Entrapment of ethyl vanillin in calcium alginate and calcium alginate/poly(vinyl alcohol) beads. Chem Pap 67 (2):221-228. doi:10.2478/s11696-012-0260-1

Lim F, Sun AM (1980) Microencapsulated islets as bioartificial endocrine pancreas. Science 210:908-909

Martín del Valle EM, Galán MA, Carbonell RG (2009) Drug Delivery Technologies: The Way Forward in the New Decade. Industrial & Engineering Chemistry Research 48 (5):2475-2486. doi:10.1021/ie800886m

Misthos P, Kakaris S, Sepsas E, Athanassiadi K, Skottis I (2006) Surgical Management of Late Postpneumonectomy Bronchopleural Fistula: The Transsternal, Transpericardial Route. Respiration 73 (4):525-528

Nazzaro F, Fratianni F, Coppola R (2012) Microtechnology and nanotechnology in food science. In: Boye JI, Arcand Y (eds) Green Technologies in Food Production and

Processing. Food Engineering Series. Springer US, pp 471-494. doi:10.1007/978-1-4614-1587-9_17

Ortakci F, Sert S (2012) Stability of free and encapsulated Lactobacillus acidophilus ATCC 4356 in yogurt and in an artificial human gastric digestion system. Journal of Dairy Science 95 (12):6918-6925

Peirone M, Ross CJD, Hortelano G, Brash JL, Chang PL (1998) Encapsulation of various recombinant mammalian cell types in different alginate microcapsules. Journal of Biomedical Materials Research 42 (4):587-596. doi:10.1002/(sici)1097-4636(19981215)42:4<587::aid-jbm15>3.0.co;2-x

Rathore S, Desai PM, Liew CV, Chan LW, Heng PWS (2013) Microencapsulation of microbial cells. Journal of Food Engineering 116 (2):369-381. doi:http://dx.doi.org/10.1016/j.jfoodeng.2012.12.022

Renggli-Zulliger N, Dudler J, Fujimuto N, Iwata K, So A (1999) Use of Encapsulated Cells Secreting Murine TIMP-2 Ameliorates Collagen-Induced Arthritis in Mice. Annals of the New York Academy of Sciences 878 (1):515-518. doi:10.1111/j.1749-6632.1999.tb07713.x

Salmons B, Gunzburg W (2010) Therapeutic Application of Cell Microencapsulation in Cancer. In: Pedraz J, Orive G (eds) Therapeutic Applications of Cell Microencapsulation, vol 670. Advances in Experimental Medicine and Biology. Springer New York, pp 92-103. doi:10.1007/978-1-4419-5786-3_9

Schrezenmeir J, Gero L, Laue C, Kirchgessner J, Muller A, Huls A, Passmann R, Hahn HJ, Kunz L, Mueller-Klieser W, Altman JJ (1992) The role of oxygen supply in islet transplantation. Transplantation Proceedings 24 (6):2925-2929

Solaro RC, F.; Battisti, A. (2010) Targeted Delivery of Protein Drugs by Nanocarriers. Materials 3:1928-1980

Southwest Research Institute S. http://www.swri.org/4org/d01/microenc/microen/release.htm.

The National Cash Register C (1963) UK Patent: 907284.

Urbanska AM, Karagiannis ED, Guajardo G, Langer RS, Anderson DG (2012) Therapeutic effect of orally administered microencapsulated oxaliplatin for colorectal cancer.

Biomaterials 33 (18):4752-4761. doi:http://dx.doi.org/10.1016/j.biomaterials.2012.03.023

Voellmy C, Speiser P, Soliva M (1977) Microencapsulation of phenobarbital by spray polycondensation. Journal of Pharmaceutical Sciences 66 (5):631-634

Zanin MP, Pettingill LN, Harvey AR, Emerich DF, Thanos CG, Shepherd RK (2012) The development of encapsulated cell technologies as therapies for neurological and sensory diseases. Journal of Controlled Release 160 (1):3-13. doi:http://dx.doi.org/10.1016/j.jconrel.2012.01.021

Zhang WJ, Laue C, Hyder A, Schrezenmeir J (2001) Purity of alginate affects the viability and fibrotic overgrowth of encapsulated porcine islet xenografts. Transplantation Proceedings 33 (7–8):3517-3519. doi:http://dx.doi.org/10.1016/S0041-1345(01)02419-8

Zhang WJ, Marx SK, Laue C, Hyder A, Juergensen A, Bickel M, Schrezenmeir J (2000) Hoe 077 reduces fibrotic overgrowth around the barium alginate microcapsules. Transplantation Proceedings 32 (1):206-209. doi:http://dx.doi.org/10.1016/S0041-1345(99)00938-0

Zimmermann U, Cramer H, Jork A, Thürmer F, Zimmermann H, Fuhr G, Hasse C, Rothmund M (2008) Microencapsulation-Based Cell Therapy. In: Biotechnology. Wiley-VCH Verlag GmbH, pp 547-571. doi:10.1002/9783527620937.ch19

CHAPTER 2.

STATE OF THE ART.

2. STATE OF THE ART

This chapter provides a description of different methods and materials to produce microparticles. The chapter focuses afterwards in the selected procedure and the specific polymer used along this research.

2.1. Microparticle production methods

There are several processes to obtain microparticles. As a matter of fact more than 200 microencapsulation patented methods can be identified in bibliography (Benita 2006).

Figure 2.1 illustrates the exponential increase in the number of scientific and non-scientific publications on the topic since middle '50s. In scheme 2.2 the most common techniques to produce microparticles are listed.

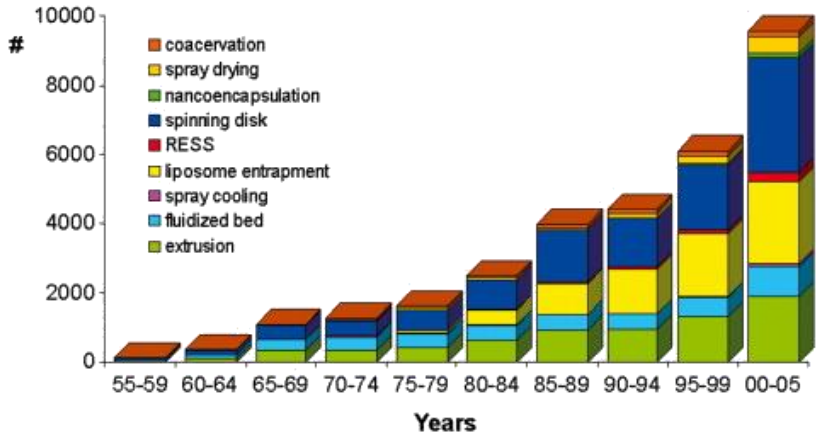

Figure 2.1: Number of publications about microencapsulation technologies (Gouin 2004).

Accordingly, several classifications of the methods of microencapsulation have been proposed, being the most general that which distinguish between physic-chemical and mechanical procedures (Dubey et al. 2009; Umer et al. 2011).

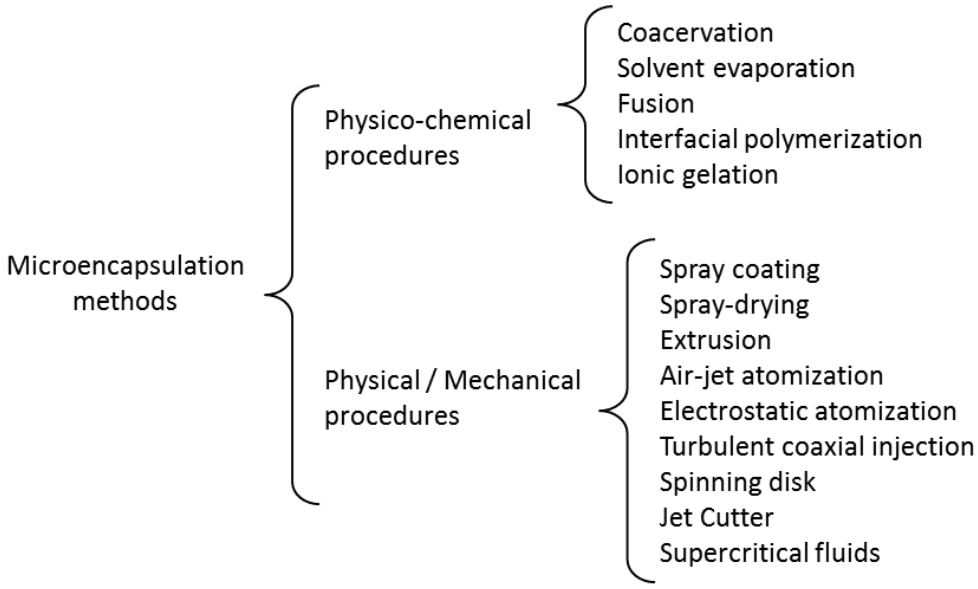

Figure 2.2: Microencapsulation techniques.

The selection of a specific procedure depends on the properties of the active ingredient to be encapsulated and the covering material, as well as the sought properties, such as granulometry, internal structure, release profile, costs, etc (Gouin 2004; Popplewell 2001).

2.1.1. Physico-chemical procedures

The most common techniques within this group are the microencapsulation by coacervation, solvent evaporation, liposome entrapment, interfacial polymerization and ionic gelation.

The term *coacervation* (phase separation) was introduced in the 20's (Bungenberg de Jong and Kruyt 1930). Nowadays it is still quite common in the pharmaceutical field. It consists of decreasing the solubility of an encapsulating polymer in an organic solution by addition of a third component. It includes the following three steps: (i) phase separation of the coating polymer solution, (ii) adsorption of the coacervate around the drug particles, and (iii) solidification and collection of the microspheres (Jain 2000).

The polymer is first dissolved in an organic solution (Lewis 1990). The water-soluble drugs like peptides and proteins are dissolved in water and dispersed in the polymer solution. Hydrophobic drugs like steroids are either solubilized or dispersed in the polymer solution. An organic nonsolvent is then added to the polymer–drug–solvent system with stirring which gradually extracts the polymer solvent. As a result the polymer is subjected to phase separation and it forms coacervate droplets (size controlled by stirring) which entrap the drug. (Figure 2.3). This system is then transferred to a large quantity of another organic nonsolvent to harden the microdroplets which are collected by washing, sieving, filtration, or centrifugation, and are finally dried (Edelman et al. 1993).

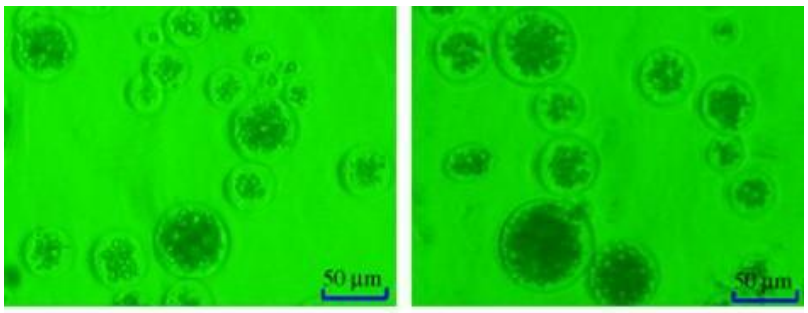

Figure 2.3: Light microscopy photograph of peppermint oil microcapsules by coacervation (Dong et al. 2011).

In a similar way in the *solvent evaporation* process, the polymer is dissolved in a suitable water immiscible solvent, and the medicament is dispersed or dissolved in this polymeric solution. The resultant solution or dispersion is then emulsified in an aqueous continuous phase to form discrete droplets. In order for the microspheres to form, the organic solvent must first diffuse into the aqueous phase and then evaporate at the water/air interface. As solvent evaporation occurs, the microspheres harden and free flowing microspheres can be obtained after suitable filtration and drying (O'Donnell and McGinity 1997).

The *interfacial polymerization* occurs between two chemically different monomers in the interface of two immiscible liquids. The ingredient to be encapsulated is commonly in an organic phase with monomers. An aqueous phase with more monomers is added and an

emulsion is formed. The monomers from both phases react at the interface producing a shell around the active ingredient (Saihi et al. 2006).

The *ionic gelation* process is based on the reaction between a charged polymer, typically a polysaccharide, and an ion of opposite charge. It does not involve rises of temperature, organic solvents or harsh conditions that can result harmful to sensitive active ingredients (Chan et al. 2002). This process will be detailed later since it is one of the methods used in this work.

The entrapment by liposomes is sometimes classified as a chemical technique. *Liposomes* are microscopic particles whose structure comprises a lipid bilayer (phospholipid vesicle). They are colloidal structures having an internal aqueous pool formed by self-assembly of amphiphilic lipid molecules in solution (Figure 2.4). Due to the presence of both lipid and aqueous phases in the vesicle, they can be employed for the entrapment, delivery, and release of water-soluble, lipid-soluble, and amphiphilic materials. Like natural membranes, they are selectively permeable to ions. The release of the ingredient can be by diffusion through the bilayer, by destruction of the vesicle, by a critical concentration of ions or by a change of pH. Their largest application has been found in the pharmaceutical industry for the release of vaccines, proteins and vitamins (Sant'Anna et al. 2011).

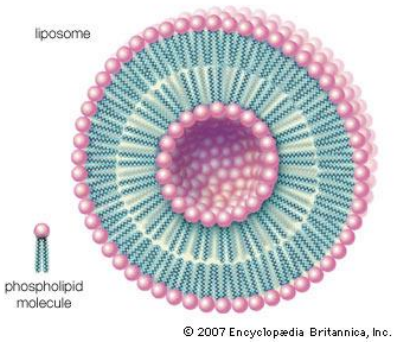

Figure 2.4: Structure of a liposome.

2.1.2. Physical and mechanical processes

This group includes the microencapsulation by different types of injection/extrusion, atomization, and supercritical fluids methods. Some of the processes here described do not

comprise the complete formation of the microcapsules but they are the first step in their generation. In those cases, droplets are formed firstly and they are later solidified by other means such as solvent evaporation, phase transition or gelation.

Several of these techniques convert bulk liquids into sprays. A spray defines a collection of liquid drops dispersed in a gas.

In the *microencapsulation by spray coating in fluidized bed* (Figure 2.5) particles of active ingredient are kept in suspension into a chamber with controlled temperature and humidity. A high velocity stream of air that contains the coating substance is sprayed into the chamber and covers the surface of the ingredient particles. The particle shell solidifies by the action of air (Dewettinck and Huyghebaert 1999).

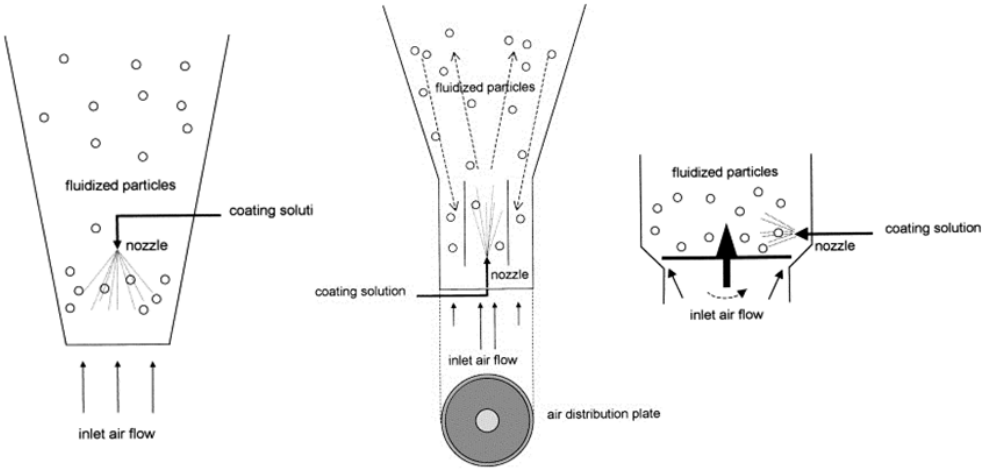

Figure 2.5: Top-spray, bottom-spray and tangential-spray fluidized bed coating (Dewettinck and Huyghebaert 1999).

In *spray-drying* the active ingredient is dispersed in a solution of encapsulating polymer which is sprayed into a chamber with hot air in vacuum (150 to 200 °C). Under these conditions, the solvent is evaporated and the encapsulating polymer solidifies on the active ingredient, to precipitate then as microparticles (Gharsallaoui et al. 2007).

Spray congealing is a similar method in which the polymer – ingredient solution at high temperature is fed into the chamber where cold air makes the polymer solidify (Ilić et al. 2009).

The *encapsulation by extrusion* or *injection* involves the flow of an emulsion of active ingredient and covering material through a nozzle. These methods generate microdroplets that have to be later solidified by cooling, gelation or solvent evaporation. Some of these methods are summarized next.

In *co-extrusion* or *turbulent coaxial injection* the active ingredient flows through the central orifice of a concentric nozzle, while the coating material flows through the outer ring. Drops are obtained at the outlet of the nozzle (Hwang et al. 2008).

In a*ir-jet assisted atomization* (see figure 2.6) the solution of coating material and active ingredient exits through a nozzle at low speed and it is surrounded by a stream of high velocity air. The friction between the liquid and the air accelerates and alters the flow stream causing atomization (Tanner et al. 2008).

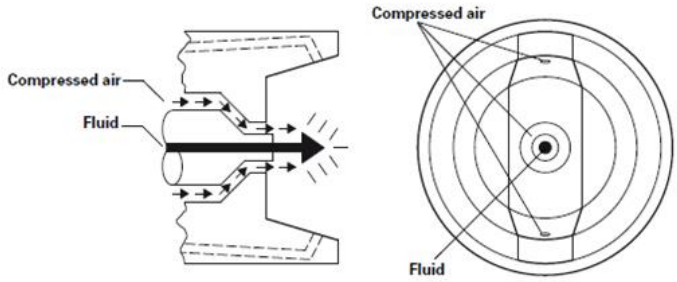

Figure 2.6: Air-assisted nozzle for jet atomization (GRACO 1995).

In *electrostatic atomization* (also called electrospray or electrohydrodynamic spray), the solution of coating - active ingredient is exposed to an intense electric field between a nozzle and a charged piece to ground. The effects of the field disperse the fluid at the outlet of the nozzle in charged droplets (Watanabe et al. 2003).

The *JetCutter technology* is a technique that cuts a jet with a rotating wire, forming regular small cylinders that take the form of drops of identical size (Prüsse et al. 1998).

The *vibrating nozzle technique* uses a simple nozzle from which the solution of coating and active ingredient issues in the form of a jet. A mechanical imposed vibration in the

nozzle is transmitted to the flow and makes the formed jet destabilize and break up in droplets (Serp et al. 2000).

The classification of the previous bunch of techniques is sometimes ambiguous. Figure 2.7 illustrates the basis of some of the detailed extrusion techniques.

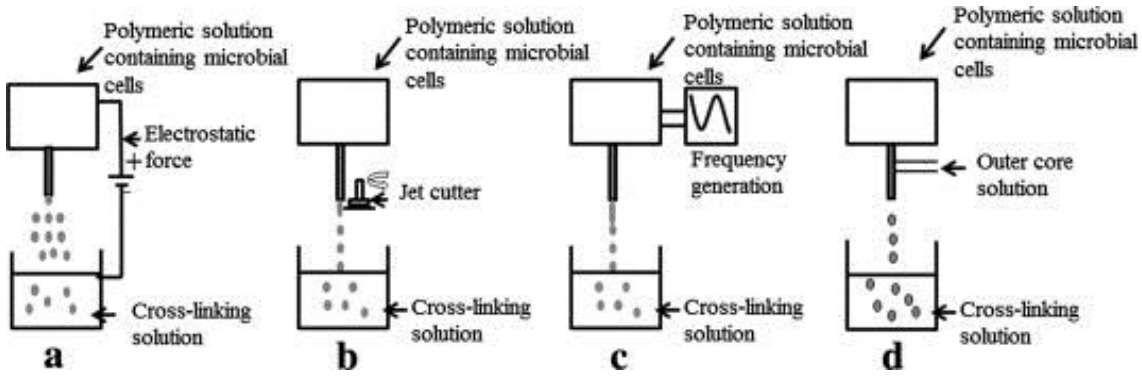

Figure 2.7: Different extrusion techniques for droplet and subsequent microspheres formation: (a) Electrostatic atomization, (b) Jet cutter, (c) Vibrating nozzle, (d) Coaxial/co-extrusion injection. (Rathore et al. 2013).

Other mechanical methods include:

Spinning disk: a nozzle directs a solution of active ingredient and encapsulating material toward the centre of a rotating disk. The centrifugal force brings the fluid to the edges of the disc and throws them as drops (Senuma et al. 2000).

Microencapsulation by fluid under supercritical conditions: Supercritical fluids are fluids at conditions of pressure and temperature higher than their critical point. They show properties halfway between a gas and a liquid, presenting a density more similar to that of the liquid and easy to tune close to the critical point. For example, small pressure changes produce large changes in density, which is the parameter characterizing the solvating power: the higher the density, the greater the solvating power. They are widely used as substitutes for organic solvents (Yeo and Kiran 2005; Reverchon 1999).

There are several techniques for producing the encapsulation of an active substance depending on the use of the supercritical fluid as solvent (RESS) or antisolvent (GAS, ASES

and SEDS). Given the fact that these techniques are far from those regarding the topic of this work no more information about them will be included.

2.2. State of the art in Bioencapsulation

As introduced in *Chapter 1: Introduction, Motivation and Objectives*, the biomedical area is one of the most selective and demanding among the various applications of the microcapsules.

The technique developed in this work aims to be applied in this area. Therefore the selection of the method must take into account the aforementioned requirements, mainly in terms of toxicity and formation kinetics.

The use of non-toxic materials and a fast, non-damaging transition from solution state to solid is a must-do particularly for cell encapsulation. Moreover the avoidance of heat, mechanical pressure or osmotic pressure in order to preserve the state of dispersion of the cells should be achieved (Cellesi and Tirelli 2005).

Therefore, among the chemical methods, gelation processes have been traditionally preferred. Other chemical techniques have been discarded due to its toxicity and slow kinetics, with some exceptions (Hill et al. 1997; Cruise et al. 1998).

Polymeric gelling substances have been commonly used to encapsulate cells during decades. They are easy to process and biocompatible most of them. Calcium or barium alginates have been common materials for biomedical applications when gelation processes are used.

Several works have been dedicated to the aim of developing reproducible and scalable processes using these polymers. Extrusion methods (Rousseau et al. 2004; Lim et al. 2013), spray drying (Coppi et al. 2002) or emulsion techniques (Fundueanu et al. 1998) are some examples.

Due to the active ingredients to be encapsulated most of the physico-chemical methods are discarded for their harsh conditions. However, mechanical processes have mildest conditions. Among these methods some of them have been assessed:

- Spinning disk: produces droplets with a range of sizes between 300 to 600 micrometres. Its main drawbacks include the deformation of the droplets and heterodispersion problems due to satellite drops (Senuma et al. 2000; Leick et al. 2010).

- Vibrating nozzles: this technique also produces microcapsules with diameters from 300 to 600 micrometres. The highest limitation of the commercial devices using this technology is the viscosity of the solutions to be treated. It is not possible to process jets with viscosities greater than 200 mPa·s (Serp et al. 2000).

- Extrusion with coaxial airflow (air-jet): produces capsules within the range of 400-800 micrometres. It allows the use of polymers with high viscosities and has few disadvantages. The appearance of small air bubbles inside the capsules, which affects the diffusion processes is of main relevance (Hwang et al. 2008).

- JetCutter technology: produces capsules within the range of 300 to 800 microns with good dispersion. It handles high viscosities. As a disadvantage we can mention the cutting losses occurring as a result of the cutting wire (Schwinger et al. 2004; Prüsse et al. 1998).

- Electrostatic atomization: generates sizes in the range of 300 to 800 microns. It prevents droplet coalescence due to the electric charge of the same polarity and it partially achieves treatment of medium viscous fluids. However, it needs to apply high voltages, up to 5 kV (Sasaki et al. 2008; Watanabe et al. 2003).

In general, all these techniques work well for low or non-viscous liquids. For medium-high viscous liquids, vibrating and air-jet nozzle commercial techniques do not work satisfactorily (Schwinger et al. 2004). Some techniques may operate under this condition with certain drawbacks (Koch et al. 2003).

2.3. Encapsulating materials

The variety of compounds used in microencapsulation is increasing gradually due to the discovery and synthesis of new biomaterials. Superficial and internal characteristics of the required particles, biocompatibility, dosage and wanted diffusion rates must be considered to choose the proper compounds.

As a first approach materials can be classified in two basic categories: natural and synthetic. The former are abundant and generally biodegradable, biocompatible and non-toxic or carcinogenic. The latter are mainly synthetic polymers, being some of them non-biodegradable.

Natural materials are classified in fats, proteins and polymers and their main disadvantage is the difficulty in developing reproducible methods to purify and modify them.

Polymers are the most common used in microencapsulation, mainly of polysaccharide nature. Alginate, dextran, xanthan gum, chitosan and gelatin stand out for their common use (Rathore et al. 2013).

Acrylic and cellulosic derivatives are within the synthetic polymers. They are used in biomedical applications, but they need to be removed after the release of the active ingredient, usually by surgery. Other synthetic polymers are biodegradable and do not require surgery for removal. Among these latter are polyesters, polyorthoesters and polyanhydrides (Kim and Mooney 1998).

Numerous materials, both natural and synthetic, have been proposed for cell encapsulation including poly(glycolic acid) (PGA), poly(lactic-co-glycolic acid) (PLGA), agarose, polyacrylates, κ-carrageenan, alginate, etc. (Chandra and Rustgi 1998). Also combinations of materials to form multicomponent and multilayer capsules have been studied (Tun et al. 1996).

Figure 2.8 and Table 2.1 provides information about how to select the best material for certain given conditions for drug delivery systems.

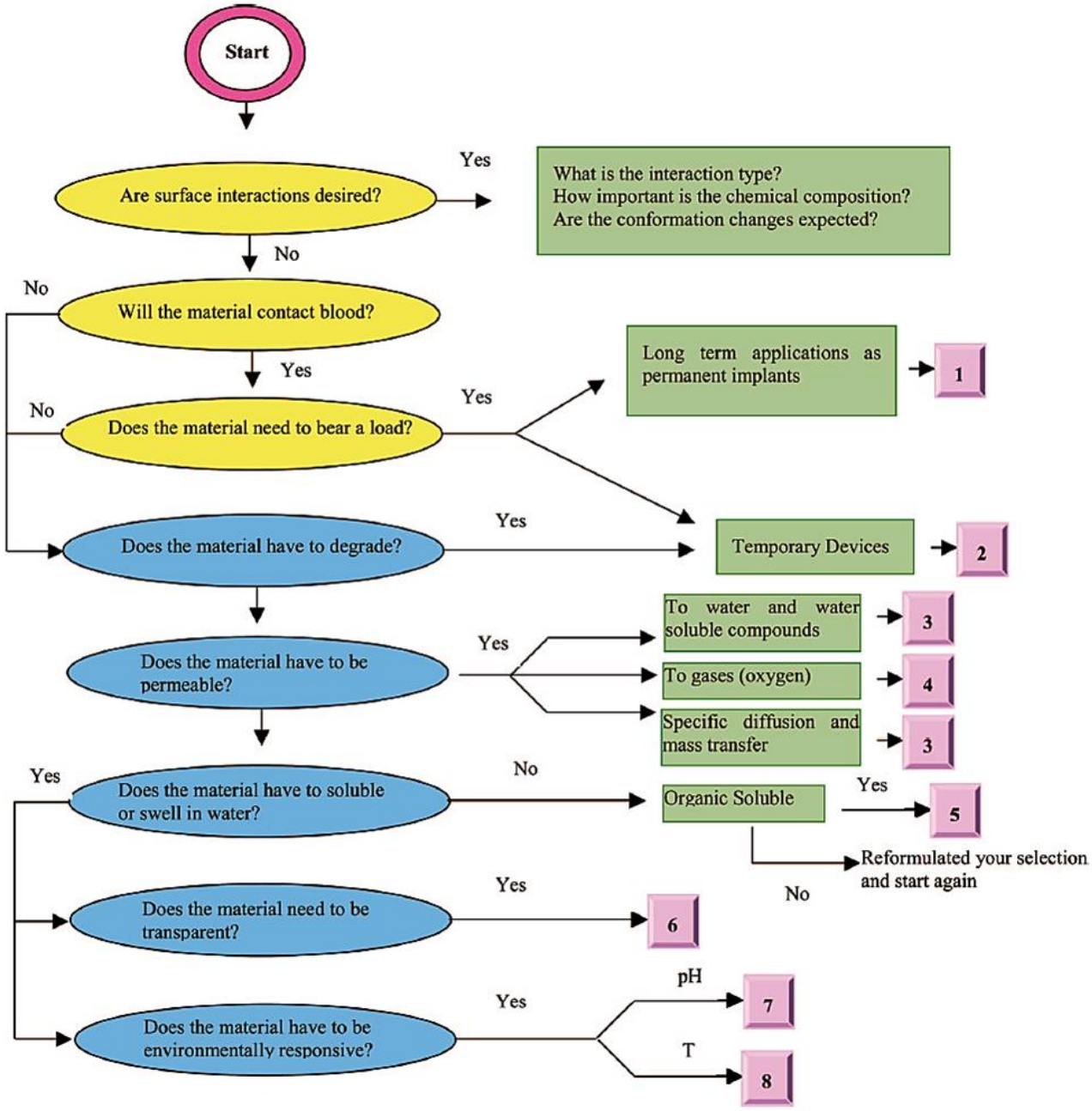

Figure 2.8: Guidelines for the selection of materials (Martín del Valle et al. 2009).

Table 2.1: Classification of polymers for drug delivery systems. Numbers in parenthesis match with numbers in Figure 2.8 (Martín del Valle et al. 2009).

Natural Polymers	
protein-based polymers (2)	polysaccharides (2)
collagen, albumin, gelatin	agarose, alginate (3), carrageenan (8), hyaluronic acid, chitosan (3, 7)
Synthetic Polymers	
biodegradable	nonbiodegradable
polyesters (2)	cellulose derivatives (7)
poly (lactic acid), poly (glycolic acid), poly(hydroxy butyrate), poly(ε-caprolactone), poly(β-malic acid), poly(dioxanones)	carboxymethyl cellulose, ethyl cellulose, cellulose acetate, cellulose acetate propionate, hydroxypropyl met hyl cellulose
polyamides (2)	silicones (6)
poly(imino carbonates), polyamino acids	colloidal silica, polysiloxanes
phosphorus-based polymers	acrylic polymers (5, 6)
polyphosphates, polyphosphonates, polyphosphazenes	polymethacrylates, poly(methyl methacrylate), poly hydro(ethylmethacrylate)
others (1)	others (8)
poly(cyano acrylates), polyurethanes, polyortho esters, polydihydropyrans, polyacetals	polyvinyl pyrrolidone, ethyl vinyl acetate, poloxamers, poloxamines

Hydrogels, of natural or synthetic polymers, are widely used. Their high water content, three-dimensional matrix structure and hydrophilic nature make them appropriate to interact with other fluids and tissues.

Of all hydrogels, alginate has been by far one of the most important coating materials (Zimmermann et al. 2007). Alginates present the following advantages:

- A relatively inert aqueous environment within the matrix.
- An encapsulation process which occurs at room temperature and does not require toxic organic solvents.
- Rapid formation of hydrogels under very mild (physiological) conditions.
- High degree of porosity that allows the diffusion of macromolecules.
- Biodegradation of the system under normal physiological conditions.
- Heat stability.

Alginates - salts of alginic acid - are linear water-soluble polysaccharides obtained from brown algae. It is a component of the cell wall of these organisms.

Alginates are heteropolymers, comprised of two monomer units: β-D manuronic acid (M) and α-L-guluronic acid (G). These are grouped into blocks of sequences MM, MG, linked glycosidically β (1-4), and blocks GG, GM, linked glycosidically α (1-4) (Zimmermann et al. 2007).

As Figure 2.9 shows, M-block regions correspond to linear chains, while G-blocks have a loop-shaped structure. The percentages of the blocks G and M vary depending on the source of algae and determine the characteristics of the gels obtained.

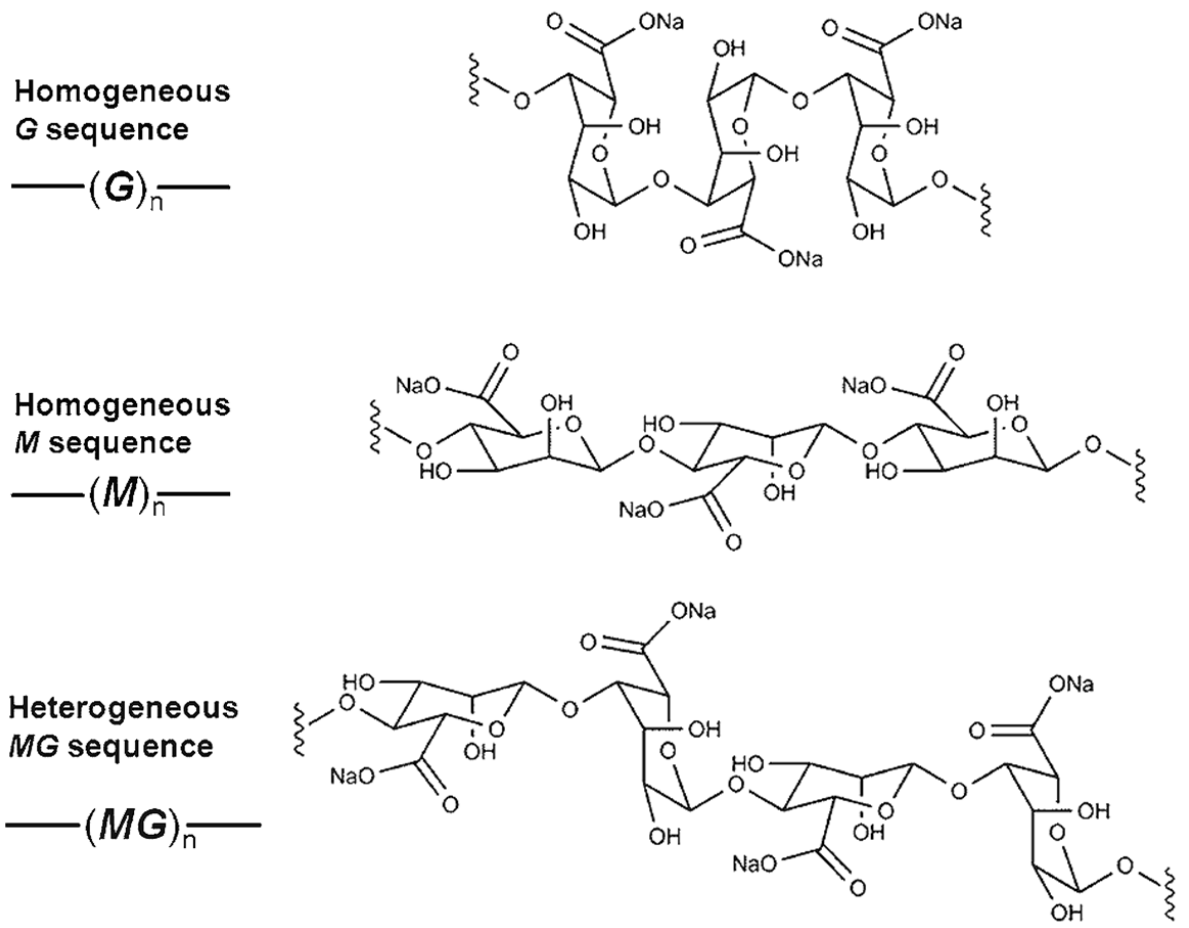

Figure 2.9: Sodium alginate sequences. (Fu et al. 2010).

Alginic acid forms water-soluble salts with monovalent cations. The commercial water soluble alginate is in sodium salt form, where the Na+ is ionically bonded to G blocks of alginate. One of the most important properties of the alginate is its ability to gel by ionic gelation reaction with polyvalent cations, becoming water-insoluble. During the gelation process, polyvalent cations replace Na^+ ions associated with carboxyl groups on G blocks.

M-blocks increase flat areas that do not react with the polyvalent cations, but when G-blocks align they leave a diamond-shaped hole that can accommodate therein the polyvalent cation, forming a dimeric structure. Consequently one alginate chain dimerizes with other chains forming a complex gel network. This model – known as "egg box" model - was proposed by Grant in 1973 to explain the gelling properties of alginates by reacting with calcium salts (Grant et al. 1973) and it is shown in Figure 2.10.

Alginates have shown affinity for polyvalent cations such as Cu^{2+}, Al^{3+} and Fe^{3+} but the most used are alkaline earth metals, whose affinity holds $Mg^{2+} << Ca^{2+} < Sr^{2+} < Ba^{2+}$ (Haug and Smidsrød 1970). Form all of these, polyvalent cations of calcium are widely used (Ishikawa et al. 1999; Shiraishi et al. 1993) but it has been extensively suggested the use of barium cations.

Apart from showing a higher affinity, barium ions give better long-term mechanical integrity, combined with calcium ions or alone (Mørch et al. 2006; Tanaka and Irie 1988). Hence, Ca^{2+} and Ba^{2+} are the most common used gelling cations.

Due to toxicity problems concerning to the Ba^{2+}, several studies have shown that the use of low amounts of barium produces very limited leakage of Ba^{2+} ions from the capsules (Thu et al. 1996). Thus, careful control of the bead manufacturing process and subsequent removal of excessive Ba^{2+} after gelation are important to maintain high cell viability (Zimmermann et al. 2008).

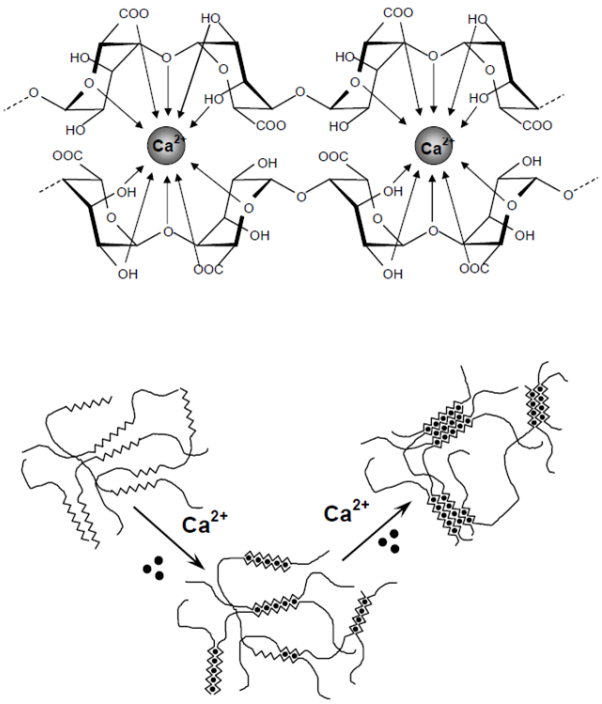

Figure 2.10: Ionic gelation process: binding of divalent cations to alginate. (a) Egg-box model. (b) Lateral association of chains (Mørch 2008)

2.4. References

Benita S (ed) (2006) Microencapsulation: Methods and Industrial Applications, Second Edition. Taylor & Francis Group.

Bungenberg de Jong HG, Kruyt HR (1930) Koazervation (Entmischung in Kolloidalen Systemen). Koll Zeitsch 50:39-48

Cellesi F, Tirelli N (2005) A new process for cell microencapsulation and other biomaterial applications: Thermal gelation and chemical cross-linking in "tandem". J Mater Sci: Mater Med 16 (6):559-565. doi:10.1007/s10856-005-0532-1

Coppi G, Iannuccelli V, Bernabei MT, Cameroni R (2002) Alginate microparticles for enzyme peroral administration. International Journal of Pharmaceutics 242 (1–2):263-266. doi:http://dx.doi.org/10.1016/S0378-5173(02)00171-0

Cruise GM, Hegre OD, Scharp DS, Hubbell JA (1998) A sensitivity study of the key parameters in the interfacial photopolymerization of poly(ethylene glycol) diacrylate upon porcine islets. Biotechnology and Bioengineering 57 (6):655-665.

Chan LW, Lee HY, Heng PWS (2002) Production of alginate microspheres by internal gelation using an emulsification method. International Journal of Pharmaceutics 242 (1–2):259-262. doi:http://dx.doi.org/10.1016/S0378-5173(02)00170-9

Chandra R, Rustgi R (1998) Biodegradable polymers. Progress in Polymer Science (Oxford) 23 (7):1273-1335

Dewettinck K, Huyghebaert A (1999) Fluidized bed coating in food technology. Trends in Food Science & Technology 10 (4–5):163-168. doi:http://dx.doi.org/10.1016/S0924-2244(99)00041-2

Dong Z, Ma Y, Hayat K, Jia C, Xia S, Zhang X (2011) Morphology and release profile of microcapsules encapsulating peppermint oil by complex coacervation. Journal of Food Engineering 104 (3):455-460. doi:http://dx.doi.org/10.1016/j.jfoodeng.2011.01.011

Dubey R, Shami TC, Rao KUB (2009) Microencapsulation Technology and Applications. Defence Science Journal 59 (1):82-95

Edelman R, Russell RG, Losonsky G, Tall BD, Tacket CO, Levine MM, Lewis DH (1993) Immunization of rabbits with enterotoxigenic E. coli colonization factor antigen

(CFA/I) encapsulated in biodegradable microspheres of poly (lactide-co-glycolide). Vaccine 11 (2):155-158. doi:http://dx.doi.org/10.1016/0264-410X(93)90012-M

Fu S, Thacker A, Sperger D, Boni R, Velankar S, Munson E, Block L (2010) Rheological Evaluation of Inter-grade and Inter-batch Variability of Sodium Alginate. AAPS PharmSciTech 11 (4):1662-1674. doi:10.1208/s12249-010-9547-0

Fundueanu G, Esposito E, Mihai D, Carpov A, Desbrieres J, Rinaudo M, Nastruzzi C (1998) Preparation and characterization of Ca-alginate microspheres by a new emulsification method. International Journal of Pharmaceutics 170 (1):11-21. doi:http://dx.doi.org/10.1016/S0378-5173(98)00063-5

Gharsallaoui A, Roudaut G, Chambin O, Voilley A, Saurel R (2007) Applications of spray-drying in microencapsulation of food ingredients: An overview. Food Research International 40 (9):1107-1121. doi:http://dx.doi.org/10.1016/j.foodres.2007.07.004

Gouin S (2004) Microencapsulation: industrial appraisal of existing technologies and trends Trends in Food Science & Technology 15 (7-8):330-347

GRACO I (1995) Atomization: Concept and Theory Training.

Grant GT, Morris ER, Rees DA, Smith PJC, Thom D (1973) Biological interactions between polysaccharides and divalent cations: The egg-box model. FEBS Letters 32 (1):195-198. doi:http://dx.doi.org/10.1016/0014-5793(73)80770-7

Haug A, Smidsrød O (1970) Selectivity of some anionic polymers for divalent metal ions. Acta Chemica Scandinavica 24:843-854

Hill RS, Cruise GM, Hager SR, Lamberti FV, Yu X, Garufis CL, Yu YAO, Mundwiler KE, Cole JF, Hubbell JA, Hegre OD, Scharp DW (1997) Immunoisolation of Adult Porcine Islets for the Treatment of Diabetes Mellitus. Annals of the New York Academy of Sciences 831 (1):332-343. doi:10.1111/j.1749-6632.1997.tb52208.x

Hwang YK, Jeong U, Cho EC (2008) Production of Uniform-Sized Polymer Core–Shell Microcapsules by Coaxial Electrospraying. Langmuir 24 (6):2446-2451. doi:10.1021/la703546f

Ilić I, Dreu R, Burjak M, Homar M, Kerč J, Srčič S (2009) Microparticle size control and glimepiride microencapsulation using spray congealing technology. International

Journal of Pharmaceutics 381 (2):176-183. doi:http://dx.doi.org/10.1016/j.ijpharm.2009.05.011

Ishikawa K, Ueyama Y, Mano T, Koyama T, Suzuki K, Matsumura T (1999) Self-setting barrier membrane for guided tissue regeneration method: Initial evaluation of alginate membrane made with sodium alginate and calcium chloride aqueous solutions. Journal of Biomedical Materials Research 47 (2):111-115.

Jain RA (2000) The manufacturing techniques of various drug loaded biodegradable poly(lactide-co-glycolide) (PLGA) devices. Biomaterials 21 (23):2475-2490. doi:http://dx.doi.org/10.1016/S0142-9612(00)00115-0

Kim B-S, Mooney DJ (1998) Development of biocompatible synthetic extracellular matrices for tissue engineering. Trends in Biotechnology 16 (5):224-230. doi:http://dx.doi.org/10.1016/S0167-7799(98)01191-3

Koch S, Schwinger C, Kressler J, Heinzen C, Rainov NG (2003) Alginate encapsulation of genetically engineered mammalian cells: Comparison of production devices, methods and microcapsule characteristics. Journal of Microencapsulation: Micro and Nano Carriers 20 (3):303 - 316

Leick S, Henning S, Degen P, Suter D, Rehage H (2010) Deformation of liquid-filled calcium alginate capsules in a spinning drop apparatus. Physical Chemistry Chemical Physics 12 (12):2950-2958. doi:10.1039/b921116k

Lewis DH (1990) Controlled release of bioactive agents from lactide/glycolide polymers. Drugs Pharma Sci 45:1-41

Lim G-P, Ong H-Y, Lee B-B, Ahmad MS, Singh H, Ravindra P (2013) Formation Of Chitosan-Alginate Capsules Using Extrusion-Dripping Method: Effect Of Stirring Speed And Biopolymers Types. Australian Journal of Basic and Applied Science 7 (5):84-90

Martín del Valle EM, Galán MA, Carbonell RG (2009) Drug Delivery Technologies: The Way Forward in the New Decade. Industrial & Engineering Chemistry Research 48 (5):2475-2486. doi:10.1021/ie800886m

Mørch ÝA (2008) Novel Alginate Microcapsules for Cell Therapy. Norwegian University of Science and Technology, Trondheim

Mørch ÝA, Donati I, Strand BL (2006) Effect of Ca2+, Ba2+, and Sr2+ on Alginate Microbeads. Biomacromolecules 7 (5):1471-1480. doi:10.1021/bm060010d

O'Donnell PB, McGinity JW (1997) Preparation of microspheres by the solvent evaporation technique. Advanced Drug Delivery Reviews 28 (1):25-42. doi:http://dx.doi.org/10.1016/S0169-409X(97)00049-5

Popplewell LM (2001) Evaluating encapsulation economics. Perfumer & Flavorist 26 (2):2-6

Prüsse U, Bruske F, Breford J, Vorlop KD (1998) Improvements to the jet cutting process for manufacturing spherical-particles from viscous polymer solutions. Chem Ing Tech 70:556-560

Rathore S, Desai PM, Liew CV, Chan LW, Heng PWS (2013) Microencapsulation of microbial cells. Journal of Food Engineering 116 (2):369-381. doi:http://dx.doi.org/10.1016/j.jfoodeng.2012.12.022

Reverchon E (1999) Supercritical antisolvent precipitation of micro- and nano-particles. The Journal of Supercritical Fluids 15 (1):1-21. doi:http://dx.doi.org/10.1016/S0896-8446(98)00129-6

Rousseau I, Le Cerf D, Picton L, Argillier JF, Muller G (2004) Entrapment and release of sodium polystyrene sulfonate (SPS) from calcium alginate gel beads. European Polymer Journal 40 (12):2709-2715. doi:http://dx.doi.org/10.1016/j.eurpolymj.2004.07.022

Saihi D, Vroman I, Giraud S, Bourbigot S (2006) Microencapsulation of ammonium phosphate with a polyurethane shell. Part II. Interfacial polymerization technique. Reactive and Functional Polymers 66 (10):1118-1125. doi:http://dx.doi.org/10.1016/j.reactfunctpolym.2006.02.001

Sant'Anna V, Malheiros PdS, Brandelli A (2011) Liposome encapsulation protects bacteriocin-like substance P34 against inhibition by Maillard reaction products. Food Research International 44 (1):326-330. doi:http://dx.doi.org/10.1016/j.foodres.2010.10.012

Sasaki E, Kurayama F, Ida J-i, Matsuyama T, Yamamoto H (2008) Preparation of microcapsules by electrostatic atomization. Journal of Electrostatics 66 (5–6):312-318. doi:http://dx.doi.org/10.1016/j.elstat.2008.02.001

Schwinger C, Klemenz A, Busse K, Kressler J (2004) Encapsulation of living cells with polymeric systems. Macromolecular Symposia 210 (1):493-499. doi:10.1002/masy.200450655

Senuma Y, Lowe C, Zweifel Y, Hilborn JG, Marison I (2000) Alginate hydrogel microspheres and microcapsules prepared by spinning disk atomization. Biotechnology and Bioengineering 67 (5):616-622.

Serp D, Cantana E, Heinzen C, Von Stockar U, Marison IW (2000) Characterization of an encapsulation device for the production of monodisperse alginate beads for cell immobilization. Biotechnology and Bioengineering 70 (1):41-53.

Shiraishi S, Imai T, Otagiri M (1993) Controlled-release preparation of indomethacin using calcium alginate gel. Biol Pharm Bull 16 (11):1164-1168

Tanaka H, Irie S (1988) Preparation of stable alginate gel beads in electrolyte solutions using Ba2+ and Sr2+. Biotechnol Tech 2 (2):115-120. doi:10.1007/bf01876161

Tanner FX, Feigl KA, Althaus TO, Windhab EJ (2008) Modeling and Simulation of an Air-Assist Atomizer for Food Sprays. Paper presented at the ILASS Americas, 21 st Annual Conference on Liquid Atomization and Spray Systems, Orlando FL.

Thu B, Bruheim P, Espevik T, Smidsrød O, Soon-Shiong P, Skjåk-Bræk G (1996) Alginate polycation microcapsules: II. Some functional properties. Biomaterials 17 (11):1069-1079. doi:http://dx.doi.org/10.1016/0142-9612(96)85907-2

Tun T, Inoue K, Hayashi H, Aung T, Gu YJ, Doi R, Kaji H, Echigo Y, Wang WJ, Setoyama H, Imamura M, Maetani S, Morikawa N, Iwata H, Ikada Y (1996) A newly developed three-layer agarose microcapsule for a promising biohybrid artificial pancreas: Rat to mouse xenotransplantation. Cell Transplantation 5 (5, Supplement 1):S59-S63. doi:http://dx.doi.org/10.1016/0963-6897(96)00042-5

Umer H, Nigam H, Tamboli AM, Nainar MSM (2011) Microencapsulation: Process, Techniques and Applications. International Journal of Research in Pharmaceutical and Biomedical Sciences 2:474-481

Watanabe H, Matsuyama T, Yamamoto H (2003) Experimental study on electrostatic atomization of highly viscous liquids. Journal of Electrostatics 57 (2):183-197. doi: 10.1016/s0304-3886(02)00139-0

Yeo S-D, Kiran E (2005) Formation of polymer particles with supercritical fluids: A review. The Journal of Supercritical Fluids 34 (3):287-308. doi:http://dx.doi.org/10.1016/j.supflu.2004.10.006

Zimmermann H, Ehrhart F, Zimmermann D, Müller K, Katsen-Globa A, Behringer M, Feilen PJ, Gessner P, Zimmermann G, Shirley SG, Weber MM, Metze J, Zimmermann U (2007) Hydrogel-based encapsulation of biological, functional tissue: fundamentals, technologies and applications. Appl Phys A 89 (4):909-922. doi:10.1007/s00339-007-4270-8

Zimmermann U, Cramer H, Jork A, Thürmer F, Zimmermann H, Fuhr G, Hasse C, Rothmund M (2008) Microencapsulation-Based Cell Therapy. In: Biotechnology. Wiley-VCH Verlag GmbH, pp 547-571. doi:10.1002/9783527620937.ch19

CHAPTER 3.

MATERIALS AND METHODS.

3. Materials and Methods

This chapter gathers information about the different chemicals, devices and software used for the completion of this thesis. Basic explanations of some of the tools considered most important are given in order to facilitate the reading of following chapters.

3.1. Chemicals

- Synthetic air ALPHAGAZ AIRE. Air Liquide España.
- Sodium Alginate (Macrocystis Pyrifera) medium viscosity. Sigma Aldrich.
- Dehydrate Barium Chloride. Reactive grade. Scharlau.
- bFGF (Fibroblastic growth factor). Sigma Aldrich.
- VEGF (Vascular endothelial growth factor). Sigma Aldrich.
- PBS (Phosphate buffer solution). Sigma Aldrich.
- TrisBuffer. Sigma Aldrich.

3.2. Devices and Components

- Particle Size Analyzer by laser diffraction. Mastersizer2000. Malvern.
- Optical microscopy DM1000. Leica with Leica DFC280 camera.
- Rotational viscometer VISCO ELITE. Fungilab S. A.
- Rotational Rheometer AR 1500ex TA Instruments.
- Capillary Breakup Extensional Rheometer CaBER (Thermo Fisher Scientific, Karlsruhe, Germany).
- Cannon-Fenske Opaque (Reverse-Flow) Viscometer.
- High Speed camera Phantom v12.1.
- Analytical balance 2442 Satorius-Werke, Explorer Ohaus.
- Grain scale JADEVER, AW-5500.
- Magnetic stirrer VELP Scientifica, Are2, with stirring controller.
- Stirrer Janke&Junkel GMBH & Co, IKA Labortechnik.
- Ultrasounds bath BRANSON 1510.

- Vacuum pump Leroy Somer DX2 8614.
- 20 µm nylon membrane filters. Scharlau.
- Glass material. Scharlau.

3.3. Specific Software

- Particle Size Analyser by laser diffraction. Mastersizer2000. Malvern.
- Optical microscopy DM1000. Leica with Leica DFC280 camera.
- Rotational Rheometer AR 1500ex TA Instruments.
- High Speed camera Phantom v12.1.
- Capillary Breakup Extensional Rheometer CaBER.
- Wolfram Mathematica (Wolfram Research).
- Ansys Workbench and Fluent package.

3.4. Particle Size Analysis

The microparticle size was measured with a particle analyser by laser diffraction. The method is based on the phenomenon of light scattering. When a particle is lightened by a monochromatic source a pattern comprising concentric rings is obtained from the scattered light. This is known as *diffraction pattern* though other scattering phenomena apart from diffraction might take place (such as refraction or reflection). This pattern, that is a function of the type and size of the particles, is then collected by a matrix of photodetectors. The size distribution is computed applying the "*Mie theory"* of light scattering, or a simplified approach through the Fraunhofer's approximation (Webb 2000).

The *Mie theory* assumes a volume-equivalent sphere model that requires knowledge of the optical properties (refractive index and imaginary component) of both the measured sample and the dispersant solution. The *Fraunhofer approximation* does not require knowledge of the optical properties of the sample.

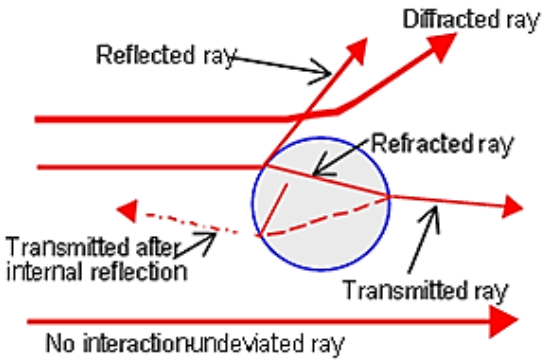

Figure 3.1: Light scattering phenomenon: interaction particle – light (Webb 2000).

This technique offers short measurement times, good reproducibility and precision, simple calibration, and high versatility. Figure 3.2 shows a generic distribution of barium-alginate microcapsules dispersed in water. The index of refraction for barium-alginate used in the calculation was 1.520 and the absorption index was 0.1.

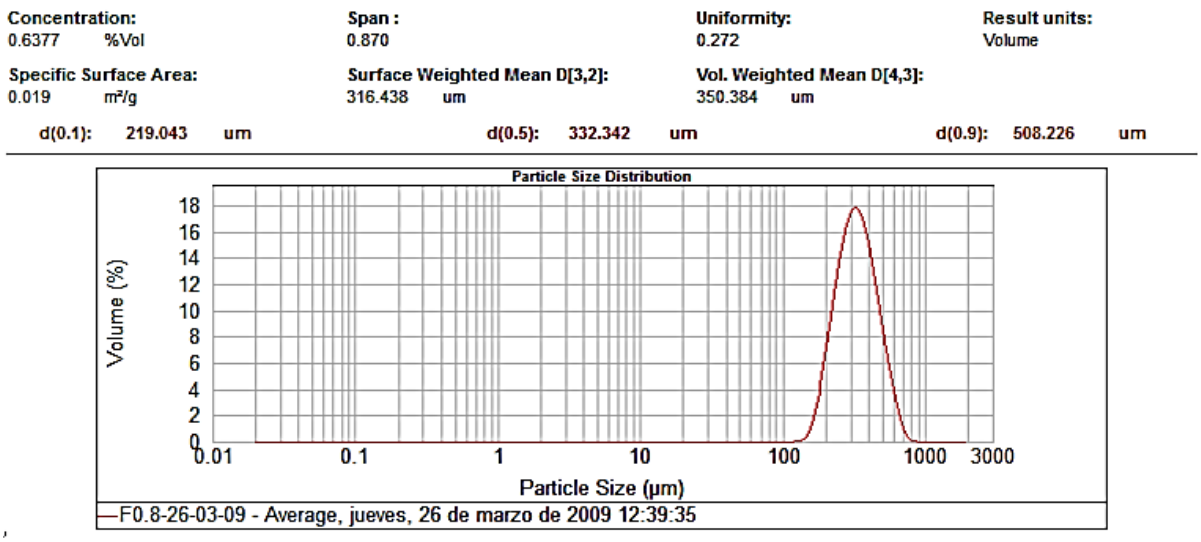

Figure 3.2: Size distribution.

Among the information given by the software the data for microparticle size in this work is referred as Sauter Mean Diameter *(SMD)*. This is a surface weighted measurement, not number-based. It uses the Moment Means concept that indicate around which central

point of the frequency the surface area distribution would rotate and it is calculated as follows:

$$SMD = D[3,2] = \frac{\int_0^\infty D^3 dN}{\int_0^\infty D^2 dN} \qquad (3.1)$$

where, *D* is the droplet diameter, and *dN* the percentage of the total number of droplets with a diameter contained in the interval *(D, D+dD)*.

As for the particle size distributions, the software computes also the span factor of the measured sample, defined as:

$$span\ factor = \frac{D_{0.9} - D_{0.1}}{D_{0.5}} \qquad (3.2)$$

where $D_{0.9}$ is the diameter at the 90th percentile, $D_{0.1}$ the diameter at the 10th percentile and $D_{0.5}$ the diameter at the 50th percentile.

3.5. Image Characterization

Optical microscopy was used to characterize the morphology of the microcapsules. The images were captured with a coupled digital camera as shown in Figure 3.3 and analysed by the processing software. Figure 3.4 shows an image captured by the microscope.

Figure 3.3: Microscope and coupled camera

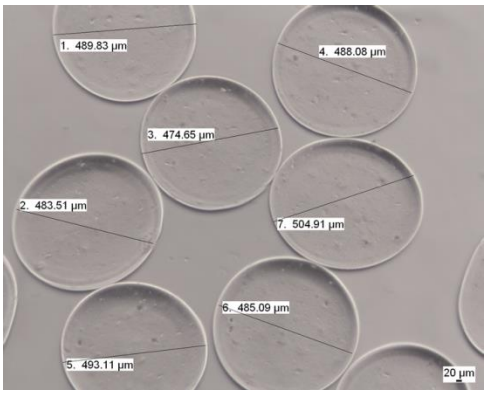

Figure 3.4: Photography of the microparticles with diameter measurements.

3.6. Determination of Viscosity

The rheological characterization of the encapsulating polymeric solution has been carried out with the help of several different devices. For the first set of experiments a unique viscosity value for every sample was determined with a rotational viscometer. After the first analysis the study of the rheology of the polymer was carried under simple shear (capillary and stress-controlled rheometer) and uniaxial extensional flow field (capillary breakup extensional rheometer).

3.6.1. Apparent viscosity in shear flow – rotational viscometer

The operating principle of a rotational viscometer relies on the torsional resistance that a fluid presents to the rotation of a spindle of known characteristics in the fluid in which is submerged. The rotating cylinder or spindle is coupled with a spring to a motor shaft that rotates at a certain speed. The angle of deviation of the shaft is measured electronically, which gives a measure of torque. The knowledge of surface area of the spindle and the rotating speed gives a direct reading of viscosity applying the general law of viscosity or Newton's law: $\eta = \frac{\tau}{\dot{\gamma}}$ where η is the viscosity, τ is the shear stress and $\dot{\gamma}$ the shear rate.

The torque is computed as the force acting on the outer surface of the spindle times the radius, which is the lever arm. Considering cylindrical spindles, the area can be computed as $\pi R^2 L$. Therefore, the following relationships can be obtained:

Shear rate (s^{-1}) $$\dot{\gamma} = \frac{2\omega R_c^2 R_b^2}{x^2\left(R_c^2 - R_b^2\right)} \quad (3.2)$$

Shear Stress (dynes/cm^2) $$\tau = \frac{M}{2\pi R_b^2 L} \quad (3.3)$$

Viscosity $$\eta = \frac{\tau}{\dot{\gamma}} \quad (3.4)$$

Where R_c is the radius of container, R_b is the radius of spindle, x is the radius at which shear rate is being measured and M is the torque measured by the instrument.

Viscometers have various types of spindles and a wide range of speeds, providing a large measure capacity. Figure 3.5 displays the device and spindles used in this work.

Figure 3.5: Rotational viscometers and set of spindles.

3.6.2. Intrinsic viscosity

There are several devices that allow measuring intrinsic viscosity values. They are based on the findings of Hagen and Poiseuille. Provided that the flow is laminar and the

fluid is Newtonian they found that the pressure drop, *Δp*, to flow in a capillary (radius *R*, length *L*) at a certain flow rate *Q* depends on the shear viscosity. The law holds as follows:

$$\eta = \frac{\Delta p}{L}\frac{\pi R^4}{8Q} \qquad (3.5)$$

where η stands for viscosity.

Through certain corrections the law also applies to non-Newtonian fluids. In this case no correction needs to be applied since the solution behaves as Newtonian for low shear rates as those reached in the viscometer.

The intrinsic viscosity was determined in this particular work by using a Cannon-Fenske (reverse-flow) viscometer with a capillary diameter of 300 µm at 40 ºC. These reverse-flow type viscometers are used for measurements of kinematic viscosity of dark Newtonian liquids according to ASTM D 445 and ISO 3104.

It consists of measuring the time that certain amount of liquid takes to flow through a capillary tube. The kinematic viscosity is obtained by multiplying the efflux time in seconds by a certain constant of the viscometer. The measurements must be done at the temperatures for which the viscometer is calibrated. The dynamic viscosity can be calculated by multiplying the kinematic viscosity by the density of the fluid.

3.6.3. Rotational rheometry - AR 1500 EX

The rotational rheometry is an analytical technique with two main approaches: controlled rate or controlled stress measurement. In both cases the sample to be studied is placed between two plates. In the second type one of the plates rotates at a fixed speed and the torsional force produced at the other plate is measured, being the strain rate the independent variable and stress the dependent variable. Inversely, in the latter approach, a torque (stress) is applied to one plate and the rotational speed (strain rate) of the same plate is measured.

The AR-1500 EX (TA Instruments, New Castle DE, USA) is a controlled stress rheometer (Figure 3.6). A Peltier plate and a solvent trap are used to control the temperature and

avoid evaporation, respectively. Most measurements were done by means of a 60 mm in diameter acrylic parallel-plate geometry with gap width between 300 to 900 µm. Data acquisition and analysis were achieved through the corporative software TA Rheology Advantage (Instrument Control AR and Data Analysis modules versions 5.7.2 and 5.7.0).

Figure 3.6: AR-1500 EX controlled stress rheometer.

3.6.4. Extensional rheometry

The Capillary Breakup Extensional Rheometer (Figure 3.7), known as CaBER (Thermo Fisher Scientific, Karlsruhe, Germany) measures the flow response of a fluid to a uniaxial extensional deformation. It studies the thinning and eventual break-up process of a fluid filament after a sudden stretch.

Figure 3.7: Capillary Breakup Extensional Rheometer.

This technique can achieve a close approximation to a shear-free purely uniaxial extensional flow by performing capillary thinning experiments. The apparatus stretches a sample of fluid contained between two plates, the lower of them fixed. The evolution of the thread after the stretching is measured at the midpoint by a laser. The mid-filament profile data, namely the radius of filament $R_{mid}(t)$, are then analysed to obtain the viscoelastic material functions under uniaxial extension.

3.7. Surface tension

The measurements to determine the surface tension of the solutions were made using a commercial tensiometer (KSV, Sigma 700, see Figure 3.8) courtesy of Iberlaser S.A. This device performs measurements through the Du Nouy ring and the Wilhelmy plate methods.

The most appropriate procedure to measure the solutions in this study was the Du Nouy ring at a speed of 1mm/min and a stabilization period of 4 hours. This method is based on measuring the force required to separate a metal ring suspended from a torsion precision balance from the surface of the liquid to be studied.

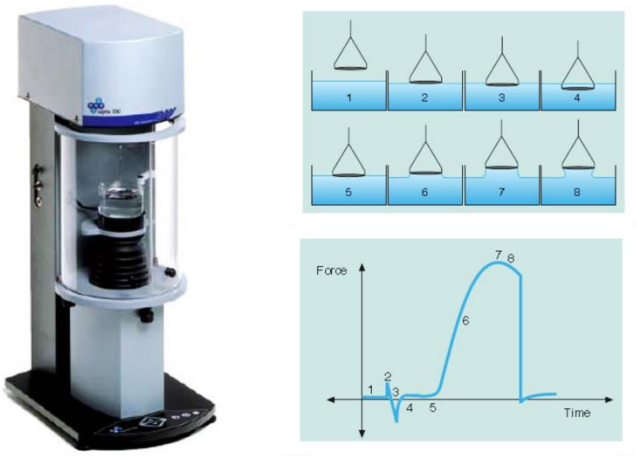

Figure 3.8: KSV Sigma 700 tensiometer and measurement procedure.

The force *F* is related to the surface tension of the liquid by the expression: $\sigma = \frac{F}{4\pi r}$ where *r* is the radius of the ring and the factor 4 refers to twice the length of the circumference, since the force acts on both sides of the ring (it has a certain thickness).

3.8. High speed camera

A CCD-based digital video camera, along with its software, was used to capture the snapshots that depict some of the experiments. The camera, PHANTOM v12.1 was able to record 6242 frames-per-second at full 1280 x 800 widescreen resolution, which was found to be enough for this research. Different lenses were used.

3.9. References

Webb PA (2000) A Primer on Particle Sizing by Static Laser Light Scattering. Technical Workshop Series: Introduction to the Latest ANSI/ISO Standard for Laser Particle Size Analysis.

CHAPTER 4.

PRELIMINARY STUDIES.

4. PRELIMINARY STUDIES

This chapter reviews the setup of the device used to produce the microparticles and also the blank runs and initial experiments are analysed, from which the behavioural curves are generated.

These curves, together with a basic review about the instabilities of jets, allow classifying the most important parameters affecting the process, such as the viscosity, flow rate, etc.

Finally semiempirical equations are computed from the wave mechanism theory and the study of adimensional numbers containing the main affecting parameters.

4.1. Description and development of the production method of microparticles

As detailed in Chapter 1 the main objective of this work comprises the development of a new technique that allows the production of monodisperse microcapsules with sizes around 300 to 600 micrometres for biomedical applications. This technique is explained next taking into account the requirements related to this field and the aimed range of sizes.

Concerning the method, the mechanical disintegration of a jet is selected among other processes for avoiding dangerous or harmful conditions to the load of the microparticles. Due to the sizes that are aimed air-assisted techniques are discarded. Thus, the instabilization of jets through a vibrating nozzle technique was considered as a feasible method.

The commercially available devices that uses this technique has a viscosity limitation (around 300 mPa·s for 150 micrometre nozzle). However, viscosities above 600 mPa·s are necessary to assure the desired high mechanical stability.

Therefore, the technique should be adapted to be suitable for processing high viscosity fluids and substantial modifications should be done.

The idea, then, is developing a process that comprises the steps that follow: (I) The active ingredient is dissolved in the encapsulating polymer to be passed through the

capillary nozzle and generate a jet, (II) the application of controlled mechanical disturbances onto the flow achieves the eventual break-up of the jet, (III) this leads to the formation of droplets, (IV) they are stabilized with a gelation process to finally obtain solid microparticles.

The physical process that develops in the jet under these conditions is known as *Rayleigh instability*. It becomes, consequently, one of the main subjects of this work and will be describe along it.

The critical point in the process lies in overcoming the high pressure drops in the capillary nozzle when medium-high viscosity (500 to 2500 mPa·s) solutions are used. Therefore, the adaptation of a high pressure system in order to push the fluid through the nozzle is suggested as the solution to overcome this problem.

4.1.1. Preliminary studies on the vibrating nozzle device

A set of experiments were conducted in order to find the upper limit of viscosity in the operation of the commercial device.

Always solutions of sodium alginate with concentrations higher than 0.8 g/dL (150 mPa·s) were used since lower values would result in quite low resistant microcapsules.

The conditions are summarized next:

- Nozzle diameter: 100 and 150 µm.
- Pushing system: peristaltic pump.
- Distance between nozzle and gelling bath: 20 cm.
- Volume of gelling solution: 100 mL.
- Gelling time: 10 minutes.
- Alginate flow rate: 5 mL/min
- Working temperature: 20 to 25 ºC.

It was possible reaching a concentration of 1.1 g/dL (260 mPa·s). However, higher viscosities involved serious difficulties, mainly leakages in connectors and blockage of flow through the nozzles. The blockages were mainly due to the impossibility to overcome the

pressure drop through the nozzle, although also sometimes clogging due to impurities was also experienced.

Table 4.1 summarizes the best found conditions for the maximum processed concentration and Figure 4.1 shows some of the obtained microcapsules. See *Appendix A: Preliminary Studies on the commercial device* to have more information about these results.

Table 4.1: Best conditions of break-up for a 260 mPa·s alginate solution and 100 micrometre nozzle.

Frequency	size	span
800	316	0.870
900	323	0.983
1100	315	1.035
1200	291	1.071

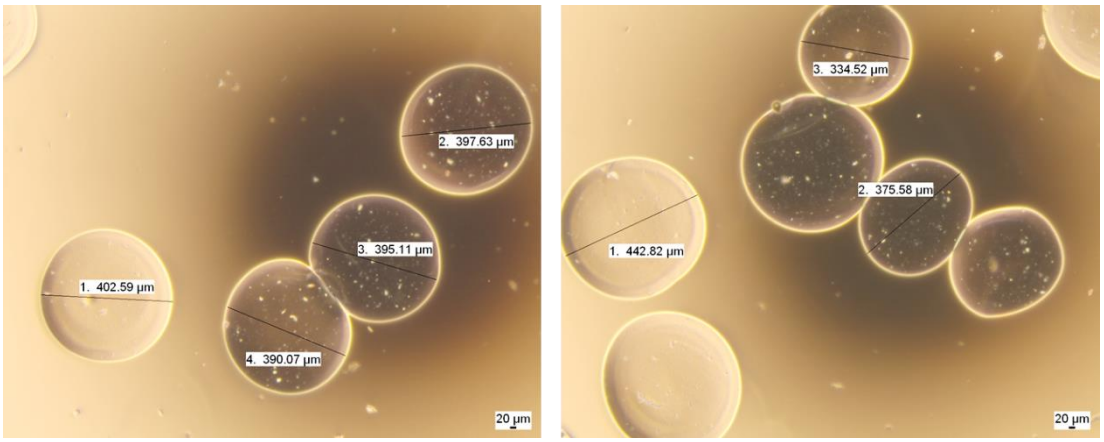

Figure 4.1: Microparticles obtained from a 260 mPa·s alginate solution applying 800 and 1100 Hz respectively.

Once the viscosity limitations have been assessed it is clear that a modification must be done.

4.2. Device description

As detailed previously, the developed technology involves a device optimized to produce microparticles from medium-high viscosity polymers combining a high-pressure system and a vibrating nozzle device.

Figure 4.2 shows a schematic diagram.

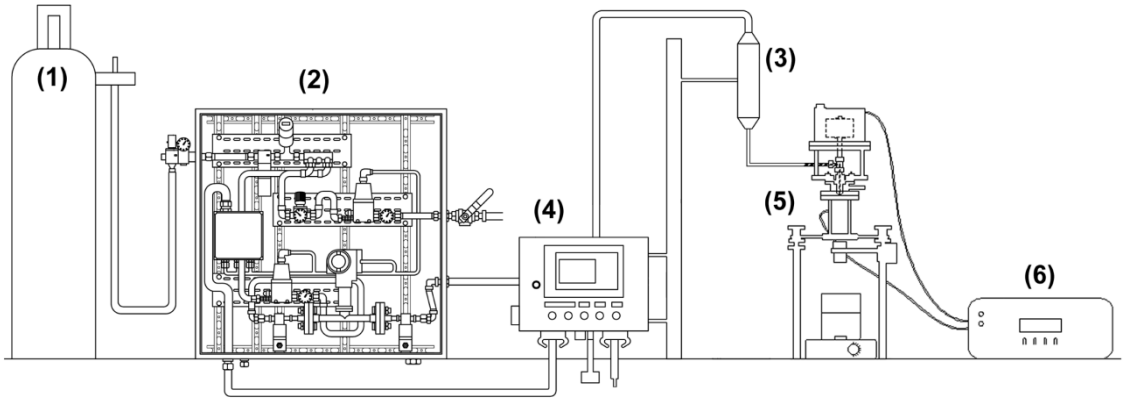

Figure 4.2: Complete system for producing microcapsules with a vibrating nozzle from high viscosity non-Newtonian fluids. Main components: (1) synthetic air bottle (2) Pneumatic cabinet. (3) Pressurized tank (4) Control board (5) Subsystem for the generation of controlled disturbances. (6) Frequency and amplitude controller.

The pneumatic cabinet (2), fed from the synthetic air cylinder (1), has the function of supplying and controlling the proper amount of air to pressurize the supply tank (3). This is the part of the installation that allows pushing high viscous solutions towards the nozzle, located in a the *vibrating nozzle subsystem* that will be detailed later. Both systems are connected through PVC tubes and steel quick connectors.

a) Pressure subsystem

It corresponds to the labelled components from (1) to (4) in Figure 4.2 and it is the centrepiece for establishing a controlled pressure in the pressurized reservoir (3). Thus, the polymer solution can flow under high pressure and overcome the pressure drop in the

nozzle. Figure 4.3 shows in detail the pneumatic cabinet. This has been designed to supply air through two different lines, one of them towards the tank and the other for air-assisted nozzles (atomization processes). In this work only the line that controls the air flow to pressurize the tank is used, blocking the other.

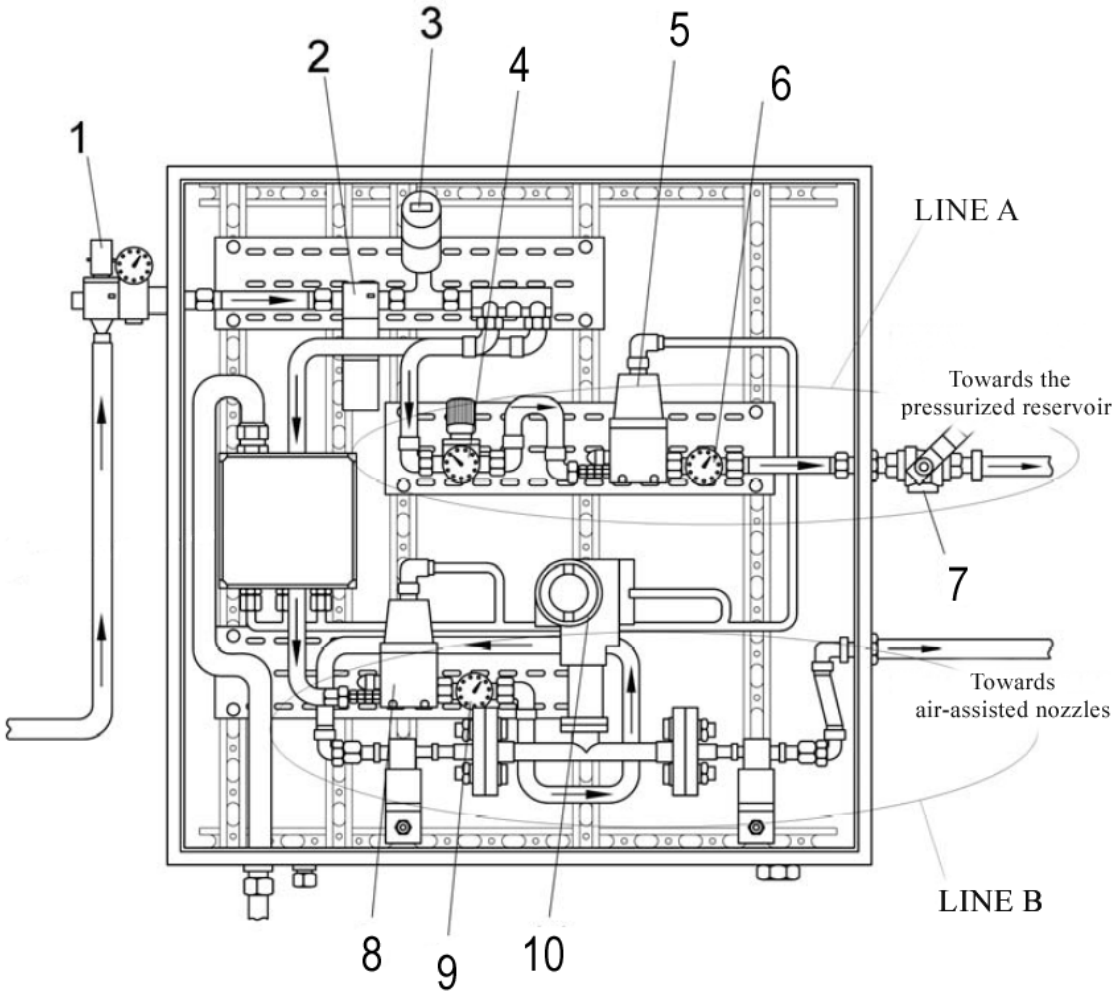

Figure 4.3: Pneumatic cabinet.

In Figure 4.3 a general valve (1) and gauge filter (2) direct the incoming air to. Next, a pressure switch (3) divides the air flow in two lines.

Line A includes a manual pressure regulator inlet (4), a proportional controller (5), a mechanical indicator (6) and a valve (7). The controller (5) is connected to the control panel and allows for accurate pressure control with feedback signal. The maximum pressure in

this line is 6 bar. Line B includes a pressure controller (8), a mechanical pressure gauge (9) and a mass flowmeter (10).

The pressure tank, (3) in Fig 4.2, collects the polymer – alginate in this case - subjected to high pressure. It is made of stainless steel and has a volume of 250 ml. The control panel (4) in Fig. 4.2 provides the software that control and monitor the process in real time.

b) Vibrating nozzle subsystem

The unit that triggers the jet disturbance by vibration corresponds to a commercial module supplied by that Swiss company *Nisco Engineering Inc*. The specific model used in this study is the VAR D Nisco that mounts a plain nozzle (Figure 4.6). Figure 4.4 displays the device. The frequency and amplitude is set digitally by a control module.

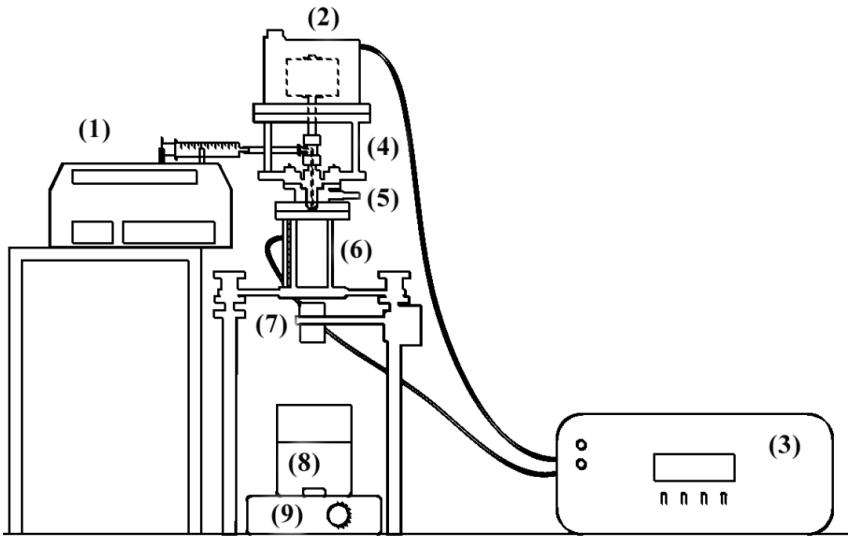

Figure 4.4: Schematic representation of the commercial encapsulator. (1) Peristaltic pump (2) Vibration unit (3) Control panel (4) T-piece (5) sapphire nozzle (6) Stroboscopic Light (7) Bypass system (8) Gelling solution (9) Magnetic stirrer.

Figure 4.5 shows an actual image of the commercial device as supplied by the manufacturer. It incorporates a peristaltic syringe pump that provides constant flow rate. The evolution of the jet after leaving the nozzle can be tracked with LED stroboscopic lights

that automatically synchronize with the selected vibration frequency. When the jet breaks a stationary string of small cylinders equally spaced can be observed with the lights.

Figure 4.5: Commercial encapsulator (Nisco Var D).

The nozzle has a sapphire tip with a hole drilled by laser, whose inner surface has been smoothed to avoid disturbances due to interior roughness (see Figure 4.6).

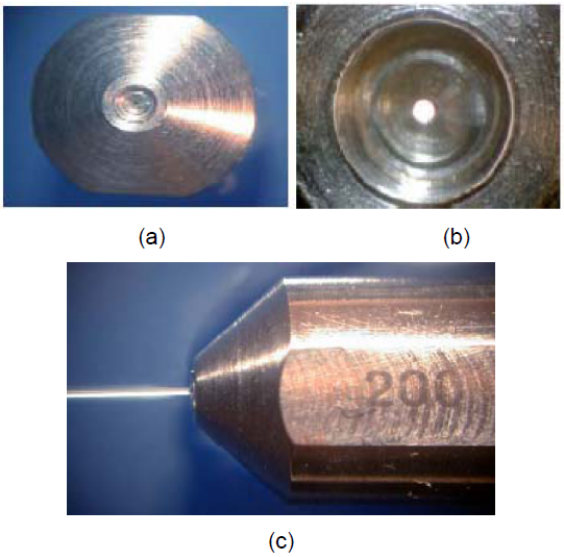

Figure 4.6: (a) Stainless steel fastening for the nozzle (b) Polished sapphire (c) Jet generation

The sapphire is mounted on a stainless steel structure. Nozzles with diameters from 50 to 600 microns can be adapted. Most of the experiments in this work were conducted using a nozzle diameter of 150 micrometres. For low viscosities the expected minimum diameter is 1.5 to 2 times the diameter of the nozzle used.

A T-piece, placed in area 4 in Fig. 4.4, connects the flexible hose that brings the fluid from the pressurized tank to the nozzle itself. One of the arms of this T-piece is blocked by a plain flat metallic layer, which transmits the vibration from the top generator by knocking of the piece.

After studying the performance of the device with higher viscosities, approximately 400 mPa·s, it was found that the connection was not adequate to bear with the generated forces by the pressurized polymer due to the presence of some leakages in the connections.

Therefore the piece was modified so that it connects to the pressurized system by stainless steel screwed metal connections. The modification can be seen in Figure 4.7.

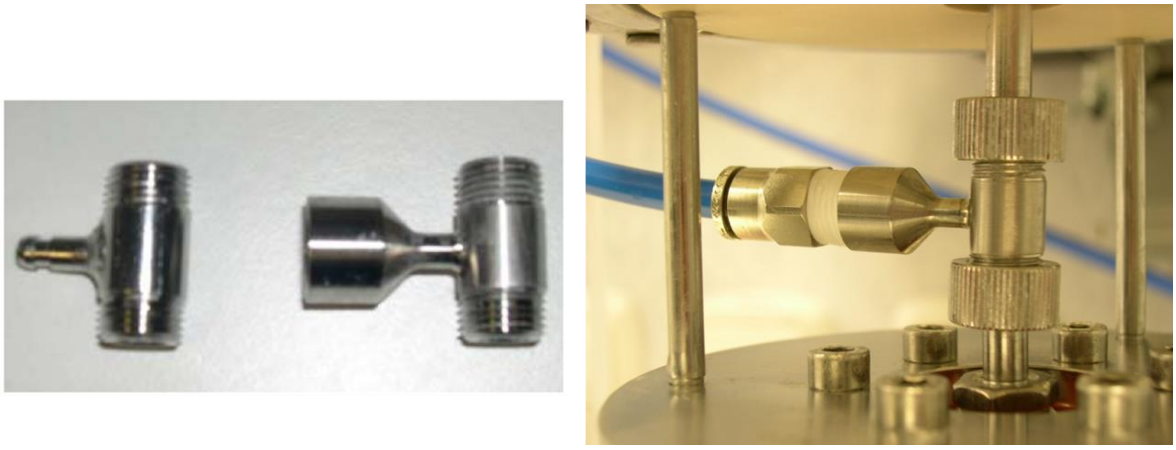

Figure 4.7: Modified T-piece to a welded steel screwed female adapter 1/8" GAS. Place where the T-piece is mounted.

The control device (3 in Fig. 4.4) provides the power supply for the vibrating mechanism and the stroboscopic light. It allows operating with two frequency ranges, up to 3000 Hz and up to 10000.

The vibration source is created by a force generator that transforms electrical current into mechanical force. It consists of a magnetic reaction mass, a drive coil and body assembly. The interaction between alternating current flowing in the coil and the magnetic field created by the magnetic mass makes the body displaces. An alternating current in the coil will produce an alternating physical displacement of the same frequency. The force generator produces a vibration from 160 to 10000 Hz.

The applied disturbance destabilizes the jet, disintegrating it in droplets that fall into the barium chloride hardening solution, at a distance of 20 cm from the nozzle. Finally the microdroplets are kept in the hardening solution during 10 minutes in order to achieve complete membrane solidification.

Figure 4.8 shows schematically the process of droplet formation from the nozzle and the gelation of these droplets in barium chloride, which generates a semipermeable solid membrane.

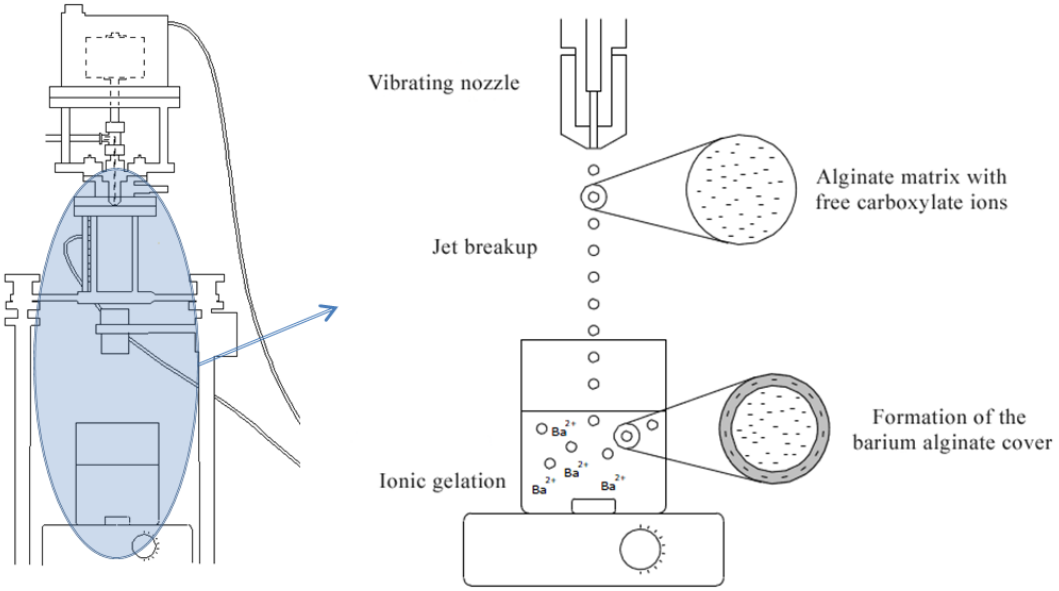

Figure 4.8: Process of droplet formation from the nozzle and gelation in Barium Chloride.

4.3. Blank runs procedure

This section describes how the behaviour of the system was assessed under different conditions of viscosity, flow rate and applied disturbances. Firstly, a basic introduction concerning instabilities in jets and more specifically in vibrating capillary nozzles is given. This allows distinguishing the most important parameters to take into account for the following experimental studies and analysis and characterize the samples for such aim.

4.3.1. Jet instabilities

When a liquid flows through a nozzle the jet formed downstream suffers variations in its shape. These changes are triggered by disturbances in the supply system, such as pressure and velocity fluctuations, as well as fluctuations in the liquid properties such as temperature, viscosity, or surface tension (Ashgriz and Yarin 2011).

As a result, an interaction between disruptive and cohesive forces on the jet gives rise to the growth of oscillations in the interface between the liquid and the surrounding medium. This changes the geometric profile of the jet.

The relationship between involved forces will lead to the increase of these oscillations until complete breakup of the jet or its decay until stabilization.

When the conditions promote the growth of the interfacial oscillations the jet eventually disintegrates into droplets. This process is sometimes referred to as *primary atomization*. Depending on the type of instability if the formed droplets exceed a critical size they can disintegrate again into smaller drops, which is known as *secondary atomization* (Chigier and Reitz 1996).

The factors accounting for the disintegration of liquid jets issuing from nozzles have been widely studied since more than a century (Savart 1833).

Different regimes have been classified to describe the disintegration processes. Wolfgang von Ohnesorge (Ohnesorge 1936) proposed a classification based on the relative importance of gravitational, inertial, surface tension and viscosity forces. He based his analysis in the dimensionless Reynolds number and the Ohnesorge number - bearing his

own name -. Among the many classifications in the bibliography this is the most common one. It is known as the Ohnesorge chart for breakup regimes (Figure 4.9).

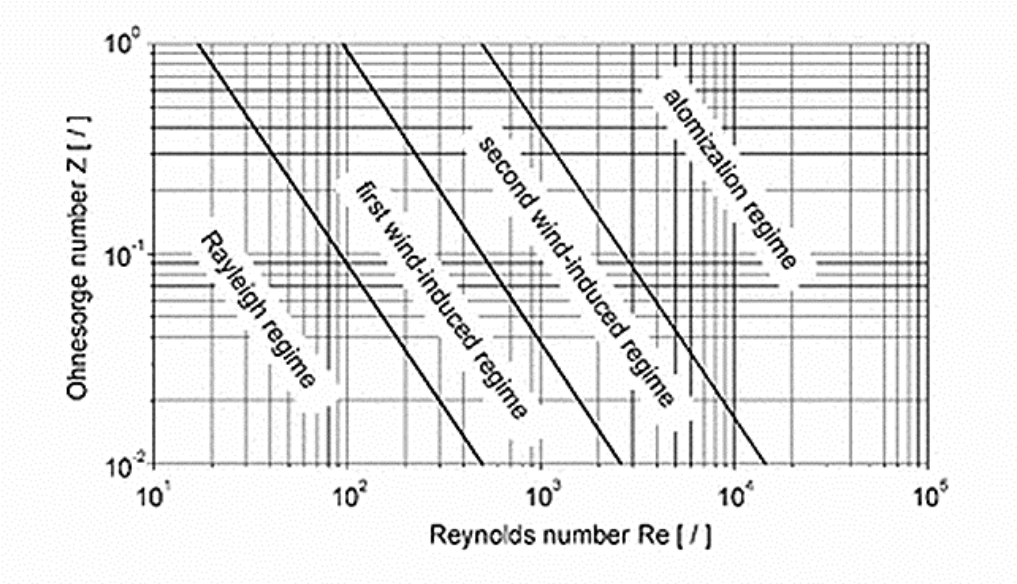

Figure 4.9: Classification of breakup regimes by the Ohnesorge chart (Baumgarten 2006).

Reitz (Reitz and Bracco 1986) described the regimes as follows:

- Rayleigh-type breakup or primary breakup mechanism: caused by the growth of axisymmetric oscillations on the surface of the jet. The size of the resulting droplets exceeds the diameter of the jet.
- First wind-induced regime: the relative velocity between the liquid and the surrounding air produces a pressure distribution which accelerates the process of breakup. The droplet diameter is similar to the jet diameter.
- Second wind-induced regime, also known as turbulent breakup: The drops are produced by the unstable growth of short-length surface waves caused by the relative movement between the jet and the surrounding air. The mean diameter of the droplets is substantially lower than the diameter of the jet.
- Atomization regime or spray: The jet disintegrates completely at the nozzle outlet and leads to droplets whose mean diameter is substantially lower than the jet diameter.

An additional criterion to classify the disintegration regime takes into account the Weber number based on the gas density together with the Weber based on the liquid properties in order to assess the aerodynamic effects (Pan and Suga 2006). The criteria are:

- Laminar: $We > 8 \; and \; We_g < 0.4$, the first condition may not be always necessary.
- Wind-induced: $1.2 + 3.4Oh^{0.9} < We_g < 13$
- Atomization: $13 < We_g < 40$

The evolution of a jet is totally different for each type of instability. It is related with unique mechanisms, which amplify the disturbances producing deviations from the cylindrical shape, as seen in Figure 4.10.

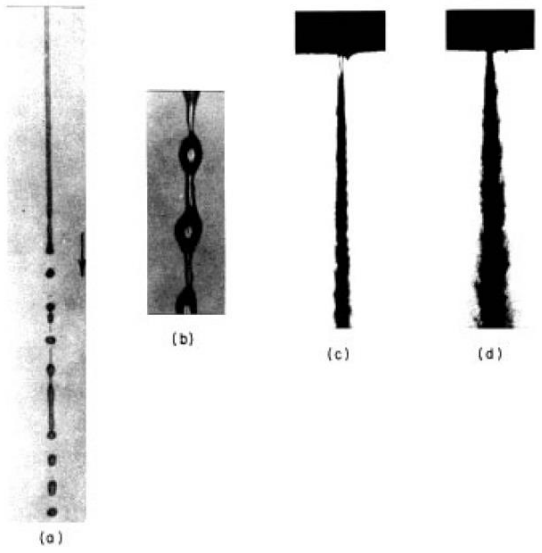

Figure 4.10: Different modes of disintegration (Lin and Reitz 1998): (1) Rayleigh breakup (2) Primary air induced breakup (3) Secondary air induced breakup (4) Spray.

Most experiments in this work were performed with alginate solutions using a circular nozzle with a 150 µm diameter, which results in a cylindrical thread of similar dimensions.

Taking characteristic values of the polymer an the process a density of 1000 kg/m^3, surface tension of 0.076 N/m, viscosity of 1.5 Pa·s and a mean velocity of 5 m/s the following magnitudes are obtained:

$$Oh = \frac{\eta}{\sqrt{\rho \cdot \sigma \cdot D}} = \frac{1.5}{\sqrt{1000 \cdot 0.076 \cdot 150 \cdot 10^{-6}}} = 14.05 \qquad (4.1)$$

$$\mathrm{Re} = \frac{\rho \cdot v \cdot D}{\eta} = \frac{1000 \cdot 5 \cdot 150 \cdot 10^{-6}}{1.5} = 0.5 \qquad (4.2)$$

$$We = \frac{\rho \cdot v^2 \cdot D}{\sigma} = \frac{1000 \cdot 5^2 \cdot 150 \cdot 10^{-6}}{0.076} = 49.34 \qquad (4.3)$$

which corresponds to the Rayleigh mechanism. This outcome holds for all the experimental range studied.

4.3.2. Rayleigh Instability

The literature on the study of break-up of laminar liquid threads begins in the early nineteenth century with the work of Savart (Savart 1833) followed by Plateau (Plateau 1873). They studied this regime in cylindrical liquid jets and found that a surface-tension driven instability at the interface of the jet with the surrounding media was leading to their breakup. Some years later Rayleigh (Rayleigh 1879) developed a numerical explanation of the phenomena, which names the type of instability, also known as Plateau-Rayleigh instability. Since then it has been a classic problem in fluid dynamics.

Plateau and Rayleigh assumed inviscid fluid conditions and infinite medium. Rayleigh noticed that the surface energy of a uniform circular cylindrical jet is not the attainable minimum energy for that given volume. He found then that the division of the jet into segments of approximated length of 2π times its radius gave rise to spherical beads, resulting in the minimum surface energy for the considered volume. Hence, he concluded that a liquid jet affected by ***surface tension forces*** becomes unstable under any axisymmetrical disturbances whose wavelength satisfies the inequality: $\lambda > 2\pi r$, being the most unstable wavelength approximately nine times the radius of the jet (Rayleigh 1879).

Rayleigh performed other studies, including a linear analysis assuming a viscous fluid without hydrodynamic interactions with air (Rayleigh 1892). However, the analysis of Weber (Weber 1931) is more known in the current literature for ***viscous effects***, because he considered the effects of Newtonian fluid viscosity and the interaction with the

surrounding air. The theory by Weber was improved by authors that proposed different approaches (Goedde and Yuen 1970; Sterling and Sleicher 1975; Bogy 1979; Chigier and Reitz 1996).

4.3.3. Characterization of polymer solutions

Different authors concluded that the instabilities in laminar jets are mainly driven by viscosity and surface tension effects. Therefore, it is of main importance the study of such parameters in the polymeric solution.

Therefore the surface tension of alginate solutions of different concentrations was measured using the method of Du Nouy ring. The results are shown in Figure 4.11.

The data report that solutions with concentrations around 2 g/dL show a surface tension value of approximately 0.076 N/m. This parameter does not vary substantially with slight changes of concentrations. The difference between the surface tension of alginates with concentrations 2.0 and 4.0 g/dL is 0.076 and 0.068 N/m respectively.

Therefore, for the range of concentrations that were tested, 1.3 to 2.1 g/dL, surface tension was taken as constant with a value of 0.076 N/m.

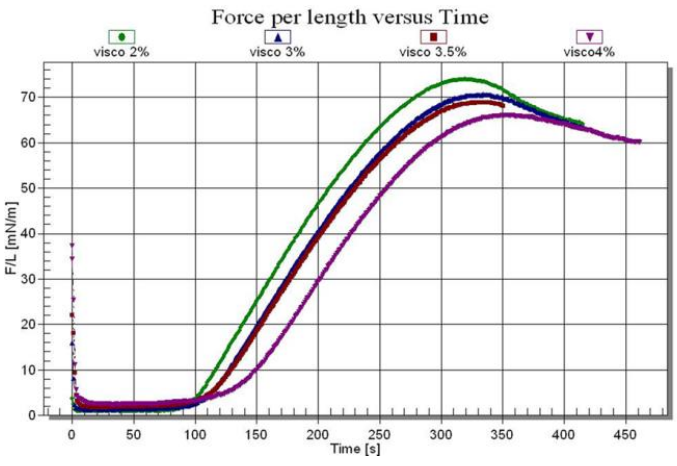

Figure 4.11: Surface tension for different alginate solutions

Regarding the viscosity, the characterization of the polymer was done by a rotating viscometer. A unique characteristic value of viscosity was considered for every

concentration. All measurements were carried out with the same spindle rotation velocity in order to have a similar shear rate affecting all the samples.

The obtained viscosities for the different tested concentrations in the blank runs are shown in Table 4.2.

Table 4.2: Viscosity values measured from the rotational viscometer.

c (g/dL)	η (Pa·s)
1.3	0.450
1.5	0.750
1.7	1.300
1.8	1.700
1.9	1.850
2.0	2.400
2.1	2.650

4.4. Generation of behavioural curves

Given the fact that the system is designed to work under different conditions, particularly of flow rate and viscosity, the generation of behavioural curves is of main interest. They provide information about the system and their analysis can lead to equations for prediction.

This section gathers information about the tests carried out in order to determine the effect of different parameters – in this case flow rate, viscosity and frequency - on the particle size, this is, the general behaviour of the system.

The considered variables for this study were the change of alginate solution concentration and flow rate (directly related to their velocity). The curves describing the overall behaviour of the system are displayed then.

As general parameters most of the experiments were carried out as follows:

- Nozzle diameter: 150 µm.
- Distance between nozzle and gelling bath: 20 cm.
- Volume of gelling solution: 100 mL.
- Gelling time: 10 minutes.
- Working temperature: 20 to 25 ºC.

The selection of the 150 µm nozzle was mainly due to the difficulties encountered working with smaller diameters. Smaller nozzles suffered frequently from clogging due to impurities or aggregates in the polymeric samples (Lee et al. 2012a). For this reason and considering the range of sizes to be targeted (300 to 600 µm) the selection of the 150 µm nozzle is justified.

4.4.1. Flow rate, viscosity and frequency conditions

Next the first experiments with the complete developed technique (pressure system and vibrating nozzle) are described. They were aimed to find out the range of viscosities and flow rates that can be processed and the range of applied frequencies leading to a homogeneous breakup.

To start with, different solution concentrations were tested at different and flow rate conditions. Data are collected in Table 4.3.

Table 4.3: Solution concentrations assayed for the set-up studies.

c (g/dL)	η (Pa·s)
1.0	0.160
1.5	0.610
2.0	2.300
2.5	3.950
3.0	5.540
3.5	14.80

The new system was able to produce continuous jets with solutions whose viscosities were up to 14000 mPa·s approximately. However, it was difficult to observe visually the breakup for such viscosities and several problems concerning the clogging of the nozzle appeared. For that reason the set-up experiments were lowered up to 2600 mPa·s.

After the viscosity limits were established, flow rates were measured. The selected flow rates for the experiments ranged from 5 to 9 mL/min. Stabilizing steady jets below 5 mL/min was not possible in most cases due to instabilities in the flow, whereas flows higher than 9 mL/min resulted in the appearance of deformations in the capsules, mainly for viscosities below 1000 mPa·s. These parameters are summarized in Table 4.4.

Table 4.4: General experimental conditions.

Parameter	Range of values
Alginate viscosity	450-2620 mPa·s
Alginate flow rate	5-9 mL/min
Surface tension	0.076 N/m
Density	1000 kg/m^3

After determining the range of viscosities and flow rates, the influence of frequency in the obtained particles was checked. A range of frequencies was tried, not taking into account yet any expression to compute them. The way to select the frequencies was based on visual observation with the help of the stroboscopic light.

Other considerations that were taken into account for selecting the frequencies to perform the experiments are detailed next:

- Schneider and Hendricks (Schneider and Hendricks 1964) studied low viscosity solutions. They suggested that an applied external vibration with a range of wavelengths $3.5d < \lambda < 7d$ causes the disintegration of the jet in uniform size drops.

- Merrington and Richardson (Merrington and Richardson 1947) observed from their experiments that a highly regular disintegration was only obtained close to the natural breakup. They considered $v/5d$ as external frequency.
- The results of Wissema and Davies (Wissema and Davies 1969) for aqueous solutions of various concentrations of glycerol indicate that the frequency required for a uniform disintegration is approximately half the optimal frequency according Weber theories.
- Rajagopalan (Rajagopalan and Tien 1973) also considered high viscosity solutions and reached similar conclusions to those of Wissema. He concluded that the minimum frequency at which uniform droplets are obtained goes from 40% of the calculated by Weber frequency.

Tables from 4.5 to 4.7 list some of the experiments that were carried out. More data are collected in Appendix A: Preliminary Studies.

Table 4.5: Experimental conditions for a 1.5 g/dL solution at 5 mL/min.

Frequency	Size (μm)	Span
600	554	0.94
800	484	0.92
1000	534	1.031
1200	535	1.004
1760	476	0.94

Table 4.6: Experimental conditions for a 1.5 g/dL solution at 6.5 mL/min.

Frequency	Size (μm)	Span
450	519	1.10
700	480	1.07
1300	533	1.12
2300	534	0.99

Table 4.7: Experimental conditions for a 2.0 g/dL solution at 6 mL/min (see Appendix A for more information).

Frequency	Size (μm)	Span
0	705	0.97
700	616	0.83
850	576	1.11
1200	623	1.01
1700	583	1.00
2050	568	0.97

Table 4.8: Summary of the experiments carried out.

Alginate	Flow rate (mL/min)	Frequencies (Hz)	Size (μm)
1 g/dL (0.160 Pa·s)	5	700-3000	486
	7	660-2800	515
	8.5	700-1600	501
1.5 g/dL (0.610 Pa·s)	5	400-1760	516
	6.5	450-2300	517
	8.8	2000-3000	520
2 g/dL (2.300 Pa·s)	6.5	700-2050	577
	7.5	700-2850	590
	9.5	700-2600	523

From these experiments it was found that there is a wide range of frequencies that lead to the breakup of the jet, in general from a minimum frequency of 600 Hz. The results do not clarify a notorious trend in the effect of the frequency on the obtained particles. It may seem that the size decreases with an increase in the frequency, being the data in disagreement those presenting high spans of the samples.

From the pictures in Figure 4.12 it is also difficult to extrapolate a clear behaviour concerning the applied frequency. However, it can be observed that there are smaller

microcapsules when higher frequencies are applied, though aggregates seem to be forming. The smallest particles could also be due to satellite droplet formation. Anyway, further analysis has to be done regarding the evolution of the jet, the coalescence of droplets and the formation of satellites.

It will be considered that the effect of the applied frequency is negligible for these set-up studies, since it cannot be further analysed for now.

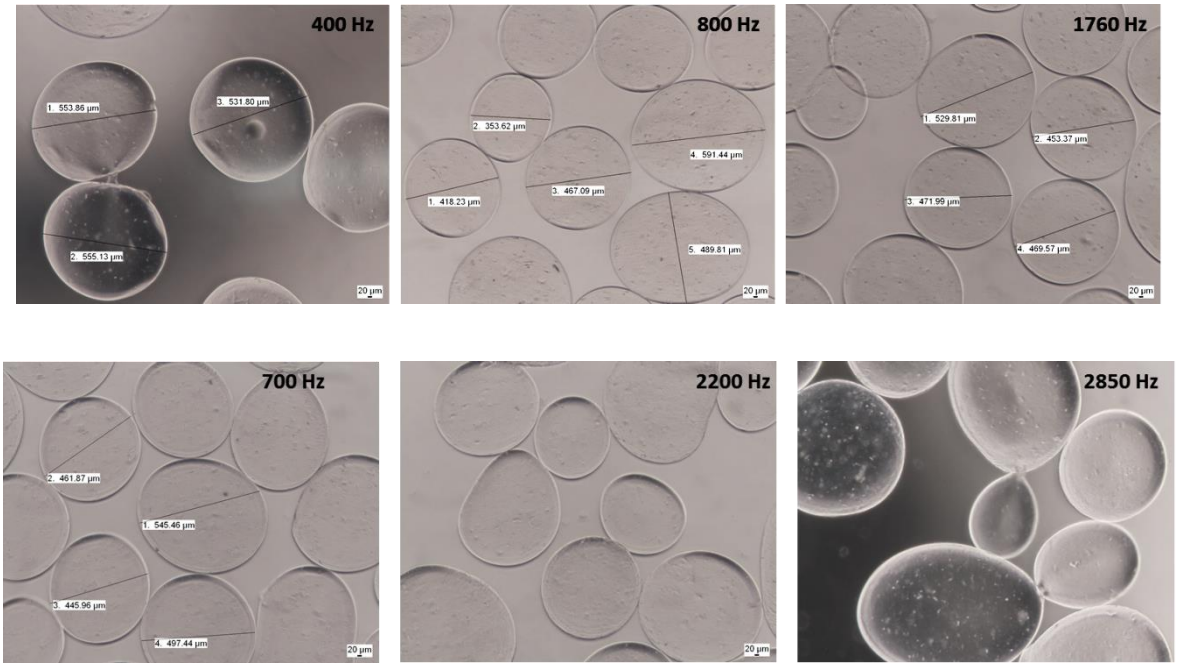

Figure 4.12 : Microcapsules from 1.5 g/dL alginate solutions under different breakup conditions. (a) Flow rate: 5 mL/min (b) Flow rate: 8.8 mL/min.

4.4.2. Disturbance frequency

The blank runs have shown that there is a wide range of frequencies leading to the break-up of the jet. However, it has been difficult to analyse the optimal frequency without the visualization of the jet evolution. Thus, the Weber equation was selected to compute a specific frequency. As described earlier, Weber (Weber 1931) studied viscous fluids and found that, in those cases, the most unstable wavelength was longer than the predicted by Rayleigh (Rayleigh 1879) studies.

The expression by Weber (4.4) includes basic physicochemical parameters of the solution and the jet to obtain an optimal wavelength (Weber 1931). From the computed wavelength, the optimal frequency to be applied can be determined by expression 4.5 knowing the velocity of the jet.

$$\lambda_{opt} = \pi \cdot \sqrt{2} \cdot d \left(1 + \frac{3\eta}{\sqrt{\rho\sigma \cdot d}} \right)^{1/2} \qquad (4.4)$$

$$f_{opt} = \frac{v}{\lambda_{opt}} \qquad (4.5)$$

Besides the frequency, it must also be taken into account the amplitude of the superimposed disturbance. This amplitude, transmitted from the force generator to the T-piece, can be controlled. As a matter of fact we did not notice differences in size, shape or span when applying amplitude scaled above 60% (referenced by the controller). The experiments were performed from the former amplitude referenced as 60%.

4.4.3. Calibration of pressure - flow rate

As it was detailed previously, the technique includes a pressurized system to facilitate the polymer flow through the capillary nozzle and overcome high pressure drops. This system can regulate the pressure from 1 to 5 bars approximately.

There is a relationship between applied pressure and flow rate of the fluid. This relationship must be determined.

Flow rates were calibrated applying a known pressure to the polymer solution and collecting the fluid into a beaker during a specific period of time. The flow rate is determined from the weight of collected fluid and time, considering a density of 1000 kg/m^3.

Figure 4.13 shows the effect of imposed pressure on the flow rate for different concentrations. In all cases a linear relationship is obtained (table 4.9). Intermediate values

to use fixed flow rates and standardise experiments were obtained by the interpolation of these relationships.

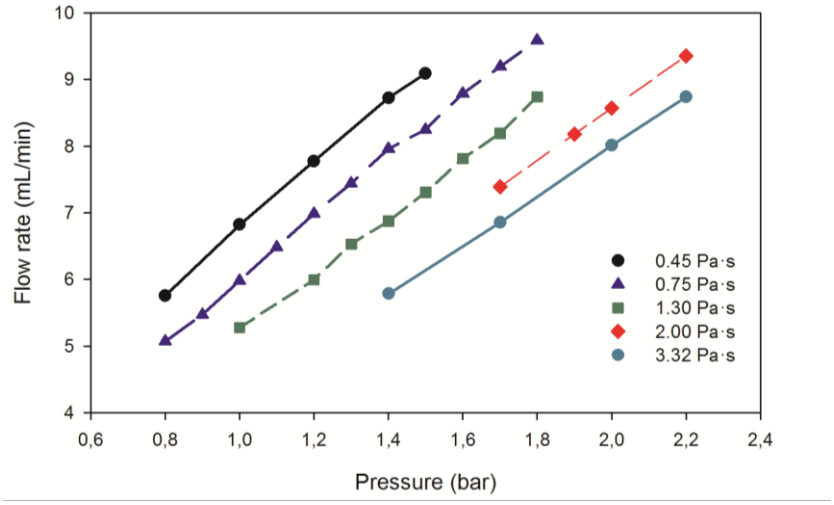

Figure 4.13: Effect of the imposed pressure on the flow rate for different samples.

Table 4.9: Linear relationships between flow rate and applied pressure to the fluid

Concentration (g/dL)	Linear relationship
1.3	$Q = 4.78P + 1.99$
1.5	$Q = 4.58P + 1.43$
1.7	$Q = 4.32P + 0.88$
1.8	$Q = 3.99P + 1.12$
1.9	$Q = 3.84P + 0.89$
2.1	$Q = 3.64P + 0.71$

From the results in table 4.9 it can be concluded that when the viscosity of the solution increases the slope of the linear relationship between pressure and flow rate decreases. This means that a further increment in pressure is required for the same increment of flow rate, given the increase in pressure drop with the viscosity.

4.5. Behavioural curves

Once the ranges of operating conditions have been determined (particularly in terms of viscosity and flow rate), a set of experiments were carried out in order to generate the behavioural curves. This will lead to a better knowledge of the system and will provide helpful information to develop theoretical analyses for predicting microparticle size saving experimental efforts.

The studied parameters through the curves are viscosity and flow rate. The effect of surface tension is not analysed here since it was previously observed its value does not significantly vary with changes in the concentration range of the polymer used in this study. Furthermore, the frequency does not show a clear effect on the size when it lies in the range where the breakup is reached. Therefore, one value of optimal frequency will be computed through Weber expression but no further analysis will be done for now.

The different frequencies for the selected ranges of flow rates and viscosities are computed as follows. On the one hand the optimal wavelength is computed considering "*d*" in expression (4.4) as the nozzle diameter - 150 µm - as authors such as Schneider and Hendriks (Schneider and Hendricks 1964). This approach is the most typically used.

On the other hand, Kurabayashi (Kurabayashi 1959) proposed a relationship between the nozzle diameter and the jet diameter that was also verified by Brandenberger et al. (Brandenberger and Widmer 1998). These latter authors used low viscosity sodium alginate samples and a laminar jet breakup technique through a vibrating nozzle.

The expression to compute the jet diameter according to Kurabayashi is as follows:

$$\frac{d_j}{d_n} = 4.33 We_n^{-0.337} \qquad (4.6)$$

$$We_n = \frac{v_n^2 \rho d_n}{\sigma} \qquad (4.7)$$

where d_n and v_n are the nozzle diameter and the velocity considering the nozzle diameter respectively.

The two procedures are assessed in order to check the differences in the computed frequencies. Table 4.10 contains the data for the computation of the optimal frequencies for a particular alginate concentration – 1.8 g/dL -.

Table 4.10: Data for the computation of optimal frequency through Weber expression to apply for the instabilization of a jet of sodium alginate 1.8 g/dL (1720 mPa·s) solution.

Q (mL/min)	v (m/s)	We_n	λ_{opt} (mm)	**f (s^{-1}) Schneider**	d_j (μm)	λ_{opt} (d_j) (mm)	**f (s^{-1}) Kurabayashi**
5	4.72	43.89	4,681	1007	182	5.408	872
5,5	5.19	53.11	"	1108	170	5.151	1007
6	5.66	63.20	"	1209	161	4.928	1148
6,5	6.13	74.17	"	1310	152	4.731	1296
7	6.60	86.03	"	1410	145	4.556	1449
7,5	7.07	98.75	"	1511	138	4.399	1608
8	7.55	112.36	"	1612	132	4.257	1772
8,5	8.02	126.84	"	1713	127	4.128	1942
9	8.49	142.21	4,681	1813	122	4.009	2117

From the data in Table 4.10 it can be seen that the frequencies between the two procedures do not vary excessively, being the highest differences around 200 to 300 s^{-1}. In most cases the two magnitudes lie in the range of frequencies previously tested for such concentration and seemed to achieve controlled breakup. Thus, considering the similarity of our process with the process studied by Brandenberger et al. (Brandenberger and Widmer 1998; Brandenberger and Widmer 1999) the frequencies obtained by applying the relationship (4.6) were selected for the experiments.

After the flow rates, viscosities and frequencies for each condition are established the experiments are carried out, measuring the obtained microparticle sizes. The data are collected in Table 4.11 and Figure 4.14. More information is given in Appendix A.

Table 4.11: Microparticle size as a function of viscosity and flow rate.

Q (mL/min)	Viscosity (mPa·s)						
	450	**750**	**1300**	**1700**	**1850**	**2400**	**2650**
5	468	526	555	618	635	658	699
5.5	473	551	585	635	668	661	708
6	509	560	575	626	650	660	707
6.5	505	515	562	-	-	650	683
7	496	502	-	608	627	-	677
7.5	499	500	539	-	-	621	680
8	-	503	521	563	605	612	662
8.5	-	505	503	553	553	580	622
9	-	-	502	517	525	540	575

Some data in Table 4.11 could not be obtained due to experimental problems. For instance, the excessive deformation of the capsules of low viscosities at high flow rates does not provide a reliable size distribution. In other cases the breakup of the jets was impossible to detect through visual observation.

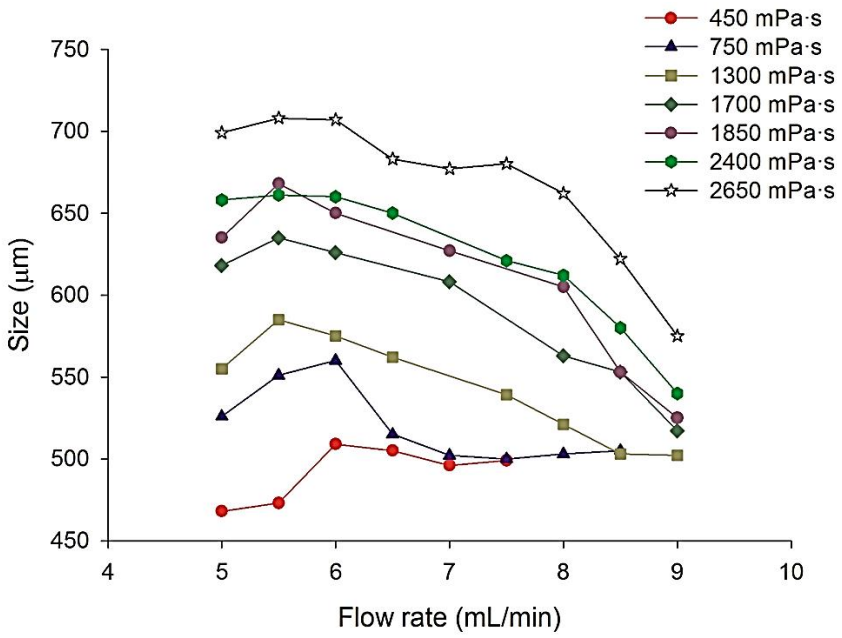

Figure 4.14: Effect of flow rate on the microparticle size.

Figure 4.14 represents the microparticle size (measured as SMD) as a function of the flow rate for several viscosities. From the collected data certain patterns are easily observed. Figure 4.15 details the different observed patterns that will be listed next.

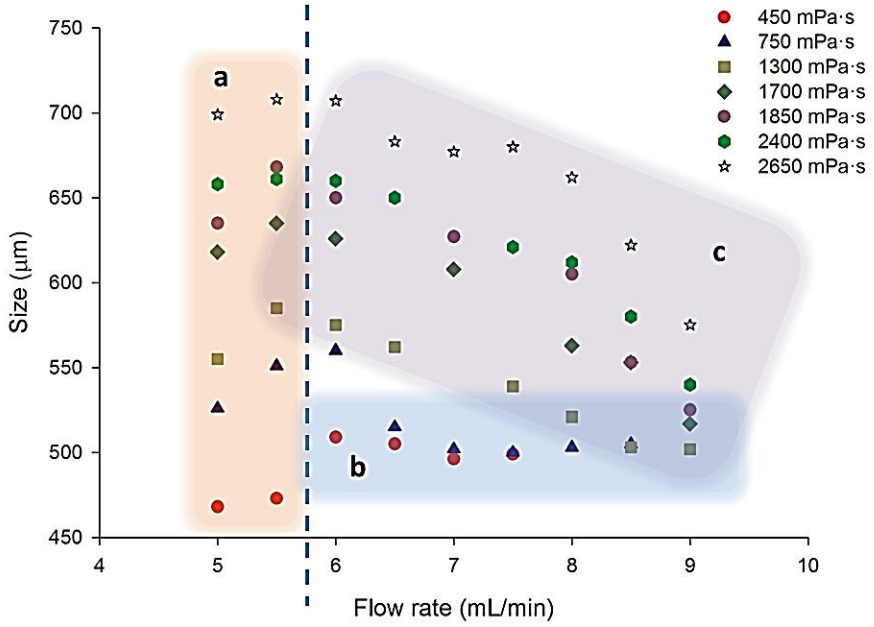

Figure 4.15: Different behaviours in the effect of viscosity and flow rate on the microparticle size.

- As a general behaviour the particle size increases when increasing the viscosity for all cases. This behaviour was expected and extensively reported, both in experimental studies and mathematical analyses (Goldin et al. 1969; Brenn et al. 2000).

The effect of the flow rate is also clear in general terms though different behaviours are observed.

a. For flow rates below 6 mL/min the tendency indicates that the particle size increases with the flow rate.
b. For flow rates above 6 mL/min and solutions with viscosities below 0.80 Pa·s the size remains constant.
c. For flow rates above 6 mL/min and solutions with viscosities above 0.80 Pa·s the size clearly decreases with an increase of the flow rate.

The last described behaviour attracted the highest interest for the study since it deals with the range of viscosities and flow rates aimed by the new technique.

In summary, certain conclusions arise from these preliminary results. The first and clearest conclusion is that the viscosity acts as a stabilizing force, damping the instability out, as it has been reported in several studies. However, as for the effect of the flow rate, the figure shows an unexpected behaviour at that time compared to other reported studies (Hartman et al. 1999; Herrero et al. 2006; Moghadam et al. 2008). It reveals a decreasing size when increasing the flow rate.

The explanation of affecting parameters on the particle size in atomization processes becomes complex since droplet size can be influenced by the aggregation of small droplets due to a higher available surface area, higher amount of droplets by unit volume, and an enhanced electrostatic attraction generated between the negatively charged droplets.

Concerning the process of study – capillary jet breakup - one of the reasons that could be influencing this situation is the frequency, which increases with the flow rate. It had been already checked in bibliography that it certainly has an influence in the *droplet size*. A relationship of the type *droplet size* $\alpha \frac{Q}{f}$, will be addressed later in *Chapter 5*. However, it had been experimentally found before that the influence of the applied frequency in the *final microparticle size* seemed not clear enough.

It was then also considered that the reason of this performance could also lie in the rheological behaviour of the polymeric solutions. An increase of shear and extensional stresses in the nozzle when the flow rate rises could lead to a decrease in the viscosity of the alginate solution, which consequently will influence also the size. Moghadam et al. also suggested that shear-thinning viscosity could be a possible reason for this unexpected behaviour (Moghadam et al. 2009). These questions will give way to later analyses.

4.5.1. Dependence of SMD on viscosity and flow rate – empirical relations

After the qualitative assessment of the main affecting parameters from Figure 4.15 a quantitative description will be extracted. With this aim the influence of the viscosity and

the flow rate on the microparticle size will be analysed independently considering the data in grey in Table 4.11 (for the behaviour detailed as "*c*" previously). These dependencies are merely illustrative with the aim of seeing more clearly the independent effect of the aforementioned parameters.

To analyse the effect of the viscosity, the Ohnesorge number will be considered in order to adimensionalize and normalize the data. The Ohnesorge number $Oh = \frac{\eta}{\sqrt{\rho \cdot \sigma \cdot d}}$ relates viscous forces to surface tension forces. As seen before it is of main interest in the analysis of jet instabilities. Similarly, the microparticle size will be adimensionalize by referring to the nozzle diameter *D*.

Regarding the analysis of the viscosity it is noteworthy saying that the effect of extensional and shear rates have not been taking into account. A similar study for an atomization nozzle conducted by Mansour and Chigier (Mansour and Chigier 1995) reported that the viscosity to be used in the Ohnesorge number to correlate data should be the infinite viscosity. Due to the lack of that information in these set-up studies the use of a viscosity value related to an intermediate shear rate has been studied. As it was previously said the applied rotation speed in the viscometer was kept constant for all solutions, trying to measure at a same shear rate.

Table 4.12 presents a summary of some of the data considered to extract the effect of the viscosity.

Table 4.12: Data for the study of the effect of viscosity on size

Viscosity (mPa·s)	Oh	Q=6 mL/min	Q=8 mL/min	Q=9mL/min
1300	12.18	575	521	502
1700	15.92	626	563	517
1850	17.33	650	605	525
2400	22.48	660	612	540
2650	24.82	707	662	575

Figure 4.16 represents in logarithmic scale the experimental SMD obtained under the different Ohnesorge numbers. An exponential dependence can be inferred, typical in instability processes (Jasuja 1982; Risk and Lefebvre 1984; Lorenzetto and Lefebvre 1977; Mansour and Chigier 1995). As concluded when the behavioural curves were studied the size increases with the viscosity and thus, a positive exponential dependence can be obtained (expression 4.8).

$$SMD = f\left(Oh^{0,267}\right) \qquad (4.8)$$

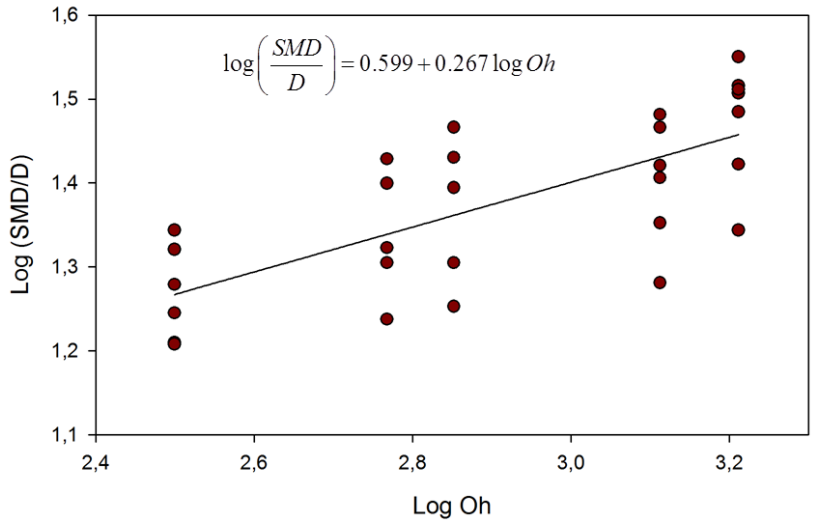

Figure 4.16: Effect of Ohnesorge number on SMD.

The influence of the flow rate on the microparticle size has been also extracted from the behavioural curves. It will be studied through the Weber number $We = \frac{v^2 \cdot \rho \cdot d}{\sigma}$ that relates inertial forces to surface tension forces. It is a quite useful relationship in the analysis of multiphase flows, where there is an interface between fluids.

Table 4.13 contains some of the data represented in Figure 4.17 in logarithmic scale.

Table 4.13: Data for the study of the effect of flow rate on size

Q (mL/min)	We	η=1700 mPa·s	η=1850 mPa·s	η=2650 mPa·s
6	63.20	626	650	707
7	86.03	608	627	677
8	112.36	563	605	662
9	142.21	517	525	575

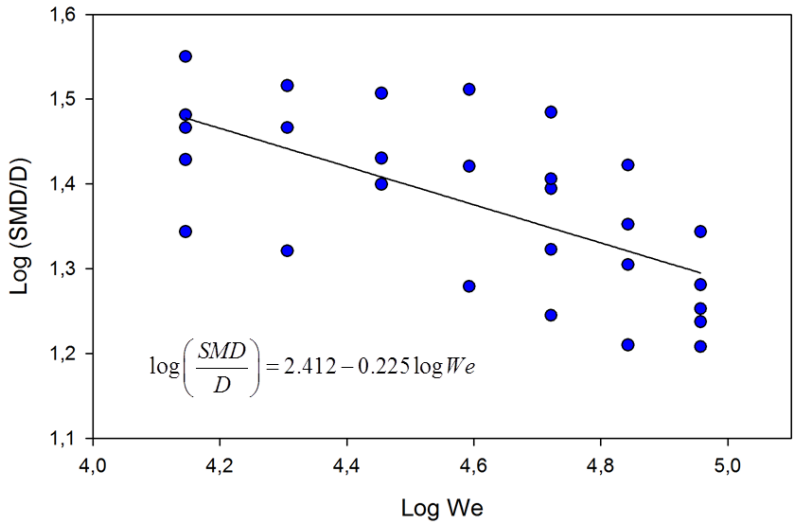

Figure 4.17: Effect of Weber number on SMD.

Contrary to viscosity, the effect of the flow rate through the Weber number leads to a negative exponential dependence of the for in expression (4.9).

$$SMD = f\left(We^{-0.225}\right) \qquad (4.9)$$

4.6. Semiempirical Approach

After the previous experiments, the behaviour of the system is now better known. A further step of high interest would comprise a study that allows the prediction of the microparticle size from the correlation of physical parameters that affect the system. As a first approach the analysis of the variables affecting the system is performed through the obtaining of semiempirical equations.

When there is a lack of knowledge about the mechanisms related to a process an empirical model must be established to represent the response of certain phenomenon from experimental measures.

At an intermediate level of approximation, a semiempirical model incorporates knowledge of the processes involved in the phenomenon by combining experimental results with conclusions and theories of other more complex models. In general it relies on a theory that is simplified with the help of empirical data.

Given the novel nature of the developed technique it was not found in the literature a semiempirical approach describing it. Regarding similar analyses on axisymmetric laminar instabilities, in most cases they estimate the droplet size - before the gelation process - through different expressions that relate in all cases jet diameter and wavelength. These approaches consider the formation of the droplet from the cylinder whose length is the wavelength of the disturbance developed in the jet (Wissema and Davies 1969; Rajagopalan and Tien 1973). However, this magnitude does not coincide with the final microparticle size and would not be valid to predict the microparticle final size. Other authors use corrector factors to estimate this parameter (Haas 1992).

However, semiempirical analyses on atomization processes are better known. Therefore, a comparative study between an atomization process and the process here developed was carried out in order to assess the possible use of the semiempirical studies found.

The first step to tackle the analysis comprises the relation of forces acting in the system. As detailed before the disintegration of a laminar liquid jet is a result of internal

and external causes. The former include shear and extensional stresses or irregularities in the geometry of the nozzle and the latter are derived from superimposed disturbances and minimal interactions with surrounding air. These cause the growth of axisymmetrical sinuous waves at the interface of the stream.

Figure 4.18 shows the system of forces considered to be acting at the interface of the jet. Viscous forces oppose to the growing of the disturbance while superimposed vibration produces pressure fluctuations at the interface due to surface tension forces and tends to increase the amplitude of the perturbation wave. Also shear and extensional stresses are agents to take into account. These latter will be considered as present in this analysis through the flow rate or velocity of the jet since the shear and extensional effects on the jet vary with its composition and velocity.

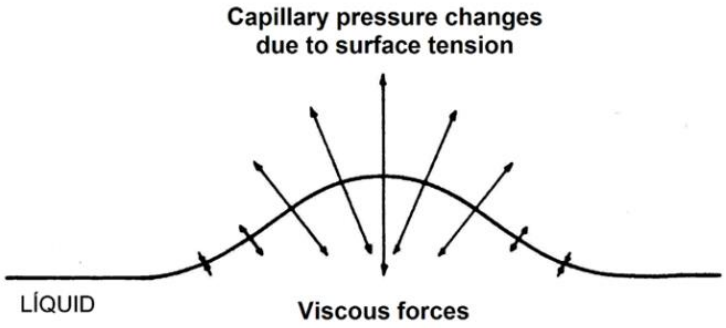

Figure 4.18: Balance of acting forces initially considered.

In a similar way, atomization processes are characterized by the interaction with the surrounding air, through air drag forces (Lefebvre 1989).

4.6.1. Wave mechanism theory

The theory that will be considered to obtain the semiempirical expressions is known as the wave mechanism theory. It describes the atomization process as a disintegration caused by the growth of unstable waves at the liquid-gas interface. These waves are generated by pressure fluctuations or turbulences in the gas and liquid streams (Adelberg

1967). The waves develop as capillary waves if the surface tension predominates or as acceleration waves when the pressure forces do (Mansour and Chigier 1995).

Basic features and parameters affect both atomization and laminar breakup processes. This can lead to suggest that this theory might also describe the process of study.

Table 4.14 compares the two processes of atomization and laminar breakup.

Table 4.14: Similarities between Rayleigh-type breakup and atomization processes

Theoretical concept: wave mechanism	***Regime / system***	
	Atomization	***Vibrating nozzle***
External perturbation / Disruptive force	Air	Vibration
Type of produced disturbance in the jet or liquid sheet: surface waves	Axisymmetric sinusoidal disturbance in the surface	Axisymmetric sinusoidal disturbance in the surface
Breakup: increase of amplitude of the surface waves by turbulences	Aerodynamic pressure	Pressure related to surface tension
Other influential parameters on the amplitude of the surface waves	Viscosity (stabilizing effect)	Viscosity (stabilizing effect)
Relevant dimensionless numbers	- Ohnesorge - Weber - Masic flows relation	- Ohnesorge - Weber

Therefore, considering the wide acceptance that this theory has among the description of the atomization processes, its application to the technique described in this work is studied.

Thus, the growth of the amplitude of the interfacial waves until the breakup for wind-induced instabilities is defined through expression (4.10) (Adelberg 1967, 1968; Jeffreys 1980; Mayer 1961)

$$\frac{dA}{dt} = A\left[\frac{\pi\beta\rho_a(U_a - v)^2}{\lambda\rho_l v} - \frac{8\pi^2\eta_l}{\rho_l\lambda^2}\right] \qquad (4.10)$$

where β: Jeffrey's sheltering parameter. The amplitude *A* is damped by the viscosity - tending to stabilize the instability - and it is promoted by the difference between gas and liquid velocities.

When the aerodynamic pressure force and the surface tension forces are significant, the velocity of the wave *v* is given by:

$$v = \left[\frac{a\lambda}{2\pi} + \frac{2\pi\sigma}{\lambda\rho_l}\right]^{\frac{1}{2}} \qquad (4.11)$$

Being '*a*' the acceleration due to the aerodynamic drag:

$$a = \frac{4C_{D_0}\sin^2\zeta}{\pi D\rho_l}\bar{\rho}_a\frac{\overline{U}_a}{2} \qquad (4.12)$$

Where C_{Do} is the drag coefficient of a cylinder in cross-flow and ζ is the angle between the jet axis and gas (in radians) and *D* the jet diameter. Air density and velocity $\bar{\rho}_a, \overline{U}_a$ are evaluated before the break-up of the liquid jet.

Substituting (4.11) in (4.10):

$$\frac{dA}{dt} = A\left[\frac{\pi\beta\rho_a\left(U_a - \left[\frac{a\lambda}{2\pi} + \frac{2\pi\sigma}{\lambda\rho_l}\right]^{\frac{1}{2}}\right)^2}{\lambda\rho_l\left[\frac{a\lambda}{2\pi} + \frac{2\pi\sigma}{\lambda\rho_l}\right]^{\frac{1}{2}}} - \frac{8\pi^2\eta_l}{\rho_l\lambda^2}\right] \qquad (4.13)$$

From where it can be concluded that viscosity opposes to the growth of the instability and the effect of surface tension should be further analysed to conclude its effect.

The minimum wavelength $\lambda_{\min}$ above which the amplitude grows exponentially with time can be determined by $dA/dt = 0$. This results in an expression of the type (4.14).

$$\lambda_{\min}^2 - \lambda_a \lambda_{\min}^2 - \lambda_\sigma^2 = 0 \qquad (4.14)$$

with: $\frac{\lambda_\sigma}{D} = \frac{4\pi 2^{1/3}}{\beta^{2/3}}\left(\frac{Oh}{We}\right)^{2/3}$ (4.15) being λ_σ the wavelength of capillary waves

$\frac{\lambda_a}{D} = \frac{64 C_{D_0} \sin^2 \zeta}{n^* \beta^2 \pi}\left(\frac{Oh^2}{We}\right)$ (4.16) being λ_a the wavelength of acceleration waves and

$n^* = \frac{\rho_a U_a^2}{\bar{\rho}_a \bar{U}_a^2}$ the shock dynamic pressure ratio.

On one hand, waves propagate as acceleration waves when aerodynamic pressure forces predominate, at a minimum wavelength $\left(a\lambda_{min}/2\pi\right)^{1/2}$. In this case $\lambda_a << \lambda_\sigma$ and the solution for the equation (4.14) is $\lambda_{min} = \lambda_\sigma$, which is governed by $(Oh/We)^{2/3}$.

On the other hand, when surface tension dominates the waves propagate as capillary waves at a minimum velocity of $\left(2\pi\sigma / \lambda_{min}\rho_l\right)^{1/2}$. Being thus $\lambda_\sigma << \lambda_a$, a solution for the equation (4.14) is $\lambda_m = \lambda_a$, governed by (Oh^2/We).

4.7. Semiempirical expressions and experimental data

Considering the wave mechanism previously detailed, Mansour and Chigier (Mansour and Chigier 1995) proposed semiempirical equations for the atomization of non-Newtonian fluids. Four relationships are proposed for the atomization of non-Newtonian fluids.

The expressions, considering the parameters that affect particularly the laminar breakup, are as follows:

$$\frac{SMD}{D} = X_2 We^{-X_1} + X_3 Oh^{X_1} \qquad (4.17)$$

$$\frac{SMD}{D} = X_2\left(\frac{Oh}{We}\right)^{X_1} \qquad (4.18)$$

$$\frac{SMD}{D} = X_2 We^{-X_1} + X_3 Oh^{2X_1} \qquad (4.19)$$

$$\frac{SMD}{D} = X_2 \left(\frac{Oh^2}{We} \right)^{X_1} \qquad (4.20)$$

The dependent variable SMD is adimensionalized dividing by the nozzle diameter, as it was done before to obtain the empirical relationships. From the theoretical solutions of equation (4.14), expressions (4.17 -4.18) with dimensionless numbers having the same exponent, implies that waves propagate as acceleration waves, predominating aerodynamic pressure forces.

However, in the case of expression (4.19) and (4.20) Ohnesorge's exponent doubles Weber's exponent, which means that surface tension forces predominate and the waves propagate as capillary waves.

Given the fact that the studied process is based on surface tension fluctuations and pressure fluctuations due to capillary effects, aerodynamic effects can be discarded and expressions 4.19 and 4.20 are proposed in order to fit the data.

To this end experimental data collected in Table 4.15 – same tests that those to generate the behavioural curves - are used for the fitting. As it was concluded, the behaviour to be studied (see c. section in list of 4.3. behavioural curves) corresponds to the data in italic and grey-shadowed.

It is worth mentioning here, before further analysis is carried out, that the previous empirical relationships fitting experimental data to microparticle sizes and the fitting to the semiempirical proposed expressions are independent approaches. Therefore, the exponents do not have to match between the studies and the implications and results of every approach are different.

Table 4.15: Data to fit the semiempirical equations.

Q (mL/min)	Viscosity (mPa·s)						
	450	**750**	**1300**	**1720**	**2000**	**2300**	**2620**
5	468	526	555	618	635	658	699
5.5	473	551	585	635	668	661	708
6	509	560	*575*	*626*	*650*	*660*	*707*
6.5	505	515	*562*	-	-	*650*	*683*
7	496	502	-	*608*	*627*	-	*677*
7.5	499	500	*539*	-	-	*621*	*680*
8	-	503	*521*	*563*	*605*	*612*	*662*
8.5	-	505	*503*	*553*	*553*	*580*	*622*
9	-	-	*502*	*517*	*525*	*540*	*575*

According to the experimental data the unknown coefficients X_1, X_2 and X_3 are computed through multiple linear regression analysis obtaining the values shown in table 4.16 and equations below.

$$\frac{SMD}{D} = 11.58 \cdot We^{-0.341} + 0.211 \cdot Oh^{0.682} \qquad (4.21)$$

$$\frac{SMD}{D} = 3.30 \cdot \left(\frac{Oh^2}{We} \right)^{0.151} \qquad (4.22)$$

Table 4.16: Data for the study of the effect of viscosity on size.

	X_1	X_2	X_3
Equation (4.12)	0.341	11.58	0.211
Equation (4.13)	0.151	3.297	-

In table 4.17 statistical data that give information about the degree of fitting for every expression are collected. The coefficients of determination compare estimated SMD/D and actual values. The closer the unit, the best is the correlation, i.e. there is no difference between the estimated value and the actual value.

Table 4.17: Statistical data concerning the fit of equations.

	Eq 4.21	*Eq 4.22*
X_1 Standard Error	0.024	0.012
X_2 Standard Error	1.583	0.056
X_3 Standard Error	0.039	-
Coefficient of Determination	0,9990	0,9986

From data in Table 4.17 both equations seem to show a good agreement of the data. However, as it is detailed next, one of the proposed equations (4.21) better predicts microparticle size.

This agreement will be checked by comparing a new set of experimental data with those predicted by the equations. The new data are collected in Table 4.18.

Table 4.18: Validation tests for the proposed fitting expressions.

Q (mL/min)	**Viscosity (mPa·s)**			
	850	**1180**	**1650**	**2190**
6	548	569	615	664
6.5	531	562	606	641
7	520	535	593	628
7.5	507	527	578	612
8	-	520	558	608
8.5	-	-	532	578

Firstly, Figures 4.19 and 4.20 represent the set of data at constant viscosity value for different flow rates – variable Weber – for the two equations respectively.

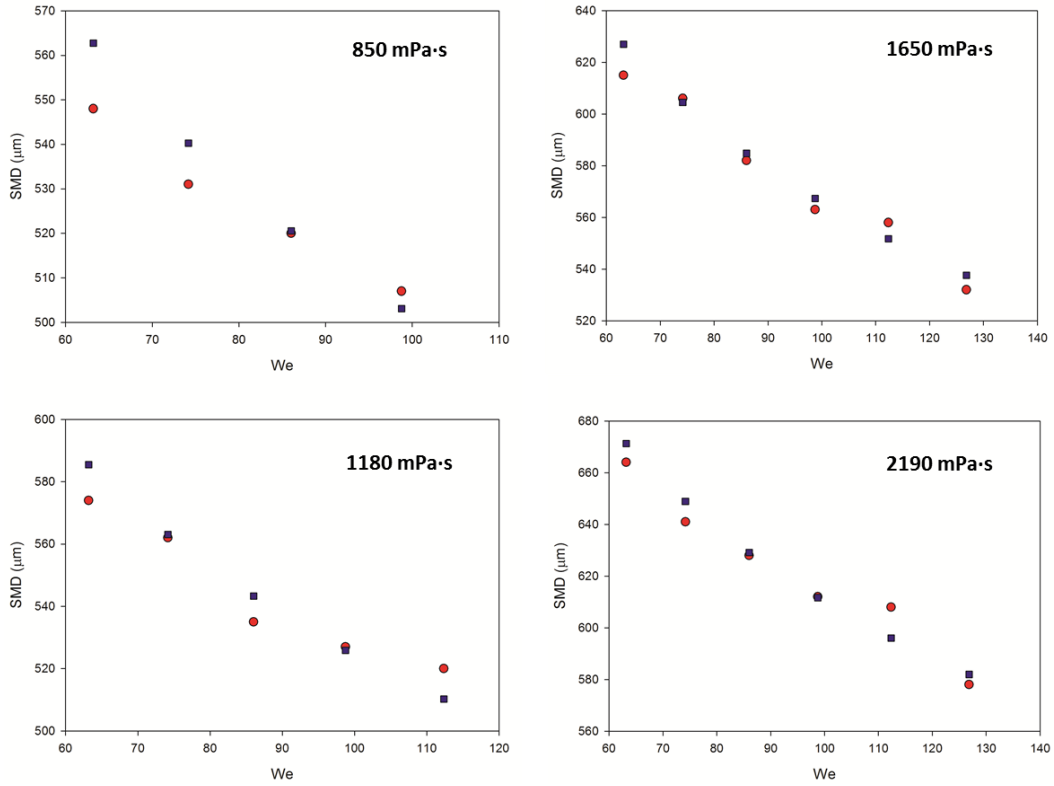

Figure 4.19: Comparison between experimental and predicted sizes of model 4.21. (•) experimental sizes (▪) predicted sizes

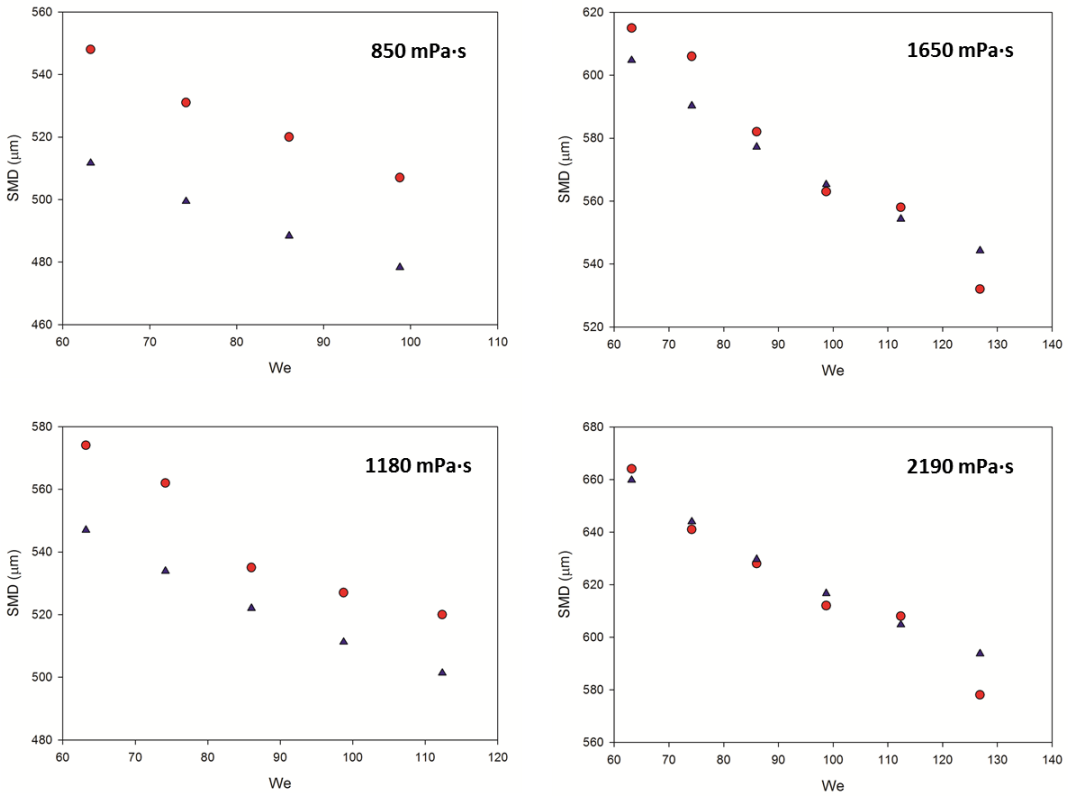

Figure 4.20: Comparison between experimental and predicted sizes of model 4.22. (●) experimental sizes (▲) predicted sizes.

Secondly, Figures 4.21 and 4.22 present a comparison between predicted and experimental data at constant flow rate and different viscosities – variable Ohnesorge – for the two expressions respectively.

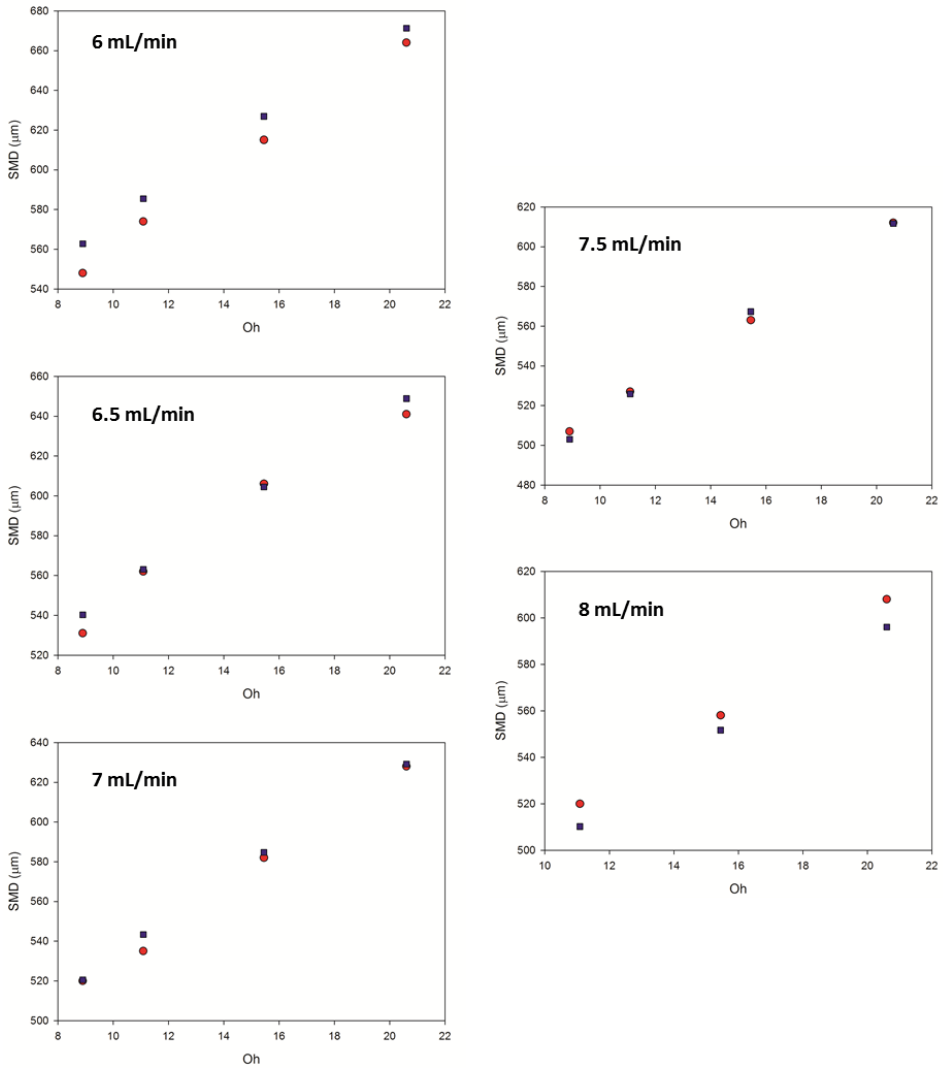

Figure 4.21: Comparison between experimental and predicted sizes of model 4.21. (•) experimental sizes (▪) predicted sizes

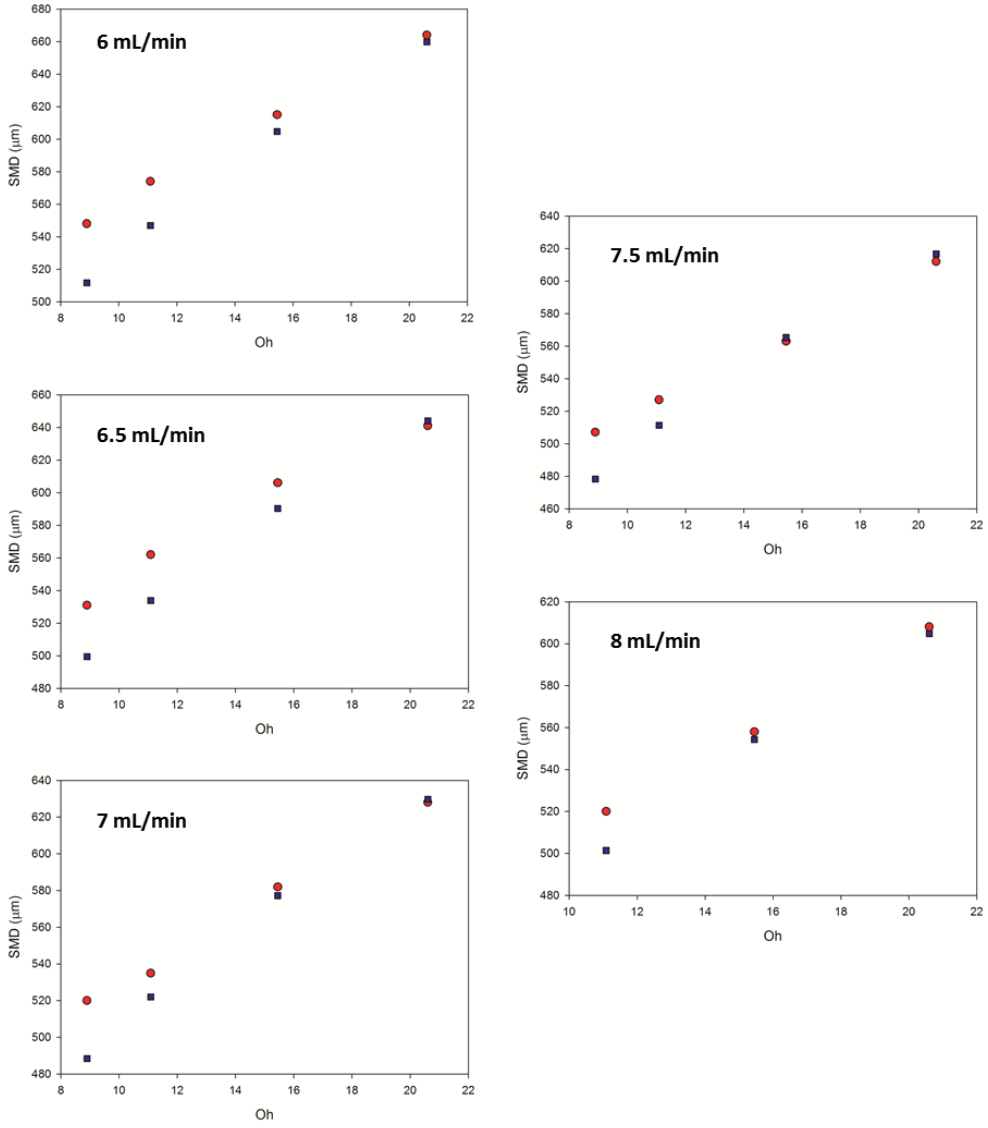

Figure 4.22: Comparison between experimental and predicted sizes of model 4.22. (•) experimental sizes (▪) predicted sizes

In general, it can be concluded that the first equation proposed $\frac{SMD}{D} = 11.58 \cdot We^{-0.341} + 0.211 \cdot Oh^{0.682}$ (4.21) predicts microparticle size with a good agreement with the experimental data. The highest deviations are found for the lowest and highest flow rates and for the lowest tested viscosities.

However, the second proposed expression (4.22) : $\frac{SMD}{D} = 3.30 \cdot \left(\frac{Oh^2}{We} \right)^{0.151}$ shows high deviations for the lowest viscosities assayed. It is noteworthy that the viscosity of 850 mPa·s is close to the limit where the behaviour of the microparticle size changes. This latter expression shows a good agreement for solutions above 1500 mPa·s, though there are few data to extract a definitive conclusion on this issue.

However, even if equation 4.22 is discarded, expression 4.21 shows a good agreement with the data. This suggests that the prediction is reliable under the range of conditions considered.

This also demonstrates that the wave mechanism, accepted for non-Newtonian liquids atomization, can also be applied to the new system developed. Thus, it allows relating some basic physical parameters through these semiempirical equations, acquiring a better knowledge of the process.

4.8. Related published work

Related to the work detailed in this chapter a research paper was published (Rodríguez-Rivero et al. 2011). It will be included next. If the reader prefers to access it by other means the citation is as follows:

Rodríguez-Rivero, C., E. M. M. Del Valle, and M. A. Galán. 2011. “Development of a new technique to generate microcapsules from the breakup of non-Newtonian highly viscous fluid jets”. AIChE Journal 57(12):3436-3447.

AIChE

Development of a New Technique to Generate Microcapsules from the Breakup of Non-Newtonian Highly Viscous Fluid Jets

C. Rodríguez-Rivero, E. M. M. Del Valle, and M. A. Galán
Dept. of Chemical Engineering, University of Salamanca, P/Los Caídos S/N, 37008 Salamanca, Spain

DOI 10.1002/aic.12549
Published online March 8, 2011 in Wiley Online Library (wileyonlinelibrary.com).

A new method to produce microcapsules ranging from 300 to 700 μm based on the droplets formation from non-newtonian high viscous liquids has been developed, characterized, and modeled. The technique involves the generation of a continuous high viscous solution jet, which is destabilized by means of a controlled vibration, breaking into droplets that undergo stabilization through a gelling process. Finally, the application of the wave-mechanisms-based theory to obtain a set of equations for the fitting of experimental data is assessed, as a first approximation for a better knowledge of the process. To find the fitting equations, the influence on the microcapsules size is studied through two-dimensionless groups, the Ohnesorge and the Weber numbers, involving the liquid viscosity and flow, respectively, and determining their exponential dependences. Further coefficients are obtained by least-squares fit of the experimental data.
 AIChE J, 57: 3436–3447, 2011
Keywords: jets, Rayleigh-type breakup, viscosity, laminar flow, vibrating nozzle

Introduction

In the last decades, the applications of microencapsulation have increased considerably, especially concerning food,[1] pharmaceutical, bioengineering, and biomedical applications.[2,3] Mainly, some of the reasons are: the microcapsules allow the controlled release of the contained active agent,[4] the masking of flavors, and the mechanical and immune protection of biological principles, such as proteins or living cells.[2,3,5]

The latter application, the microencapsulation of living cells or biomolecules, is the most selective among all of them, as some restrictive requirements concerning toxicity, kinetics formation, mechanical stability, and monodispersion have to be taken into account.[6,7]

Multiple techniques to produce microparticles have been developed, which are usually classified into physico–chemical and mechanical methods.[8] Coacervation and emulsion are common among the first techniques, from which several problems arise regarding size control and hazardous conditions for the active agent. Hence, the use of mechanical processes, combined with gelation methods of stabilization, has become especially relevant and developed, mainly for biomedical applications.[7,9]

However, in some of these mechanical processes difficulties also arise in controlling the size and shape, principally dealing with viscous fluids. For instance, when the spinning disk technique works with high viscosity fluids, it produces satellite drops and high heterodispersion[10]; in the extrusion by coaxial gas flow (airjet), some troubles related to the intrusion of air bubbles and a low throughput present themselves[7] and the jet cutting method works properly but suffers from what is called cut losses.[11]

On the other hand, the techniques concerning the breakup of laminar jets have become really important, and several studies with the aim of getting a better understanding of these processes are being carried out. These methods involve

Correspondence concerning this article should be addressed to E. M. D. Valle at emvalle@usal.es.

Table 1. Viscosity Values in Respect to Alginate Solutions Concentration

% w/w	μ (mPa s)
1	163
1.5	750
2	2300
2.5	3950
3	5540
3.5	14800

the control of the disturbance that a liquid undergoes when emerging from a circular nozzle,[12,13] achieving through this control a good monodispersion of the samples. Experimentally, the jet may be disturbed through several ways: mechanically, piezoelectrically, and acoustically[14–17] or magnetically,[18–20] undergoing Rayleigh-type breakup, widely known amongst others in inkjet printing applications.[21]

Some of the main disadvantages of Rayleigh-type breakup techniques are also problems regarding the work with high viscous fluids and their low productivity rate, though this second inconvenience can be solved with multinozzle systems.[22,23] Current bibliography only reports few studies of systems running with high viscosity fluids, up to 1400 mPa s[24] or 3000 mPa s.[25,26]

To ensure a good mechanical stability of the microcapsules, the viscosity of alginate solutions should reach over 1000 mPa s.[25] With this new system, we have obtained continuous jets up to 14,000 mPa s, though we have only shown in this study experiments up to 2620 mPa s.

Taking into account the restrictions in relation to polymer viscosities, the aim of this study has been, on one hand, the development of a new technique based on Rayleigh-type breakup that allows to work with high viscous liquid jets producing monodisperse microcapsules and, on the other hand, the study of factors affecting the system and the obtaining of a set of semiempirical models which predict the particle size, giving an initial perspective of the instability taking place.

Materials and Methods

Materials

Same batch of sodium alginate, purchased from Sigma Aldrich (alginic acid sodium salt from brown algae medium viscosity, powder) was used during the whole study. All solutions were prepared dissolving sodium alginate in water under hard stirring for 2 h. The required solutions consist of concentrations between 1.0 and 3.5% w/w.

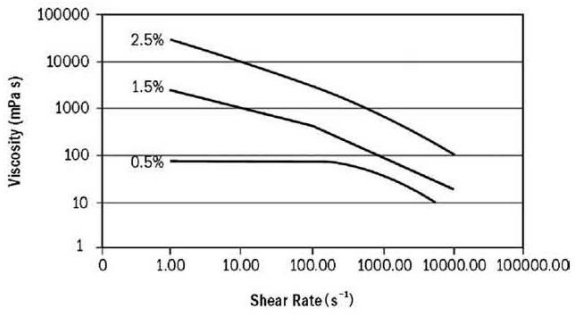

Figure 1. Viscosity values against shear rate.[27]

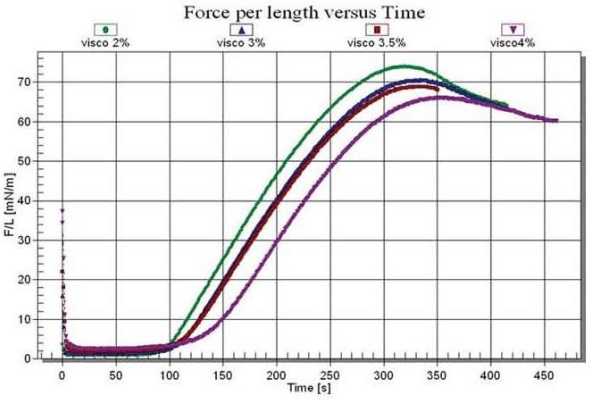

Figure 2. Surface tension values for different concentrations of alginate solutions.

The value decreases slightly when increasing the concentration. [Color figure can be viewed in the online issue, which is available at wileyonlinelibrary.com.]

Barium chloride dihydrate, reagent grade purchased from Scharlau, was used to obtain the hardening solutions dissolving in water in a concentration 2% w/w.

Solutions properties measurements

The viscosity of alginate solutions was determined by using a rotational viscometer (Visco Elite, Fungilab S.A.), at a temperature of 20°C and 6.28 rad/s (60 rpm) with the corresponding spindle in every case (values shown in Table 1). This value for the angular velocity has been chosen constant to following a method of reference for all cases.

The rheology of alginate solutions determines one of the most important physical behaviors of this polymer: its pseudoplasticity, which means that the viscosity of the solution decreases as the shear stresses or shear rate applied increase, as shown in Figure 1.[27]

The surface tension was determined by a tensiometer performing Du Nouy ring measurements (courtesy of Iberlaser S.A. using tensiometer model Sigma 700, KSV), obtaining the values shown in Figure 2. It can be observed that the surface tension values do not almost vary when the polymer concentration changes.

Experimental device

The device that has been optimized to produce microbeads based on a laminar viscous jet breakup induced by a superimposed controlled vibration is shown in Figure 3:

The pneumatic cabinet (2) has been previously designed to develop an air blast atomization technique by Herrero et al.[28] and, for the current application here described, it has the function of supplying and controlling the proper amount of air to pressurize the supply tank (3), fed from the synthetic air cylinder (1). This pneumatic cabinet differentiates this system from commercial devices and allows pushing high viscous solutions towards the nozzle. The nozzle is located in a commercial system that generates the continuous jet (Nisco VARD Encapsulator, Nisco Engineering AG). Both systems are connected through a PVC (polyvinyl chloride) pipe and steel quick connectors.

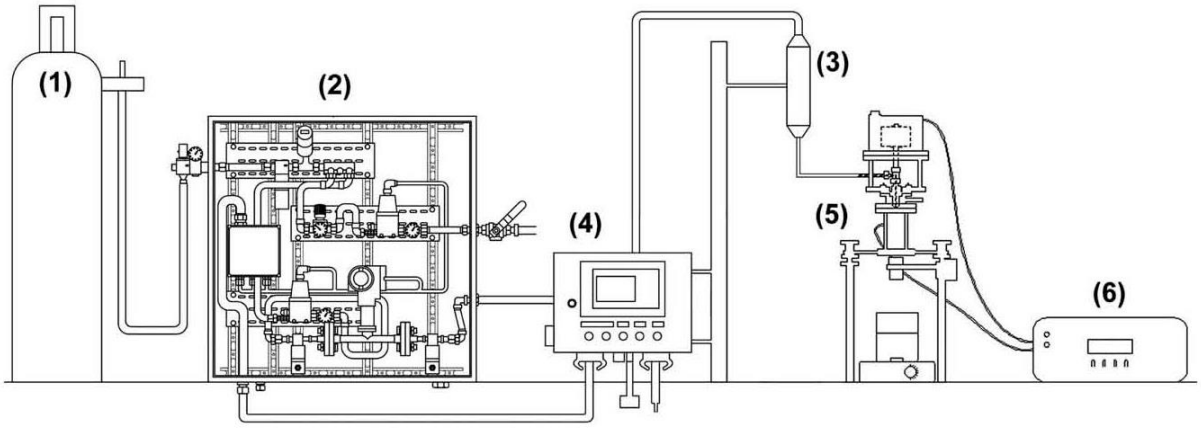

Figure 3. Experimental device to generate monodisperse microcapsules from high viscous non-Newtonian fluids.

(1) Compressed syntethic air cylinder, (2) pneumatic cabinet, (3) pressurized tank, (4) control board, (5) commercial system to impose external perturbation, and (6) frequency and amplitude controller.

Some other authors have also used pressurized air to force the liquid through a nozzle[16,23] but applied to lower viscosity values, whereas others have also carried out similar studies with commercial vibrating nozzles devices.[17,29,30]

The high viscous alginate solution is pushed from the pressurized tank towards the nozzle, producing a steady flow through it. Nozzles with diameters from 50 to 600 μm may be adapted. When a steady flow through the nozzle is achieved the external vibration source, a piezoelectric device connected to the nozzle through a T-piece, produces a controlled disturbance in the thread. The piezoelectric element can generate a vibration from 160 to 10,000 Hz. The applied disturbance destabilizes the jet, disintegrating it in droplets that fall into the barium chloride hardening solution, at a distance of 20 cm from the nozzle. Finally, the microdroplets are maintained in the hardening solution during 10 min to achieve complete membrane solidification.

The formation of droplets can be directly observed through a glass window by means of a stroboscopic light. The parameters of air pressure, which controls the alginate flow rate, and the frequency and amplitude of the superimposed vibration can be controlled by (4) and (5), respectively.

Particle size analysis

The values of particle size and distributions are determined using a particle analyzer (Mastersizer2000, Malvern Instruments) by laser diffraction technology. The size used in the analysis is characterized by the Sauter mean diameter (SMD), which is the diameter of a droplet that has the same volume-surface area ratio as the arithmetic mean of volume-surface area ratio of the total of droplets, this means the diameter of a droplet presenting the same volume-surface area ratio as the ratio of the total volume of droplets and the total surface area. Thus, mathematically expressed:

$$\mathrm{SMD} = \frac{\int_0^\infty D^3 dN}{\int_0^\infty D^2 dN} \quad (1)$$

where D is the droplet diameter, and dN the percentage of the total number of droplets with a diameter contained in the interval $[D, D + dD]$.

After analyzing the size, an image characterization of the particles is carried out using an optical microscope DM1000 Leica (Leica Microsystems) with camera Leica DFC280.

Theory

One of the classical studies in fluid dynamics has been the instability of a capillary liquid jet under the effect of surface tension. When a liquid flows through an orifice or a nozzle at certain velocity, the stream generated at the exit is perturbed simply due to noise, or the way of creating the perturbation can be also specifically imposed. Because of surface tension the disturbance is amplified and, depending on the balance of acting forces, it may grow in time and space. This growth may lead to the break up, which means that the jet breaks into droplets downstream, or it might decay and eventually stabilize.[31]

Plateau[12] observed that a cylindrical jet does not have the minimal surface energy according to the given volume and he noticed that, when the thread splits up in segments $\sim 2\pi$ times its radius, the droplets produced have the minimal surface energy for that volume. Rayleigh[13] came to the same conclusion and used a theoretical linear temporal analysis to determine the optimal wavelength corresponding to the maximal growth rate, though he considered a Newtonian fluid surrounded by an infinite and inviscid fluid. The expression

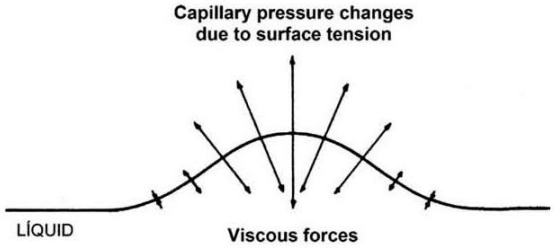

Figure 4. Balance of forces acting in Rayleigh instability.

Table 2. Similarities Between Rayleigh-Type Breakup and Atomization Processes

	Expression in the system	
Theoretical concept: wave mechanism	Atomization	Vibrating nozzle
External perturbation/Disruptive force	Air	Vibration
Type of produced disturbance in the jet or liquid sheet: surface waves	Axisymmetric sinusoidal disturbance in the surface	Axisymmetric sinusoidal disturbance in the surface
Breakup background: increase of the amplitude in the surface waves by turbulences	Aerodynamic pressure	Pressure related to surface tension
Other influential parameters on the amplitude of the surface waves	Viscosity (stabilizing effect)	Viscosity (stabilizing effect)
Dimensionless numbers relevant for the model	Ohnesorge Weber Masic flows ralation	Ohnesorge Weber

that he obtained to calculate the optimal wavelength (when the growth rate of the disturbance is maximum) was:

$$\lambda_{opt} = \pi \cdot \sqrt{2} \cdot d \cong 4.44 \cdot d \tag{2}$$

After Rayleigh, Weber[32] studied viscous fluids and found that, in those cases, the most unstable wavelength was longer than that predicted by Rayleigh studies:

$$\lambda_{opt} = \pi \cdot \sqrt{2} \cdot d \left(1 + \frac{3\mu}{\sqrt{\rho\sigma \cdot d}}\right)^{1/2} \tag{3}$$

Once the optimal wavelength is obtained, the frequency to be applied is calculated as followed:

$$f_{opt} = \frac{v}{\lambda_{opt}} \tag{4}$$

where v is the velocity of the jet.

All mentioned authors concluded that a thread might break up into droplets through a finite wavelength causing an axisymmetric capillary instability. One of the ways to externally create that destabilizing wavelength and control the breakup and monodispersion of samples is by applying a frequency and amplitude controlled disturbance to the flow of liquid forming the jet, in the form of a controlled vibration.

Development of a Semi-Empirical Model to Predict Microparticle Size

Acting forces in Rayleigh instability

The system of forces that acts on the interface of the described system under instability is shown in Figure 4. The viscous forces oppose to the growth of the disturbance as the superimposed vibration produces pressure fluctuations at the interface due to surface tension forces and tends to increase the amplitude of the wave.

Table 3. Viscosity Values in Respect to Alginate Solutions Concentration Used for the Experimentation

% w/w	μ (mPa s)
1.3	450
1.5	750
1.7	1300
1.8	1720
1.9	2000
2	2300
2.1	2620

Wave mechanism theory

As explained before, the disintegration of a liquid laminar jet is a result of internal and external causes. The first ones involve shear stresses, friction, or irregularities in the geometry of the nozzle. The external ones are derived from superimposed disturbances and certain minimal interactions with surrounding air.[33] All of them cause the growth of axisymmetrical sinuous waves at the interface of the stream, having as main acting agents the viscosity and surface tension forces.

In a similar way, atomization processes are also characterized by the flow properties in and out of the atomizers, the surrounding air, and the development of waves at the interface of the jet, controlling the mechanism viscosity and surface tension.[31,34] In the case of atomization processes, the aerodynamical forces and the geometry of the nozzle are more relevant than those in processes based on Rayleigh-type breakup, being that the aerodynamical forces in these processes usually neglected. In Table 2, the basic characteristics and parameters affecting both instabilities, laminar jet breakup and atomization processes, are compared, where several similarities can be seen.

Therefore, considering the wide acceptance that the wave mechanism theory has among the atomization processes, its application to the new technique described has been studied as a first approximation.

This theory describes the disintegration process caused by the growth of unstable waves at the liquid–gas interface, when the air interacts with the liquid, being these waves generated by pressure fluctuations or turbulences in the gas or liquid streams.[35] The waves continue as capillary waves if the surface tension predominates or as acceleration wave when the pressure forces predominate.[36]

Thus, Adelberg,[35,37] Jeffreys,[38] and Mayer[39] studied wind-induced instabilities and found that the amplitude of the

Table 4. Experimental Conditions in Which Set-Up Experiments have been Carried Out

Alginate viscosity (mPa s)	450–2620
Alginate flow rate (cm^3/min)	5–9
Surface tension (N/m)	0.076
Nozzle diameter = jet diameter (μm)	150
Density (kg/m^3)	1000
Reynolds number	0.29–2.32

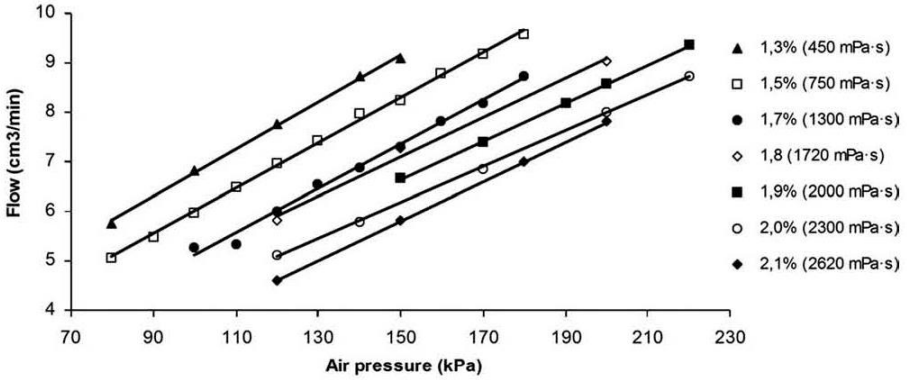

Figure 5. Relation between pressure imposed inside the tank by means of compressed air and the flow of alginate solutions of different concentrations.

waves at the interface grows when exceeding a minimum value and, when becoming large enough, the jet breaks. The expression describing the amplitude of surface waves is:

$$\frac{dA}{dt} = A\left[\frac{\pi\beta\rho_a(U_a - u)^2}{\lambda\rho_1 u} - \frac{8\pi^2\mu_1}{\rho_1\lambda^2}\right] \tag{5}$$

From the expression (5), it can be seen that the amplitude is damped by the viscosity—tending to stabilize the instability—as it increases as the difference between the gas and liquid phases velocities increases.

When the aerodynamic pressure force and the surface tension forces are significant, the velocity of the wave u is given by:

$$u = \left[\frac{a\lambda}{2\pi} + \frac{2\pi\sigma}{\lambda\rho_1}\right]^{1/2} \tag{6}$$

Being the acceleration due to the aerodynamic drag:

$$a = \frac{4C_{Do}\sin^2\zeta}{\pi D\rho_1}\left(\overline{\rho_a}\overline{U_a^2}/2\right) \tag{7}$$

Substituting (6) and (7) in (5):

$$\frac{dA}{dt} = A\left[\frac{\pi\beta\rho_a U_a^2}{\lambda\rho_1\left[\frac{a\lambda}{2\pi} + \frac{2\pi\sigma}{\lambda\rho_1}\right]^{1/2}} - \frac{8\pi^2\mu_1}{\rho_1\lambda^2}\right] \tag{8}$$

From which can be concluded that surface tension and viscosity oppose to the growth of the instability. The minimum wavelength above which the amplitude grows exponentially with time can be determined by $dA/dt = 0$, leading to the expression:

$$\lambda_m^2 - \lambda_a\lambda_m^2 - \lambda_\sigma^2 = 0 \tag{9}$$

$$\text{With}: \frac{\lambda_\sigma}{D} = \frac{2\pi(16)^{1/3}}{\beta^{2/3}}(Z/We)^{2/3} \tag{10}$$

where λ_σ the wavelength of capillary waves

$$\frac{\lambda_a}{D} = \frac{64C_{Do}\sin^2\zeta}{n*\beta^2\pi}(Z^2/We) \tag{11}$$

where λ_a the wavelength of acceleration waves and

$$n* = \rho_a U_a^2/\overline{\rho_a}\overline{U_a^2}$$

the shock dynamic pressure ratio

When aerodynamic pressure forces predominate waves propagate as acceleration waves at a minimum wavelength $(a\lambda_m/2\pi)^{1/2}$. In this case, $\lambda_a \ll \lambda_\sigma$ and the solution of the Eq. 9 is $\lambda_m = \lambda_\sigma$, which is governed by $(Z/We)^{2/3}$.

On the other hand, when the surface tension dominates the waves propagate as capillary waves at a minimum velocity of $(2\pi\sigma/\lambda_m\sigma_1)^{1/2}$. Being thus $\lambda_\sigma << \lambda_a$, a solution for the Eq. 9 is $\lambda_m = \lambda_a$, governed by (Z^2/We).

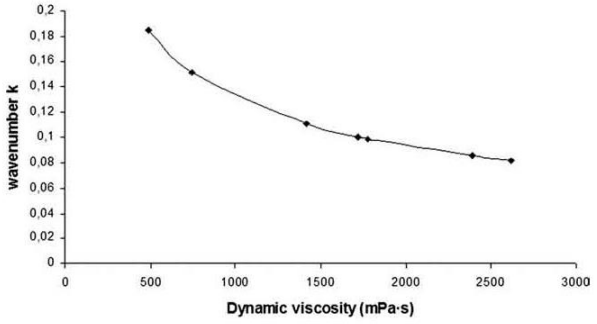

Figure 6. Values of the wavenumber for the different analyzed solutions.

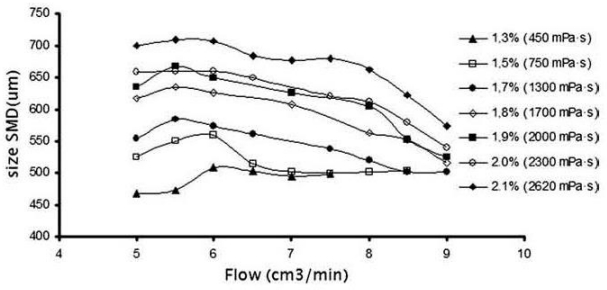

Figure 7. System behavior curves for nine different flows and seven viscosities.

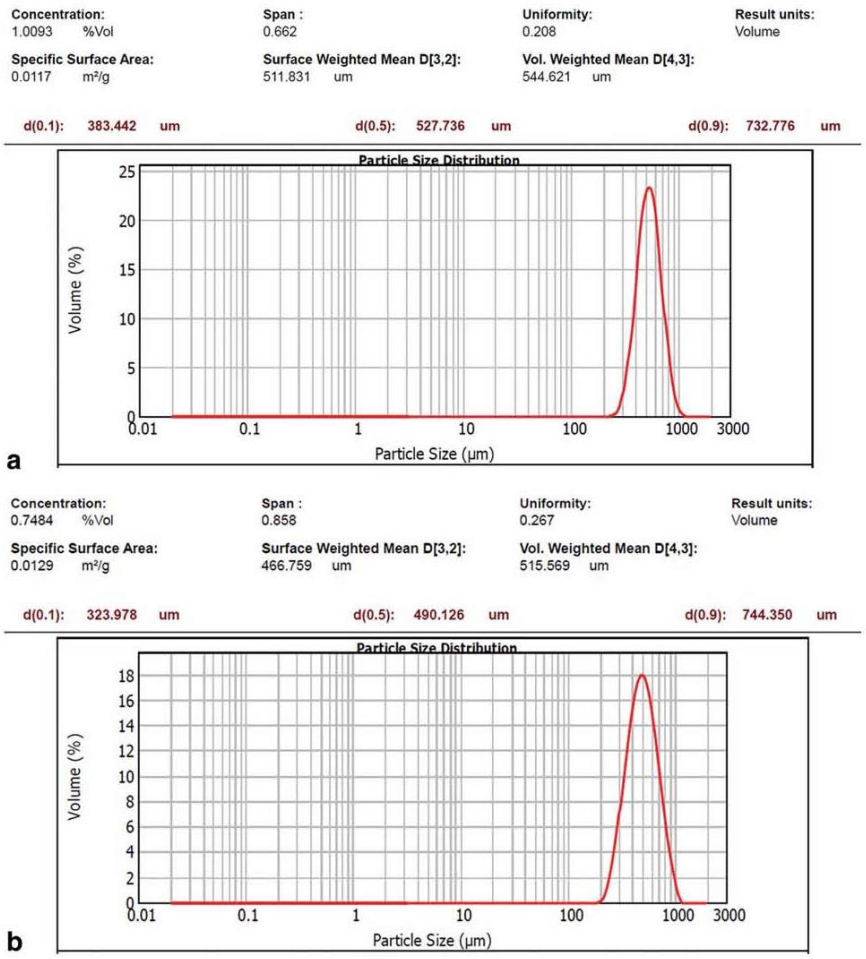

Figure 8. Size distributions (a) for capsules from 1.9% alginate and (b) for capsules from 1.7% alginate, both issuing from a 150 μm nozzle.

[Color figure can be viewed in the online issue, which is available at wileyonlinelibrary.com.]

Summarizing, both dimensionless numbers, *We* and *Z*, have either the same exponents or *Z* exponent is twice that of *We*'s. This is the reason why both will be considered and analyzed through the development of the semi-empirical model.

Set-Up Studies

The new system allowed us to create a continuous jet up to 14,000 mPa s approximately, though for such viscosity values some obstacles affected the system, first difficulties to observe visually the breakup appeared and secondly, the plugging of the nozzle sometimes was becoming a problem after generating such high viscous jets (around 14,000 mPa s) during a long period of time, probably due to solidification of the polymer in the nozzle. The first problem will be solved by acquiring a high speed camera to analyze properly the breakup when increasing the viscosity of the solutions and concerning the plugging we have checked that this effect is well minimized applying ultrasounds and maintaining a proper cleanliness of the nozzle.

Therefore, the viscosity used in the set-up experiments was lowered up to 2620 mPa s, as waiting for the acquisition of a high speed camera which permits the capture of the breakup. In Tables 3 and 4, the experimental conditions are summarized.

The flow tested range from 5 to 9 cm^3/min, which corresponds to the impossibility of creating a steady jet below 5 cm^3/min and the appearance of deformations in the capsules when increasing the flow over 9 cm^3/min, overall for viscosities below 2000 mPa s, due to the high energy in the impact, which will also be named later. On the other hand, the tested viscosities are above 260 mPa s, maximum value that could be processed previously with the commercial device, and below 2700 mPa s due to difficulties described before.

The frequency to be applied can be calculated knowing the physicochemical parameters of the alginate solution, the nozzle diameter, and the jet velocity. In our studies, we have considered the use of Weber equation to determine the optimal wavelength, and then obtaining the frequency to be applied with the velocity of the thread by means of the expressions (3) and (4).

Nozzle flow properties

Depending on the physical properties of the solutions and the air pressure applied to generate the stream, the frequency for the breakup changes, corresponding to the Weber expression shown before (3) and (4).

The flow regime is always laminar and in a jetting mode, not dripping, as Reynolds numbers clearly indicate with very low values, from 0.29 to 2.32, due to the high viscosities.

The liquid flow through the nozzle, this is the jet velocity, is controlled by regulating the pressure inside the pressurized reservoir. The first parameter is determined experimentally, by measuring the amount of alginate collected in a certain period of time and calculating the volumetric flow rate as $F = m/\rho$ (where m is the mass flow rate and ρ the density of the fluid). The velocity of the jet is obtained by the expression $v = F/\pi r^2$ (where r is the jet radius, in our study, it is considered the same as the nozzle radius).

It can be seen in Figure 5, as expected, that an increase in the incoming air pressure is needed in order to provoke an increase in the flow. It is also logic that an increase in the viscosity involves higher air pressures.

Breakup properties

The frequency applied, as mentioned before, corresponds to Weber expressions (3) and (4). It was checked that, for the corresponding values, the breakup always happened, though the wavenumber ranges between 0.082 and 0.18 for the different solutions studied, this is, as Figure 6 shows, increasing the viscosity the wavelength also increases, decreasing the frequency to be applied.

$$k = \frac{2\pi}{\lambda}$$

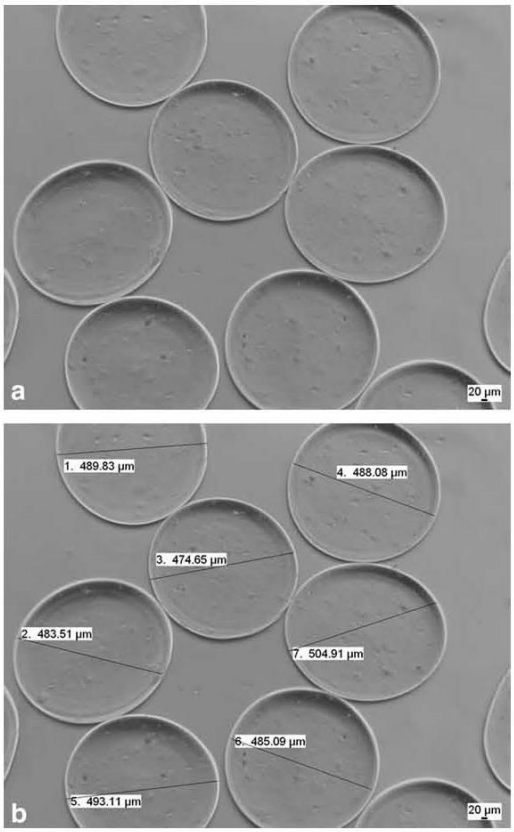

Figure 9. Microphotographs of capsules from alginate 1.8% in concentration (a) as captured from the camera (b) measured by means of the software.

Results and Discussion

Behavior curves

To study the behavior of the system several experiments were carried out, analyzing different flow and viscosity conditions, considering the limitations described previously. Thus, seven viscosities (420–2620 mPa s) and nine different flow regimes (5–9 cm^3/min) were tested, collecting the data in Figure 7, where size is plotted against flow and different behaviors can be distinguished.

From Figure 7, it can be seen as a general behavior that the particle size increases when increasing the viscosity. Observing flows below 6 cm^3/min, the tendency seems to indicate that the particle size increases with the flow, but on the other hand, above 6 cm^3/min we can observe two different behaviors: the first one for solutions with viscosities below 800 mPa s, where the size remains constant as increasing the flow, and second, for solutions with viscosities above 800 mPa s, where the size clearly decreases with the increase of the flow. This latter behavior is the one that we have studied more deeply.

From these results, it can be concluded that the viscosity acts as a stabilizing force, this is it damps the instability out, as it has been reported in several studies. Furthermore, the figure shows a special behavior that clearly differs from other similar studies, this is the decreasing of size when increasing the flow, which proposes the special relevance that pseudoplastic behavior takes in the system. The reason why that performance takes place seems to be the increase of shear stresses in the nozzle when rising the flow, what makes the viscosity of the fluid to decrease, and consequently also the size.

Particle size distribution and image characterization

From the measurements taken by laser diffractometry, the particle size distributions are obtained. The software used gives the span factor of the measured sample, defined as:

$$\text{span factor} = \frac{D_{0.9} - D_{0.1}}{D_{0.5}}$$

where $D_{0.9}$ is the diameter of the 90th percentile, $D_{0.1}$ the diameter of the 10th percentile, and $D_{0.5}$ the diameter of the 50th percentile.

In general, the relative span factor falls within 0.600 and 0.900 as shown in Figure 8.

Several microimages were taken, using the optical microscope DM1000 Leica with an integrated Leica DFC280 camera, to evaluate visually the size and shape of the microparticles. The images were kept by means of

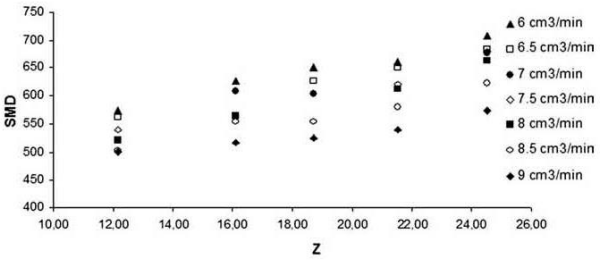

Figure 10. Variation of SMD with Ohnesorge number.

specific Leica IM50 software. An example is shown in Figure 9.

Influence of viscosity on SMD

The liquid properties of the polymer are described by using the Ohnesorge number (Z), which relates the importance of viscous forces to surface tension forces. The Ohnesorge number is expressed by the following equation:

$$Z = \frac{\mu}{\sqrt{\rho \cdot \sigma \cdot D}} \tag{12}$$

Figure 10 collects the experimental SMD values obtained under different Ohnesorge numbers. It can easily be seen that the size increases with the viscosity as shown before. An exponential dependence can be obtained from Figure 11, being the type: SMD = $f(Z^{X_Z})$, obtaining finally SMD = $f(Z^{0.2817})$.

Obtaining a positive dependence of the Ohnersorge number on SMD determines that increasing the affecting properties, in this case, the viscosity (the rest of parameters are considered constant) makes larger the capsules diameter.

Influence of flow on SMD

In a similar way, the flow regime is characterized by the Weber number, which relates inertial forces of the jet with liquid surface tension.

$$We = \frac{\rho \cdot u^2 \cdot D}{\sigma} \tag{13}$$

From Figure 12, it can be seen that the size decreases when increasing the Weber number due to an increase in the flow, as expected and explained in Figure 7.

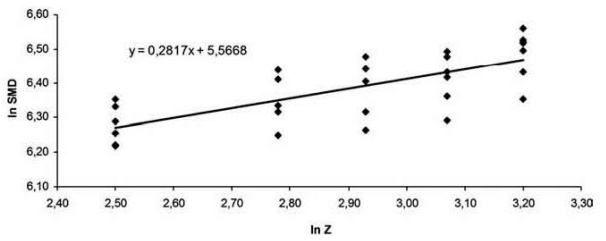

Figure 11. Influence of the Ohnesorge number on the SMD of the microcapsules.

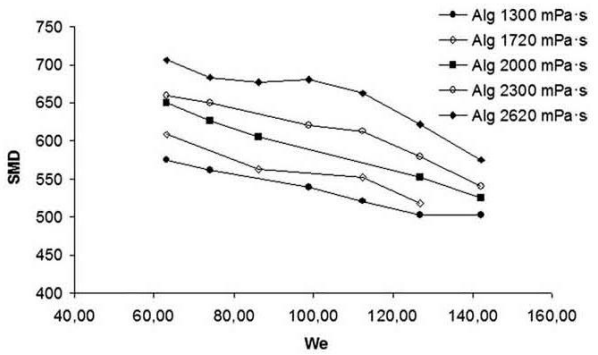

Figure 12. Variation of SMD with Weber number.

Collecting the data, the exponential dependence between Weber number and size can be obtained by the linear expression calculated from Figure 13, obtaining a value: SMD = $f(We^{-0.2247})$.

Obtaining a negative dependence of the Weber number on SMD implies that the higher is the velocity or flow rate of the fluid, the smaller is the capsules size.

Semi-empirical models

As it has been described above, the alginate is a pseudoplastic fluid and this nature seems to become apparent through the behavior that is being studied. However, it has been considered a constant viscosity for each solution, not being the zero shear viscosity or the apparent viscosity for the different flow velocities (with their associated different shear conditions), but a representative value. The reason why the pseudoplastic nature of the polymer has not been taken into consideration for the development of the semi-empirical model is that we first want to check, as a first approach, whether the equations proposed from the wave mechanism, not considering the non-Newtonian terms but a constant viscosity value, agree with our system. Thus, this approach has been considered for us as a first basic knowledge of the behavior of the system.

After the development of this semi-empirical model, we will develop a theoretical analysis in which non-Newtonian terms will be considered and its agreement will be checked also using rheological measurements by means of a rheometer.

Based on wave mechanism theory and selecting from models that Mansour and Chigier[36] propose, the equations collected in Table 5 are studied to determine the agreement with experimental data obtained from this study.

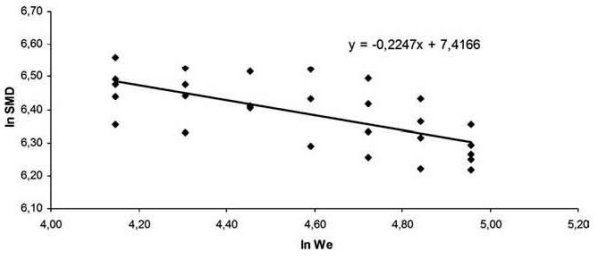

Figure 13. Influence of the Weber number on the SMD of the microcapsules.

Table 5. Proposed Equations to Fit the Data

$$\frac{\text{SMD}}{D} = X_2 We^{-X_1} + X_3 Z^{X_1} + C \quad (14)$$

$$\frac{\text{SMD}}{D} = X_2 We^{-X_1} + X_3 Z^{2X_1} + C \quad (15)$$

$$\frac{\text{SMD}}{D} = X_2 \left(\frac{Z}{We}\right)^{X_1} \quad (16)$$

For Eqs. 17 and 19 both dimensionless numbers have same exponent values, as described before this implies that waves propagate as acceleration waves, predominating aerodynamic pressure forces.

In the case of (18), exponent X_Z is double than exponent X_{We}, which means that surface tension forces predominate, hence the waves propagate as capillary waves.

After substituting the exponential dependence values: $\text{SMD} = f(Z)^{0.2817}$ and $\text{SMD} = f(We)^{-0.2247}$ as well as considering the correlation exponent X_1 by calculating its mean value: $X_1 = (0.2817 + 0.2247)/2 = 0.2532$, according to the experimental data, the unknown coefficients X_2, X_3 in proposed Eqs. 17–19 are calculated through multiple linear regression analysis obtaining the values shown in Table 6 and the equations below

Table 6. Unknown Coefficients for the Eqs. 17–19

	X_2	X_3	C
Equation 17	10.6210	2.0898	−3.7324
Equation 18	10.6203	0.5077	−1.5909
Equation 19	6.0474	–	–

$$\frac{\text{SMD}}{D} = 10.6210 \cdot We^{-0.2532} + 2.0898 \cdot Z^{0.2532} - 3.7324 \quad (17)$$

$$\frac{\text{SMD}}{D} = 10.6203 \cdot We^{-0.2532} + 0,5077 \cdot Z^{0.5064} - 1.5909 \quad (18)$$

$$\frac{\text{SMD}}{D} = 6.0474 \cdot \left(\frac{Z}{We}\right)^{0,2532} \quad (19)$$

Comparison between the experimental size of microparticles and the predicted size by the model

A set of experiments is carried out to compare the experimental data with those predicted by the equations obtained from the

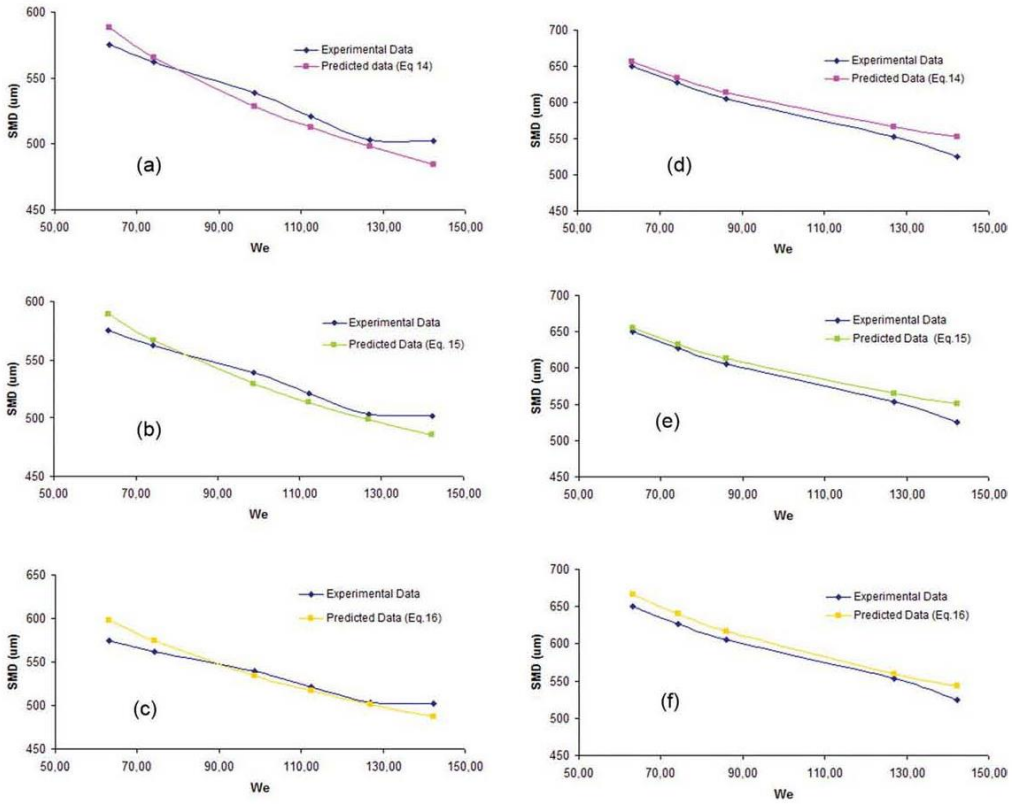

Figure 14. Comparison between experimental and predicted sizes.

[Color figure can be viewed in the online issue, which is available at wileyonlinelibrary.com.]

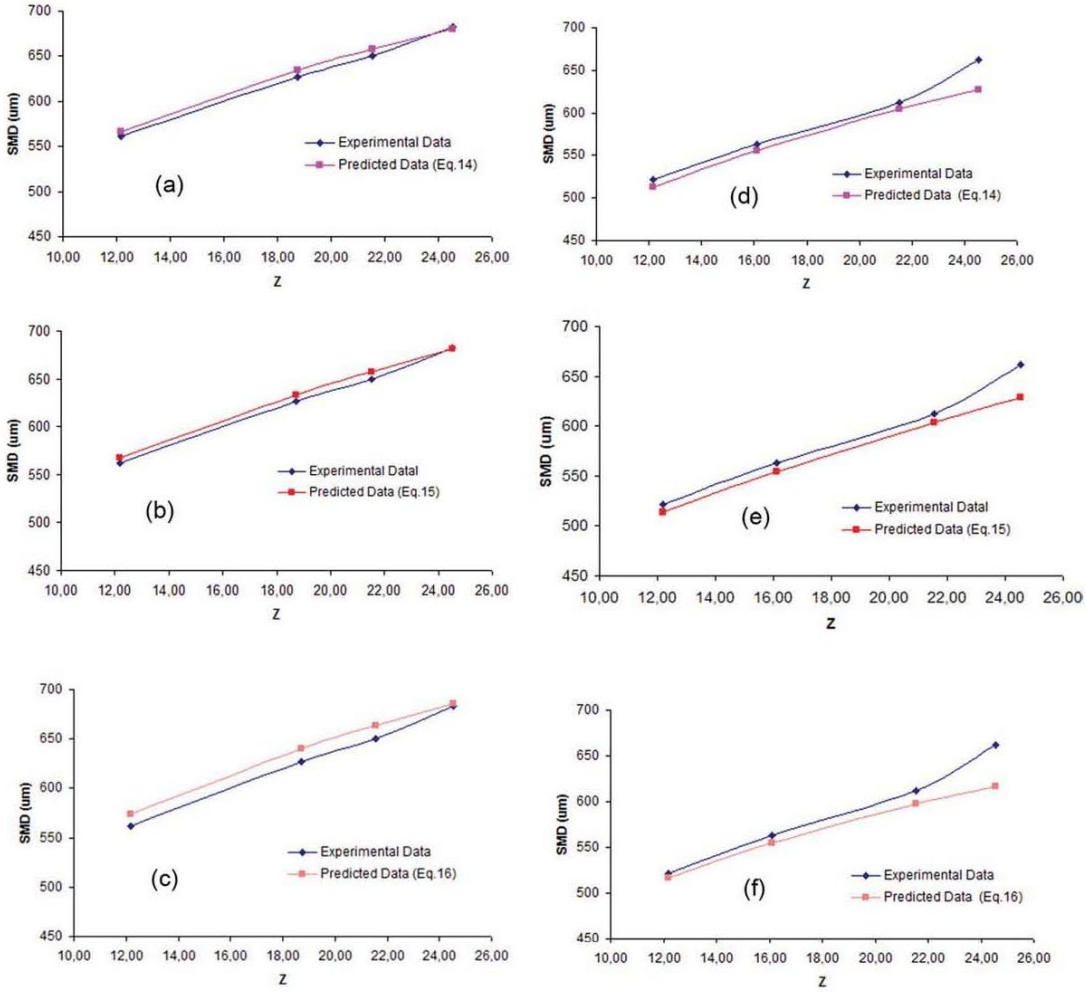

Figure 15. Comparison between experimental and predicted sizes.

At a constant flow of 6.5 cm^3/min (a–c). At a constant flow of 8 cm^3/min (d–f). [Color figure can be viewed in the online issue, which is available at wileyonlinelibrary.com.]

wave mechanism theory. First set of data is taken at constant value for the viscosity for different flows, this is variable Weber, in Figure 14.

A second set of comparative data is taken at constant flow—Weber—and different viscosities, this is variable Ohnesorge, as shown in Figure 15.

In general, it can be concluded that all three proposed equations predict microparticle size with a good agreement with the experimental data, though finding some deviations under certain conditions described next.

After analyzing the value of errors for the different data, it can be observed that the dispersion in the data is wider for the highest flows and the fitting of predicted data is consequently worse than considering medium flow values. That is due to the high energy when capsules impact in the hardening solution, provoking their deformation and reducing the reliability of measurements, increasing errors, as shown in Figures 16a–c.

Second, errors can also be observed for the highest of the viscosity analyzed, 2620 mPa s, what can be produced due to the difficulty to observe visually the breakup of the jet, probably incurring in the use of non optimal breakup frequencies, which leads to heterodispersion, producing higher errors as shown in Figures 16d–f.

Hence, it can be finally concluded that all three equations acceptably predict, under our study conditions, the size of particles. Errors between experimental and predicted size are collected in Table 7. Thus, it seems to be demonstrated that wave mechanism, accepted for non-Newtonian liquids atomization, can also be applied to the new system developed, which allows relating some basic physical parameters through these semi-empirical equations, acquiring a better knowledge of the process.

Conclusions

This study reports the development of a new technology able to generate polymeric microparticles, ranging from 300 to 700 μm in size with high monodispersión, from high viscous polymers. From the experiments here reported, it can be concluded that the new technology developed succeeded in working with high

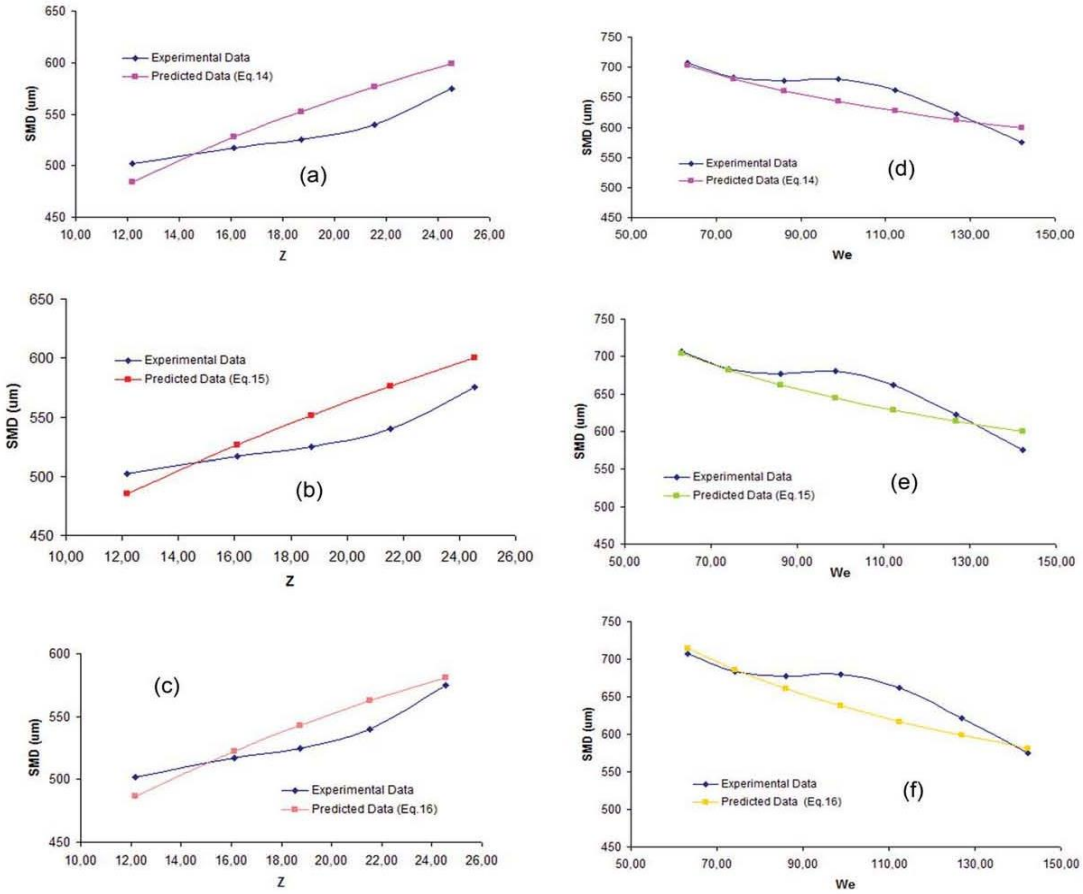

Figure 16. Comparison between experimental and predicted sizes.

Deviations (a–c) at a constant flow of 9 cm^3/min. At a constant viscosity of 2620 mPa s (d–f). [Color figure can be viewed in the online issue, which is available at wileyonlinelibrary.com.]

viscous solutions, creating continuous jets up to 14,000 mPa s. We also verified the stabilizing behavior of the viscosity, as expected, and the special relevance of the pseudoplasticity of alginate.

Besides the development and characterization of the system, a semi-empirical model stemming from the wave mechanism theory has been developed to predict microparticle size. It has been concluded that the obtained equations predict the size of particles acceptably, demonstrating that wave mechanism, accepted for non-Newtonian liquids atomization, can also be applied to the new system developed.

Table 7. Error Values Between Experimental and Predicted Size Using the Semiempirical Equations

	Equation 17	Equation 18	Equation 19
Lowest error (%)	0.14	0.17	0.17
Highest error (%)	6.71	6.65	6.78
Average error (%)	2.25	2.17	2.36

Acknowledgments

This research was supported by funds from the Ministerio de Ciencia e Innovación (Spain), project CTQ2009-08222 (PPQ subprogram). Cristina Rodríguez is also supported by a F.P.U. grant from the Ministerio de Ciencia y Innovación (Spain). This grant is also appreciated by the author.

Notation

A = amplitude of the surface disturbance
C_{Do} = Drag coefficient of a cylinder in cross flow
D or d = jet diameter, considered the same as jet nozzle
F = volumetric flow rate
f = frequency of the disturbance
k = wavenumber
m = liquid mass flow rate
U = air average velocity
u = velocity of the wave
v = velocity of the liquid
We = Weber number
Z = Ohnesorge number
X_{We} = power dependence of SMD on Weber number
X_Z = power dependence of SMD on Ohnesorge number
X_1 = general correlation exponent
$X_{2,3}$ = general correlation coefficients

Greek letters

β = Jeffrey's sheltering parameter
λ = wavelength
ρ = density of the jet
σ = surface tension
ζ = angle between the jet axis and gas
μ = dynamic viscosity

Literature Cited

1. Gouin S. Microencapsulation: industrial appraisal of existing technologies and trends. *Trends Food Sci Technol*. 2004;15:330–347.
2. Hernández RM, Orive G, Murua A, Pedraz JL. Microcapsules and microcarriers for in situ cell delivery. *Adv Drug Delivery Rev*. 2010;62:711–730.
3. Chang TMS, Prakash S. Therapeutic uses of microencapsulated genetically engineered cells. *Mol Med Today*. 1998;4(5):221–227.
4. Venkatesan P, Manavalan R, Valliappan K. Microencapsulation: a vital technique in novel drug delivery system. *J Pharm Sci Res*. 2009;1:26–35.
5. Teramura Y, Iwata H. Bioartificial pancreas. Microencapsulation and conformal coating of islet of Langerhans. *Adv Drug Delivery Rev*. 2010;62:827–840.
6. Peirone M, Ross CJD, Hortelano G, Brash JL, Chang PL. Encapsulation of various recombinant mammalian cell types in different alginate microcapsules. *J Biomed Mater Res*. 1998;42:587–596.
7. Koch S, Schwinger C, Kressler J, Heinzen C, Rainov NG. Alginate encapsulation of genetically engineered mammalian cells: comparison of production devices, methods and microcapsule characteristics. *J Microencapsul*. 2003;20:303–316.
8. Poncelet D. *Microencapsulation: fundamentals, methods and applications*. In: Blitz J, Gun'ko V, editors. *Surface Chemistry in Biomedical and Environmental Science*. The Netherlands: Springer, 2006:23–34.
9. DeGroot AR, Neufeld RJ. Encapsulation of urease in alginate beads and protection from α-chymotrypsin with chitosan membranes. *Enzyme Microb Technol*. 2001;29:321–327.
10. Senuma Y, Lowe C, Zweifel Y, Hilborn JG, Marison I. Alginate hydrogel microspheres and microcapsules prepared by spinning disk atomization. *Biotechnol Bioeng*. 2000;67:616–622.
11. Prüsse U, Bruske F, Breford J, Vorlop KD. Improvements to the jet cutting process for manufacturing spherical-particles from viscous polymer solutions. *Chem Ing Technol*. 1998;70:556–560.
12. Plateau J, editor. *Statique expérimentale et théorique des liquides soumis aux seules forces moléculaires*. Paris: Gauthier-Villars, 1873.
13. Rayleigh L. On the capillary phenomena of jets. *Proc R Soc London*. 1879;29:71–97
14. Bousfield DW, Stockel IH, Nanivadekar CK. The breakup of viscous jets with large velocity modulations. *J Fluid Mech*. 1990;218:601–617.
15. Chaudhary KC, Redekopp LG. The nonlinear capillary instability of a liquid jet, part 1. Theory. *J Fluid Mech*. 1980;96:257–274.
16. Rutland DF, Jameson GJ. Theoretical prediction of the sizes of drops formed in the breakup of capillary jets. *Chem Eng Sci*. 1970; 25:1689–1698.
17. Berkland C, Kim K, Pack DW. Fabrication of PLG microspheres with precisely controlled and monodisperse size distributions. *J Controlled Release*. 2001;73:59–74.
18. Chandrasekhar S, editor. *Hydrodynamic and Hydromagnetic Stability*. Oxford: The Clarendon Press, 1961.
19. Zeleny J. On the conditions of instability of electrified drops, with applications to the electrical discharge from liquid points. *Proc Cambridge Philos Soc*. 1915;18:71–83
20. Zeleny J. Instability of electrified liquid surfaces. *Phys Rev*. 1917; 10(1):1–6.
21. Heinzl J, Hertz CH. *Ink-jet printing*. In: Hawkes PW, editor. *Electronics and Electron Physics*, Vol. 65. Orlando, Florida: Academic Press, Inc., 1985:91–166.
22. Brandenberger H, Widmer F. A new multinozzle encapsulation/immobilisation system to produce uniform beads of alginate. *J Biotechnol*. 1998;63:73–80.
23. Brenn G, Helpio T, Durst F. A new apparatus for the production of monodisperse sprays at high flow rates. *Chem Eng Sci*. 1997; 52:237–244.
24. Wissema JG, Davies GA. The formation of uniformly sized drops by vibration-atomization. *Can J Chem Eng*. 1969;47:530–535.
25. Moghadam H, Samimi M, Samimi A, Khorram M. Electro-spray of high viscous liquids for producing mono-sized spherical alginate beads. *Particuology*. 2008;6:271–275.
26. Watanabe H, Matsuyama T, Yamamoto H. Experimental study on electrostatic atomization of highly viscous liquids. *J Electrostat*. 2003;57:183–197.
27. ISP Pharmaceuticals, Inc. Alginate for Pharmaceutical and Medical Applications. *Performance Enhancing Products. ISP Pharmaceuticals Product Guide*. USA. 2008.
28. Herrero EP, Valle EMMD, Galán MA. Development of a new technology for the production of microcapsules based in atomization processes. *Chem Eng J*. 2006;117:137–142.
29. Del Gaudio P, Colombo P, Colombo G, Russo P, Sonvico F. Mechanisms of formation and disintegration of alginate beads obtained by prilling. *Int J Pharm*. 2005;302:1–9.
30. Seifert DB, Phillips JA. Production of small, monodispersed alginate beads for cell immobilization. *Biotechnol Prog*. 1997; 13:562–568.
31. Lefebvre AH, editor. *Atomization and Sprays*. New York: Hemisphere Publishing Corporation, 1989.
32. Weber C. Zum Zerfall eines Flüssigkeitsstrahls. Zeit für angewandte Mathematik und Mechanik. 1931;11:136–141.
33. Hanif H. *Formation and Break Up of Microscale Liquid Jets*. Georgia Institute of Technology, 2009.
34. Chigier N, editor. *Spray Technology Short Course*. Pittsburgh, Pensylvania: Carnegie Mellon University, 1995.
35. Adelberg M. Breakup rate and penetration of a liquid jet in a gas stream. *AIAA J*. 1967;5:1408–1415.
36. Mansour A, Chigier N. Air-blast atomization of non-Newtonian liquids. *J Non-Newtonian Fluid Mech*. 1995;58:161–194.
37. Adelberg M. Mean drop size resulting from the injection of a liquid jet into a high-speed gas stream. *AIAA J*. 1968;6:1143–1147.
38. Jeffreys H. On the formation of water waves by wind. *Proc R Soc London, Ser A*. 1925;107:189–206.
39. Mayer E. Theory of Liquid Atomization in Hugh Velocity Gas Streams. *ARS J*. 1961;31(12):1783–1785.

Manuscript received Oct. 15, 2010, and revision received Jan. 3, 2011.

4.9. Conclusions extracted from the published work

This study reports the development of a new technology able to generate polymeric microparticles from high viscous polymers ranging from 300 to 700 microns in size with high monodispersion. From the experiments here reported it can be concluded that the new technology developed succeeded in processing high viscous solutions, creating continuous jets up to 14000 mPa·s. We also verified the stabilizing behavior of the viscosity, as expected, and the special relevance of the pseudoplasticity of alginate.

Besides the development and characterization of the system a semiempirical model stemming from the wave mechanism theory has been developed in order to predict microparticle size. It has been concluded that the obtained equations predict acceptably the size of particles, demonstrating that wave mechanism, accepted for non-Newtonian liquids atomization, can also be applied to the new system developed.

4.10. Conclusions from the Chapter in this thesis

Through this chapter the behaviour of a new technique designed to generate polymeric microparticles from medium-high viscosity polymers has been studied.

From the set-up experiments it can be concluded that the new developed technology succeeded in processing high viscous solutions, creating continuous jets up to 10000 mPa·s.

The effect of key parameters such as viscosity and flow rate were analysed through the generation of behavioural curves. The stabilizing behavior of the viscosity was easily observed. However, the effect of flow rate posed certain questions, highlighting the special relevance of shear and extensional effects on the rheology of alginate for further considerations.

Finally, a semiempirical model stemming from the wave mechanism theory was assessed as tool for the prediction of microparticle size. It was concluded that the obtained semiempirical equations acceptably predict the size of particles under certain conditions, namely for viscosities above 1500 mPa·s. However, particularly one of the two proposed expressions shows a good agreement under all tested conditions. This demonstrates that

the wave mechanism, accepted for non-Newtonian liquids atomization, can be also applied to the new developed system.

Finally, the effect of the frequency, which could not be concluded by the studies in this chapter, should be further addressed. It is known that it affects the droplet size. Moreover, another important characteristic parameter of the breakup process is the breakup length. These effects and parameters cannot be studied by naked-eye inspection due to the magnitudes given in the process and high-speed imaging techniques should be used instead.

These issues will be addressed in the following chapters.

4.11. References

Adelberg M (1967) Breakup rate and penetration of a liquid jet in a gas stream. AIAA J 5:1408-1415

Adelberg M (1968) Mean drop size resulting from the injection of a liquid jet into a high-speed gas stream. AIAA J 6:1143-1147

Ashgriz N, Yarin AL (2011) Capillary Instability of Free Liquid Jets. In: Ashgriz N (ed) Handbook of Atomization and Sprays. Springer.

Baumgarten C (2006) Fundamentals of Mixture Formation in Engines. In: Mixture Formation in Internal Combustion Engine. Heat, Mass Transfer. Springer Berlin Heidelberg, pp 5-46. doi:10.1007/3-540-30836-9_2

Bogy DB (1979) Drop Formation in a Circular Liquid Jet. Annual Review of Fluid Mechanics 11 (1):207-228. doi:10.1146/annurev.fl.11.010179.001231

Brandenberger H, Widmer F (1998) A new multinozzle encapsulation/immobilisation system to produce uniform beads of alginate. Journal of Biotechnology 63 (1):73-80. doi: 10.1016/s0168-1656(98)00077-7

Brandenberger HR, Widmer F (1999) Immobilization of Highly Concentrated Cell Suspensions Using the Laminar Jet Breakup Technique. Biotechnology Progress 15 (3):366-372. doi:10.1021/bp990033m

Brenn G, Liu Z, Durst F (2000) Linear analysis of the temporal instability of axisymmetrical non-Newtonian liquid jets. International Journal of Multiphase Flow 26 (10):1621-1644. doi: 10.1016/s0301-9322(99)00115-9

Chigier NA, Reitz RD (1996) Regimes of jet breakup and breakup mechanisms. In: Kuo K (ed) Progress in Astronautics and Aeronautics, vol 1. pp 109–136

Goedde EF, Yuen MC (1970) Experiments on liquid jet instability. Journal of Fluid Mechanics 40 (03):495-511. doi:10.1017/S0022112070000289

Goldin M, Yerushalmi J, Pfeffer R, Shinnar R (1969) Breakup of a laminar capillary jet of a viscoelastic fluid. Journal of Fluid Mechanics 38 (04):689-711. doi:10.1017/S0022112069002540

Haas PA (1992) Formation of uniform liquid drops by application of vibration to laminar jets. Industrial & Engineering Chemistry Research 31 (3):959-967. doi:10.1021/ie00003a043

Hartman RPA, Brunner DJ, Camelot DMA, Marijnissen JCM, Scarlett B (1999) Electrohydrodynamic atomization in the cone–jet mode physical modeling of the liquid cone and jet. Journal of Aerosol Science 30 (7):823-849. doi:http://dx.doi.org/10.1016/S0021-8502(99)00033-6

Herrero EP, Del Valle EMM, Galán MA (2006) Modelling prediction of the microcapsule size of polyelectrolyte complexes produced by atomization. Chemical Engineering Journal 121 (1):1-8. doi: 10.1016/j.cej.2006.04.003

Jasuja AK (1982) Plain-jet airblast atomization of alternative liquid petroleum fuels under high ambient air pressure conditions. ASME 82-GT-32

Jeffreys H (1980) On the formation of water waves by wind. Proc Roy Soc Lond A 107:189

Kurabayashi T (1959) Atomization of liquid by means of rotating nozzle. Trans Jpn Soc Mech Eng 25 (160):1266-1273

Lee A, Sudau K, Ahn KH, Lee SJ, Willenbacher N (2012) Optimization of Experimental Parameters to Suppress Nozzle Clogging in Inkjet Printing. Industrial & Engineering Chemistry Research 51 (40):13195-13204. doi:10.1021/ie301403g

Lefebvre AH (ed) (1989) Atomization and Sprays. Hemisphere Publishing Corporation, New York

Lin SP, Reitz RD (1998) Drop and spray formation from a liquid jet. Annual Review of Fluid Mechanics 30 (1):85-105. doi:10.1146/annurev.fluid.30.1.85

Lorenzetto GE, Lefebvre AH (1977) Measurements of drop size on a plain jet airblast atomizer. AIAA J 15:1006-1010

Mansour A, Chigier N (1995) Air-blast atomization of non-Newtonian liquids. Journal of Non-Newtonian Fluid Mechanics 58:161-194

Mayer E (1961). ARS J 31:1783-1785

Merrington AC, Richardson EG (1947) The break-up of liquid jets. Proceedings of the Physical Society 59 (1):1

Moghadam H, Samimi M, Samimi A, Khorram M (2008) Electro-spray of high viscous liquids for producing mono-sized spherical alginate beads. Particuology 6 (4):271-275. doi: 10.1016/j.partic.2008.04.005

Moghadam H, Samimi M, Samimi A, Khorram M (2009) Study of Parameters Affecting Size Distribution of Beads Produced from Electro-Spray of High Viscous Liquids. Iranian Journal of Chemical Engineering 6 (3 (Summer)):88-98

Ohnesorge WV (1936) Die Bildung von Tropfen an Düsen und die Auflösung flüssiger Strahlen. ZAMM - Journal of Applied Mathematics and Mechanics / Zeitschrift für Angewandte Mathematik und Mechanik 16 (6):355-358. doi:10.1002/zamm.19360160611

Pan Y, Suga K (2006) A numerical study on the breakup process of laminar liquid jets into a gas. Physics of Fluids 18 (5):052101

Plateau J (ed) (1873) Statique expérimentale et théorique des liquides soumis aux seules forces moléculaires. Gauthier-Villars, Paris

Rajagopalan R, Tien C (1973) Production of mono-dispersed drops by forced vibration of a liquid jet. The Canadian Journal of Chemical Engineering 51 (3):272-279. doi:10.1002/cjce.5450510302

Rayleigh L (1879) On the capillary phenomena of jets. Proc R Soc London 29

Rayleigh L (1892) XVI. On the instability of a cylinder of viscous liquid under capillary force. Philosophical Magazine Series 5 34 (207):145-154. doi:10.1080/14786449208620301

Reitz RD, Bracco FV (1986) Mechanisms of breakup of round liquids jets. In: Cheremisnoff N (ed) The encyclopedia of Fluid Mechanics. pp 233-249

Risk NK, Lefebvre AH (1984) Spray Characteristics of plain-jet airblast atomizers. Trans ASME J Eng Gas Turbines Power 106:639-644

Rodríguez-Rivero C, Del Valle EMM, Galán MA (2011) Development of a new technique to generate microcapsules from the breakup of non-Newtonian highly viscous fluid jets. AIChE Journal 57 (12):3436-3447. doi:10.1002/aic.12549

Savart F (1833) Mémoire sur la constitution des veines liquides lancées par des orifices circulaires en mince paroi. Annali di Chimica 53:337-386

Schneider JM, Hendricks CD (1964) Source of Uniform-Sized Liquid Droplets. Review of Scientific Instruments 35 (10):1349-1350. doi:10.1063/1.1718742

Sterling AM, Sleicher CA (1975) The instability of capillary jets. Journal of Fluid Mechanics 68 (03):477-495. doi:10.1017/S0022112075001772

Weber C (1931) Zum Zerfall eines Flüssigkeitsstrahls. Zeit für angewandte Mathematik und Mechanik. 11:136

Wissema JG, Davies GA (1969) The formation of uniformly sized drops by vibration-atomization. The Canadian Journal of Chemical Engineering 47 (6):530-535. doi:10.1002/cjce.5450470609

CHAPTER 5.

PHYSICAL STUDY.

5. PHYSICAL STUDY

As it has been mentioned in previous chapters this work deals with the analysis of a technique to generate biocompatible microparticles from the controlled capillary instability of medium-high viscosity polymeric jets.

This chapter addresses in particular a deeper analysis of the physical process of the instability in sodium alginate solutions, attempting to tackle certain concerns that were extracted in the conclusions of C*hapter 4: Preliminary studies* about the new developed technique.

It was firstly concluded that the effect of shear and extensional rates may be having an influence in the behaviour of the jet when the flow rate and viscosity change. This leads to the need of a deeper rheological characterization of the samples.

In a second instance, the lack of techniques to analyse the influence of the frequency on the microparticle formation pointed out the need of tracking the evolution of the instability and breakup of the polymeric jets. Thus, the use of a high speed visualisation technique allows studying the effect of the applied frequency in the shape of the jet, droplets and breakup length.

Finally, a mathematical model is proposed in order to characterize theoretically the process. To this end, a linear temporal model leads to an expression that relates wave parameters – wavenumber – to the growth rate of the wave. It allows comparing experimental and theoretical optimal frequency data to check the theoretical model.

5.1. Fluid rheology

For understanding the flow behaviour of the polymer it is very important to tackle the analysis of the rheology of the solutions.

The nature and flow properties of fluids can be investigated through *rheology*, which is defined as the science of the deformation and flow of matter. A basic introduction about the discipline of rheology is reviewed next.

Most of encountered fluids in physical and industrial processes, namely polymers, behave as non-Newtonian (Chhabra and Richardson 2008). Non-Newtonian fluids are those that do not follow the Newton's model. This model is mathematically described by (5.1):

$$\frac{F}{A} = \tau_{yx} = \mu\left(-\frac{dV_x}{dy}\right) = \mu\dot{\gamma}_{yx} \qquad (5.1)$$

This law stands that the shear stress is proportional to the shear rate for a Newtonian fluid in a streamline flow (see Figure 5.1).

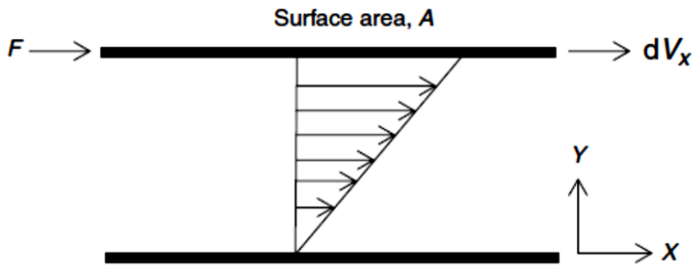

Figure 5.1: Application of shear force to a fluid.

By definition, a Newtonian fluid is that in which the value of μ is independent of the shear rate $\dot{\gamma}_{yx}$, and it depends only on temperature and pressure. The constant of proportionality μ is a characteristic property of each substance and it is known as Newtonian viscosity, shear viscosity, dynamic viscosity, or simply viscosity.

If shear stress τ_{yx} is plotted against shear rate $\dot{\gamma}_{yx}$ for a Newtonian fluid, a straight line of slope μ that passes through the origin is obtained. These representations - τ_{yx} vs $\dot{\gamma}_{yx}$ - are known as flow curves or rheograms (see Figure 5.2). Thus, the viscosity μ completely characterizes the flow behaviour of a Newtonian fluid at a fixed temperature and pressure (Macosko 1994).

A fluid is called Non-Newtonian when its flow curve is nonlinear or it is linear but it does not pass through the origin (see Figure 5.2). Then, its viscosity is not constant at a given temperature and pressure and it exhibits non equal and nonzero normal stress in

simple shear flow. Thus, the magnitude of the viscosity depends on flow conditions, such as flow geometry, applied stress, time of shearing, kinematic history of the sample, etc, (Chhabra and Richardson 2008).

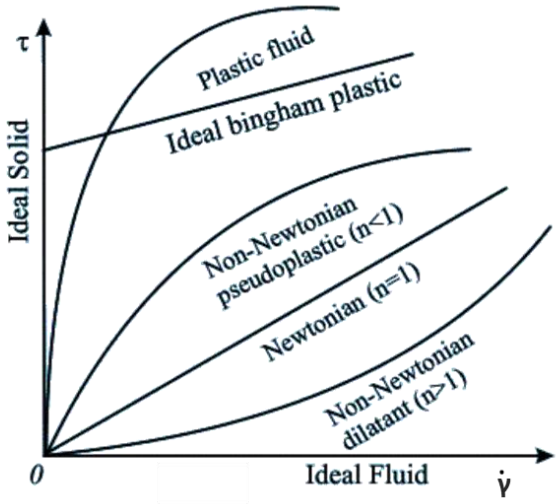

Figure 5.2: Schematic flow curves for Newtonian and non-Newtonian fluids.

The non-Newtonian fluid behaviour is generally classified into three general categories as (Barnes 2000):

1. Purely viscous, time-independent, or generalized Newtonian fluids (GNF): the shear rate is dependent only on the value of the shear stress. A generalized Newtonian fluid is defined by its independence on the second invariant of the rate of deformation tensor. Among them, a subdivision can be made: shear-thinning or pseudoplastics, visco-plastics and shear-thickening or dilatant.

2. Time-dependent systems: the relation between the shear stress and the shear rate also depends on the duration of shearing, the previous kinematic history, etc. They can be thixotropic or rheopectic.

3. Viscoelastic fluids: present characteristics of both an elastic solid and a viscous fluid. They show partial elastic and recoil recovery after deformation.

Most materials display a combination of two or even all the three types of non-Newtonian characteristics, but in general one of the three types can be extracted as dominant and allows studying the material in such way.

Shear and extensional flow have a different influence in the material behaviour. This is due to the relative movement of the molecules under these different types of flows.

In shear flows liquid elements flow *over* or *past* each other, while in extensional flow, adjacent elements flow *towards* or *away from* each other (Barnes 2000).

The simplest form of extensional flow is the uniaxial flow, in which the material is stretched in one direction, corresponding with size reduction in the other directions as shown in Figure 5.3.

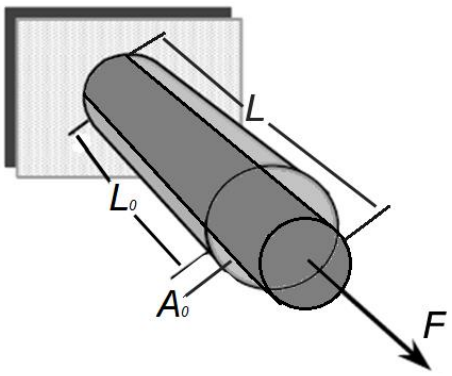

Figure 5.3: Application of axial force to a fluid (Barnes 2000).

This type of uniaxial flow can be found in several situations such as flow in and out orifices, dies, atomization, suction, molding by compression, injection, extrusion and flow through porous means (Chhabra and Richardson 2008). Blow molding, fiber spinning, thermoforming, and film blowing are all commercial polymer forming operations with strong extensional flow fields.

Similarly to the depiction used in shear flow, the uniaxial extensional flow is described by the extensional stress (σ_e), Hencky strain (ε_h), extensional velocity from the flow velocity gradient (extensional strain rate) and the uniaxial extensional viscosity (η_e) (Steffe 1992).

The true or Hencky strain, ε_h, when the specimen with an initial length L_0 is extended to a length L, is defined as:

$$\varepsilon_h = \int_{L_0}^{L} \frac{dL}{L} = \ln \frac{L}{L_0} \qquad (5.2)$$

The extensional velocity or strain rate is defined from the Hencky strain as:

$$\dot{\varepsilon}_h = \frac{d\varepsilon_h}{dt} = \frac{1}{L}\frac{dL}{dt} \qquad (5.3)$$

The extensional stress is defined as the force by area unit as:

$$\sigma_e = \frac{FL}{A_0 L_0} \qquad (5.4)$$

5.1.1. Polymer rheology and jet breakup

Polymers behave as non-Newtonian fluids, showing in most cases viscoelasticity, with partial elastic and recoil recovery after deformation (Muller and Davidson 1994). This will determine the evolution of polymeric jets.

Middleman (Middleman 1965), Goldin (Goldin et al. 1969) or Bousfield (Bousfield et al. 1986) were authors that first studied the breakup of viscoelastic fluids. From their works and more recent studies (Yarin 1993; Christanti and Walker 2001) differences between the breakup of viscoelastic and Newtonian fluids are defined. These can be summarized in:

- A delay for the onset of the disturbance growth.
- A faster disturbance growth, enhanced compared to Newtonian fluids with same Ohnesorge number.
- A retarded and lengthened breakup length due to extensional stresses.

Thus in general the patterns of deformation differ. This means that the viscoelastic fluids show a different response and consequently different relationships and characteristic parameters describe their behaviour.

Therefore, complex constitutive equations are needed in order to study the response of the fluids under the application of external stresses. A constitutive equation or rheological equation of state is an expression that relates stress and deformation variables. They may be derived from a microscale perspective – i.e. solvent and polymer molecules as distinct entities - or from a continuum (macroscopic) point of view – i.e. polymer solution treated as a homogeneous continuum- (Barnes 2000).

One of the general linear viscoelastic fluid constitutive equations is known as Maxwell model (Bird et al. 1987), where time constants such as the called "relaxation time"- λ_1 in the following expression - come into play:

$$\boldsymbol{\tau}_{yx} + \lambda_1 \frac{\partial}{\partial t} \boldsymbol{\tau}_{yx} = -\eta_0 \dot{\boldsymbol{\gamma}}_{yx} \qquad (5.5)$$

More characteristic times take place when the complexity of the relationships increases. These parameters give information about the extent to which the molecules are able to change or rearrange their configuration after external applied forces cease (Bird et al. 1987).

These temporal parameters have been taken into account for the characterization of the samples in this study. Furthermore, they will be necessary for the mathematical model.

5.2. Sodium alginate in salt-free solutions rheology

The characterization of the commercial sodium alginate solutions used in the analysis is detailed along the next sections.

The specific product used in this work was medium viscosity alginic acid sodium salt from brown algae purchased to Sigma-Aldrich. The salt contains approximately 61% mannuronic and 39% guluronic acid - M/G ratio of 1.56 - and a molecular weight ranges between 80-120 kg/mol.

The solutions are obtained as detailed in *Chapter 4*. The alginate salts were dissolved in ultrapure water (salt-free solutions) under stirring for 1.5 hours keeping similar rotation conditions (500 to 2000 rpm), obtaining solutions with pH 7 (± 0.5).

Haug et al (Haug and Smidsrød 1962) examined solutions of polyelectrolytes in water and reported that the viscosity is not affected for pH between 4 and 12.

Given the fact that the polymer solutions are subjected to both shear and extensional flow fields, three main characterizations were done: determination of intrinsic viscosity, simple shear properties and uniaxial extensional properties.

The instruments used for the characterization of the aforementioned properties were capillary viscometer and controlled stress rotational rheometer (simple shear) and Capillary Breakup Extensional rheometer –CaBER - respectively.

5.2.1. Determination of intrinsic viscosity and concentration regimes

The intrinsic viscosity [η] provides information about the interaction between solute and solvent. It is defined as the solute ability of isolated polymer molecule to increase the solvent viscosity (Marani et al. 2013). It does not have the units of absolute viscosity but rather dL/g, essentially representing the volume occupied by the solute per unit mass of solute.

Expressions (5.6) and (5.7) define [η] and what is known as specific viscosity, η_{sp}, where η_0 is the solution zero-shear viscosity, $\eta_{solvent}$ is the solvent Newtonian viscosity, η_{sp} is the specific viscosity, η_r is the relative viscosity, c the solution concentration and η_{sp}/c the reduced viscosity.

$$[\eta] = \lim_{c \to 0} \frac{\eta_{sp}}{c} \qquad (5.6)$$

$$\eta_{sp} = \frac{\eta_0 - \eta_{solvent}}{\eta_{solvent}} = \eta_r - 1 \qquad (5.7)$$

[η] must be determined by extrapolation to zero concentration, as defined by (5.6). For that purpose the viscosity of solutions from 0.01 to 1.5 g/dL was measured using a Cannon-Fenske (reverse-flow) viscometer with a capillary diameter of 300 µm at 40 ºC to accelerate the measurements with respect to room temperature.

In table 5.1 lists the data obtained from the viscometer measurements (working principle in *Chapter 3*). The computed specific viscosity is obtained from the measured zero-shear viscosity and the viscosity of the solvent – water 0.000653 Pa·s for 40 ºC –.

Table 5.1: Obtained data from capillary viscometer measurements.

Concentration (g/dL)	η_0 (Pa·s)	Specific viscosity η_{sp}
1.5	0.537	820.91
1.2	0.271	413.38
1	0.165	251.24
0.8	0.088	133.47
0.6	0.046	70.71
0.5	0.031	46.68
0.4	0.0231	34.45
0.3	0.0162	23.94
0.25	0.0126	18.35
0.2	0.0103	14.89
0.15	0.0084	11.90
0.1	0.0060	8.24
0.075	0.0052	6.98
0.05	0.0039	4.92

Figure 5.4 shows the effect of concentration on the reduced viscosity η_{sp}/c. It shows that, for the lowest concentrations, the reduced viscosity decreases when concentration increases until 0.25 g/dL, after which it increases continuously with concentration.

The behaviour shown in the figure differs from the results commonly reported for alginate solutions. Certain authors (Mancini et al. 1996; Gómez Díaz and Navaza 2002) reported that the reduced viscosity η_{sp}/c increases for the whole range of concentration.

Contrary, Xiao et al (Xiao et al. 2012) reported a decrease of η_{sp}/c for the whole range of concentrations that they studied.

Other authors who have published on alginate do not show data of reduced viscosity dependence on concentration and present only specific viscosity or $\eta_0 - \eta_{solvent}$ data instead (Storz et al. 2010; Simeone et al. 2004).

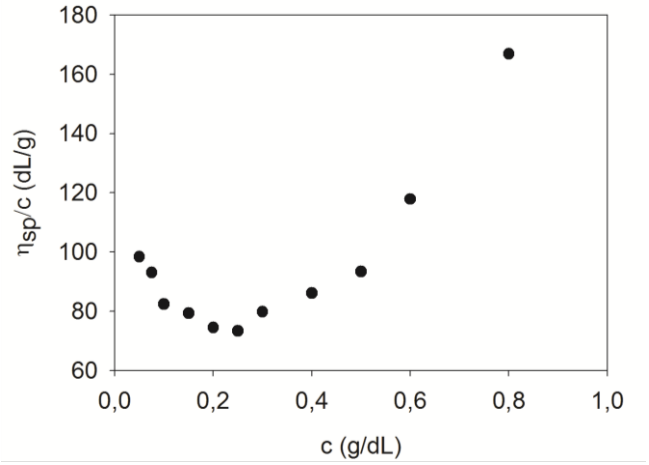

Figure 5.4: Effect of concentration on the reduced viscosity η_{sp}/c for concentrations from 0.05 to 0.8 g/dL.

The observed behaviour can be possibly explained by the effect of the ionic strength of the solutions.

Since alginate is a polyelectrolyte, its addition to water changes the ionic strength. Fuoss et al (Fuoss and Strauss 1949) found that certain polyelectrolytes exhibited a marked dependence on their ionic strength. Additionally, Smidsrød (Smidsrød 1970) published studies on sodium alginate aqueous solutions and demonstrated that they presented high ionic strength dependence.

The intrinsic and reduced viscosities are decreasing functions of the ionic strength, because the polymer macromolecular conformation changes with the charges on the chain (Smidsrød 1970; Hilliou et al. 2009). Hence, a decrease is expected at low alginate

concentration, where the ionic strength has more effect, what confirms that the effect of free sodium ions released in water from the solutions affects the behaviour of the samples.

However, at larger concentration the chain interaction screens the effect of the polyelectrolyte increasing the reduced viscosity with the concentration. In this case, a behaviour reminiscent from the theoretical predictions for polyelectrolytes in salt free solutions is expected (Dobrynin et al. 1995).

The non-monotonic increase of η_{sp}/c with the polysaccharide concentration precludes approximating the reduced viscosity values closest to zero concentration to a straight line and, following the definition of [η] - equation (5.6) - by extrapolation to zero concentration.

An alternative approach to compute [η] is considered neglecting the data for concentrations below 0.25 g/dL – for the calculations following -.

Storz et al (Storz et al. 2010) proposed a pseudo-truncated three terms Taylor expansion to describe the concentration dependence of the specific viscosity η_{sp} for all concentration regimes (diluted, moderately concentrated and concentrated).

In the corresponding equation (5.8), k_H is the Huggins coefficient, which is expected to be of the order of 0.5 (Storz et al. 2010; Haward et al. 2012; Fuoss and Strauss 1949). *A* and *n* are also fitting parameters:

$$\eta_{sp} = [\eta]c + k_H [\eta]^2 c^2 + A[\eta]^n c^n \qquad (5.8)$$

The fitting that best matches with the expected value for k_H collects concentrations from 0.5 g/dL. The result of the fitting gives:

$$\eta_{sp} = 19.245c + 0.319\cdot[\eta]^2 c^2 + 0.00119[\eta]^{3.87} c^{3.87} \qquad (5.9)$$

with [η] = 19.25 dL/g. The intrinsic viscosity [η] is of the order of other reported values for alginate solutions (Mancini et al. 1996; Storz et al. 2010; Haug and Smidsrød 1962; Gómez Díaz and Navaza 2002).

Storz et al (Storz et al. 2010) concluded that exponent *n* was universal for all alginates, with a value of 4.32. If the value of the exponent n is considered 4.32 to calculate k_H and [η] the following expression for data ranging from 0.25 to 1.5 g/dL is obtained:

$$\eta_{sp} = 18.06c + 0.456\cdot[\eta]^2 c^2 + 2.97\cdot 10^{-4}[\eta]^{4.32} c^{4.32} \qquad (5.10)$$

The value of intrinsic viscosity [η] does not vary much between the two approximations. Once [η] is obtained, the different regimes of concentration are determined.

Figure 5.5 shows the specific viscosity as a function of concentration in logarithmic scale, where the continuous longest line corresponds to the fitting of the experimental data to the equation (5.9).

The concentration dependence of η_{sp} in a log-log format for a direct comparison with the scaling laws theories for neutral and charged polymers.

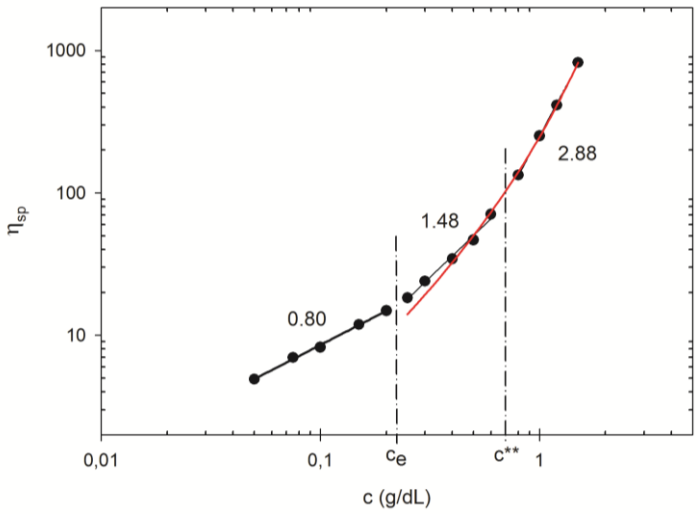

Figure 5.5: Effect of alginate concentration (c) on the specific viscosity (η_{sp}) of sodium alginate aqueous solutions: Experimental data (symbols) and data fitting to the last approximation of equation (5.9) (thick line).

The dilute regime is usually expected to be finished when the polymer concentration reaches a critical value c* of the order of 1/[η] (Böhm and Kulicke 1999; Duxenneuner et al.

2008). For many polysaccharides, where long range interactions (H-bonding) come into play, the critical concentration c* correspond to 4/[η] (Morris et al. 1981; Kulicke et al. 2005). c* determines the onset of interaction between macromolecules that defines the semi-dilute unentangled regime of concentration.

Therefore, a change in the concentration dependence of η_{sp} is expected for concentrations in the range from 1/[η] and 4/[η], i.e. 0.06 to 0.22 g/dL. Furthermore, the onset of the semi-dilute regime starts when η_{sp} is nearly 1.

Colby reviews in one of his works (Colby 2010) that slopes of unity are expected by the Zimm model in dilute solution (c < c*) for values $\eta_{sp} < 1$, and slopes of ½ and 1.3 are expected by the Rouse model for semidilute unentangled solutions of polyelectrolytes and neutral polymers respectively, for values $1 < \eta_{sp} < 20$. At higher concentrations, entangled solutions are consistent with larger slopes.

Figure 5.5 shows that η_{sp} is nearly 10 for concentration between 0.06 and 0.22 g/dL. This suggests that c* is not located in this range of concentration, since the dilute regime should end before the onset of the semi-dilute regime, when η_{sp} is nearly 1.

In addition, data in Figure 5.5 suggest that three concentration regimes with scaling laws of 1/2, 3/2 and 2.9 can be identified. The two first power law exponents correspond respectively to the semi-dilute unentangled and entangled regimes of polyelectrolytes in salt free solutions (Hilliou et al. 2009; Dobrynin et al. 1995; Colby 2010), whereas the last exponent is indicative of entanglements in neutral polymer solutions.

Such concentration scaling is not predicted by equation (5.9) which suggests that [η] computed using this equation is largely underestimated because, as it has been said before, c*should be lower than the computed concentrations from 1/[η] and 4/[η], i.e. 0.06 to 0.22 g/dL., to fulfil the criteria of η_{sp} nearly 1, which would require a higher value of [η].

Indeed, since the low concentration regime shows a power law scaling with exponent close to 1/2, a linear scaling is expected at lower concentrations which correspond to the dilute regime.

The overlap concentration c* that would indicate the onset of the unentangled semidilute regime lies below the experimental data shown in Figure 5.5. Therefore, two other critical concentrations are assigned to the two changes of slope displayed in Figure 5.5, namely c_e which signals the onset of an entangled semi-dilute regime, and c** which indicates the concentrated regime.

5.2.2. Characterization under simple shear by rotational rheometry

The characterization of the samples centred on solutions covering a range of concentrations up to zero-shear viscosities of about 5.5 Pa·s.

The samples are characterized under steady-shear measurements by flow curves that measure the steady strain response to an applied stress in a steady simple-shear flow.

They are also characterized under dynamic measurements by SAOS (Small Amplitude Oscillatory Shear), applying an oscillatory stress of established amplitude and variable frequency to the fluid and measuring the fluid's linear response.

Figure 5.6 shows the flow curves obtained from solutions of different concentrations.

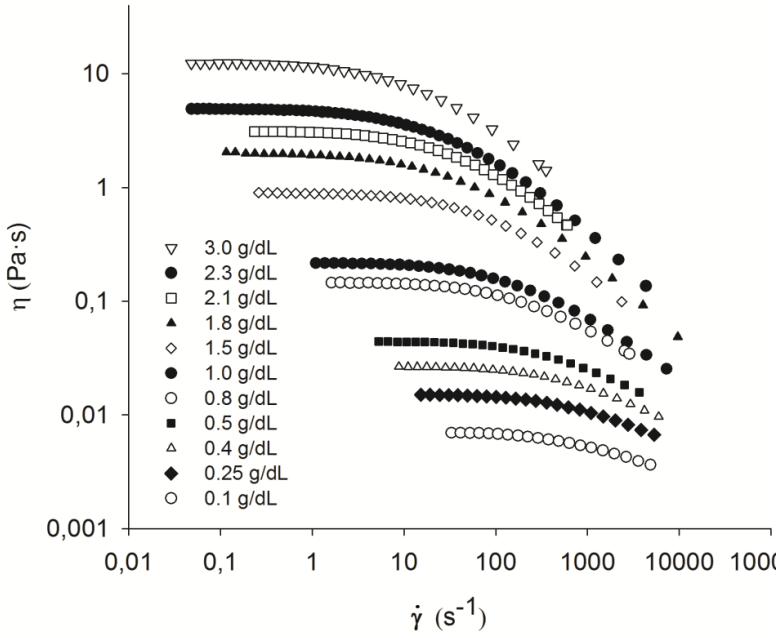

Figure 5.6: Flow curves – shear viscosity as a function of shear rate –.

The data collected in the figure show a shear rate dependent viscosity above certain value of shear rate, known as critical shear rate $\dot{\gamma}^*$. From this parameter a characteristic time scale under steady-shear flow can be extracted as $\lambda_c = 1/\dot{\gamma}^*$.

It indicates the onset of the transition between the constant viscosity region (first Newtonian plateau) and the shear thinning regime.

The data in Figure 5.6 were fitted to the most known generalized non-Newtonian models. Among them, the modified Cross constitutive equation (Cross 1965; Barnes 1989) (5.11) resulted in the best fit for the different flow curves.

$$\frac{\eta - \eta_\infty}{\eta_0 - \eta_\infty} = \frac{1}{1 + \left(\lambda_c \dot{\gamma}\right)^m} \qquad (5.11)$$

The fittings allow extracting the values for Newtonian plateau viscosities η_0 (at zero shear rate), relaxation times λ_C and exponents *m*, which indicates the power law relation between shear stress and shear rate in the shear-thinning region (*m = n-1* where *n = 1* or *m = 0* indicates a Newtonian behaviour). It is not possible to observe experimentally the Newtonian plateaus at large shear rates and thus it will be considered $\eta_\infty = 0$.

The estimated parameters by applying Cross model for the different solutions are summarized in Table 5.2.

Figure 5.7 shows the concentration dependence of the relaxation times and the exponent *m* gathered in Table 5.2. The log-log representation again allows a direct comparison of data with scaling laws predictions for polymer solutions (Colby 2010).

Table 5.2: Fitting parameters for the Cross model for different solution concentrations. The fitting errors are between 2 and 4 % except for 0.1 g/dL with a 14 % error.

C (g/dL)	η_0 (Pa·s)	λ_C (s)	m	$\dot{\gamma}$ *(s^{-1})	n
0.1	$7.19 \cdot 10^{-3}$	$5.55 \cdot 10^{-4}$	0.828	1802	0.172
0.25	0.0154	$6.18 \cdot 10^{-4}$	0.857	1633	0.143
0.4	0.0270	$7.17 \cdot 10^{-4}$	0.838	1394	0.162
0.5	0.0450	$1.13 \cdot 10^{-3}$	0.846	884	0.154
0.8	0.1485	$2.53 \cdot 10^{-3}$	0.787	394	0.213
1	0.222	$3.16 \cdot 10^{-3}$	0.726	317	0.274
1.5	0.911	$7.66 \cdot 10^{-3}$	0.759	130	0.241
1.8	2.032	0.0169	0.722	59	0.278
2.0	2.744	0.0175	0.758	57	0.242
2.1	3.228	0.0180	0.765	56	0.235
2.3	4.953	0.0259	0.744	39	0.256
3.0	12.70	0.0481	0.730	21	0.270

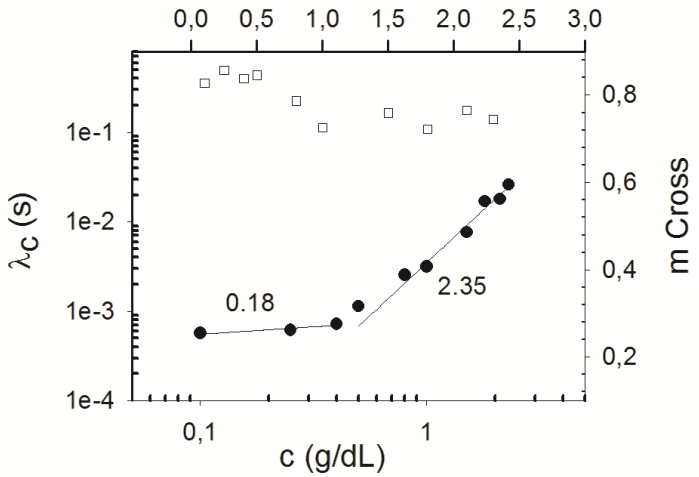

Figure 5.7: Concentration dependence of parameter *m* (hollow squares) and relaxation times λ_C obtained from Cross equation.

Figure 5.7 reveals that λ_C increases with the concentration in two different tendencies. The first three data disagree with the expected power law scaling $c^{-1/2}$ predicted for polyelectrolytes in salt free solutions (Colby 2010) at $c < c_e$.

Rather, the plateau at lower concentrations is reminiscent from the scaling c^0 expected for entangled polyelectrolytes ($c > c^{**}$). However, such behavior is only predicted for highly charged polyelectrolytes (Hilliou et al. 2009), and data in Figure 5.5 suggest that the plateau in λ_C occurs in a concentration regime corresponding to $c^* < c < c_e$. At larger concentrations, the scaling $c^{7/3}$ expected for entangled neutral polymers in theta solvent is recovered.

Thus, the relaxation times of all solutions suggest a transition from an entangled polyelectrolyte behavior to an entangled neutral behavior at larger concentrations, which is in harmony with results displayed in Figure 5.4.

Such transition is also described by the concentration dependence of the shear thinning index *m*.

The decrease of *m* with the concentration already suggests that a master curve cannot be built by simply shifting the flow curves on both axes, as illustrated in Figure 5.8. It is the transition from polyelectrolyte to neutral polymer behavior what precludes the overlapping of flow curves.

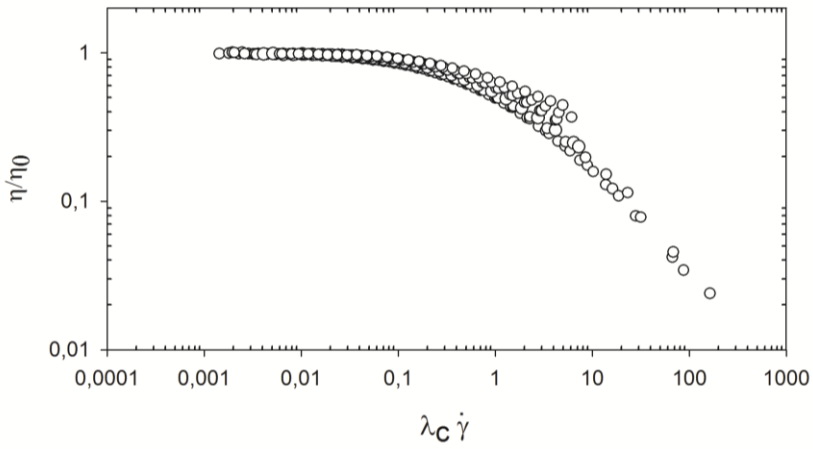

Figure 5.8: Attempt to generate a master flow curve.

Next, dynamic measurements are carried out through SAOS (small amplitude oscillatory shear) – also known as oscillation stress sweeps tests - within the linear viscoelastic region (LVER). The LVER was checked by performing stress sweeps at 1, 0.1 and 0.01 Hz and selecting different values of oscillation stress or % strain depending on the concentration studied, in the range of 2 to 5 %.

The tests were conducted applying a frequency range from 10^{-2} to $5 \cdot 10^{2}$ rad/s. The chosen amplitude for the shear deformation sinusoidally changing in time was around 3% and previously checked to be in the linear viscoelastic region through strain sweep tests.

The parameters extracted from a frequency sweep are defined by equation 5.11 where γ_0 and σ_0 are the strain and stress amplitudes, respectively, and δ the phase shift between stress and strain (90° for purely viscous response and 0° for purely elastic response), measured for each frequency ω.

$$G' = \frac{\gamma_0}{\sigma_0}\cos\delta, \quad G'' = \frac{\gamma_0}{\sigma_0}\sin\delta \qquad (5.11)$$

Figure 5.9 presents a set of frequency sweeps for different concentrations ranging from 0.1 to 3 g/dL.

In the figure a cross-over frequency between *G'* and *G''* for the most concentrated solutions can be observed. The effects of inertia limit the frequency range and makes impossible to capture cross-over points for smaller concentrations.

Below the cross-over point the loss modulus *G''* is higher than the storage modulus *G'*, which means that the samples show a predominantly viscous behaviour.

When *G'* exceeds *G''* the behaviour turns to be elastic, since the polymer coils are not able to relax completely. Thus, the inverse of the cross-over point frequency value defines the relaxation time related to polymer entanglements in semi-dilute and concentrated solutions.

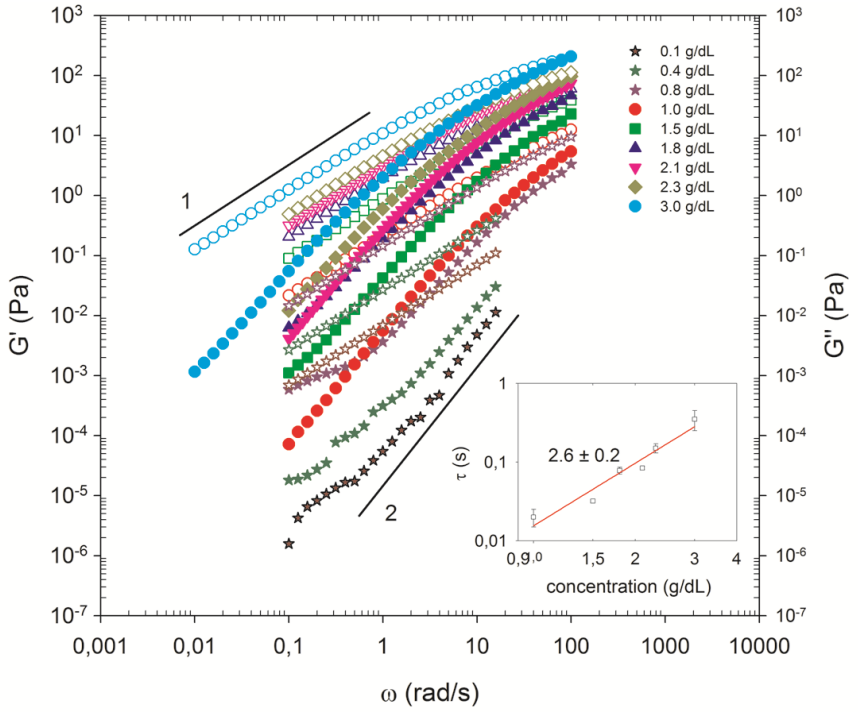

Figure 5.9: Storage modulus G' (hollow symbols) and loss modulus G'' (solid symbols) as a function of the angular frequency.

The longest relaxation time of the solution, here considered τ, is related to the full polymer disengagement from the network of neighbouring chains, and it is estimated from the cross-over frequency extrapolated from the terminal behaviour of *G'* and *G''* with slopes 2 and 1 respectively (Willenbacher et al. 2008).

Table 5.3 gathers the two relaxation times obtained for now – the one from Cross equation fitting λ_C and the one extrapolated from the terminal regions in SAOS τ -. The concentration dependence of τ is presented in the inset in Figure 5.9, where the power law exponent displayed in the inset matches nicely the exponent found for λ_C (Figure 5.7), which indicates the consistency of the two sets of experiments.

Table 5.3: Relaxation times λ_C obtained from fitting the flow curves (Cross model) and relaxation times τ obtained as described in the text.

c (g/dL)	η_0 (Pa·s)	λ_C (s)	τ (s)
1	0.222	$3.16 \cdot 10^{-3}$	0.02 ± 0.005
1.5	0.911	$7.66 \cdot 10^{-3}$	0.032 ± 0.002
1.8	2.032	0.0169	0.078 ± 0.008
2.1	3.228	0.0180	0.084 ± 0.004
2.3	4.953	0.0259	0.15 ± 0.02
3.0	12.70	0.0481	0.35 ± 0.10

The validity of the Cox-Merz rule (Cox and Merz 1958) is tested and shown in Figure 5.10. This empirical rule states that the value of the dynamic viscosity η^* equals the value of the steady shear viscosity η measured under similar flow conditions, i.e. for $\omega = \dot{\gamma}$.

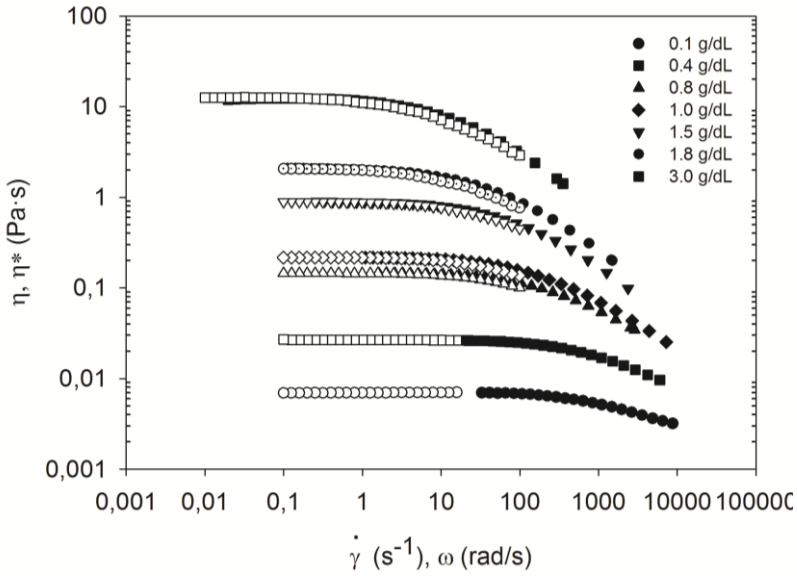

Figure 5.10: Viscosity as a function of shear rate (filled symbols) and complex viscosity as a function of frequency (hollow symbols).

The zero shear viscosity, which defines the Newtonian viscosity η_0, does not depend on the experimental method used to measure it, and thus in the limit of slow flows, η^* should match η.

Figure 5.10 shows that the rule holds very well for the Newtonian plateau, thus indicating that the two sets of experimental data – flow curve and dynamic measurements - are consistent. Note that, even when Figure 5.10 does not present the same dimensional units in the x-axis for the two rheological tests, this is the common representation in rheology text books.

5.2.3. Characterization under uniaxial extensional flow

The phenomena of extensional effects on jets were already addressed in the XIX century and have been studied in deep since then (Aleksandrov and Lazurkin 1940; Entov 1986).

Several instruments have been developed in the last decades for the study of uniaxial extensional properties. Among them, the two or four roll mills accessories, opposed jet devices, Filament Stretching rheometers (Tirtaatmadja and Sridhar 1993) (FiSER) or Capillary Breakup Extensional rheometers (Entov and Hinch 1997) – CaBER - are well known. The extensional properties can also be studied by relatively simple drop pinch-off or breakup experiments and a high-speed camera.

The Capillary Breakup Extensional Rheometer – CaBER – was used in this work to determine the extensional properties of the alginate solutions. This technique can achieve a close approximation to a shear-free purely uniaxial extensional flow by performing capillary thinning experiments. The apparatus stretches a sample of fluid contained between two plates, the lower of them fixed. The evolution of the thread after the stretching is measured at the midpoint by a laser and the mid-filament profile data, namely the radius of filament $R_{mid}(t)$, are then analysed to characterize the fluid behaviour. Figure 5.11 shows the working principle of this device.

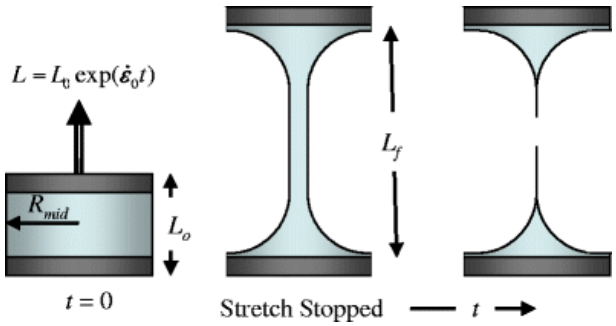

Figure 5.11 : Schematic diagram of capillary breakup extensional rheology (CaBER) experiment (Miller et al. 2009)

For the purpose of analysing the midfilament temporal profile, the mechanism that opposes the capillary forces after the stretching must be identified. Equations 5.12 to 5.15 are widely found in literature concerning the topic (Rodd et al. 2005; Stelter et al. 2000) to describe the thinning process.

For a low-viscosity fluid an inertia-capillary balance defines the thinning process and the diameter decay follows a power law expression (5.12). For viscous Newtonian fluids the balance is viscous-capillary and the radius decays linearly following expression (5.13). For solutions where elasticity is at play extra tensile stress that slows the thinning process appears and, if sufficiently large, an elasto-capillary balance takes place which leads to an exponential decay given by equation (5.14).

$$R_{mid}(t) = 0.64\left(\frac{\sigma}{\rho}\right)^{1/3}\left(t_{bu} - t\right)^{2/3} \quad (5.12)$$

$$R_{mid}(t) = R_0 - \frac{\sigma}{14.1\eta}t \quad (5.13)$$

$$\frac{R_{mid}(t)}{R_0} = \left(\frac{GR_0}{2\sigma}\right)^{1/3}\exp[-t/3\lambda] \quad (5.14)$$

where t_{bu} is the filament breakup time, R_0 is the radius after the stretching of the filament finishes, which is at the beginning of the filament thinning, λ is the so-called stress relaxation time, which determines the growth characteristic scale of elastic stresses in the

necking filament, *G* is known as the relaxation modulus and refers to the value of the linear stress-relaxation function *G(t)* when the material is subjected to a particular shear spectrum (Entov and Hinch 1997), *σ* is the surface tension and *ρ* the density and η is the Newtonian shear viscosity.

In addition, power law fluids that show an inelastic shear thinning behaviour follow a power law relationship (5.15)

$$\frac{R_{mid}(t)}{R_0} = \Phi(n)\frac{\sigma}{K}(t_{bu} - t)^n \quad (5.15)$$

where *n* is the power law exponent and *Φ(n)* is a numerical constant defined in several works (McKinley 2005b; Niedzwiedz et al. 2009) as:

$$\Phi(n) = 0.0709 + 0.239(1-n) + 0.548(1-n)^2 + 0.2848(1-n)^3 \quad for\ n \geq 0.6$$

$$\Phi(n) = 2^{-\frac{n}{3}} \quad for\ n < 0.6$$

The measurements using CaBER are easy to perform though sagging, gravity drainage and other problems have to be avoided. To keep an adequate cylindrical configuration some conditions are recommended: the use of initial gaps smaller than the *capillary length* $l_{cap} = \sqrt{\sigma / \rho g}$, and initial aspect ratios $\Lambda_0 = h_0/D_0$ between 0.5 and 1.

These experimental conditions were varied to establish those for which the relaxation process and times would not become affected, also checking that no instabilities in D(t) were present (Rodd et al. 2005).

Certain dimensionless numbers help to know better what and when will be the main driving process for the filament thinning (Clasen et al. 2012; McKinley 2005a; Clasen et al. 2006b), and thus to use the appropriate equation to describe $R_{mid}(t)$.

On one hand, the Ohnesorge number $Oh = \frac{\eta}{\sqrt{\rho\sigma R}}$ relates the viscous and inertial effects. If *Oh > 0.2077* viscous effects will dominate over inertial effects. The viscosity *η* of the sample is considered the zero-shear viscosity η_0 obtained by steady shear (see Table

5.2) or the Newtonian extensional viscosity as three times η_0. R is the radius of the sample thread.

Owing to the high zero shear viscosities that we are dealing with, the Oh numbers calculated from the filament conditions predict a predominant viscous behaviour against inertia; *Oh* is higher than 0.2077 for the larger radius of the thread (3 mm), which implies that the reduction of the radius when the stretching is applied would increase the Oh value.

On the other hand, the elastocapillary number $Ec = \frac{\lambda\sigma}{\eta R}$ compares the viscous and elastic effects. Its critical value for controlling the dynamics of the thinning process is 4.7015 so it is expected a process controlled by elastic effects when *Ec > 4.7015* (Clasen 2010), sometimes directly considered the unit (as it is computed below). λ is the characteristic time scale of elastic thinning.

Similarly, the elastocapillary number also varies with the radius, and it increases when the radius decreases. Given the information gathered before λ can be considered as the relaxation time computed from the fit of steady flow curves to the Cross model (λ_C, see Table 5.2) or as the relaxation time extrapolated from the terminal regime in SAOS (τ, see Table 5.3). Two critical radii R_V from which the process would change from a viscous to an elastic controlled process can be obtained.

The Deborah number $De = \frac{\lambda}{\sqrt{\rho R^3/\sigma}}$ also gives information about the thinning process. It compares inertia with elasticity. As done for *Ec*, critical radii R_E can be computed, at which the thinning starts to be controlled by the solution elasticity.

For values greater than the unit elasticity dominates over inertia (Vadillo et al. 2012). In general it is considered that the fluid exhibits both viscous and elastic behaviour for *0.5 < De < 10*, which is the region of greater importance when studying viscoelastic fluids.

The critical radii computed from *De= 1* or *Ec=1* are presented in Table 5.4. Two different values for every critical radius are obtained. This is due to the two different values

that were extracted previously through different measurements (steady-shear - λ_C – and oscillatory shear – τ -).

Table 5.4: Comparison between the radii computed from the elastocapillary number - R_V - and the Deborah number - R_E - using either λ_C or τ (larger radii).

c (g/dL)	η_0 (Pa·s)	λ_C (s) Cross (5.11)	τ (s) SAOS	R_V (mm) *Ec = 1*	R_E (mm) *De = 1*	Initial radius (mm)	Breakup time t_b (s)
1.5	0.911	$7.66 \cdot 10^{-3}$	0.032	0.64 – 2.67	1.65 – 4.27	0.78	0.0901
2.0	2.744	0.0175	0.08	0.48 – 2.22	2.86 – 7.86	0.875	0.1772
3.0	12.7	0.0481	0.35	0.29 – 2.09	5.6 - 21	0.885	0.3570

Certain conclusions can be extracted from the data in table 5.4. In the case of the critical radii calculated from the condition of Deborah being the unit - R_E - both computed radii are above the initial stretching radii. Thus, Deborah number keeps higher than the unit for the whole stretching process and elasticity rules over inertia for the whole range of radii measured experimentally.

However, *Rv* critical radii in Table 5.4 are lower than the initial stretching radii when the relaxation times λ_C from the steady shear measurements are considered. This suggests that viscous effects could overcome elastic effects in a range of times corresponding to early thinning. This is the filament thinning behaviour reported by certain authors (Clasen 2010; Clasen et al. 2012; Haward et al. 2012) for weakly elastic fluids such as semi-diluted polymer solutions.

In the cases reported then, the filament time evolution follows a linear thinning (equation 5.13), then a power law thinning (equation 5.12) and eventually an elastocapillary thinning (equation 5.14) which should be used to extract λ_{ext}. The relaxation time λ_{ext} associated with the thinning of the filament is different from λ_C and τ and it is

related to “the characteristic time scale for viscoelastic stress growth in an uniaxial elongational flow” (Rodd et al. 2005).

However, if *Rv* is computed using the longest relaxation time τ from SAOS, as proposed for more diluted systems (Clasen et al. 2012; Vadillo et al. 2012), larger critical diameters than those experimentally occurring are obtained and filament thinning should be essentially ruled by elasticity.

The computed *Rv* and R_E are simply indicative to help in opting for the use of a specific equation to analyse the thinning. Thus, both approaches will be studied, starting with the elasticity dominating behaviour.

In this case, it is expected an exponential filament thinning to show up prior to finite extensional behaviour of polymer chains and eventually filament break-up. This exponential thinning has been documented for non-dilute Guar solutions (Duxenneuner et al. 2008) and ultra-high viscosity alginate solutions (Storz et al. 2010). Thus, λ_{ext} should be extracted by fitting equation (5.8) to data exhibiting an exponential decay prior to the final linear process.

The semi-log plots in Figure 5.12 show a linear decay at early time indicating that a constant deformation rate is reached and that the extensional stress increases exponentially. After this, a terminal regime develops, with a fast decay until breakup of the thread.

The relaxation time λ_{ext} can be obtained from fitting expression (5.14) to the first linear regime in Figure 5.12. The corresponding extracted times are gathered in table 5.5. The experimental data for one of the solutions assayed are gathered in Appendix B.

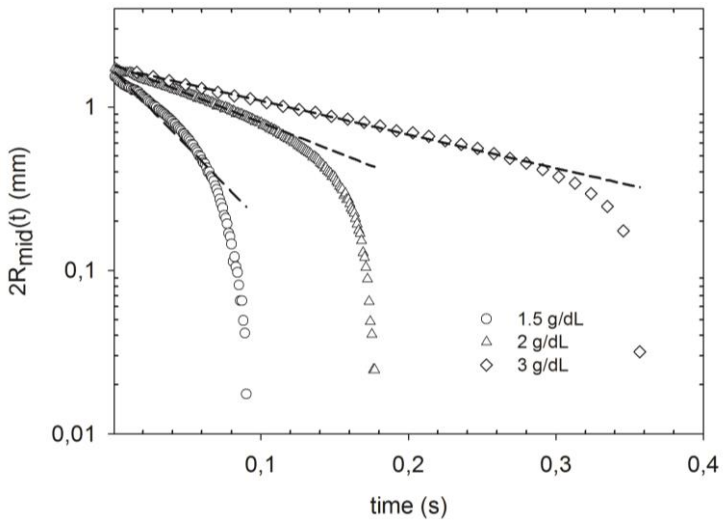

Figure 5.12: Evolution of the filament thinning process: diameter *D(t)* as a function of time for different concentrations of alginate solutions.

After fitting the data the following expressions were obtained:

$$\text{1.5 g/dL:} \quad \frac{R_{mid}(t)}{R_0} = 1.109\exp[-21.048\ t] \qquad (5.16)$$

Data until *t = 0.07 s* were selected and a relaxation time $\lambda_{ext} = 0.0157\ s$ is obtained.

$$\text{2.0 g/dL:} \quad \frac{R_{mid}(t)}{R_0} = 0.997\exp[-7.654\ t] \qquad (5.17)$$

Data until *t = 0.1001 s* were selected and a relaxation time $\lambda_{ext} = 0.041\ s$ is obtained.

$$\text{3.0 g/dL:} \quad \frac{R_{mid}(t)}{R_0} = 0.982\exp[-4.617\ t] \qquad (5.18)$$

Data until *t = 0.269 s* were selected and a relaxation time $\lambda_{ext} = 0.0703\ s$ is obtained.

After the first approach has been assessed in the second approach it is possible that viscous effects overcome elastic effects at early stages (Clasen 2010).

Table 5.5 contains the data to be introduced in the proposed fitting equations.

Table 5.5: Experimental data for the solutions assayed.

Concentration (g/dL)	Initial radius R_0 (mm)	Breakup time (s)	η_0 (Pa·s)
1.5	0.780	0.0901	0.911
2.0	0.875	0.1772	2.744
3.0	0.885	0.3570	12.70

The *regime I* describing gravitational sagging is not given in any of the three solutions assayed. Gravitational sagging is expected when the Bond number $Bo = \frac{\rho g R^2}{\sigma}$ exceeds a value of 0.2, which happens when a radius of 1.24 mm is attained. All of our initial radii are below this value, which gives Bond numbers higher than the critical one.

After discarding this first regime the *regime II* would describe a visco-capillary balance where the filament radius is still large. Next, the analysis regarding this regime for the solution of 1.5 g/dL is detailed as reference for the calculation, since the other two solutions encountered the same issues here analysed. This regime is characterised by the linear equation (5.13).

The obtained expression (5.19) is plotted with the list of measured data in Figure 5.13, from which it can be easily seen that there is a high deviation.

$$R_{mid}(t) = R_0 - 0.0709\frac{\sigma}{\eta}t = 0.780 - 1000 \cdot 0.0709\frac{0.076}{0.911}t = 0.780 - 5.91665t \qquad (5.19)$$

Clasen (Clasen 2010) also proposed the expression (5.20) with the same slope though a different ordinate at the origin. Experimental data and expression (5.21) are plotted in Figure 5.14 and also a high deviation is obtained between the fitting and the data.

$$R_{mid}(t) = 0.0709\frac{\sigma}{\eta}(t_{bu} - t) \quad (5.20)$$

$$R_{mid}(t) = 0.0709\frac{\sigma}{\eta}(t_{bu} - t) = 0.0709\frac{0.076}{0.911} \cdot 1000(0.0901 - t) = 0.5329 - 5.9148t \quad (5.21)$$

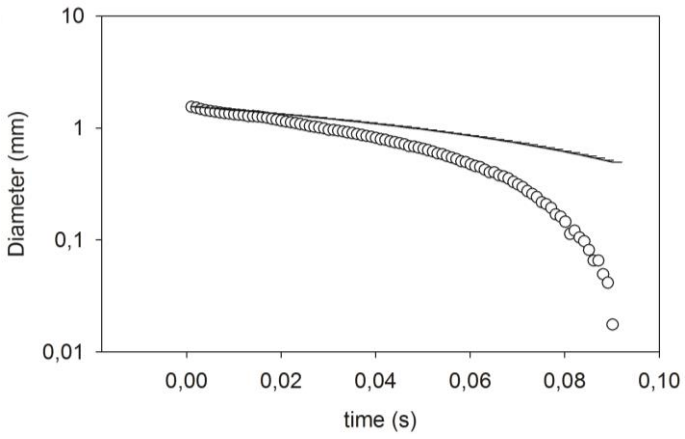

Figure 5.13: Fitting of equation (5.19) for the 1.5 g/dL solution.

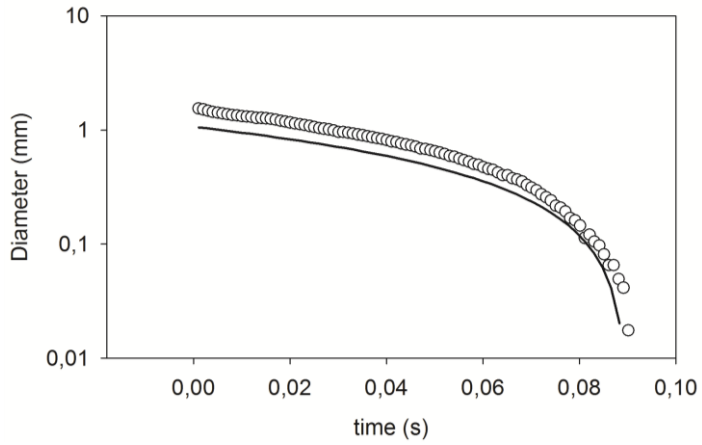

Figure 5.14: Fitting of equation (5.21) for the 1.5 g/dL solution.

However, if the data are fitted to a generic linear expression as (5.22) the obtained expression (5.23) does nicely match the data (see Figure 5.15).

$$R_{mid}(t) = R_0 - mt \qquad (5.22)$$

Nevertheless, the new slope reveals that the computed Newtonian shear viscosity is smaller than the experimentally measured (0.602 Pa·s in this particular case).

$$R_{mid}(t) = 0.7780 - 8.95t \qquad (5.23)$$

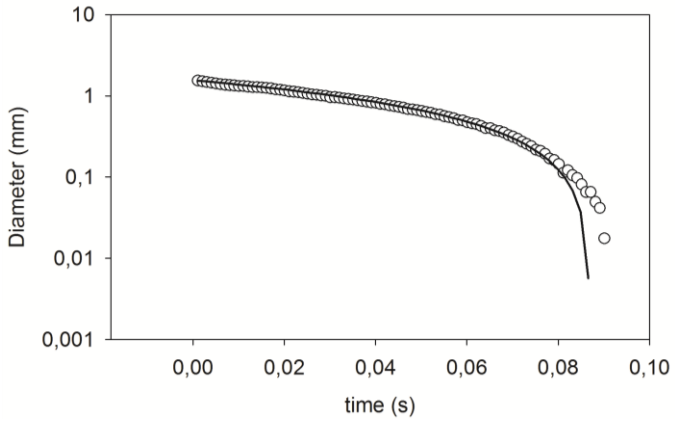

Figure 5.15: Fitting of equation 5.22 to *D(t)* as a function of time for the 1.5 g/dL solution.

Figure 5.16 reveals how the linear equation nicely reproduces the filament thinning (thick lines) for the three solutions, but the computed Newtonian shear viscosities are much smaller than the ones measured in shear rheometry (0.60 Pa.s, 1.13 Pa.s and 2.17 Pa.s for solutions with 1.5 g/dL, 2 g/dL and 3 g/dL alginate, respectively). The fittings of data to equations (5.13) and (5.14) are displayed as solid lines and dot lines, respectively. The inset figure shows a double logarithmic plot of the time evolution of the mid filaments where thick lines indicate power law behaviour with exponents corresponding to shear thinning exponents *n* computed in Table 5.2.

The third regime still corresponds to a visco-capillary balance but now showing extensional thinning, in which the extensional viscosity follows a power law expression.

The radius would evolve as described by (5.15), where the *n* index is commonly taken as the one obtained from shear data (Clasen, 2010) (see Table 5.2).

The inset in Figure 5.16 shows how finding the correct time domain showing power law behaviour involves serious difficulties, considering also the problems in the determination of the value of *k* in the equation, which has been tried to be extracted from a power law fitting of the flow curve. Furthermore, the time domain for the fitting is short and thus few points are available for such analysis.

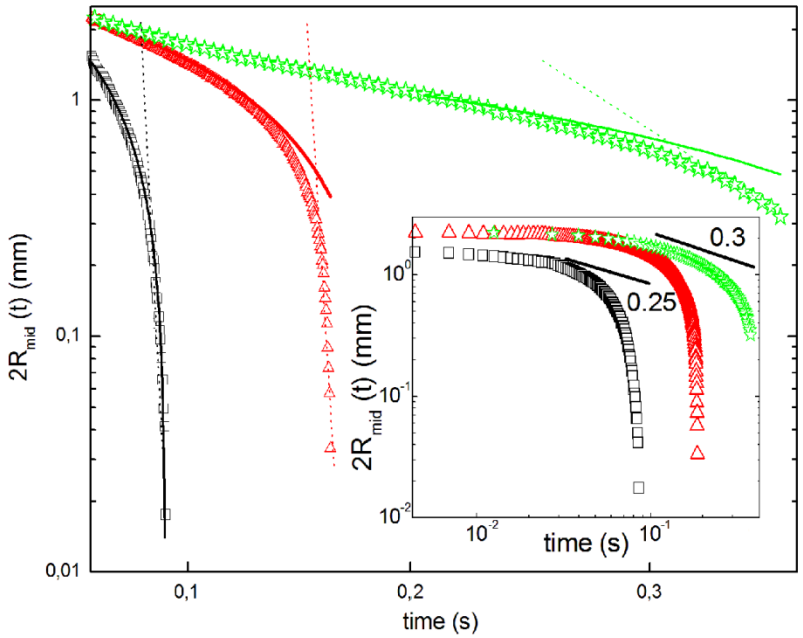

Figure 5.16: Time evolution of the mid filament diameter for 1.5 g/dL (squares), 2 g/dL (triangles) and 3 g/dL (stars) alginate solutions.

Finally, the elasto-capillary regime, corresponding to equation (5.14), would take place at late temporal stages. Figure 5.16 shows the fits of equation (5.14) to the data in the corresponding long time regime in dot lines. The fitted expressions resulted as follows:

1.5 g/dL: $\frac{R_{mid}(t)}{R_0} = 82986 \exp[-169.32\ t]$ (5.24)

Data selected from *t = 0.080 s* (11 data in total) lead to a relaxation time λ_{ext} *= 0.0020 s*.

2.0 g/dL: $\frac{R_{mid}(t)}{R_0} = 2.41 \cdot 10^8 \exp[-130.89\ t]$ (5.25)

Data from *t = 0.159 s* were selected (19 data) and λ_{ext} *= 0.0025 s*.

3.0 g/dL: $\frac{R_{mid}(t)}{R_0} = 900529 \exp[-47.94\ t]$ (5.26)

Data from *t = 0.313 s* were selected (5 data) and λ_{ext} *= 0.0070 s*.

Few data points are available for the fits and thus the computation of the relaxation time λ_{ext} remains uncertain.

Table 5.6 compares the relaxation times obtained from the different approaches. These are one order of magnitude different. Consequently extensional times from the second approach are also one order of magnitude smaller than the relaxation times extracted from steady shear, in agreement with results reported for semi-dilute and entangled polymer solutions (Arnolds et al. 2010; Clasen 2010).

Table 5.6: Extensional relaxation times of sodium alginate solutions of different concentrations and comparison to steady-shear relaxation times.

Concentration (g/dL)	λ_{ext} (s)		$\lambda_{ext} / \lambda_C$		λ_{ext} / τ	
	Fig. 5.12	*Fig. 5.16*	*Fig. 5.12*	*Fig. 5.16*	*Fig. 5.12*	*Fig. 5.16*
1.5 g/dL	0.0157	0.0020	2.1	0.26	0.49	0.06
2.0 g/dL	0.0410	0.0025	2.3	0.14	0.51	0.03
3.0 g/dL	0.0703	0.0070	1.5	0.15	0.20	0.02

Whereas the relaxation times obtained in steady shear and filament thinning flows are of the same order of magnitude, the longest relaxation time τ obtained in oscillatory shear is roughly one to two orders of magnitude larger than the extensional characteristic time.

Similar results were reported for a set of acrylic thickener solutions (Kheirandish et al. 2009). The difference between extensional and shear relaxation times was assigned to the break-up of aggregates in elongational flows. Moreover, two orders of magnitudes were recently found between λ_C and λ_{ext} for a set of semi-dilute and entangled ultra high molecular mass alginates in NaCl solutions (Storz et al. 2010). However, the removal of aggregates by centrifugation of the solutions did not affect the discrepancy between the two relaxation times.

Figure 5.17 shows the power law behaviour found for the concentration dependence of the relaxation times λ_{ext} obtained from the two previous approaches (Figures 5.12 and 5.16).

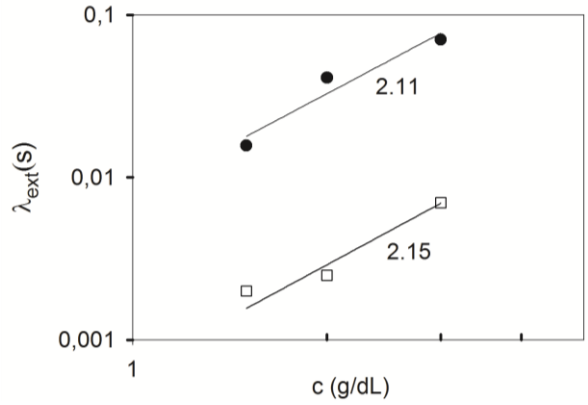

Figure 5.17: Concentration dependence of the relaxation time λ_{ext} from the first approach (•) and the second approach (▫).

In spite of the small set of data available it is noteworthy that the computed exponents - 2.11 ± 0.55 and 2.15 ± 0.41 - are in agreement with the concentration dependence found for both λ_C and τ, previously extracted.

The characteristic times extracted from filament stretching and thinning strongly depend on the choice of equation and time regime to be used for data analysis, this is depending on the approach considered.

Thus, this simple experimental technique does not allow for a straightforward estimation of the relaxation time which is at play during extension. However, since the second approach does not match properly previous regimes it will be considered the first approach as a more valid computation in later analyses.

5.2.4. Apparent extensional viscosity

Considering the first approach for extracting the relaxation time under uniaxial extensional flow, after the exponential decay that indicates the elasto-capillary regime and

just before the breakup, the polymer chains are fully extended and the diameter decays linearly with time.

This behaviour is described by expression (5.27) (Storz et al. 2010):

$$D_{mid}(t) = D_0 - \frac{\sigma}{\eta_E}\, t \qquad (5.27)$$

which essentially resembles equation (5.13) with an apparent extensional viscosity η_E replacing the Newtonian shear viscosity η_0.

Table 5.7 shows the extensional viscosity obtained from fitting expression (5.27) to the data that were dismissed for the exponential fits illustrated in Figure 5.11. Furthermore, the viscosities computed from the direct measurements of CaBER using the time derivative of the filament diameter (5.28) are displayed in Figure 5.18.

$$\eta_e = -\frac{\sigma}{2\frac{\partial R_{mid}(t)}{\partial t}} \qquad (5.28)$$

Table 5.7: Shear and extensional characteristics of sodium alginate solutions of different concentrations.

concentration	η_E (Pa·s)	η_e (Pa·s)	η_e/η_0
1.5	4.48 ± 0.04	4.3 ± 0.5	4.72
2.0	7.43 ± 0.09	12 ± 2	4.37
3.0	20.31 ± 0.68	45 ± 5	3.54

Figure 5.18 shows a constant $\eta_{e,app}$ which does not depend on the extensional rate (for medium values). From the results it is concluded that there is no strain hardening, which complies with earlier reports for polysaccharides studied in the non-entangled semi-dilute regime (Duxenneuner et al. 2008).

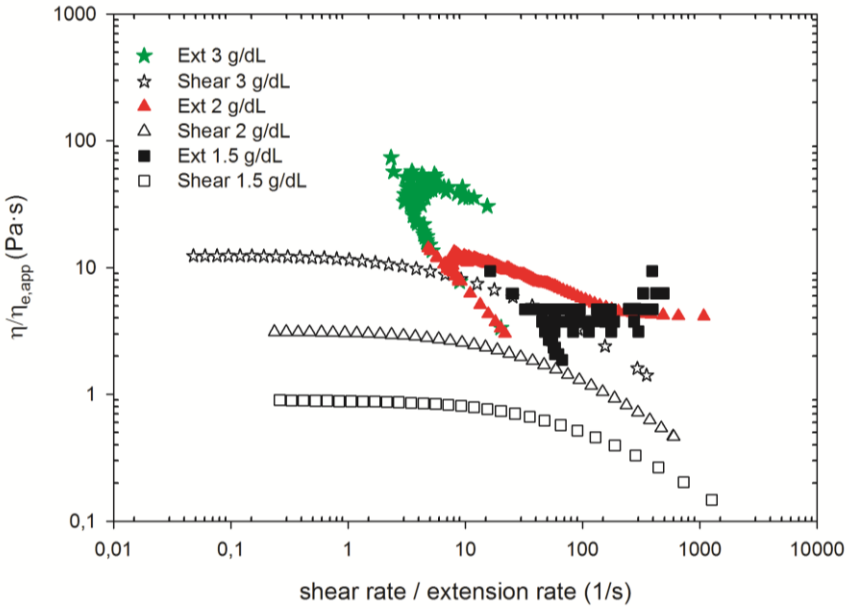

Figure 5.18: Apparent extensional viscosity as a function of the extension rate and steady shear viscosity as a function of the shear rate.

However, at large Hencky strains, the apparent extensional viscosity of the two more concentrated solutions decreases while the apparent extensional rate increases rapidly with time (inset in Figure 5.19). Extensional viscosity thinning is observed, which explains the lower extensional viscosity η_E computed in this regime.

Semi-dilute polymer solutions usually exhibit a shear thinning viscosity when the shear stress increases, caused by the deformation of the polymer coils and their subsequent orientation in the flow direction. At larger concentrations, disentanglement of polymer coils occurs at smaller stresses prior to flow orientation.

Conversely, in extensional flows it is common to find strain hardening over part of the deformation regime due to "coil-stretching" transition given at high deformation rates (Stelter et al. 2000). However, this strain-hardening effect can be balanced with the strain-thinning effects of the disentanglements of shear deformation depending on the concentration and shear rate of the polymer (Meadows et al. 1995).

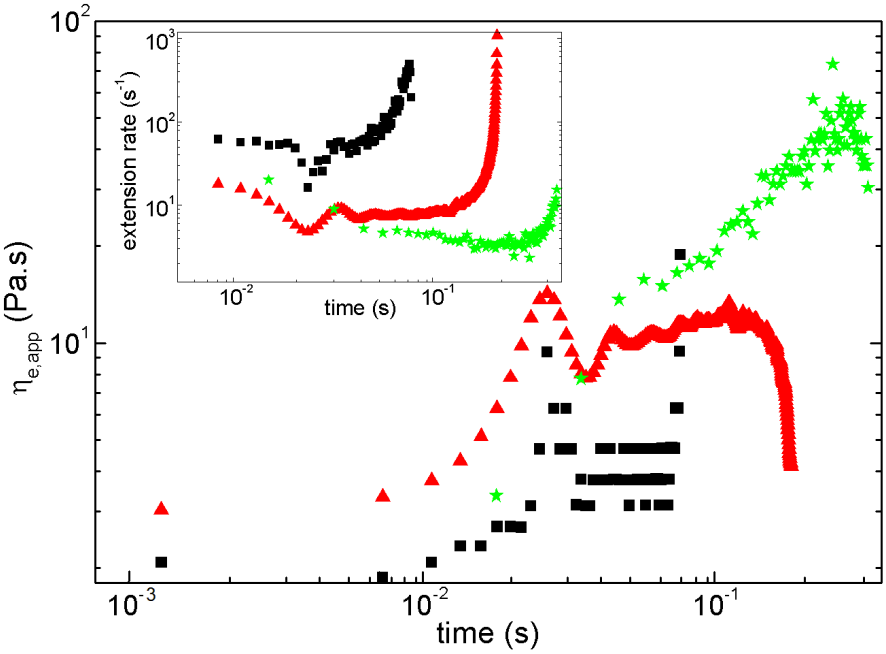

Figure 5.19: Time dependence of the apparent extensional viscosity. Inset: time dependence of the extension rate during the filament thinning.

The Trouton ratio η_e/η_0 in the samples studied decreases with the concentration, in qualitative agreement with data reported for semi-dilute and non-entangled modified guar gum solutions (Duxenneuner et al. 2008). The decrease in Trouton ratio was explained by the strong inter-chain interactions existing in guar gum solutions. Here, these interactions are replaced by the entanglements evidenced in shear rheometry.

5.3. Experimental and linear analysis of the laminar instability of polymeric jets

As it has been described before, this work addresses the formation of microparticles from polymeric solutions of sodium alginate that are driven towards a capillary nozzle to form jets whose instability is controlled by mechanical vibration, developing a Rayleigh-type jet breakup.

Chapter 4 included a detailed description about previous studies on this mechanism (Savart 1833; Plateau 1873; Rayleigh 1879; Weber 1931).

Most of the studies about jet disintegration depict instabilities in Newtonian fluids. Studies dealing with non-Newtonian fluid jets are less found in the literature. However, it has long been known that the addition of polymers to a liquid affects the stability and consequently the breakup of jets due to their viscoelastic behaviour (Lin and Reitz 1998).

As mentioned in section *5.1.1. Polymer rheology and jet breakup* it is known that viscoelastic fluids show a different response to shear and extensional stresses compared to Newtonian fluids, and therefore they require the use of complex constitutive equations when mathematical models are tackled.

In this chapter a linear temporal mathematical model will be obtained in order to describe the system. An expression that relates the growth rate and the wavenumber for a viscoelastic liquid is derived from the model, commonly known as dispersion relation, from which representations known as dispersion curves are obtained.

5.3.1. Description of the jet and breakup

The experimental methodology performed to address the following mathematical model comprises the recording of the formation and evolution of jets and droplets under different conditions. The conditions selected were similar to those used in *Chapter 4: Preliminary Studies*.

Solutions with zero-shear viscosities from 0.9 to 2.7 Pa·s pass through a 150 micrometres diameter nozzle with flow rates from 5 to 8 mL/min.

Several recordings were obtained at different distances from the nozzle by means of a high-speed camera. However, it was not possible to film just from the tip of the nozzle because the design of the device hampers from visualizing the nozzle exit.

Therefore only measurements from 1.5 cm from the nozzle are attainable and most of the measurements were taken from 3 to 5 cm downstream the exit to capture the breakup and evolution of the falling droplets.

Table 5.8 contains a summary of the experiments carried out to record the evolution of the jet. Not in all cases the droplets are solidified and collected. In general the range of frequencies was covered applying those at intervals of 100 Hz.

The parameters that can be measured from the recordings include the breakup length or the interdroplet size. However, to measure the jet diameter or the microdroplet size the captured images do not provide reliable information due to insufficient resolution.

Table 5.8: Experimental conditions recorded

Concentration (g/dL)	Flow rate (mL/min)	Frequency (s^{-1})
1.3	5	0 – 2000
1.5	6	0 – 3000
1.6	5 - 8	0 – 4000
1.8	5 - 8	0 – 4000
1.9	5.5 – 8	0 – 6000
2.0	5 - 8	0 – 6000

The alginate solutions analysed shown patterns like those in Figures 5.20 and 5.21 where sinusoidal axisymmetric waves are observed short after the nozzle exit, when controlled disturbances are applied, turning into a bead on a string - BOAS - pattern downstream. Beads of solution are then connected by thin ligaments or threads, and the breakup and size are determined by the behaviour of the main droplets and ligaments (Clasen et al. 2006a). Newtonian liquid jets show behaviours as those in Figure 5.22.

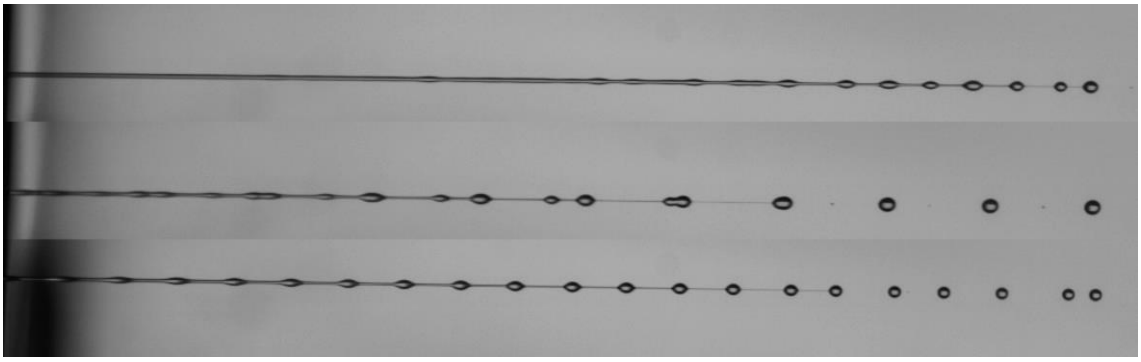

Figure 5.20: Droplet formation for a 1.3 g/dL solution – 5 mL/min - applying from top to bottom: 0, 800 and 1650 Hz.

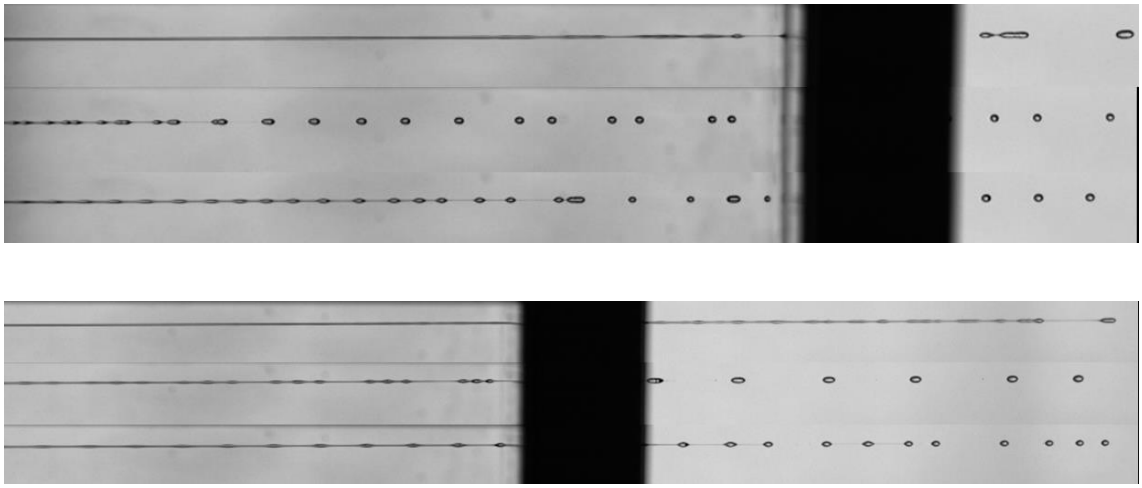

Figure 5.21: (a) Droplet formation for a 1.8 g/dL solution – 5 mL/min – applying different frequencies (0, 800 and 1400 Hz). (b) Droplet formation for a 1.8 g/dL solution – 7 mL/min - applying different frequencies (0, 800 and 1400 Hz).

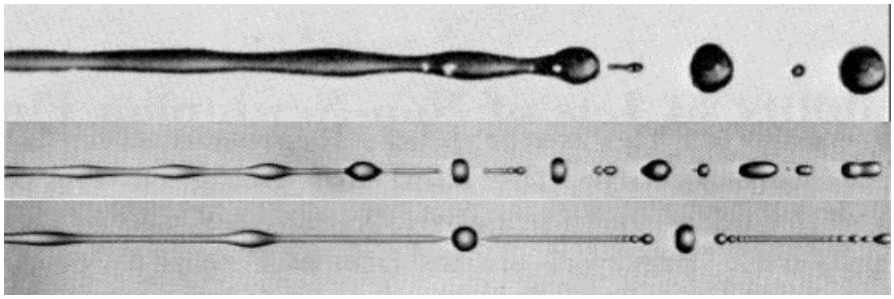

Figure 5.22: Breakup of Newtonian jets (Gordon et al. 1973)

Figures 5.20 and 5.21 provide information about certain behaviours that are in agreement with a first rough analysis of the effects of viscosity, flow rate and external vibration frequency applied.

When the viscosity increases the breakup length increases considerably for the same flow rate and frequencies (similar wavenumbers). This should be related to a shorter growth rate in the dispersion curves. Moreover the formation of droplets exhibits more irregularities or non-linear effects with a rise of viscosity.

When the flow rate increases, keeping a constant concentration and frequency applied, the breakup length increases in most cases. The growth rate obtained from the dispersion curves should also decrease with the flow rate for the same applied frequencies. It is noteworthy to say here that a same value for the frequency of the interfacial wave under larger flow rates means shorter wavenumbers.

Finally and similarly to the conclusion obtained in Chapter 4 it is important to note that the range of frequencies that lead to jet breakup is wide but not all frequencies achieve homogeneous microdroplets. Thus, an optimal range is observed in all cases and, in general, there is a minimum frequency from which the jet does not exhibit satellite droplets.

It was also checked that the applied frequency and the frequency of the wave developed by the disturbed interphase match.

Concerning the objectives of generating a mathematical model the main aim is to determine through a dispersion relation the best optimal conditions agreeing with the experimental range of frequencies that achieve homogeneous breakup.

Figure 5.23 shows how the formation of satellite droplets from the ligaments can mislead to a wrong characterization of the wave-like pattern developed by the jet. The frequency calculated from considering the gaps between droplets as wavelength differs considerably with the frequency applied when satellites are present.

Sometimes the satellite droplets attach to the main blobs, going backwards or forwards. This allows seeing a post-breakup pattern from where the real wavelength can be

more easily measured (see Figure 5.24). Other times they attach between them and form a new droplet or simply stay detached, which lead to heterodisperse samples.

These non-linear phenomena of migration, oscillation and merging of droplets in viscoelastic fluids and periodic jets has been studied in the literature (Li and Fontelos 2003).

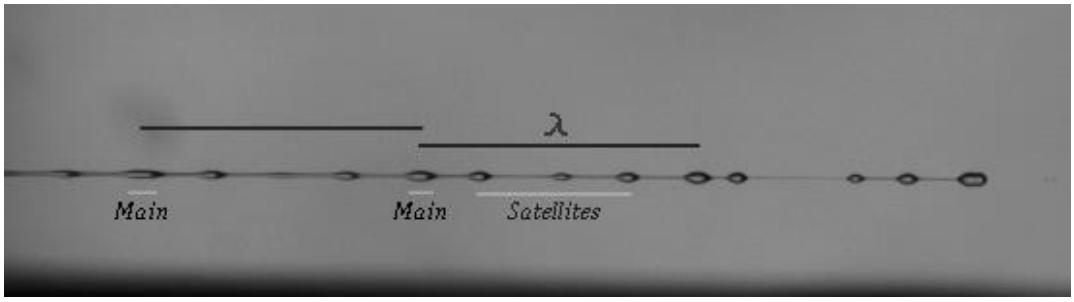

Figure 5.23: Droplet formation for a 1.5 g/dL solution – 6 mL/min – applying an external vibration of frequency 600 Hz. Main and secondary droplets growing from ligaments.

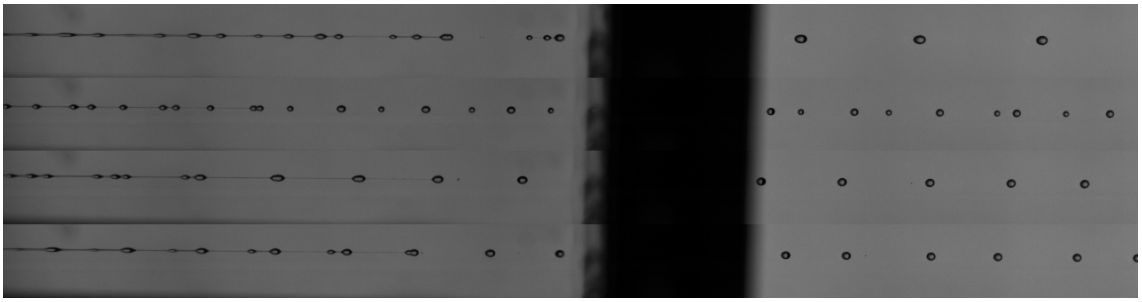

Figure 5.24: Droplet formation for a 1.5 g/dL solution – 6 mL/min - applying from top to bottom: 600, 850, 900 and 1000 Hz.

5.4. Theoretical study and determination of the dispersion equation

The mathematical approach adopted in this study comprised a temporal linear analysis.

The common ways to tackle fluid instabilities are temporal or spatial and, in turn, linear or non-linear. The temporal analysis considers solutions that are periodic in space and exponential in time, as observed previously for the process.

The linear analysis supposes that the disturbance initially shows a wave-like pattern with infinitesimal amplitude compared to its wavelength and the unperturbed jet radius (see Figure 5.25). However, it has been checked that the prediction from this approach is still valid even when the amplitude increases considerably for certain cases at low velocities. This suggests that the non-linear terms in the momentum equations do not affect significantly the jet in certain cases (Goldin et al. 1969; Li and Fontelos 2003).

The decision to focus on a linear approach instead of a non-linear analysis based on the results observed from experimentation. In all cases the natural instability - not applying any external vibration - leads to uneven disturbances in terms of wavelength and amplitude, increasing in unevenness with the concentration.

Conversely, when an external vibration from 600 Hz is applied, waves with constant wavelengths are observed and the obtained droplets are found regularly in distance. The amplitude of the perturbed jet seems to be growing exponentially on time (see Figures 5.20 and 5.21).

Therefore it is suggested that this pattern may be described by a temporal linear analysis. Hence, it could lead us to a dispersion equation that would indicate the wavelength of the disturbance that becomes in a faster growth for particular conditions. From this parameter also the theoretical size of the resulting droplets could be predicted.

The final objective is the assessment of whether the dispersion relation is appropriate to indicate the best conditions of breakup by comparison with the experimental data and, thus, also predict droplet sizes for these conditions. The description of the nonlinear effects, such as satellite droplet formation and migration will not be considered because

the model is aimed to determine optimal ranges where these nonlinear effects are not observed.

It is worth explicitly mentioning that the model is not intended to describe strictly the microdroplet formation but the optimal frequency to achieve monodisperse samples and the determination of the effect of parameters such as viscosity or flow rate in the evolution and breakup of the jet.

Figure 5.25 shows a perturbed jet moving through an inviscid gas at a mean velocity $\overline{V}$ where the z-axis is parallel and the x-axis is normal to the flow. Some authors have already carried out linear temporal analyses considering the expressions and similar assumptions to those that we will address once again here (Brenn et al. 2000; Gao 2009; Liu and Liu 2006).

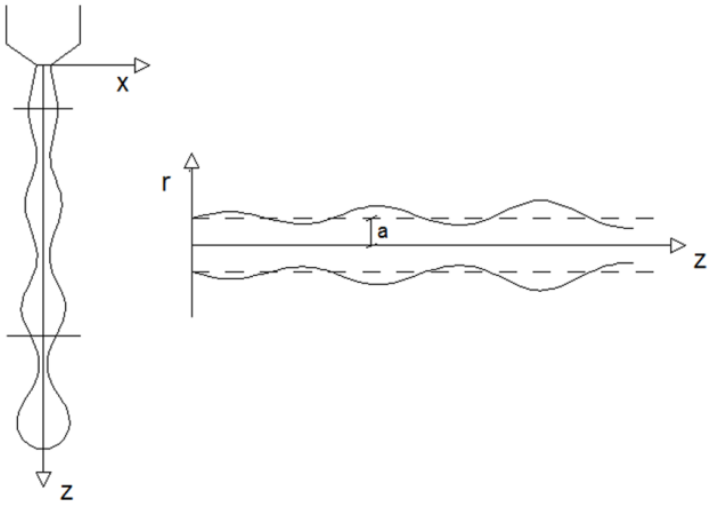

Figure 5.25: Schematic description of the coordinate system and basic parameters of the jet.

The way in which a jet progresses depends on the balance of forces acting on it. These are body forces (gravity, electromagnetic forces and inertial effects), liquid pressure, stresses on the liquid –related mainly to the viscosity term - and surface tension.

The Bond number $Bo = \frac{\rho \cdot g \cdot D^2}{\sigma}$, used before in this study to analyse other phenomena, gives information about the pressure forces acting in the system. It relates

hydrostatic pressure - due to fluid weight – and Laplace contribution - linked to surface tension – (Gennes et al. 2004).

$Bo \approx 10^{-3}$ are obtained with the properties of sodium alginate solutions and considering a 150 μm diameter jet. This indicates that surface tension forces dominate over gravitational effects and control the process. Therefore, gravity forces are considered negligible.

Regarding other physical assumptions heat and mass transfer are also neglected, the fluid is incompressible and constant surface tension is assumed along the jet. Gas inertia is also neglected since the density of the surrounding gas is negligible compared to the liquid density.

It is also assumed that the jet surface is perturbed in a symmetric way, with null velocity component in azimuthal direction.

The analysis starts from the general equations of continuity and momentum:

$$\frac{\partial \rho}{\partial t} + \nabla \cdot \rho \mathbf{v} = 0 \qquad (5.29)$$

$$\rho \left(\frac{\partial}{\partial t} + \mathbf{v} \cdot \nabla \right) \mathbf{v} = -\nabla \cdot \mathbf{T} \qquad (5.30)$$

T is the total stress tensor of the liquid $\mathbf{T} = p\mathbf{I} + \tau$, *p* is the pressure of the fluid, ***I*** is the identity tensor and **τ** is the viscous stress tensor or extra-stress tensor (also called stress deviatoric tensor).

As it was extensively analysed before, sodium alginate solutions exhibit non-Newtonian viscoelastic behaviour. Thus, the analysis requires a non-Newtonian constitutive equation to account for the relationship between the viscous stresses and strain rate.

One of the most general viscoelastic model - the corotational Oldroyd-B (5.31) - is considered for the study. Its constants are zero-shear stress viscosity η_0 and time constants t_1 and t_2, relaxation and retardation times respectively.

$$\boldsymbol{\tau}+t_1\frac{D\boldsymbol{\tau}}{Dt}-\left(\nabla\mathbf{v}\right)^T\cdot\boldsymbol{\tau}-\boldsymbol{\tau}\left(\nabla\mathbf{v}\right)=2\eta_0\left[\mathbf{D}+t_2\frac{D\mathbf{D}}{Dt}-\left(\nabla\mathbf{v}\right)\cdot\mathbf{D}-\mathbf{D}\left(\nabla\mathbf{v}\right)^T\right] \qquad (5.31)$$

Where the deformation tensor is defined as: $\mathbf{D}=\frac{1}{2}\left\{\nabla\mathbf{v}+\left(\nabla\mathbf{v}\right)^T\right\}$

Considering incompressible flow and linearizing the constitutive equation expressions (5.29 - 5.31) become (5.32 – 5.34):

$$\nabla\cdot\mathbf{v}=0 \qquad (5.32)$$

$$\rho\left(\frac{\partial}{\partial t}+\overline{V}\cdot\frac{\partial}{\partial z}\right)\mathbf{v}=-\nabla\cdot\left(p\mathbf{I}+\boldsymbol{\tau}\right) \qquad (5.33)$$

$$\boldsymbol{\tau}+t_1\left(\frac{\partial}{\partial t}+\overline{V}\cdot\frac{\partial}{\partial z}\right)\boldsymbol{\tau}=-\eta_0\left[\dot{\boldsymbol{\gamma}}+t_2\left(\frac{\partial}{\partial t}+\overline{V}\cdot\frac{\partial}{\partial z}\right)\dot{\boldsymbol{\gamma}}\right] \qquad (5.34)$$

As basis of the study and as observed, the instability in the cylindrical jet induces an axisymmetric wave in the surface of the fluid which applies to surface displacement but also velocities, pressure and stress and strain tensors profiles.

The harmonic perturbations are of the form (5.35) according to a linear temporal analysis with varicose perturbation mode. Altered profiles for velocity, pressure, stress tensor and strain rate tensor are described by (5.36-5.39):

$$r_s=a+A_0e^{(\omega t+ikz)} \qquad (5.35)$$

where *a* is the radius of the unperturbed jet, *z* is the axial component, *ω* is a complex frequency (its real part ω_r represents the growth rate of the disturbance and its imaginary part the frequency), *t* is time, A_0 is the amplitude of the perturbation at t_0, and *k* is the wave number.

$$\mathbf{v}=\mathbf{V}(r)e^{(\omega t+ikz)}:\quad v_r=v_{r0}e^{(\omega t+ikz)}\ ,\quad v_z=v_{z0}e^{(\omega t+ikz)} \qquad (5.36)$$

$$p=P(r)e^{(\omega t+ikz)} \qquad (5.37)$$

$$\boldsymbol{\tau}=\mathbf{T}(r)e^{(\omega t+ikz)} \qquad (5.38)$$

$$\dot{\boldsymbol{\gamma}} = \dot{\boldsymbol{\Gamma}}(r)e^{(\omega t + ikz)} \qquad (5.39)$$

Substituting expression (5.38 - 5.39) into (5.34) the expression (5.40) is obtained

$$\tau = \eta(\omega)\dot{\gamma} \qquad (5.40)$$

Where $\eta(\omega) = \eta_0 \dfrac{1 + t_2\left(\omega + ik\overline{U}\right)}{1 + t_1\left(\omega + ik\overline{U}\right)}$ (5.41)

These last expressions into (5.32-5.33), expressed in scalar and cylindrical coordinates, leads to the partial differential equations (5.42-5.44):

$$\frac{1}{r}\frac{\partial}{\partial r}(rv_r) + \frac{\partial v_z}{\partial z} = 0 \qquad (5.42)$$

$$\rho\left(\frac{\partial v_r}{\partial t} + \bar{V}\frac{\partial v_r}{\partial z}\right) = -\frac{\partial p}{\partial r} + \eta(\omega)\left[\frac{\partial}{\partial r}\left(\frac{1}{r}\frac{\partial}{\partial r}(rv_r)\right) + \frac{\partial^2 v_r}{\partial z^2}\right] \qquad (5.43)$$

$$\rho\left(\frac{\partial v_z}{\partial t} + \bar{V}\frac{\partial v_z}{\partial z}\right) = -\frac{\partial p}{\partial z} + \eta(\omega)\left[\frac{1}{r}\frac{\partial}{\partial r}\left(r\frac{\partial v_z}{\partial r}\right) + \frac{\partial^2 v_z}{\partial z^2}\right] \qquad (5.44)$$

These PDEs are reduced to ordinary differential equations by substituting (5.36 - 5.37) into (5.42 – 5.44). The resulting ODEs are of the form of Bessel functions with respect to the variable *r*.

The boundary conditions here considered at the gas-liquid interface to solve the system of ODEs were already applied by Tomotika (Tomotika 1935).

The kinematic condition or no slipping condition at the surface of the jet (5.45) requires that the velocity components are continuous at the surface.

The dynamic boundary conditions (5.46-5.47) define the tangential stress parallel to the surface as continuous at the surface of the column and relate the difference in the normal stress between the inside and outside of the column to the interfacial surface tension.

$$v_r = \left(\frac{\partial}{\partial t} + \overline{V} \cdot \nabla \right) \left(A_0 e^{(\omega t - jkz)} \right) \qquad (5.45)$$

$$\mathbf{T} \times \mathbf{n} = 0 \qquad (5.46) \quad \text{(there are no eddies)}$$

$$\mathbf{T} \cdot \mathbf{n} + \sigma \nabla \cdot \mathbf{n} = 0 \qquad (5.47)$$

Expressions (5.48-5.52) result from linearizing and defining parameters in (5.46-5.47).

$$v_r = \left(\frac{\partial \left(A_0 e^{(\omega t - jkz)} \right)}{\partial t} + \overline{V} \cdot \frac{\partial \left(A_0 e^{(\omega t - jkz)} \right)}{\partial z} \right) \qquad r = a \qquad (5.48)$$

$$T_{rz} = \tau_{rz} = -\eta(\omega) \left(\frac{\partial v_z}{\partial r} + \frac{\partial v_r}{\partial z} \right) = 0 \qquad r = a \qquad (5.49)$$

$$T_{rr} + p_\sigma = 0 \qquad r = a \qquad (5.50)$$

$$\text{Where } T_{rr} = p + \tau_{rr} = p - 2\eta(\omega) \frac{\partial v_r}{\partial r} \qquad (5.51)$$

$$p_\sigma = \frac{\sigma_0}{a^2} \left(A_0 e^{ikz+\omega t} + a^2 \frac{\partial^2 \left(A_0 e^{ikz+\omega t} \right)}{\partial z^2} \right) = \frac{\sigma_0}{a^2} \left(1 - a^2 k^2 \right) A_0 e^{ikz+\omega t} \qquad (5.52)$$

The profiles (5.53 - 5.55) are obtained after solving the system of ODEs

$$v_r = \left[\frac{l^2 + k^2}{I_1(ka)} I_1(kr) - \frac{2k^2}{I_1(la)} I_1(lr) \right] \frac{\eta(\omega)}{\rho} A_0 e^{(\omega t - jkz)} \qquad r \le a \qquad (5.53)$$

$$v_z = i \left[\frac{l^2 + k^2}{I_1(ka)} I_0(kr) - \frac{2kl}{I_1(la)} I_0(lr) \right] \frac{\eta(\omega)}{\rho} A_0 e^{(\omega t - jkz)} \qquad r \le a \qquad (5.54)$$

$$p = \frac{l^2 + k^2}{k I_1(ka)} I_0(kr) \eta(\omega) \left(\omega + ik\overline{V} \right) A_0 e^{(\omega t - jkz)} \qquad r \le a \qquad (5.55)$$

$$\text{Where} \quad l^2 = k^2 + \frac{\rho\left(\omega + ik\bar{V}\right)}{\eta(\omega)} \qquad (5.56)$$

The normal stress T_{rr} in the liquid is obtained from substituting the corresponding equations of velocity and pressure profiles into (5.51):

$$T_{rr} = -\left\{\frac{l^2+k^2}{I_1(ak)}\left[\frac{\rho}{k}\left(\omega + ik\bar{V}\right)I_0(kr) + 2k\eta(\omega)I_1'(kr)\right] - \frac{4k^2 l\eta(\omega)}{I_0(la)}I_1'(lr)\right\}\frac{\eta(\omega)}{\rho}A_0 e^{(\omega t + ikz)} \quad (5.57)$$

The dispersion equation (5.58) is obtained when expressions (5.52) and (5.57) are introduced to define the normal stress boundary condition (5.50)

$$\omega^2 \frac{ak}{2}\frac{I_0(ak)}{I_1(ak)} + \omega\frac{\eta_0}{\rho a^2}\frac{1+\lambda_2\left(\omega + ik\bar{V}\right)}{1+\lambda_1\left(\omega + ik\bar{V}\right)}k^2a^2\left[2ak\frac{I_0(ak)}{I_1(ak)}\frac{l^2}{l^2-k^2} - 1 - 2al\frac{I_0(al)}{I_1(al)}\frac{k^2}{l^2-k^2}\right] = \quad (5.58)$$
$$= \frac{\sigma k^2 a^2}{2\rho a^3}\left(1-k^2a^2\right)$$

Expression (5.59) is obtained from taking the real part and rearranging terms in (5.58)

$$\omega_r^2 \frac{ak}{2}\frac{I_0(ak)}{I_1(ak)} + \omega_r\frac{\eta(\omega)}{\rho}k^2\left[2ak\frac{I_0(ak)}{I_1(ak)}\frac{l^2}{l^2-k^2} - 1 - 2al\frac{I_0(al)}{I_1(al)}\frac{k^2}{l^2-k^2}\right] = \quad (5.59)$$
$$= \frac{\sigma k^2 a^2}{2\rho a^3}\left(1-k^2a^2\right)$$

The expression is adimensionalised (5.63) by using a ratio of deformation retardation time to stress relaxation time $\bar{t} = t_2/t_1$ (time ratio), the Ohnesorge number which denotes the ratio of viscous force to surface tension force: $Oh = \frac{\eta_0}{\sqrt{\rho\sigma a}}$

El, known as elasticity number (Kroesser and Middleman 1969), that represents a relationship between viscous effect and elastic effect in the fluid:

$$El = \frac{t_1 \cdot \eta_0}{\rho \cdot a^2} \qquad (5.60)$$

Ω_r is the non-dimensional growth rate: $\Omega_r = \dfrac{\omega_r}{\sqrt{\sigma/\left(\rho a^3\right)}}$ (5.61)

al can be expressed in dimensionless form by prior parameters as:

$$al = \sqrt{(ak)^2 + \frac{\Omega_r}{Oh}\frac{Oh + El\cdot\Omega_r}{Oh + \bar{t}El\cdot\Omega_r}} \qquad (5.62)$$

$$\left[Oh\frac{Oh+\bar{t}\cdot El\cdot\Omega}{Oh+El\cdot\Omega}\right]^2\left\{2(ak)^2\left[1-\left(\frac{al}{ak}\right)^2\right]+(ak)^3\left[1+\left(\frac{al}{ak}\right)^2\right]^2\frac{I_0(ak)}{I_1(ak)}-4(ak)^2(al)\frac{I_0(al)}{I_1(al)}\right\}= \qquad (5.63)$$

$$=1-(ak)^2$$

(Gao 2009)

5.4.1. Involved parameters in the dispersion relation

The dispersion relation (5.63) includes the rheological parameters of zero-shear viscosity, relaxation time and retardation time - η_0, t_1 and t_2 -.

Zero shear viscosity values can be extracted from the data of the flow curves (see Figure 5.6 in section *5.2.2. Characterization under simple shear flow*).

Table 5.9 shows basic parameters obtained from the fitting of the flow curves to the Cross equation (5.10).

Table 5.9: Rheological parameters obtained by fitting data to the Cross equation.

c (g/dL)	η_0 (Pa·s)	λ_C (s)	m	Ohnesorge
1.5	0.911	$7.66 \cdot 10^{-3}$	0.759	11.33
1.8	2.032	0.0169	0.722	25.28
2.0	2.744	0.0175	0.758	34.14
2.3	4.953	0.0259	0.744	61.62
3.0	12.70	0.0481	0.730	158.01

However, the stress relaxation time was computed from different type of measurements since the concept describe the relaxation of the polymer chains under different external field conditions (such as simple shear or uniaxial extensional fields). Thus, three different values can be extracted from the previous rheological studies, from steady-shear, dynamic-shear and uniaxial extensional flow measurements.

Table 5.10 contains the characteristic relaxation times obtained after applying the three different types of described measurements.

Compared with similar studies the characteristic relaxation times obtained are one order of magnitude higher than those found for other polymeric systems, though the viscosities in this study are higher (Gordon et al. 1973; Kroesser and Middleman 1969). Wloka et al (Wloka et al. 2004) studied extracellular polymeric substances obtaining a lifetime of junction points of 17 ms.

Table 5.10: Characteristic relaxation times obtained from steady shear, SAOS and uniaxial extensional fields. * Data have been extrapolated.

c (g/dL)	η_0 (Pa·s)	$t_{1,SHEAR}$ (s) (λ_C)	$t_{1,SAOS}$ (s) (τ)	$t_{1,CaBER}$ (s) (λ_{ext})
1.5	0.911	$7.66 \cdot 10^{-3}$	0.032	0.0157
1.8	2.032	0.0169	0.078	0.0330*
2.0	2.744	0.0175*	0.080*	0.0410
3.0	12.70	0.0481	0.350	0.0703

As for the parameter t_2 or deformation retardation time (Malkin 1994), the obtaining of satisfactory data through creep analyses was not possible to achieve. The larger viscous nature of the samples compared to the elastic response for low strain rates precluded from obtaining satisfactory data.

Therefore, information found in the literature was considered for the determination of t_2. For instance Bird et al. (Bird et al. 1987) concluded that the ratio between retardation and relaxation time is less than the unit from the analysis of linear viscoelastic models. In most studies the retardation time is considered ten times less than the relaxation times (Gordon et al. 1973; Kroesser and Middleman 1969; Brenn et al. 2000). Thus, the same consideration will be taken in this work, so the dimensionless parameter $\bar{t} = t_2/t_1 = 0.1$.

5.5. Study of the dispersion equation

In the next sections the study of different parameters affecting the behaviour of the system will be assessed through the dispersion curves derived from the mathematical model. Thus, the effect of the rheology of the sample (viscosity and elasticity) and the effect of the flow rate (or velocity) will be analysed.

Authors mentioned before (Brenn et al. 2000; Gao 2009) have checked the applicability of the theoretical dispersion relation derived from a temporal linear model in the disintegration of viscoelastic liquids jets at small Weber and Ohnesorge numbers. The formation of bending instabilities on the jets appear when Weber numbers exceed the order of 10^3 (Yarin 1993) and axisymmetric disturbances are not developed in the jet anymore, invalidating the obtained dispersion relation.

However, no limitations related to high Ohnesorge numbers have been found. Thus, the applicability of the expression for maximum values of Weber numbers around 150 and Ohnesorge values up to 25 will be checked, being another of the followed aims.

Mathematica® software was used to solve and plot the adimensional growth rate Ω as a function of the wavenumber k. These two variables are in implicit form (see expression 5.63).

In order to estimate the maximum value of the function, the Newton's method was used, with the imposed condition of null derivative.

Figures 5.26 shows screen shots of a generic Mathematica notebook containing the basic information to plot and calculate the maximum values of the dispersion curves under specific flow and solution conditions.

In order to determine the theoretical size of droplets, for the fastest growth rate or any other condition, the definition of wavenumber $k = \frac{2\pi}{\lambda}$ is applied, where λ is the interface wave wavelength. For any k given from the dispersion relation (5.63) the wavelength λ can be computed. The estimated droplet size will be calculated as the diameter of a sphere whose volume is that of a cylinder having a length equal to the wavelength so that the volume of the sphere (droplet) equals the volume of the jet cylinder: $\frac{4}{3}\pi r_d^3 = \pi r_j^2 \lambda$ where r_d and r_j are the radii of the droplet and jet respectively. Now frequencies can be computed as $f = \frac{v_j}{\lambda}$ where v_j is the mean jet velocity.

```
Clear["Global`*"]
Off[General::spell, General::spell1]
```

Variable magnitudes and definitions

```
t1 = 0.0157;
t2 = 0.00157;
visc0 = 0.911;
d = 1000;
ST = 0.076;
a = 163.19 * 10^-6 / 2;
v = 4.79;
```

$$El = \frac{t1 * visc0}{d * a^2}$$

$$\lambda = t2 / t1$$

$$Z = \frac{visc0}{(d * ST * a)^{0.5}}$$

```
2148.28

0.1

11.5686
```

$$al := Sqrt\left[(a * k)^2 + \frac{\Omega}{Z}\,\frac{Z + El * \Omega}{Z + \lambda\, El * \Omega}\right]$$

Representation

```
plot1 =
 ContourPlot[
  (Z (Z + λ El Ω)/(Z + El Ω))^2
    (2 (a k)^2 (1 - (al/(a k))^2) + (a k)^3 (1 + (al/(a k))^2)^2 BesselI[0, a k]/BesselI[1, a k] -
      4 (a k)^2 al BesselI[0, al]/BesselI[1, al]) == 1 - (a k)^2, {k, 10, 12000}, {Ω, 0.001, 0.25},
  ContourStyle → {Thick, Blue},
  FrameLabel → {"Wavenumber k (1/m)", "Adimensional growth rate Ω"},
  LabelStyle → Directive[FontFamily → "Helvetica", FontSize → 13, Italic],
  ImageMargins → 50]
```

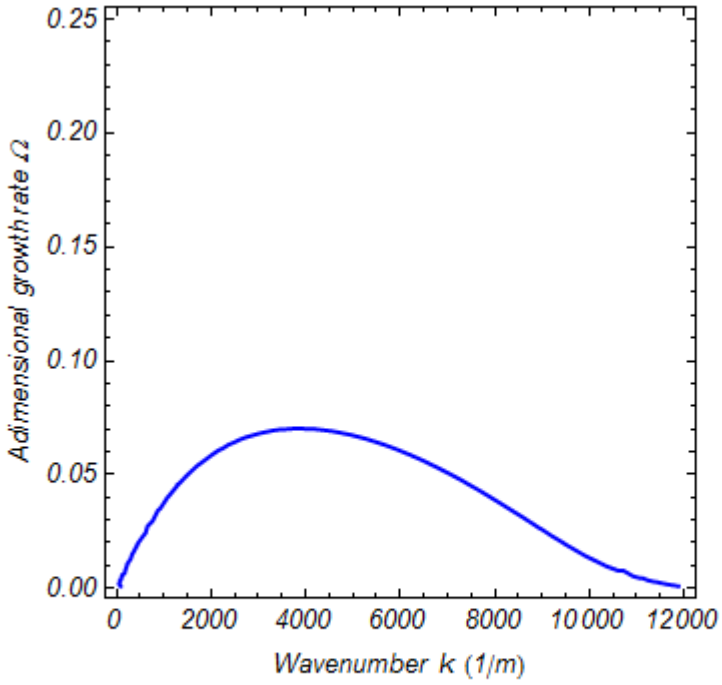

Finding the maximum growth rate, wavenumber and optimum frequency and wavelength

```
expr1 :=
 (Z (Z + λ El Ω)/(Z + El Ω))^2
   (2 (a*k)^2 (1 - (al/(a*k))^2) + (a*k)^3 (1 + (al/(a*k))^2)^2 BesselI[0, a*k]/BesselI[1, a*k] -
     4 (a*k)^2 al BesselI[0, al]/BesselI[1, al]) == 1 - (a*k)^2

expr1d :=
 D[
  (Z (Z + λ El Ω)/(Z + El Ω))^2
    (2 (a*k)^2 (1 - (al/(a*k))^2) + (a*k)^3 (1 + (al/(a*k))^2)^2 BesselI[0, a*k]/BesselI[1, a*k] -
      4 (a*k)^2 al BesselI[0, al]/BesselI[1, al]) - 1 + (a*k)^2, {k}]

sol1 = FindRoot[{expr1, expr1d == 0}, {{Ω, 0.01}, {k, 0.1}}]

{Ω → 0.0702432, k → 3861.56}

sol1 = {Ω, k} /. %
lambda1 = 2 * Pi / sol1[[2]]
f1 = v / lambda1

{0.0702432, 3861.56}

0.00162711

2943.87
```

Figure 5.26: Screen shots of the Mathematica code to approximate the maximum value of the dispersion curve.

As covered in Chapter 4 the expression obtained by Weber (Weber 1931) was used to compute the optimal frequency to impose at the nozzle (5.64). In next sections Weber's wavelengths and linked frequencies will be compared to data from the dispersion relation.

$$\lambda_{opt} = \pi \cdot \sqrt{2} \cdot d_j \left(1 + \frac{3\eta}{\sqrt{\rho\sigma \cdot d_j}}\right)^{1/2} \quad (5.64)$$

5.5.1. Relaxation time effect

The data and recordings obtained experimentally showed certain patterns and behaviours as detailed before (see Fig. 5.20 – 5.21). With the help of these data the concurrent determination of the relaxation time that best defines the behaviour is obtained by comparison between the predicted and experimental conditions.

As explained previously three different values of the relaxation time were determined for every concentration – λ_C from steady shear measurements, τ from dynamic shear measurements and λ_{ext}.from uniaxial extensional measurements -. It is not clear in the literature how the relaxation times are measured in similar studies for the computation of dispersion curves. Therefore, the effect of the different obtained magnitudes will be checked on the results and compare with the experimental data.

Both shear stresses (particularly high in the nozzle) and normal stresses are affecting the jet, however the stretching or extensional effect keeps further downstream the nozzle and is expected to control the breakup process. Therefore, the expectations were finding the best agreement for the relaxation time obtained from extensional measurements.

Pearson (Pearson 1976) already suggested that the pronounced molecular orientation that arises in uniaxial extension was the protagonist of the different effects in jets. He also reported that the orientation of the molecules in uniaxial extension relaxes more slowly than orientation due to simple shear. The way the flow develops in the nozzle is of major importance. A sudden contraction near the exit of the nozzle will produce a profound uniaxial extensional flow combined with shear flow. A long capillary will lead to a fully developed shear profile. In both cases the relaxation behaviours are different.

Furthermore, for the study of uniaxial flow fields, the thinning and break-up of complex liquids have been studied surface conformations to extract characteristic times.

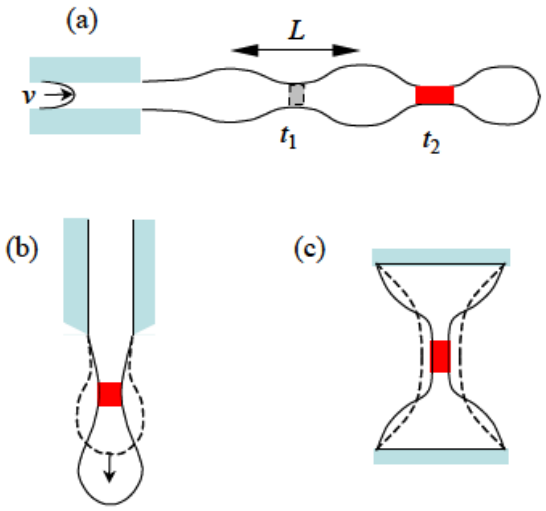

Figure 5.27 : Three prototypical geometries for studying breakup of complex fluids; (a) continuous jetting instability; (b) dripping from a nozzle; (c) necking and breakup of a liquid bridge (McKinley 2005b).

Table 5.10 is copied here for an easy check of the data that the section is dealing with.

Table 5.10: Characteristic relaxation times obtained from steady shear, SAOS and uniaxial extensional fields. * Data have been extrapolated.

c (g/dL)	η_0 (Pa·s)	$t_{1,SHEAR}$ (s) (λ_C)	$t_{1,SAOS}$ (s) (τ)	$t_{1,CaBER}$ (s) (λ_{ext})
1.5	0.911	$7.66 \cdot 10^{-3}$	0.032	0.0157
1.8	2.032	0.0169	0.078	0.0330*
2.0	2.744	0.0175*	0.080*	0.0410
3.0	12.70	0.0481	0.350	0.0703

Figure 5.28 and Table 5.11 reveal the influence of the relaxation time on the growth rate for a 1.8 g/dL solution and 6 mL/min flow rate. The higher the relaxation time the higher the growth rate and the optimal wavenumber *k*, so it is the optimal frequency.

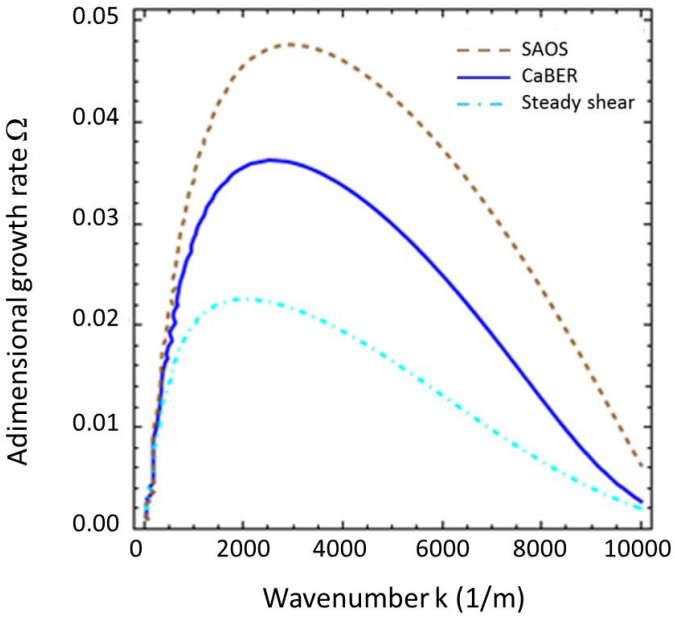

Figure 5.28: Effect of different relaxation times. Sample of 1.8 g/dL at 6 mL/min. Relaxation times: SAOS (dashed line), CaBER (thick line), steady shear (dot-dashed line).

Table 5.11: Predicted and experimental values for the optimal wavenumber, wavelength, droplet size, frequencies and final microparticle size for the different relaxation times obtained for 1.8 g/dL solution at 6 mL/min.

	$t_{1,SHEAR}$ (s)	$t_{1,CaBER}$ (s)	$t_{1,SAOS}$ (s)
t_1 (s)	0.017	0.033	0.078
k (m^{-1})	2034	2577	2952
Ω	0.023	0.036	0.047
λ (m)	0.0076	0.0024	0.0021
Theoretical Size (μm)	523	483	462
Theoretical Frequency (s^{-1})	1335	1691	1938
Experimental size (μm)		≈561	
Experimental frequency (s^{-1})		1500 - 1800	

As said before the best experimental conditions are found for an enclosed range of frequencies. Within this range the obtained microcapsules are more homogeneous.

From the data extracted in Table 5.11 (similarly checked for different samples and flow rates) it is concluded that the computations using the extensional relaxation time are in a better agreement with the experimental conditions. This conclusion agrees with the expected behaviour (extensional effects dominate the process) and therefore, the extensional relaxation time will be considered for the rest of the study.

Regarding the difference between the computed droplet size and the experimental microparticle size it is likely to be due to a swelling of the structure when it solidifies in the gelling bath. The lack of particular studies on the topic precludes from giving more information. Further studies should be done on the issue.

5.5.2. Concentration effect

Already in *Chapter 4: Preliminary studies* it was checked that a variation in concentration means a variation in viscosity, whereas the surface tension remains constant. The effect of viscosity in the dispersion curves can be easily assessed as shown in Figure 5.29. It reveals a pronounced decrease in the dimensionless growth rate when the viscosity increases. The viscous forces oppose to the growth of the capillary instability, causing also a lengthening of the breakup length. At the same time k decreases when viscosity increases. This will cause bigger droplets under the predicted optimal conditions, which agrees with experimental data.

Table 5.12 reveals that the unique optimal Weber's wavelength values for every viscosity are larger than the optimal theoretical ones. This also involves that theoretical optimal frequencies are larger than Weber's dominant frequencies. With Weber conditions the predicted droplet diameters are larger than the theoretical and experimental data.

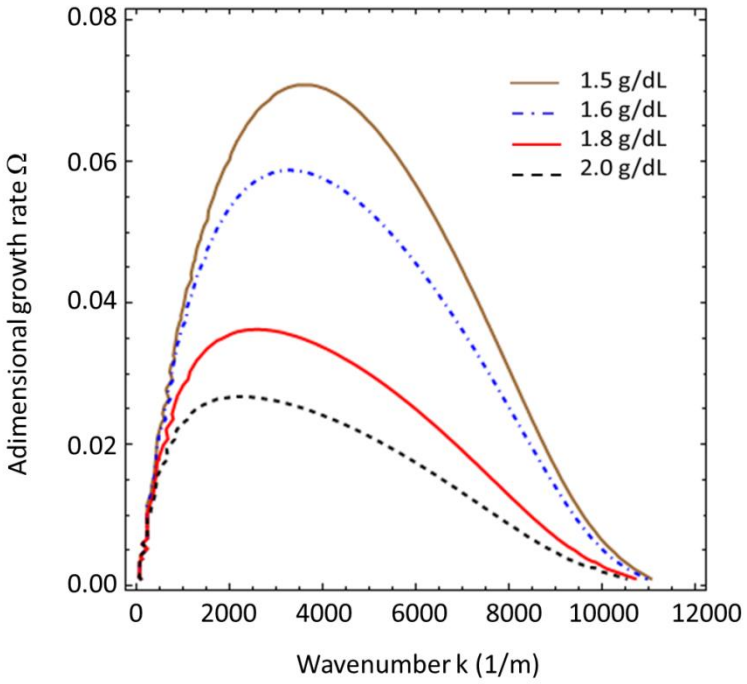

Figure 5.29: Dispersion curves for different concentrations keeping a constant flow rate (6 mL/min): 1.5 g/dL (thick line), 1.6 g/dL (dot-dashed line), 1.8 g/dL (thick line) and 2 g/dL (dashed line).

Table 5.12: Predicted optimal parameters: from the Weber expression (We), the dispersion relation (Th), compared to the experimental parameters (Exp).

Conc (g/dL)	λ_{We} (mm)	λ_{Th} (mm)	ω (s^{-1})	f_{We} (s^{-1})	f_{Th}(s^{-1})	f (s^{-1})	$Size_{We}$ (µm)	$Size_{Th}$ (µm)	$Size_{Exp}$ (µm)
1.50	3.85	1.76	750.3	1070	2365	2100-2500	563	432	508
1.60	4.52	1.92	622.3	913	2153	1900-2200	594	446	512
1.80	5.72	2.44	383.8	721	1691	1500-1800	642	483	561
2.00	6.63	2.84	283.4	622	1453	1200-1500	675	508	625

5.5.3. Flow rate effect

The flow rate has been the most difficult parameter to assess, which reminds about the conclusions collected from the preliminary studies. A change in the flow rate directly affects the velocity of the jet but also its diameter. Whereas the velocity does not appears directly in the dispersion equation (5.62) the variation of the jet radius directly affects it.

Figure 5.30 displays the jet radii as function of flow rate for 1.6, 1.8 and 1.9 g/dL. It indicates that, for this range of concentrations, the diameters remains constant for the same flow rates.

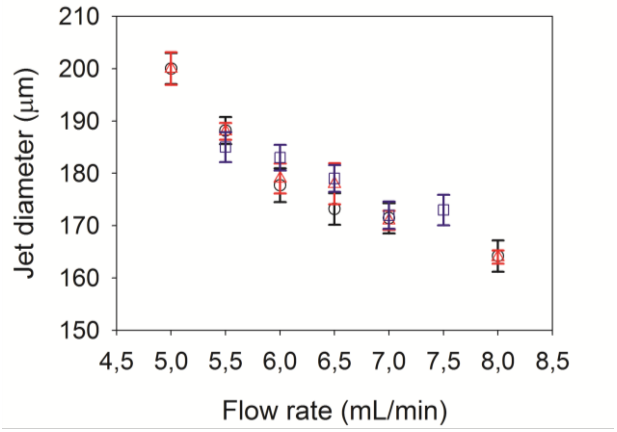

Figure 5.30: Effect of flow rate on the jet diameter.

Figure 5.31 presents dispersion curves for different flow rates keeping a constant concentration of 1.6 g/dL. The figure shows a shift towards higher wavenumbers when the flow rate increases, involving higher optimal frequencies. This tendency agrees with the experimental measurements, where the recordings show that the best conditions are achieved where the dominant conditions in the curve.

The curves in Figure 5.31 represent the growth rate in its adimensional form. Table 5.13 gathers the dimensional data for a better understanding of the phenomena.

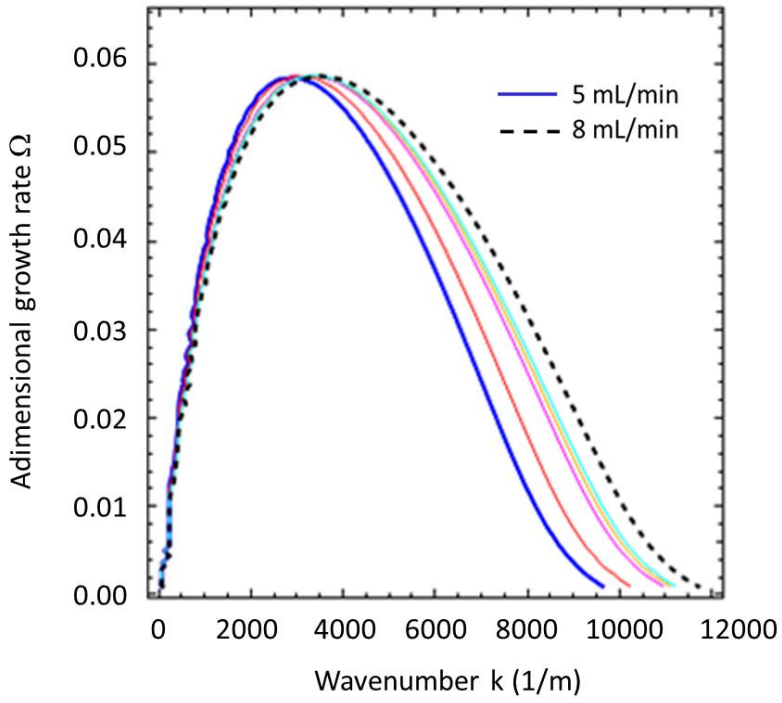

Figure 5.31: Dimensionless growth rate as a function of wavenumber for a 1.6 g/dL alginate solution under different flow rates. Lowest flow rate in thick line – 5 mL/min -, highest flow rate in dashed line – 8 mL/min -.

Data in Table 5.13 show that an increase in the liquid flow rate destabilizes the jet – maximum Ω increases-. It was observed that, in general for the optimal conditions, the breakup length remains almost constant (particularly for low flow rates, see Figure 5.32) or it increases with the flow rate. Therefore, it seems that there is a disagreement between the predicted growth rate and the experimental breakup length. A further study on this issue is needed.

Table 5.13: Optimal wavenumber, growth rate, frequency and size applying different flow rates for a 1.6 g/dL solution.

Q mL/min	λ_{We} (mm)	λ_{Th} (mm)	ω (s^{-1})	f_{We} (s^{-1})	f_{Th} (s^{-1})	f (s^{-1})	$Size_{We}$ (μm)	$Size_{Th}$ (μm)	$Size_{Exp}$ (μm)
5	4.98	2.18	511	533	1215	1100-1300	669	508	-
5.5	4.76	2.05	561	693	1607	1500-1700	633	478	538
6	4.52	1.92	622	913	2154	1900-2200	594	446	512
6.5	4.47	1.88	647	1029	2449	2400-2600	586	440	503
7	4.43	1.87	645	1141	2705	2700-2900	580	435	506
8	4.29	1.79	688	1376	3296	3200-3500	558	417	473

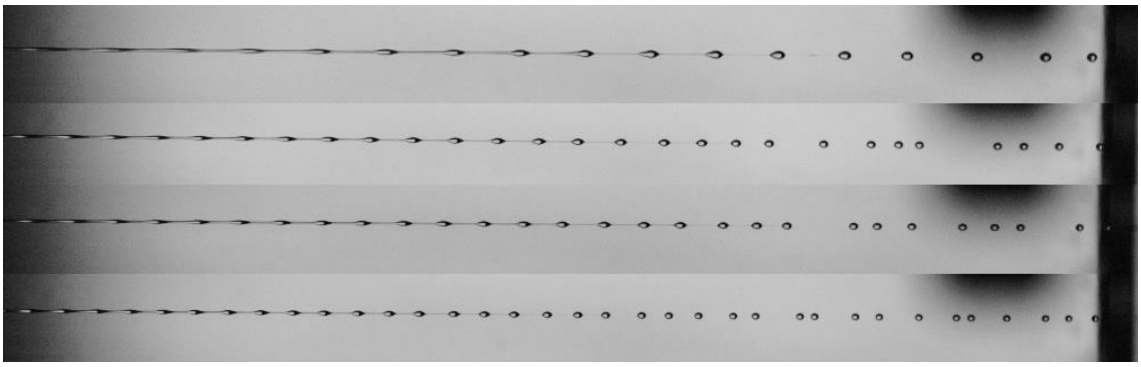

Figure 5.32: Theoretical optimal breakup conditions for jets of 1.6 g/dL alginate solution under different flow rates – 5, 5.5, 6 y 6.5 mL/min -.

5.6. Conclusions

Some conclusions were extracted from the information collected in this chapter are summarized.

Regarding the rheological properties of sodium alginate in salt-free solutions the scaling theories shows their accordance with a polyelectrolyte behaviour for low concentrations with a shift to a neutral polymer behaviour at larger concentrations corresponding to the semi-dilute and entangled regime, as predicted by theory (Dobrynin et al. 1995; Colby 2010).

This behaviour was also supported by the effect of the concentration on the specific viscosity, the relaxation times from steady shear and the longest relaxation times from SAOS measurements.

After analysing the extensional behaviour of the samples under different approaches it was concluded that an exponential filament thinning followed by an eventual break-up result the best regimes that describe the experimental data. Besides, the data pointed out that alginate in salt-free concentrated solutions shows strain thinning of the extensional viscosity.

Finally, a linear analysis accounting for the mechanism of laminar polymeric jet breakup was proposed as a more complete mathematical approach. Previous studies were based on semiempirical procedures.

The linear analysis accounts for viscoelastic effects that were not considered previously.

The analysis allows predicting the optimal range of frequencies to achieve homogeneous samples. Furthermore, it reveals the effects that most influence the system behaviour through the comparison of dispersion curves with the experimental data. Therefore, it could be concluded that the proposed approach is valid for describing the jet breakup mechanism of medium-viscosity viscoelastic polymers.

It was verified that elastic effects rule over simple shear effects through the assessment of different magnitudes of relaxation time, obtained from different flow field measurements. However, it is important to note that the retardation time was not possible to be measured and the data relied on similar studies found in the bibliography.

It is also worth saying that rheological characterization for complex processes such as jet instabilities are experiencing great advances nowadays. As an example, common oscillatory shear measurements are based on assays applying low shear stress measurements (SAOS).

A new technique that superposes an oscillatory motion onto a steady-state shear flow - orthogonal and parallel superposition – is shredding light into the combination of these flow fields. Thus, several authors (Vermant et al. 1998; Kim et al. 2013) have demonstrated that increasing the steady-state shear rate, the crossover of storage and loss moduli G' and G'', shifts to higher frequencies. The relaxation times are rate-dependent. This could lead to the determination of new constitutive equations.

The equation used in this work, Oldroyd-B, has resulted appropriate for the range of concentrations studied.

In the future it would be of highly interest to study non-linear inertial terms and analyse the non-linearity of the viscoelasticity through non-linear approaches. It would help to describe the system further, for instance the satellite droplet formation. Besides, it would also be of high interest to find a relationship between the growth rate and breakup length.

5.7. References

Aleksandrov AP, Lazurkin YS (1940) A Study of Polymers. I. Highly Elastic Deformation of Polymers. Rubber Chemistry and Technology 13 (4):886-898. doi:10.5254/1.3546566

Arnolds O, Buggisch H, Sachsenheimer D, Willenbacher N (2010) Capillary breakup extensional rheometry (CaBER) on semi-dilute and concentrated polyethyleneoxide

(PEO) solutions. Rheologica Acta 49 (11-12):1207-1217. doi:10.1007/s00397-010-0500-7

Barnes HA (1989) Shear-Thickening (``Dilatancy'') in Suspensions of Nonaggregating Solid Particles Dispersed in Newtonian Liquids. Journal of Rheology 33 (2):329-366

Barnes HA (2000) A Handbook of Elementary Rheology

Bird RB, Armstrong RC, Hassager O (eds) (1987) Dynamics of polymeric liquids: Fluid Mechanics, vol 1. Second edn. John Wiley & Sons.

Böhm N, Kulicke W-M (1999) Rheological studies of barley (1→3)(1→4)-β-glucan in concentrated solution: investigation of the viscoelastic flow behaviour in the sol-state. Carbohydrate Research 315 (3–4):293-301. doi:http://dx.doi.org/10.1016/S0008-6215(99)00035-X

Bousfield DW, Keunings R, Marrucci G, Denn MM (1986) Nonlinear analysis of the surface tension driven breakup of viscoelastic filaments. Journal of Non-Newtonian Fluid Mechanics 21 (1):79-97. doi: 10.1016/0377-0257(86)80064-7

Brenn G, Liu Z, Durst F (2000) Linear analysis of the temporal instability of axisymmetrical non-Newtonian liquid jets. International Journal of Multiphase Flow 26 (10):1621-1644. doi: 10.1016/s0301-9322(99)00115-9

Clasen C (2010) Capillary breakup extensional rheometry of semi-dilute polymer solutions. Korea-Australia Rheology Journal 22 (4):331-338

Clasen C, Eggers J, Fontelos MA, Li J, McKinley GH (2006a) The beads-on-string structure of viscoelastic threads. Journal of Fluid Mechanics 556:283-308

Clasen C, Phillips PM, Palangetic L, Vermant, Jan (2012) Dispensing of rheologically complex fluids: The map of misery. AIChE Journal 58 (10):3242-3255. doi:10.1002/aic.13704

Clasen C, Plog JP, Kulicke WM, Owens M, MacOsko C, Scriven LE, Verani M, McKinley GH (2006b) How dilute are dilute solutions in extensional flows? Journal of Rheology 50 (6):849-881

Colby R (2010) Structure and linear viscoelasticity of flexible polymer solutions: comparison of polyelectrolyte and neutral polymer solutions. Rheologica Acta 49 (5):425-442. doi:10.1007/s00397-009-0413-5

Cox WP, Merz EH (1958) Correlation of dynamic and steady flow viscosities. Journal of Polymer Science 28 (118):619-622. doi:10.1002/pol.1958.1202811812

Cross MM (1965) Rheology of non-Newtonian fluids: A new flow equation for pseudoplastic systems. Journal of Colloid Science 20 (5):417-437. doi:10.1016/0095-8522(65)90022-x

Chhabra RP, Richardson JF (eds) (2008) Non-Newtonian Flow and Applied Rheology

Christanti Y, Walker LM (2001) Surface tension driven jet break up of strain-hardening polymer solutions. Journal of Non-Newtonian Fluid Mechanics 100 (1-3):9-26. doi: 10.1016/s0377-0257(01)00135-5

Dobrynin AV, Colby RH, Rubinstein M (1995) Scaling theory of polyelectrolyte solutions. Macromolecules 28 (6):1859-1871

Duxenneuner MR, Fischer P, Windhab EJ, Cooper-White JJ (2008) Extensional Properties of Hydroxypropyl Ether Guar Gum Solutions. Biomacromolecules 9 (11):2989-2996. doi:10.1021/bm800553v

Entov VM (1986) Effect of elastic deformations in the flow of polymer solution. Heat transfer Soviet research 18 (1):60-73

Entov VM, Hinch EJ (1997) Effect of a spectrum of relaxation times on the capillary thinning of a filament of elastic liquid. Journal of Non-Newtonian Fluid Mechanics 72 (1):31-53. doi:http://dx.doi.org/10.1016/S0377-0257(97)00022-0

Fuoss RM, Strauss UP (1949) The Viscosity of mixtures of Polyelectrolytes and simple Electrolytes. Annals of the New York Academy of Sciences 51 (4):836-851. doi:10.1111/j.1749-6632.1949.tb27309.x

Gao Z (2009) Instability of non-Newtonian jets with a surface tension gradient. Journal of Physics A: Mathematical and Theoretical 42 (6):065501

Gennes P-Gd, Brochard-Wyart F, Quere D (eds) (2004) Capillarity and Wetting Phenomena: drops, bubbles, pearls, waves. Springer, New York, USA

Goldin M, Yerushalmi J, Pfeffer R, Shinnar R (1969) Breakup of a laminar capillary jet of a viscoelastic fluid. Journal of Fluid Mechanics 38 (04):689-711. doi:10.1017/S0022112069002540

Gómez Díaz D, Navaza JM (2002) Caracterización reológica de dispersiones agua-alginato sódico con aplicación en la industria alimentaria. Ciencia y Tecnología Alimentaria 3 (5):302-306

Gordon M, Yerushalmi J, Shinnar R (1973) Instability of Jets of Non-Newtonian Fluids. Transactions of the Society of Rheology 17 (2):303-324

Haug A, Smidsrød O (1962) Determination of Intrinsic Viscosity of Alginates. Acta Chemica Scandinavica 16:1569-1578

Haward SJ, Sharma V, Butts CP, McKinley GH, Rahatekar SS (2012) Shear and Extensional Rheology of Cellulose/Ionic Liquid Solutions. Biomacromolecules 13 (5):1688-1699. doi:10.1021/bm300407q

Hilliou L, Freitas F, Oliveira R, Reis MAM, Lespineux D, Grandfils C, Alves VD (2009) Solution properties of an exopolysaccharide from a Pseudomonas strain obtained using glycerol as sole carbon source. Carbohydrate Polymers 78 (3):526-532. doi:http://dx.doi.org/10.1016/j.carbpol.2009.05.011

Kheirandish S, Gubaydullin I, Willenbacher N (2009) Shear and elongational flow behavior of acrylic thickener solutions. Part II: effect of gel content. Rheologica Acta 48 (4):397-407. doi:10.1007/s00397-008-0324-x

Kim S, Mewis J, Clasen C, Vermant J (2013) Superposition rheometry of a wormlike micellar fluid. Rheologica Acta:1-14. doi:10.1007/s00397-013-0718-2

Kroesser FW, Middleman S (1969) Viscoelastic jet stability. AIChE Journal 15 (3):383-386. doi:10.1002/aic.690150316

Kulicke WM, Clasen C, Lohman C (2005) Characterization of Water-Soluble Cellulose Derivatives in Terms of the Molar Mass and Particle Size as well as Their Distribution. Macromolecular Symposia 223 (1):151-174. doi:10.1002/masy.200550511

Li J, Fontelos MA (2003) Drop dynamics on the beads-on-string structure for viscoelastic jets: A numerical study. Physics of Fluids 15 (4):922-937

Lin SP, Reitz RD (1998) Drop and spray formation from a liquid jet. Annual Review of Fluid Mechanics 30 (1):85-105. doi:10.1146/annurev.fluid.30.1.85

Liu Z, Liu Z (2006) Linear analysis of three-dimensional instability of non-Newtonian liquid jets. Journal of Fluid Mechanics 559:451-459. doi:10.1017/S0022112006000413

Macosko CW (ed) (1994) RHEOLOGY: Principles, Measurements and Applications.

Malkin AY (1994) Viscoelasticity. In: Rheology Fundamentals. ChemTec Publishing, Toronto, pp 245-307

Mancini M, Moresi M, Sappino F (1996) Rheological behaviour of aqueous dispersions of algal sodium alginates. Journal of Food Engineering 28 (3–4):283-295. doi:http://dx.doi.org/10.1016/0260-8774(95)00068-2

Marani D, Hjelm J, Wandel M (2013) Use of Intrinsic Viscosity for Evaluation of Polymer-Solvent Affinity. Annual Transactions of the Nordic Rheology Society 21:255-262

McKinley GH (2005a) Dimensionless Groups For Understanding Free Surface Flows of Complex Fluids. Society of Rheology Bulletin 74 (2):6-10

McKinley GH (2005b) Visco-Elasto-Capillary Thinning and Break-Up of Complex Fluids. Hatsopoulos Microfluids Laboratory, Dept. of Mechanical Engineering, Massachusetts Institute of Technology, Cambridge, USA,

Meadows J, Williams PA, Kennedy JC (1995) Comparison of the extensional and shear viscosity characteristics of aqueous hydroxyethyl cellulose solutions. Macromolecules 28 (8):2683-2692. doi:10.1021/ma00112a013

Middleman S (1965) Stability of a viscoelastic jet. Chemical Engineering Science 20 (12):1037-1040. doi: 10.1016/0009-2509(65)80105-1

Miller E, Clasen C, Rothstein J (2009) The effect of step-stretch parameters on capillary breakup extensional rheology (CaBER) measurements. Rheologica Acta 48 (6):625-639. doi:10.1007/s00397-009-0357-9

Morris ER, Cutler AN, Ross-Murphy SB, Rees DA, Price J (1981) Concentration and shear rate dependence of viscosity in random coil polysaccharide solutions. Carbohydrate Polymers 1 (1):5-21. doi:http://dx.doi.org/10.1016/0144-8617(81)90011-4

Muller FL, Davidson JF (1994) Rheology of Shear Thinning Polymer Solutions. Industrial & Engineering Chemistry Research 33 (10):2364-2367. doi:10.1021/ie00034a016

Niedzwiedz K, Arnolds O, Willenbacher N, Brummer R (2009) How to characterize yield stress fluids with capillary breakup extensional rheometry (CaBER)? Applied Rheology 19 (4)

Pearson JRA (1976) Instability in Non-Newtonian Flow. Annual Review of Fluid Mechanics 8 (1):163-181. doi:10.1146/annurev.fl.08.010176.001115

Plateau J (ed) (1873) Statique expérimentale et théorique des liquides soumis aux seules forces moléculaires. Gauthier-Villars, Paris

Rayleigh L (1879) On the capillary phenomena of jets. Proc R Soc London 29

Rodd LE, Scott TP, Cooper-White JJ, McKinley GH (2005) Capillary Break-up Rheometry of Low-Viscosity Elastic Fluids. Applied Rheology 15:12-27

Savart F (1833) Mémoire sur la constitution des veines liquides lancées par des orifices circulaires en mince paroi. Annali di Chimica 53:337-386

Simeone M, Alfani A, Guido S (2004) Phase diagram, rheology and interfacial tension of aqueous mixtures of Na-caseinate and Na-alginate. Food Hydrocolloids 18 (3):463-470. doi:http://dx.doi.org/10.1016/j.foodhyd.2003.08.004

Smidsrød O (1970) Solution properties of alginate. Carbohydrate Research 13 (3):359-372. doi:http://dx.doi.org/10.1016/S0008-6215(00)80593-5

Steffe JF (ed) (1992) Rheological Methods in Food Process Engineering. Freeman Press.

Stelter M, Brenn G, Yarin AL, Singh RP, Durst F (2000) Validation and application of a novel elongational device for polymer solutions. Journal of Rheology 44 (3):595-616

Storz H, Zimmermann U, Zimmermann H, Kulicke W-M (2010) Viscoelastic properties of ultra-high viscosity alginates. Rheologica Acta 49 (2):155-167. doi:10.1007/s00397-009-0400-x

Tirtaatmadja V, Sridhar T (1993) A filament stretching device for measurement of extensional viscosity. Journal of Rheology 37 (6):1081-1102

Tomotika S (1935) On the Instability of a Cylindrical Thread of a Viscous Liquid Sorrounded by Another Viscous Fluid. Proc R Soc Lond A:322-337

Vadillo DC, Mathues W, Clasen C (2012) Microsecond relaxation processes in shear and extensional flows of weakly elastic polymer solutions. Rheologica Acta 51 (8):755-769

Vermant J, Walker L, Moldenaers P, Mewis J (1998) Orthogonal versus parallel superposition measurements. Journal of Non-Newtonian Fluid Mechanics 79 (2–3):173-189. doi:http://dx.doi.org/10.1016/S0377-0257(98)00105-0

Weber C (1931) Zum Zerfall eines Flüssigkeitsstrahls. Zeit für angewandte Mathematik und Mechanik. 11:136

Willenbacher N., Matter Y., Gubaydullin I, Schaedler V (2008) Effect of aggregation on shear and elongational flow properties of acrylic thickeners. Korea-Australia Rheology Journal 20(3):109-116.

Wloka M, Rehage H, Flemming HC, Wingender J (2004) Rheological properties of viscoelastic biofilm extracellular polymeric substances and comparison to the behavior of calcium alginate gels. Colloid & Polymer Science 282 (10):1067-1076. doi:10.1007/s00396-003-1033-8

Xiao Q, Tong Q, Lim L-T (2012) Pullulan-sodium alginate based edible films: Rheological properties of film forming solutions. Carbohydrate Polymers 87 (2):1689-1695. doi:http://dx.doi.org/10.1016/j.carbpol.2011.09.077

Yarin AL (1993) Free Liquid Jets and Films: Hydrodynamics and Rheology. New York

CHAPTER 6.

CONCLUSIONS AND FUTURE WORK.

6. CONCLUSIONS AND FUTURE WORK

6.1. Conclusions

As general conclusions:

- A new equipment to work with high viscosity polymers for the production of controlled microparticles has been developed. The effect of different parameters on the final microparticles and the preceding microdroplet formation has been modelled under different approaches.

- This new technology successfully generates microparticles with controlled size and high mechanical resistance for their use in biomedical applications.

- The microparticles range from 300 to 600 micrometres and are produced from medium-high viscosity polymers.

From the experimental and theoretical studies performed in this work the following particular conclusions can be extracted.

- A **new technique** based in a combined technology of vibrating nozzle and pressurized system overcomes the difficulties concerning the processing of medium/high viscosity bulk solutions into capillary stable continuous jets. From the set-up experiments the new developed technology succeeded in processing high viscous solutions, creating continuous jets up to 10000 mPa·s.

- This technique controls the evolution of laminar instabilities on continuous jets, which leads eventually to jet breakup and droplet formation, followed by a process of solidification. A study of the influence of physic-chemical variables on the microparticle size is carried out through the generation of behavioural curves and the analysis of the dependence of SMD on viscosity, flow rate and surface tension employing dimensionless numbers.

- The stabilizing behaviour of the viscosity was clearly observed. However, the effect of flow rate posed questions. The special relevance of shear and extensional effects on the behaviour of the systems comes into play as for further considerations (rheology of the solutions).

- Considering the influence of viscosity and flow rate, a first approach to the physical process is tackled by relating particle size and these variables through mathematical expressions. Thus, a set of semiempirical equations based on the wave mechanism theory are assessed as tool for predicting microcapsule size.

- The obtained semiempirical equations acceptably predict the size of particles under certain conditions, namely for viscosities above 1500 mPa·s. One of the proposed expressions shows a good agreement under all assayed conditions, demonstrating that the wave mechanism, accepted for non-Newtonian liquids atomization, can be also applied to the new developed system. For this analysis the applied frequency is computed from the Weber equation for viscous Newtonian fluids.

- The **rheological properties** of sodium alginate in salt-free solutions were determined in order to analyse the influence of the different flow fields affecting the process.

- The salt-free solutions of sodium alginate show polyelectrolyte behaviour for low concentrations, shifting to a neutral polymer behaviour at larger concentrations. This is confirmed by scaling theories applied to the effect of the concentration on the specific viscosity and on different relaxation times.

The analysis of the behaviour of the samples under extensional field was computed under two different approaches.

- An exponential filament thinning followed by an eventual break-up result the best regimes that describe the experimental data. Moreover, the solutions show strain thinning of the extensional viscosity.

Once the rheology of the polymer is characterized a more complete **physical approach** to the analysis of the instability is addressed, with the help of image analysis for comparison.

- The images captured by a high-speed camera show a Bead-on-a-String (BOAS) structure, typically encountered in the breakup of viscoelastic materials. The range of frequencies that lead to the breakup of the jet is wide but not all frequencies lead to homogeneous microcapsules. Thus, an optimal range is observed in all cases and, in general, there is a minimum frequency from which the jet does not exhibit satellite droplets. Non-linear phenomena of migration, oscillation and merging of droplets are not observed inside these optimal ranges.

- The patterns and tendencies from the experimental observation show that when the viscosity increases, for the same flow rate and disturbance condition, the breakup length increases. Besides, when the flow rate increases, using the best breakup conditions, the breakup length increases or maintain relatively constant.

A temporal linear analysis is proposed to account for the mechanism of laminar polymer jet breakup, with the main aim of determining the best optimal conditions matching with the optimal experimental range of frequencies.

- The linear analysis allows predicting the optimal range of frequencies to achieve homogeneous samples and reveals the effects that most affect the system behaviour through a dispersion relation - relating wavenumber and growth rate of the waves – and by comparison of the related dispersion curves with the experimental data.

- Through the assessment of different magnitudes of the relaxation time (obtained from measurements under different flow fields) it was verified that extensional effects rule over simple shear effects.

- The dispersion curves predict shorter growth rates with an increase in the viscosity and relatively constant growth rates when the flow rate increases. This latter

behaviour does create uncertainties once again about the prediction concerning the effect of the flow rate.

- The proposed approach is valid for describing the jet breakup mechanism of medium-viscosity polymers. The equation used in this work, Oldroyd-B, has resulted appropriate in the range of concentrations studied.

- **Computational Fluid Dynamics (CFD) analyses** were carried out in order to set up solvers and conditions that allowed comparing numerical solutions with the experimental results to provide a solid base for a possible scale-up. The inclusion of viscoelastic models was attempted through UDFs but was not successful.

- The obtained trends showed interesting qualitative results, in agreement with the trends observed in the experimental data. However, the use of generalized Newtonian models does not account for the formation of a bead-on-a-string (BOAS) structure as the one seen in the experimental images.

- The use of the Volume of Fluid (VOF) model and the considered set-up deals reasonably well with the interface tracking. The results show coherency and lead us to consider the use of VOF adequate for the study of capillary laminar instabilities.

6.2. Improvements and Future work

During the process and completion of this work certain new ideas and possible ideas for improving the study have come up. Some of them are highlighted next, trying to keep a logical order with the thesis contents.

In order to improve the **experimental conditions**, the effects concerning coalescence of droplets that affect the dispersion of the resulting microparticles, should be minimized. To avoid aggregates during the droplet fall and during the hardening step an electrostatic field can be applied to the droplets (Serp et al. 2000). The system comprises the generation of an electrostatic field with the help of a charged electrode installed close down the nozzle exit and an earth-electrode in the hardening solution.

Figure 8.1 represents the scheme of a commercial device including the described system. The electrostatic effect makes the particles present the same charge in its surface – negative charges in the case of sodium alginate solutions - and repel each other.

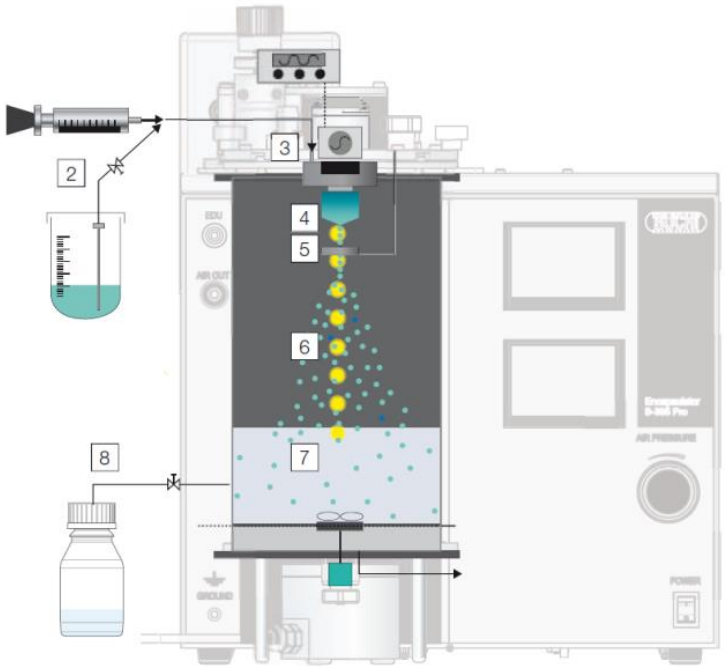

Figure 8.1: Scheme of a *BÜCHI Labortechnik AG* commercial device that includes an electrostatic dispersion unit.

During the experimentation performed in this work the application of an electrostatic field was implemented with the help of a high voltage power source and two electrodes (drilled metal disk or washer in the fall and metallic plate in the hardening solution).

Figure 8.2 shows the obtained results increasing the voltage – 2, 4 and 6 kV-. The results in terms of separating the droplets were satisfactory. However, the need to high voltages and the lack of protective measurements precluded from working under these conditions.

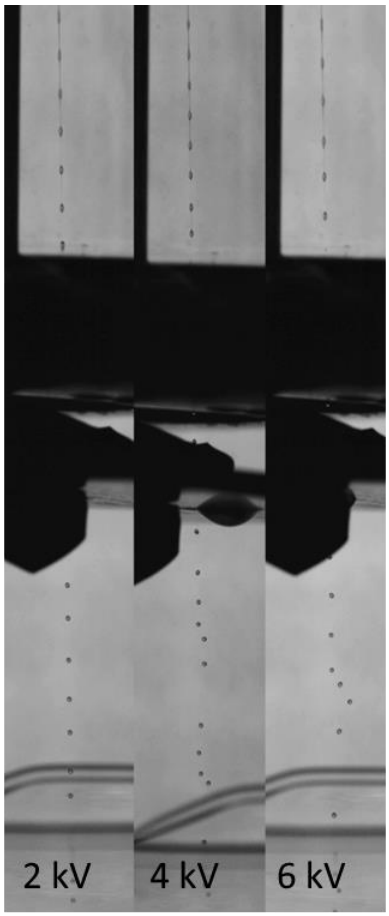

Figure 8.2: Effect on the droplet fall under the application of electrostatic fields from 2, 4 and 6 kV.

The use of surrounding accelerated air would also modify the evolution of the droplets. Depending on the air conditions even the breakup regime could change, though

this could be the aim of a different type of work. However, not changing the instability regime the effects of accelerated air could be studied.

In relation to the **characterization of the samples** some other studies could be performed. A detailed chemical analysis of the solutions, such as molecular weight distribution of the polymer or ionic strength of the samples, would help to analyse the behaviour of the system.

A study of the effect of salt content in the rheological properties, as complementary to the free-salt solutions analysis, could provide information to tune settings for better experimental results.

As for **viscoelastic properties**, it would be of high interest the experimental determination of the retardation time. It could not be measured and the data were obtained from similar studies found in the literature. Checking further information of possible ways to measure it should be addressed.

Furthermore, the determination of rheological properties, such as relaxation times, by Large Amplitude Oscillatory Shear (LAOS) (Ewoldt et al. 2008) or superposition analyses (Vermant et al. 1998) could shred light into the characterization of this type of systems, subjected to high shear stresses, where the relaxation times is generally characterized in the linear viscoelastic region when the process actually takes place in the non-linear viscoelastic region.

Regarding both the **mathematical analysis** of the process and rheological aspects, the non-linearity of the phenomenon (through nonlinear analysis) and other rheological models should be assessed (such as FENE-P or Giesekus) (Fontelos and Li 2004).

A relationship between the breakup length and the growth rate should also be established, as to predict the former as a function of the latter when the dispersion curves are evaluated.

Concerning **CFD studies,** the inclusion of more complex constitutive equations than Generalized Newtonian models must be addressed (such as Oldroyd-B, FENE-P or Giesekus

as mentioned before). Also the interaction with an electrostatic field or air drag forces could be studied.

Furthermore, the study of mass transfer and structural stability of the droplets when hitting and introducing in the gelling bath should be performed for a better knowledge of the process and the classification of more physical phenomena involved that allow a more robust predictive modelling (swelling / shrinkage and transport phenomena in the gelation process should be further analysed).

After a better modelling of the system CFD studies dealing with the behaviour of the microcapsules under physiological or transport conditions would also be of high interest (couples CFD-DEM models).

Other approaches would include the study of variables that have not been modified in this work, such as the surface tension or the nozzle diameter. The addition of surfactants or changes in the surface tension induced by thermal variations could be analysed by experimentation and considered in mathematical and computational models.

6.3. References

Ewoldt RH., Hosoi AE, McKinley GH (2008) New measures for characterizing nonlinear viscoelasticity in large amplitude oscillatory shear. Journal of Rheology (1978-present) 52(6):1427-1458.

Fontelos, MA., Jie L (2004) On the evolution and rupture of filaments in Giesekus and FENE models. Journal of Non-Newtonian Fluid Mechanics 118(1):1-16.

Serp D, Cantana E, Heinzen C, Von Stockar U, Marison IW (2000) Characterization of an encapsulation device for the production of monodisperse alginate beads for cell immobilization. Biotechnology and Bioengineering 70 (1):41-53.

Vermant J, Walker L, Moldenaers P, Mewis J (1998) Orthogonal versus parallel superposition measurements. Journal of Non-Newtonian Fluid Mechanics 79 (2–3):173-189. doi:http://dx.doi.org/10.1016/S0377-0257(98)00105-0

APPENDIXES

APPENDIX A – Data of blank runs and set-up experiments

I) Preliminary studies on the commercial device

Tested conditions for a 260 mPa·s alginate solution (maximum viscosity processed)

Frequency	size	span
800	316	0.870
900	323	0.983
1100	315	1.035
1200	291	1.071

Images

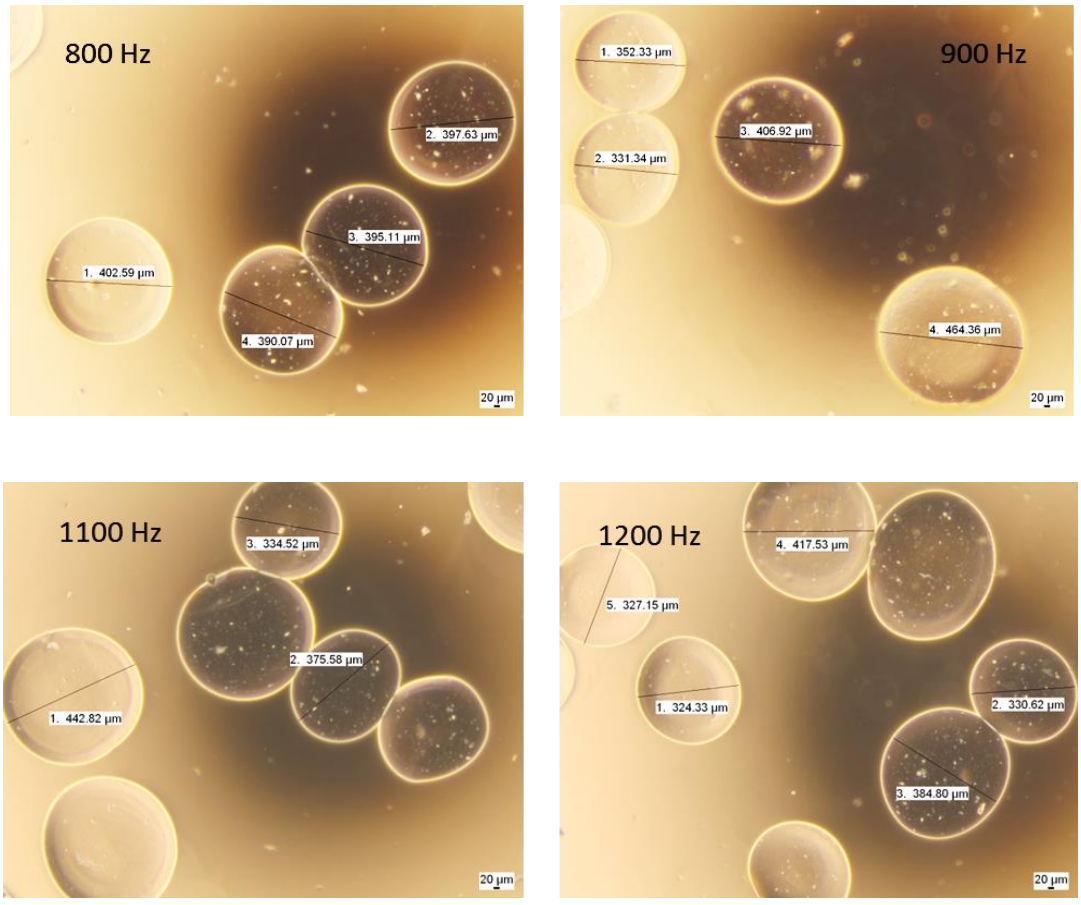

Microparticles obtained from a 260 mPa·s alginate solution -800, 900, 1100 and 1200 Hz -.

Distributions

Concentration:	Span :	Uniformity:	Result units:
0.6377 %Vol	0.870	0.272	Volume
Specific Surface Area:	**Surface Weighted Mean D[3,2]:**	**Vol. Weighted Mean D[4,3]:**	
0.019 m²/g	316.438 um	350.384 um	

d(0.1): 219.043 um **d(0.5): 332.342 um** **d(0.9): 508.226 um**

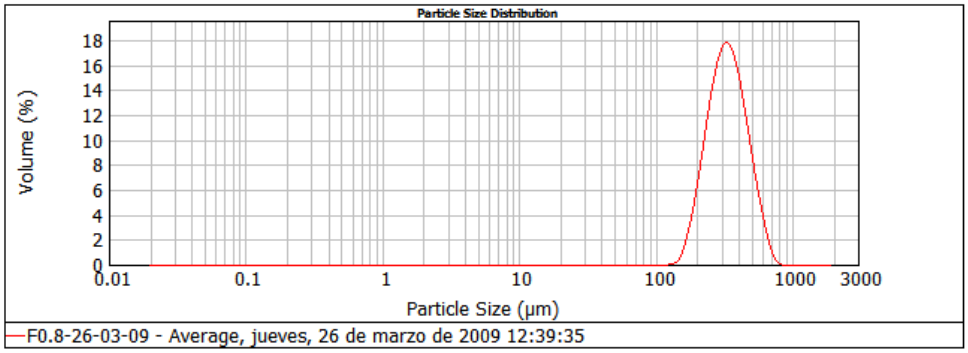

Distribution for a 260 mPa·s alginate solution applying 800 Hz.

Concentration:	Span :	Uniformity:	Result units:
.6270 %Vol	0.983	0.302	Volume
Specific Surface Area:	**Surface Weighted Mean D[3,2]:**	**Vol. Weighted Mean D[4,3]:**	
.0186 m²/g	323.185 um	367.279 um	

d(0.1): 214.101 um **d(0.5): 345.495 um** **d(0.9): 553.684 um**

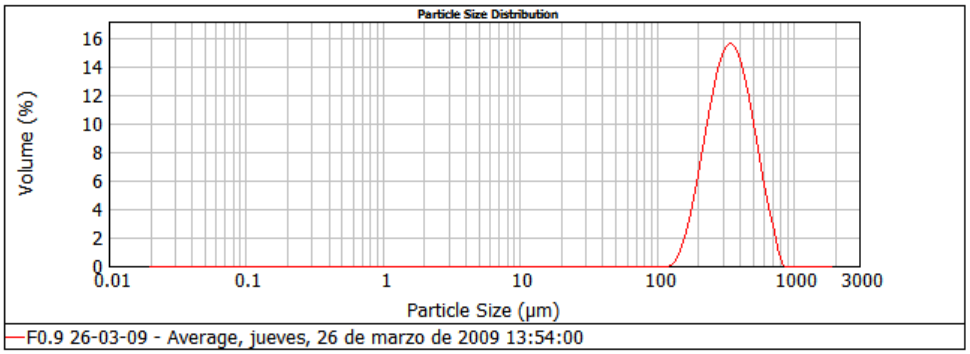

Distribution for a 260 mPa·s alginate solution applying 900 Hz.

Concentration:	Span :	Uniformity:	Result units:
1.5858 %Vol	1.035	0.319	Volume
Specific Surface Area:	**Surface Weighted Mean D[3,2]:**	**Vol. Weighted Mean D[4,3]:**	
1.0191 m²/g	314.777 um	362.098 um	

d(0.1): 204.202 um d(0.5): 339.393 um d(0.9): 555.419 um

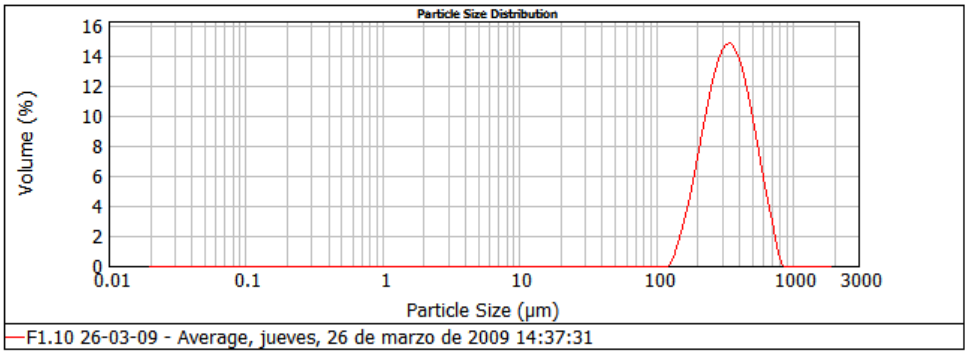

Distribution for a 260 mPa·s alginate solution applying 1100 Hz.

Concentration:	Span :	Uniformity:	Result units:
0.5073 %Vol	1.071	0.334	Volume
Specific Surface Area:	**Surface Weighted Mean D[3,2]:**	**Vol. Weighted Mean D[4,3]:**	
0.0206 m²/g	291.317 um	352.342 um	

d(0.1): 192.398 um d(0.5): 331.749 um d(0.9): 547.607 um

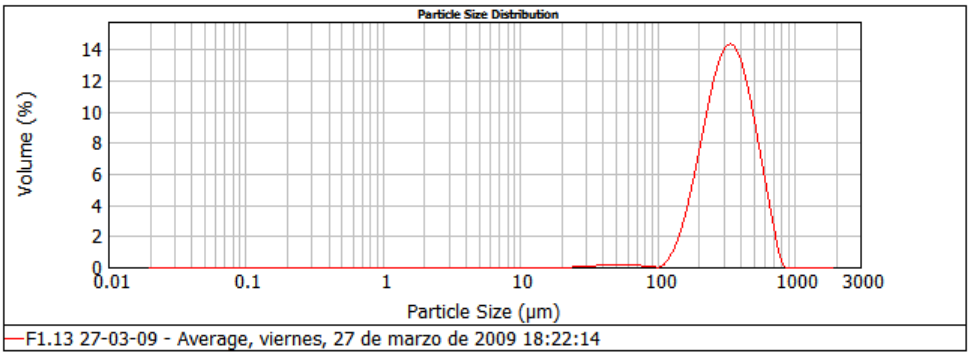

Distribution for a 260 mPa·s alginate solution applying 1200 Hz.

II) Preliminary studies on the commercial device

Preliminary studies with the complete system

Alginate 1.0 % w/w	**Flow rate 5 mL/min**	
Frequency (s^{-1})	Size (µm)	Span
0	563	1.112
400	468	1.007
700	508	0.878
900	505	0.942
1850	477	0.951
2650	467	0.961
3000	472	0.906

Alginate 1.0 % w/w	Flow rate 7 mL/min	
Frequency (s^{-1})	Size (µm)	Span
0	542	1.333
660	527	1.281
1500	510	1.300
1800	482	1.216
2300	521	1.310
2800	533	1.277

Alginate 1.0 % w/w	Flow rate 8.5 mL/min	
Frequency (s^{-1})	Size (µm)	Span
0	520	1.511
700	489	1.434
1600	515	1.446
2000	498	1.536

Alginate 1.5 % w/w Flow rate 5 mL/min		
Frequency (s^{-1})	Size (µm)	Span
400	512	0,662
600	554	0,94
800	484	0,915
1000	534	1,031
1200	535	1,004
1760	476	0,941

Alginate 1.5 % w/w Flow rate 6.5 mL/min		
Frequency (s^{-1})	Size (µm)	Span
450	519	1,095
700	480	1,07
1300	533	1,117
2300	534	0,987

Alginate 1.5 % w/w Flow rate 8.8 mL/min		
Frequency (s^{-1})	Size (µm)	Span
2000	511	1,38
3000	528	1,246

Alginate 2.0 % w/w Flow rate 6 mL/min		
Frequency (s^{-1})	Size (µm)	Span
0	705	0.973
700	616	0.826
850	566	1.106
1200	623	1.014
1700	543	1.003
2050	538	0.967

Alginate 2.0 % w/w Flow rate 6.7 mL/min		
Frequency (s^{-1})	Size (µm)	Span
0	705	1.071
700	575	0.933
1550	633	0.980
2200	544	1.088
2850	606	1.012

Alginate 2.0 % w/w Flow rate 8.8 mL/min		
Frequency (s^{-1})	Size (µm)	Span
0	608	1.144
700	542	0.911
1700	482	1.165
2050	535	1.042
2600	534	1.123

Distributions

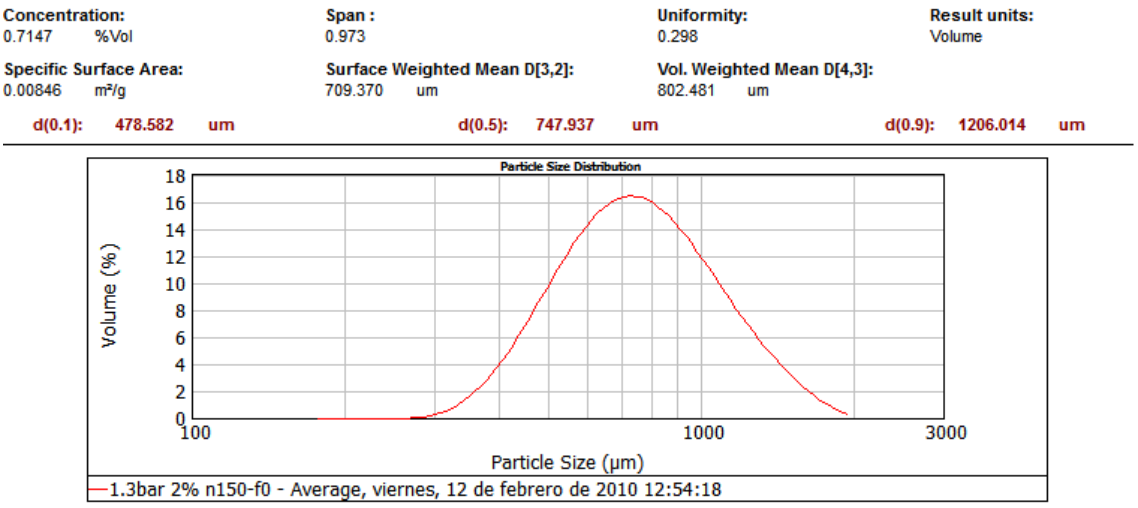

Distribution for a 2.3 Pa·s alginate solution (0 Hz).

Concentration:	Span :	Uniformity:	Result units:
0.8302 %Vol	0.793	0.244	Volume
Specific Surface Area:	**Surface Weighted Mean D[3,2]:**	**Vol. Weighted Mean D[4,3]:**	
0.0096 m²/g	625.322 um	681.567 um	

d(0.1): 447.380 um **d(0.5): 648.770 um** **d(0.9): 962.049 um**

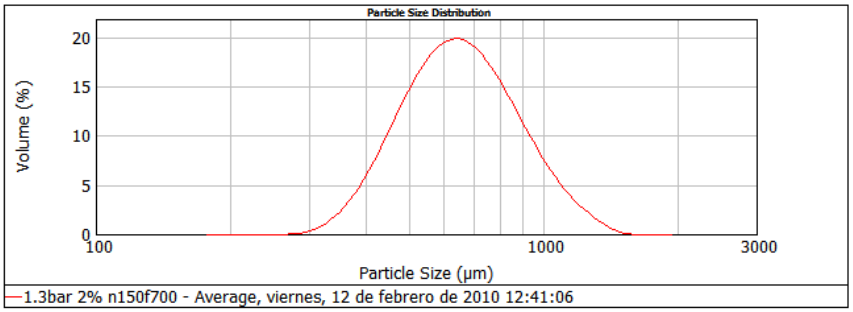

Distribution for a 2.3 Pa·s alginate solution (700 Hz).

Concentration:	Span :	Uniformity:	Result units:
0.8415 %Vol	1.108	0.342	Volume
Specific Surface Area:	**Surface Weighted Mean D[3,2]:**	**Vol. Weighted Mean D[4,3]:**	
0.0106 m²/g	566.690 um	659.618 um	

d(0.1): 364.904 um **d(0.5): 606.996 um** **d(0.9): 1037.371 um**

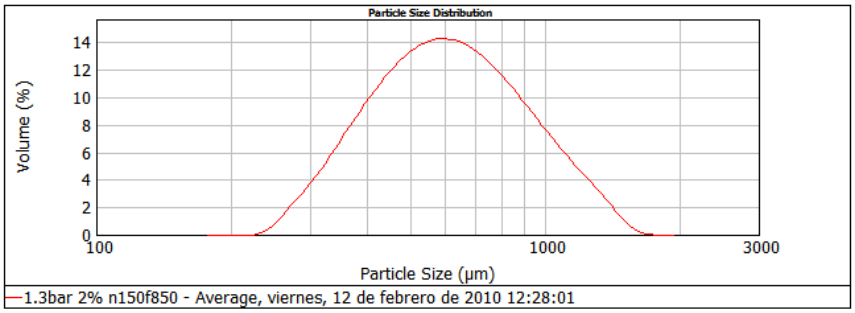

Distribution for a 2.3 Pa·s alginate solution (850 Hz).

Concentration:	Span :	Uniformity:	Result units:
0.6839 %Vol	0.987	0.307	Volume
Specific Surface Area:	**Surface Weighted Mean D[3,2]:**	**Vol. Weighted Mean D[4,3]:**	
0.00948 m²/g	632.871 um	719.229 um	

d(0.1): 423.207 um **d(0.5): 671.492 um** **d(0.9): 1086.225 um**

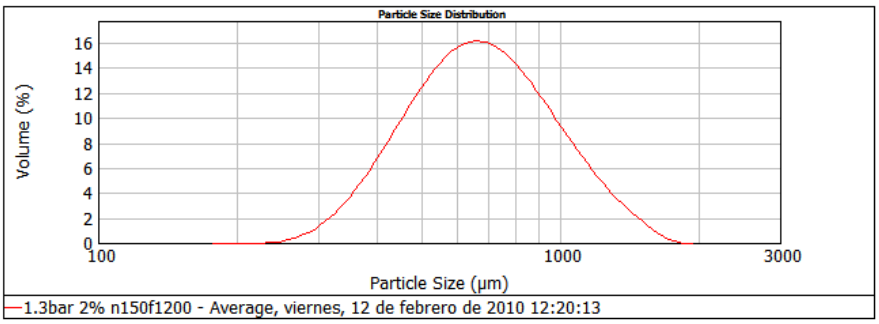

Distribution for a 2.3 Pa·s alginate solution (1200 Hz).

Concentration:	Span :	Uniformity:	Result units:
1.0433 %Vol	0.936	0.293	Volume
Specific Surface Area:	**Surface Weighted Mean D[3,2]:**	**Vol. Weighted Mean D[4,3]:**	
0.0109 m²/g	549.425 um	617.882 um	

d(0.1): 372.689 um **d(0.5):** 579.962 um **d(0.9):** 915.316 um

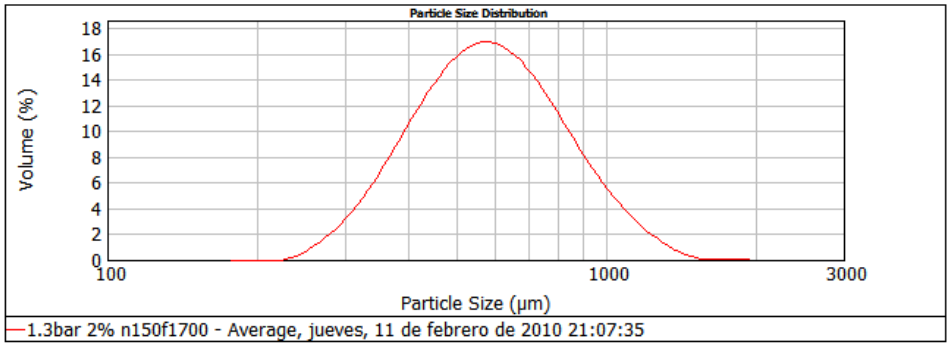

Distribution for a 2.3 Pa·s alginate solution (1700 Hz).

Concentration:	Span :	Uniformity:	Result units:
0.6367 %Vol	0.984	0.306	Volume
Specific Surface Area:	**Surface Weighted Mean D[3,2]:**	**Vol. Weighted Mean D[4,3]:**	
0.0112 m²/g	535.795 um	609.543 um	

d(0.1): 356.809 um **d(0.5):** 570.844 um **d(0.9):** 918.670 um

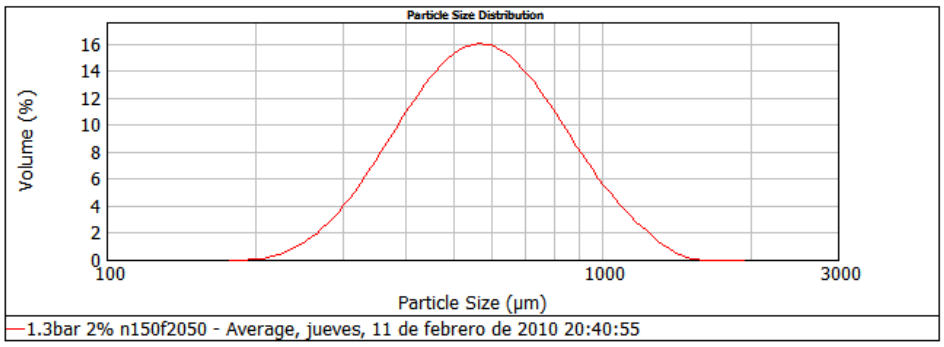

Distribution for a 2.3 Pa·s alginate solution (2050 Hz).

Images

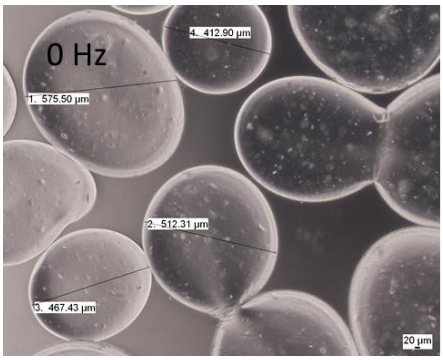

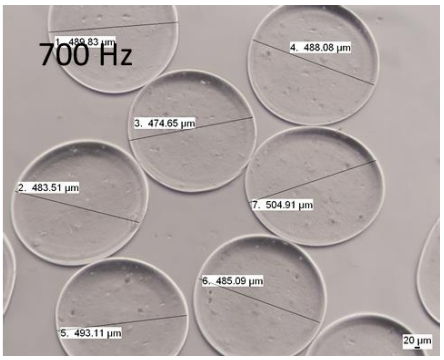

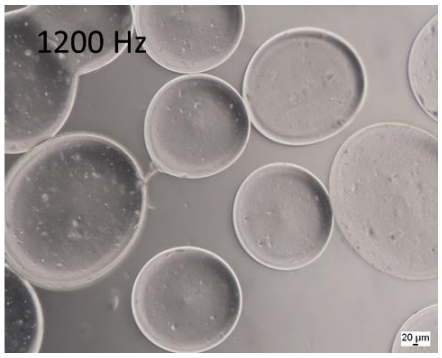

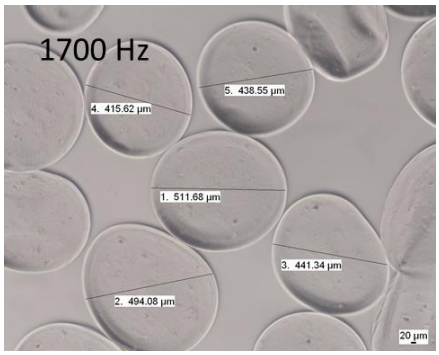

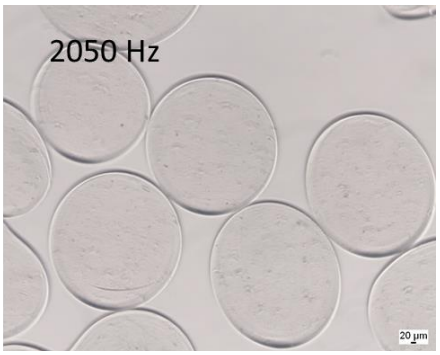

Microparticles obtained from a 2.3 Pa·s alginate solution – different frequencies applied -.

II) Experiments for the built-up of behavioural curves

Microparticle size as a function of viscosity and flow rate.

Q (mL/min)	Viscosity (mPa·s)						
	450	**750**	**1300**	**1720**	**2000**	**2300**	**2620**
5	468	526	555	618	635	658	699
5.5	473	551	585	635	668	**661**	708
6	509	560	**575**	**626**	650	660	707
6.5	505	515	562	-	-	**650**	683
7	496	502	-	**608**	627	-	677
7.5	499	500	539	-	-	621	680
8	-	503	**521**	**563**	605	**612**	662
8.5	-	505	503	**553**	553	580	622
9	-	-	502	**517**	525	**540**	575

Distributions: applying optimal frequencies computed from the Weber expression (4.4).

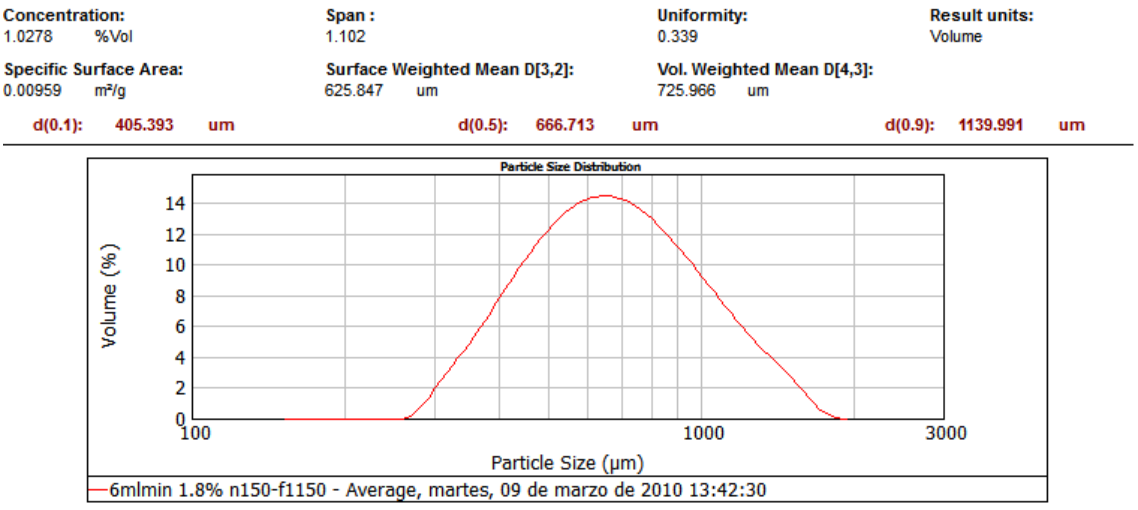

Distribution for a 1.720 Pa·s alginate solution at 6 mL/min.

Concentration:	Span :	Uniformity:	Result units:
0.7692 %Vol	0.991	0.303	Volume
Specific Surface Area:	**Surface Weighted Mean D[3,2]:**	**Vol. Weighted Mean D[4,3]:**	
0.00987 m²/g	607.928 um	690.017 um	

d(0.1): 408.466 um **d(0.5): 641.212 um** **d(0.9): 1043.943 um**

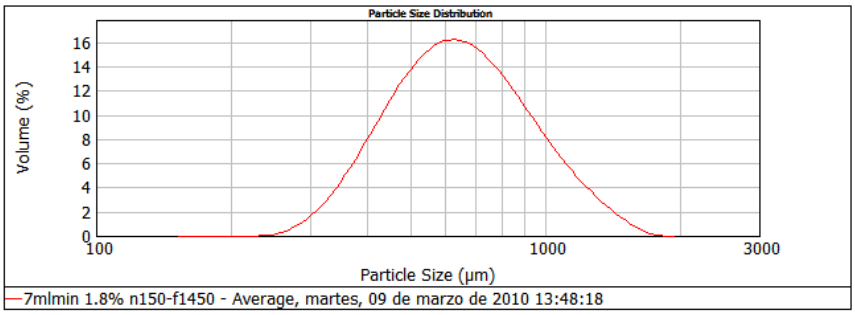

Distribution for a 1.720 Pa·s alginate solution at 7 mL/min.

Concentration:	Span :	Uniformity:	Result units:
0.6861 %Vol	0.973	0.303	Volume
Specific Surface Area:	**Surface Weighted Mean D[3,2]:**	**Vol. Weighted Mean D[4,3]:**	
0.0107 m²/g	562.566 um	636.380 um	

d(0.1): 378.779 um **d(0.5): 594.381 um** **d(0.9): 957.383 um**

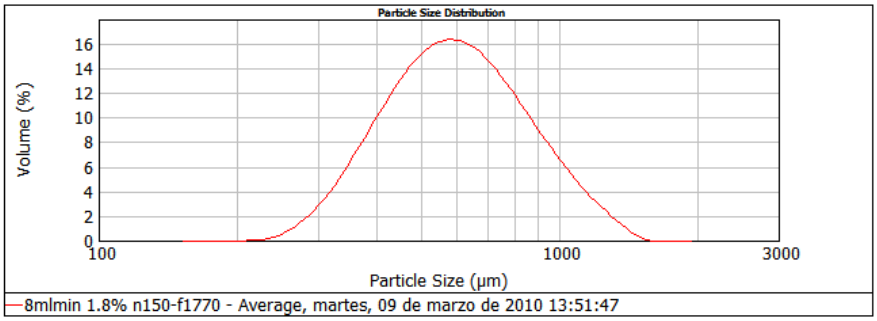

Distribution for a 1.720 Pa·s alginate solution at 8 mL/min.

Concentration:	Span :	Uniformity:	Result units:
0.9545 %Vol	1.092	0.341	Volume
Specific Surface Area:	**Surface Weighted Mean D[3,2]:**	**Vol. Weighted Mean D[4,3]:**	
0.0108 m²/g	553.050 um	643.368 um	

d(0.1): 360.846 um **d(0.5): 588.701 um** **d(0.9): 1003.589 um**

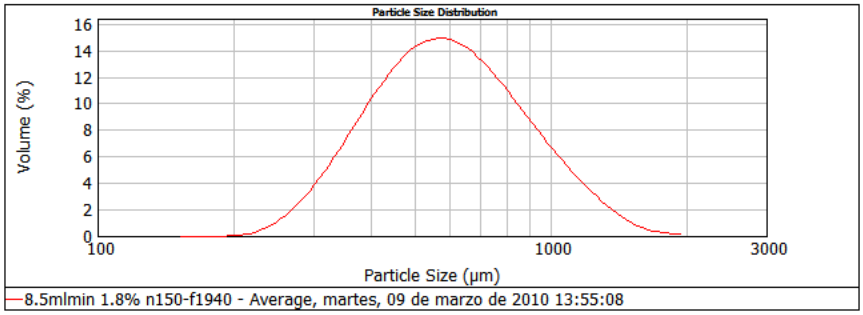

Distribution for a 1.720 Pa·s alginate solution at 8.5 mL/min.

Concentration:	Span :	Uniformity:	Result units:
1.1138 %Vol	0.974	0.301	Volume
Specific Surface Area:	**Surface Weighted Mean D[3,2]:**	**Vol. Weighted Mean D[4,3]:**	
0.0116 m²/g	517.036 um	586.173 um	

d(0.1): 347.590 um **d(0.5): 546.822 um** **d(0.9): 880.166 um**

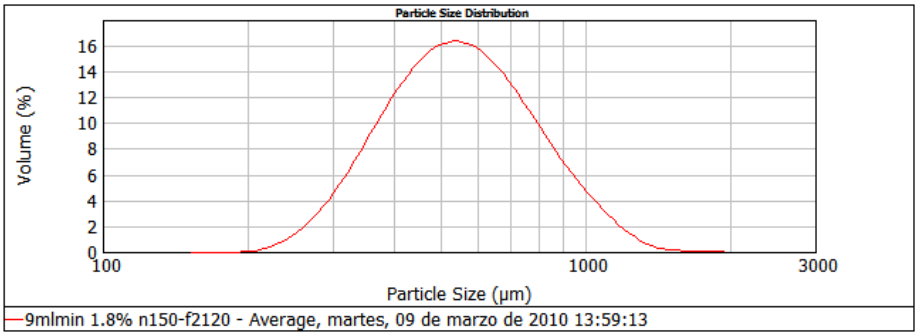

Distribution for a 1.720 Pa·s alginate solution at 9 mL/min.

Images: applying optimal frequencies computed from the Weber expression (4.4).

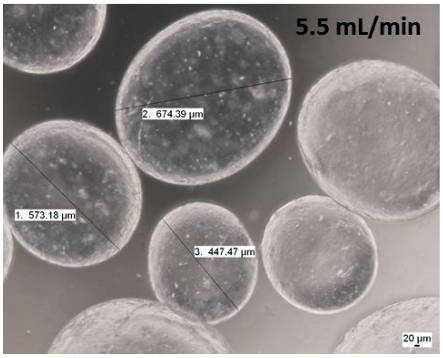

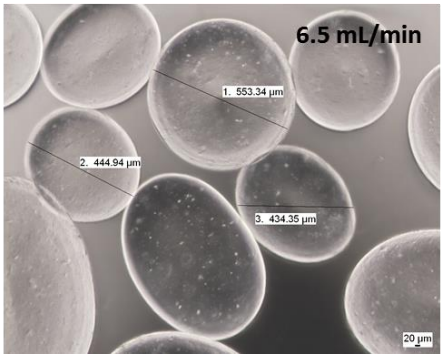

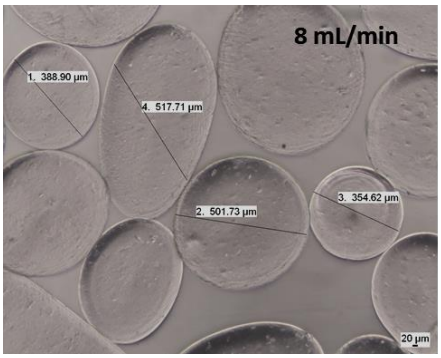

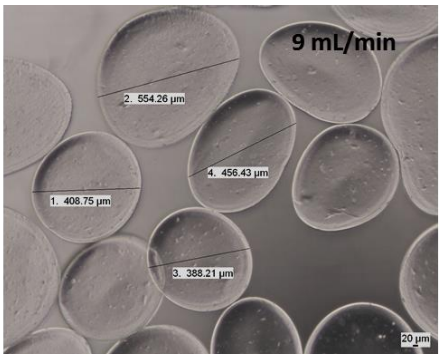

Obtained microparticles for a 2.3 Pa·s alginate solution at different flow rates.

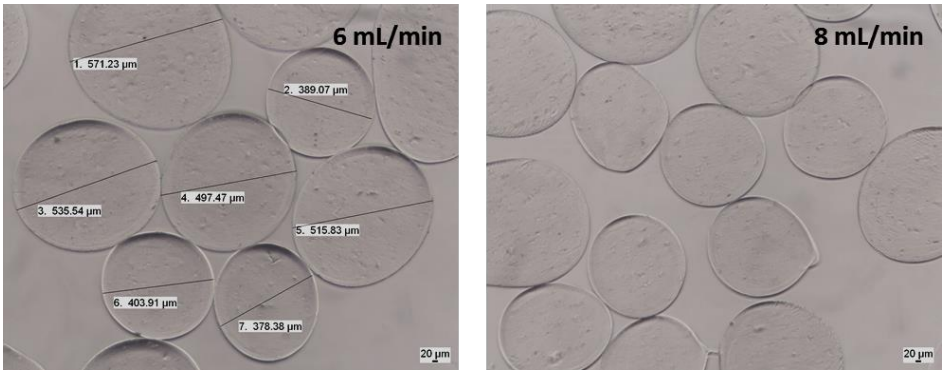

Obtained microparticles for a 1.3 Pa·s alginate solution at different flow rates.

APPENDIX B – Data of extensional experiments

CaBER Software Version: CaBER V4.50 Build 11-29-04

Drive System Used: Linear Drive

Exponential Strike (upload) Strike Time [ms]: 50.00

1.5 % - Initial gap 3 mm

Temperature Probe 1 [°C]: 25.9

Sample End height (mm) 13.16 Sample start height (mm) 3.010

Time	Diameter	Strain	Strain Rate
-0.05	5.94951	0.016901	-2.75979
-0.049	5.95772	0.014143	-2.75607
-0.048	5.96593	0.011389	-1.10089
-0.047	5.95772	0.014143	-0.55123
-0.046	5.96593	0.011389	-0.27496
-0.04499	5.96593	0.011389	-1.64273
-0.04399	5.97413	0.008642	-1.91522
-0.04299	5.98234	0.005895	0.548962
-0.04199	5.97413	0.008642	0.824222
-0.04099	5.95772	0.014143	0.551198
-0.03999	5.97413	0.008642	1.099064
-0.03899	5.97413	0.008642	0.274507
-0.03799	5.94951	0.016901	3.586192
-0.03699	5.96593	0.011389	4.401681
-0.03599	5.92489	0.025195	16.31381
-0.03498	5.80185	0.067165	41.38639
-0.03398	5.60515	0.136147	67.31107
-0.03298	5.35954	0.225763	93.40506
-0.03198	5.09789	0.325866	107.0506
-0.03098	4.80396	0.444638	113.797
-0.02998	4.51861	0.56711	115.4191
-0.02898	4.28249	0.67445	111.3632
-0.02798	4.05479	0.783721	107.4512
-0.02698	3.84359	0.890705	109.9066
-0.02598	3.64883	0.994706	107.7587
-0.02497	3.46238	1.099607	108.6733

-0.02397	3.27611	1.210205	108.9514
-0.02297	3.11427	1.311529	108.0452
-0.02197	2.95258	1.41816	104.5641
-0.02097	2.78294	1.536503	98.09194
-0.01997	2.66994	1.619407	88.26937
-0.01897	2.57313	1.693273	77.11226
-0.01797	2.4683	1.77646	75.12051
-0.01697	2.38771	1.842849	75.6105
-0.01597	2.2991	1.918484	72.66092
-0.01496	2.21857	1.989793	70.13718
-0.01396	2.15418	2.048699	64.08766
-0.01296	2.08981	2.109373	57.74687
-0.01196	2.0335	2.164002	55.37448
-0.01096	1.97721	2.220145	51.24087
-0.00996	1.92897	2.269547	49.17444
-0.00896	1.88879	2.311646	46.80457
-0.00796	1.84057	2.363368	44.52641
-0.00696	1.8004	2.407501	44.6234
-0.00596	1.76828	2.443504	41.66519
-0.00495	1.72812	2.489451	49.0576
-0.00395	1.67192	2.555574	46.92989
-0.00295	1.65587	2.574866	38.78081
-0.00195	1.62376	2.61403	35.5853
-0.00095	1.59166	2.653964	38.31595
5E-05	**1.55957**	**2.694699**	**36.00991**
0.00105	1.5355	2.725807	37.61251
0.00205	1.51144	2.757393	40.3271
0.00305	1.47134	2.811172	44.69262
0.00405	1.43927	2.855247	44.42377
0.00506	1.41522	2.888949	37.23644
0.00606	1.39117	2.923229	44.47159
0.00706	1.36712	2.958106	39.31419
0.00806	1.35109	2.981696	36.09895
0.00906	1.33507	3.005551	41.60636
0.01006	1.31904	3.029711	60.65138
0.01106	1.31103	3.041893	53.22297
0.01206	1.29501	3.066482	61.03458
0.01306	1.27097	3.103958	52.6945
0.01406	1.27097	3.103958	45.07731
0.01507	1.26296	3.116603	42.63389
0.01607	1.24694	3.142134	61.76755
0.01707	1.23092	3.167995	63.82997
0.01807	1.19889	3.220727	67.40127
0.01907	1.18288	3.247615	59.25839
0.02007	1.15886	3.288645	55.92496

0.02107	1.13484	3.330536	55.27016
0.02207	1.11883	3.358952	54.33764
0.02307	1.10283	3.38776	58.23010
0.02407	1.07882	3.431783	66.84466
0.02508	1.06281	3.461686	61.80324
0.02608	1.03881	3.507367	56.47657
0.02708	1.02281	3.538411	58.10836
0.02808	1.00681	3.569945	51.70117
0.02908	0.99081	3.601984	53.27386
0.03008	0.95882	3.667623	54.80108
0.03108	0.95882	3.667623	48.09328
0.03208	0.94283	3.701257	32.32134
0.03308	0.92683	3.735489	16.29225
0.03408	0.91084	3.770295	24.84316
0.03509	0.89485	3.805717	33.6712
0.03609	0.87887	3.841755	25.46518
0.03709	0.86288	3.878478	34.84451
0.03809	0.84689	3.915888	53.38433
0.03909	0.83091	3.953986	45.30635
0.04009	0.81492	3.99285	56.69342
0.04109	0.79095	4.05256	57.77271
0.04209	0.78296	4.072866	49.56773
0.04309	0.75899	4.135052	50.57014
0.04409	0.74302	4.177584	41.2808
0.0451	0.72704	4.221067	53.24955
0.0461	0.71107	4.265488	54.39415
0.0471	0.68711	4.334041	44.48071
0.0481	0.67912	4.357434	57.25542
0.0491	0.66315	4.405027	58.58866
0.0501	0.64719	4.45375	61.0177
0.0511	0.63122	4.503721	62.54402
0.0521	0.61525	4.554972	51.29559
0.0531	0.59131	4.634349	66.68117
0.0541	0.58332	4.661558	83.36671
0.05511	0.55938	4.745371	56.35468
0.05611	0.54342	4.803264	58.82248
0.05711	0.52746	4.862884	75.75614
0.05811	0.50353	4.955743	78.99426
0.05911	0.49555	4.987693	81.56197
0.06011	0.47162	5.086682	67.77242
0.06111	0.45567	5.155492	89.25732
0.06211	0.44769	5.190827	113.1233
0.06311	0.42377	5.300648	97.95121
0.06411	0.39984	5.416901	81.56686
0.06512	0.39984	5.416901	108.5873

0.06612	0.37592	5.540277	88.78059
0.06712	0.36795	5.583135	95.1145
0.06812	0.35201	5.67171	124.1568
0.06912	0.3281	5.812393	134.1712
0.07012	0.31215	5.912062	176.0762
0.07112	0.29622	6.016825	155.875
0.07212	0.27231	6.185147	132.9801
0.07312	0.25637	6.305786	184.6032
0.07412	0.24044	6.434088	153.3759
0.07513	0.21654	6.643479	173.31
0.07613	0.20858	6.718384	298.6875
0.07713	0.19265	6.877279	276.3934
0.07813	0.16875	7.142193	247.2983
0.07913	0.16079	7.238831	282.2894
0.08013	0.14486	7.447494	330.7373
0.08113	0.11302	7.9439	396.2428
0.08213	0.12098	7.807779	329.743
0.08313	0.10506	8.089966	422.6547
0.08413	0.09709	8.247753	491.9652
0.08514	0.08117	8.605938	392.3114
0.08614	0.06525	9.042577	415.6352
0.08714	0.06525	9.042577	345.2654
0.08814	0.04934	9.601559	358.6251
0.08914	0.04138	9.953434	402.6532
0.09014	0.01751	11.67349	378.5213

REFERENCES

Acarregui A, Orive G, Pedraz JL, Hernández RM (2013) Therapeutic applications of encapsulated cells. Methods in Molecular Biology 1051:349-364

Adelberg M (1967) Breakup rate and penetration of a liquid jet in a gas stream. AIAA J 5:1408-1415

Adelberg M (1968) Mean drop size resulting from the injection of a liquid jet into a high-speed gas stream. AIAA J 6:1143-1147

Aleksandrov AP, Lazurkin YS (1940) A Study of Polymers. I. Highly Elastic Deformation of Polymers. Rubber Chemistry and Technology 13 (4):886-898. doi:10.5254/1.3546566

Anna SL, McKinley GH (2001) Elasto-capillary thinning and breakup of model elastic liquids. Journal of Rheology 45 (1):115-138

ANSYS (2011) ANSYS FLUENT Theory Guide. Release 14.0. ANSYS, Inc.

Arnolds O, Buggisch H, Sachsenheimer D, Willenbacher N (2010) Capillary breakup extensional rheometry (CaBER) on semi-dilute and concentrated polyethyleneoxide (PEO) solutions. Rheologica Acta 49 (11-12):1207-1217. doi:10.1007/s00397-010-0500-7

Ashgriz N, Mostaghimi J (2002) An Introduction to Computational Fluid Dynamics. In: Editor JS (ed) Fluid Flow Handbook. McGraw-Hill Handbooks.

Ashgriz N, Yarin AL (2011) Capillary Instability of Free Liquid Jets. In: Ashgriz N (ed) Handbook of Atomization and Sprays. Springer.

Bagle AV, Jadhav RS, Gite VV, Hundiwale DG, Mahulikar PP (2013) Controlled release study of phenol formaldehyde microcapsules containing neem oil as an insecticide. International Journal of Polymeric Materials and Polymeric Biomaterials 62 (8):421-425

Barnes HA (1989) Shear-Thickening (``Dilatancy'') in Suspensions of Nonaggregating Solid Particles Dispersed in Newtonian Liquids. Journal of Rheology 33 (2):329-366

Barnes HA (2000) A Handbook of Elementary Rheology

Baumgarten C (2006) Fundamentals of Mixture Formation in Engines. In: Mixture Formation in Internal Combustion Engine. Heat, Mass Transfer. Springer Berlin Heidelberg, pp 5-46. doi:10.1007/3-540-30836-9_2

Benita S (ed) (2006) Microencapsulation: Methods and Industrial Applications, Second Edition. Taylor & Francis Group.

Bird RB, Armstrong RC, Hassager O (eds) (1987) Dynamics of polymeric liquids: Fluid Mechanics, vol 1. Second edn. John Wiley & Sons.

Bisceglie V (1933) Uber die antineoplastische immunitat; heterologe Einpflnzung von Tumoren in Huhner-embryonen. Ztschr Krebsforsch 40:122–140

Bogy DB (1979) Drop Formation in a Circular Liquid Jet. Annual Review of Fluid Mechanics 11 (1):207-228. doi:10.1146/annurev.fl.11.010179.001231

Böhm N, Kulicke W-M (1999) Rheological studies of barley (1→3)(1→4)-β-glucan in concentrated solution: investigation of the viscoelastic flow behaviour in the sol-state. Carbohydrate Research 315 (3–4):293-301. doi:http://dx.doi.org/10.1016/S0008-6215(99)00035-X

Bousfield DW, Keunings R, Marrucci G, Denn MM (1986) Nonlinear analysis of the surface tension driven breakup of viscoelastic filaments. Journal of Non-Newtonian Fluid Mechanics 21 (1):79-97. doi: 10.1016/0377-0257(86)80064-7

Brandenberger H, Widmer F (1998) A new multinozzle encapsulation/immobilisation system to produce uniform beads of alginate. Journal of Biotechnology 63 (1):73-80. doi: 10.1016/s0168-1656(98)00077-7

Brandenberger HR, Widmer F (1999) Immobilization of Highly Concentrated Cell Suspensions Using the Laminar Jet Breakup Technique. Biotechnology Progress 15 (3):366-372. doi:10.1021/bp990033m

Brenn G, Liu Z, Durst F (2000) Linear analysis of the temporal instability of axisymmetrical non-Newtonian liquid jets. International Journal of Multiphase Flow 26 (10):1621-1644. doi: 10.1016/s0301-9322(99)00115-9

Bungenberg de Jong HG, Kruyt HR (1930) Koazervation (Entmischung in Kolloidalen Systemen). Koll Zeitsch 50:39-48

Carreau PJ (1972) Rheological Equations from Molecular Network Theories. Transactions of The Society of Rheology (1957-1977) 16 (1):99-127. doi:http://dx.doi.org/10.1122/1.549276

Cellesi F, Tirelli N (2005) A new process for cell microencapsulation and other biomaterial applications: Thermal gelation and chemical cross-linking in “tandem”. J Mater Sci: Mater Med 16 (6):559-565. doi:10.1007/s10856-005-0532-1

Clasen C (2010) Capillary breakup extensional rheometry of semi-dilute polymer solutions. Korea-Australia Rheology Journal 22 (4):331-338

Clasen C, Eggers J, Fontelos MA, Li J, McKinley GH (2006a) The beads-on-string structure of viscoelastic threads. Journal of Fluid Mechanics 556:283-308

Clasen C, Phillips PM, Palangetic L, Vermant, Jan (2012) Dispensing of rheologically complex fluids: The map of misery. AIChE Journal 58 (10):3242-3255. doi:10.1002/aic.13704

Clasen C, Plog JP, Kulicke WM, Owens M, MacOsko C, Scriven LE, Verani M, McKinley GH (2006b) How dilute are dilute solutions in extensional flows? Journal of Rheology 50 (6):849-881

Colby R (2010) Structure and linear viscoelasticity of flexible polymer solutions: comparison of polyelectrolyte and neutral polymer solutions. Rheologica Acta 49 (5):425-442. doi:10.1007/s00397-009-0413-5

Cook MT, Tzortzis G, Charalampopoulos D, Khutoryanskiy VV (2012) Microencapsulation of probiotics for gastrointestinal delivery. Journal of Controlled Release 162 (1):56-67. doi:http://dx.doi.org/10.1016/j.jconrel.2012.06.003

Coppi G, Iannuccelli V, Bernabei MT, Cameroni R (2002) Alginate microparticles for enzyme peroral administration. International Journal of Pharmaceutics 242 (1–2):263-266. doi:http://dx.doi.org/10.1016/S0378-5173(02)00171-0

Cox WP, Merz EH (1958) Correlation of dynamic and steady flow viscosities. Journal of Polymer Science 28 (118):619-622. doi:10.1002/pol.1958.1202811812

Cross MM (1965) Rheology of non-Newtonian fluids: A new flow equation for pseudoplastic systems. Journal of Colloid Science 20 (5):417-437. doi:10.1016/0095-8522(65)90022-x

Cruise GM, Hegre OD, Scharp DS, Hubbell JA (1998) A sensitivity study of the key parameters in the interfacial photopolymerization of poly(ethylene glycol) diacrylate upon porcine islets. Biotechnology and Bioengineering 57 (6):655-665.

Chaikof EL (1999) Engineering and Material Considerations in Islet Cell Transplantation. Annual Review of Biomedical Engineering 1 (1):103-127. doi:10.1146/annurev.bioeng.1.1.103

Chan LW, Lee HY, Heng PWS (2002) Production of alginate microspheres by internal gelation using an emulsification method. International Journal of Pharmaceutics 242 (1–2):259-262. doi:http://dx.doi.org/10.1016/S0378-5173(02)00170-9

Chandra R, Rustgi R (1998) Biodegradable polymers. Progress in Polymer Science (Oxford) 23 (7):1273-1335

Chhabra RP, Richardson JF (eds) (2008) Non-Newtonian Flow and Applied Rheology

Chick W, Like A, Lauris V (1975) Beta cell culture on synthetic capillaries: an artificial endocrine pancreas. Science 187 (4179):847-849. doi:10.1126/science.187.4179.847

Chigier NA, Reitz RD (1996) Regimes of jet breakup and breakup mechanisms. In: Kuo K (ed) Progress in Astronautics and Aeronautics, vol 1. pp 109–136

Christanti Y, Walker LM (2001) Surface tension driven jet break up of strain-hardening polymer solutions. Journal of Non-Newtonian Fluid Mechanics 100 (1-3):9-26. doi: 10.1016/s0377-0257(01)00135-5

Chung TJ (ed) (2010) Computational Fluid Dynamics. Cambridge University Press.

De La Puente P, Ludeña D, Fernández A, Aranda JL, Varela G, Iglesias J (2011) Autologous fibrin scaffolds cultured dermal fibroblasts and enriched with encapsulated bFGF for tissue engineering. Journal of Biomedical Materials Research - Part A 99 A (4):648-654. doi:10.1002/jbm.a.33231

de Souza JRR, Feitosa JPA, Ricardo NMPS, Trevisan MTS, de Paula HCB, Ulrich CM, Owen RW (2013) Spray-drying encapsulation of mangiferin using natural polymers. Food Hydrocolloids 33 (1):10-18

Dewettinck K, Huyghebaert A (1999) Fluidized bed coating in food technology. Trends in Food Science & Technology 10 (4–5):163-168. doi:http://dx.doi.org/10.1016/S0924-2244(99)00041-2

Dobrynin AV, Colby RH, Rubinstein M (1995) Scaling theory of polyelectrolyte solutions. Macromolecules 28 (6):1859-1871

Dong Z, Ma Y, Hayat K, Jia C, Xia S, Zhang X (2011) Morphology and release profile of microcapsules encapsulating peppermint oil by complex coacervation. Journal of Food Engineering 104 (3):455-460. doi:http://dx.doi.org/10.1016/j.jfoodeng.2011.01.011

Duane T. Birnbaum, Brannon-Peppas L (2003) Microparticle Drug Delivery Systems. Drug Delivery Systems in Cancer Therapy. Humana Press, Totowa, New Jersey

Dubey R, Shami TC, Rao KUB (2009) Microencapsulation Technology and Applications. Defence Science Journal 59 (1):82-95

Duxenneuner MR, Fischer P, Windhab EJ, Cooper-White JJ (2008) Extensional Properties of Hydroxypropyl Ether Guar Gum Solutions. Biomacromolecules 9 (11):2989-2996. doi:10.1021/bm800553v

Edelman R, Russell RG, Losonsky G, Tall BD, Tacket CO, Levine MM, Lewis DH (1993) Immunization of rabbits with enterotoxigenic E. coli colonization factor antigen (CFA/I) encapsulated in biodegradable microspheres of poly (lactide-co-glycolide). Vaccine 11 (2):155-158. doi:http://dx.doi.org/10.1016/0264-410X(93)90012-M

Entov VM (1986) Effect of elastic deformations in the flow of polymer solution. Heat transfer Soviet research 18 (1):60-73

Entov VM, Hinch EJ (1997) Effect of a spectrum of relaxation times on the capillary thinning of a filament of elastic liquid. Journal of Non-Newtonian Fluid Mechanics 72 (1):31-53. doi:http://dx.doi.org/10.1016/S0377-0257(97)00022-0

Ewoldt RH., Hosoi AE, McKinley GH (2008) New measures for characterizing nonlinear viscoelasticity in large amplitude oscillatory shear. Journal of Rheology (1978-present) 52(6):1427-1458.

Fontelos, MA., Jie L (2004) On the evolution and rupture of filaments in Giesekus and FENE models. Journal of Non-Newtonian Fluid Mechanics 118(1):1-16.

Fu S, Thacker A, Sperger D, Boni R, Velankar S, Munson E, Block L (2010) Rheological Evaluation of Inter-grade and Inter-batch Variability of Sodium Alginate. AAPS PharmSciTech 11 (4):1662-1674. doi:10.1208/s12249-010-9547-0

Fundueanu G, Esposito E, Mihai D, Carpov A, Desbrieres J, Rinaudo M, Nastruzzi C (1998) Preparation and characterization of Ca-alginate microspheres by a new emulsification method. International Journal of Pharmaceutics 170 (1):11-21. doi:http://dx.doi.org/10.1016/S0378-5173(98)00063-5

Fuoss RM, Strauss UP (1949) The Viscosity of mixtures of Polyelectrolytes and simple Electrolytes. Annals of the New York Academy of Sciences 51 (4):836-851. doi:10.1111/j.1749-6632.1949.tb27309.x

Gao Z (2009) Instability of non-Newtonian jets with a surface tension gradient. Journal of Physics A: Mathematical and Theoretical 42 (6):065501

Gennes P-Gd, Brochard-Wyart F, Quere D (eds) (2004) Capillarity and Wetting Phenomena: drops, bubbles, pearls, waves. Springer, New York, USA

Gharsallaoui A, Roudaut G, Chambin O, Voilley A, Saurel R (2007) Applications of spray-drying in microencapsulation of food ingredients: An overview. Food Research International 40 (9):1107-1121. doi:http://dx.doi.org/10.1016/j.foodres.2007.07.004

Goedde EF, Yuen MC (1970) Experiments on liquid jet instability. Journal of Fluid Mechanics 40 (03):495-511. doi:10.1017/S0022112070000289

Goldin M, Yerushalmi J, Pfeffer R, Shinnar R (1969) Breakup of a laminar capillary jet of a viscoelastic fluid. Journal of Fluid Mechanics 38 (04):689-711. doi:10.1017/S0022112069002540

Gómez Díaz D, Navaza JM (2002) Caracterización reológica de dispersiones agua-alginato sódico con aplicación en la industria alimentaria. Ciencia y Tecnología Alimentaria 3 (5):302-306

Gordon M, Yerushalmi J, Shinnar R (1973) Instability of Jets of Non-Newtonian Fluids. Transactions of the Society of Rheology 17 (2):303-324

Gouin S (2004) Microencapsulation: industrial appraisal of existing technologies and trends Trends in Food Science & Technology 15 (7-8):330-347

GRACO I (1995) Atomization: Concept and Theory Training.

Grant GT, Morris ER, Rees DA, Smith PJC, Thom D (1973) Biological interactions between polysaccharides and divalent cations: The egg-box model. FEBS Letters 32 (1):195-198. doi:http://dx.doi.org/10.1016/0014-5793(73)80770-7

Green BK (1945) US Patent: 2374862.

Haas PA (1992) Formation of uniform liquid drops by application of vibration to laminar jets. Industrial & Engineering Chemistry Research 31 (3):959-967. doi:10.1021/ie00003a043

Hartman RPA, Brunner DJ, Camelot DMA, Marijnissen JCM, Scarlett B (1999) Electrohydrodynamic atomization in the cone–jet mode physical modeling of the liquid cone and jet. Journal of Aerosol Science 30 (7):823-849. doi:http://dx.doi.org/10.1016/S0021-8502(99)00033-6

Haug A, Smidsrød O (1962) Determination of Intrinsic Viscosity of Alginates. Acta Chemica Scandinavica 16:1569-1578

Haug A, Smidsrød O (1970) Selectivity of some anionic polymers for divalent metal ions. Acta Chemica Scandinavica 24:843-854

Haward SJ, Sharma V, Butts CP, McKinley GH, Rahatekar SS (2012) Shear and Extensional Rheology of Cellulose/Ionic Liquid Solutions. Biomacromolecules 13 (5):1688-1699. doi:10.1021/bm300407q

Herrero EP, Del Valle EMM, Galán MA (2006) Modelling prediction of the microcapsule size of polyelectrolyte complexes produced by atomization. Chemical Engineering Journal 121 (1):1-8. doi: 10.1016/j.cej.2006.04.003

Hill RS, Cruise GM, Hager SR, Lamberti FV, Yu X, Garufis CL, Yu YAO, Mundwiler KE, Cole JF, Hubbell JA, Hegre OD, Scharp DW (1997) Immunoisolation of Adult Porcine Islets for the Treatment of Diabetes Mellitus. Annals of the New York Academy of Sciences 831 (1):332-343. doi:10.1111/j.1749-6632.1997.tb52208.x

Hilliou L, Freitas F, Oliveira R, Reis MAM, Lespineux D, Grandfils C, Alves VD (2009) Solution properties of an exopolysaccharide from a Pseudomonas strain obtained using glycerol as sole carbon source. Carbohydrate Polymers 78 (3):526-532. doi:http://dx.doi.org/10.1016/j.carbpol.2009.05.011

Hollaus PH, Lax F, El-Nashef BB, Hauck HH, Lucciarini P, Pridun NS (1997) Natural history of bronchopleural fistula after pneumonectomy: A review of 96 cases. The Annals of Thoracic Surgery 63 (5):1391-1396. doi:http://dx.doi.org/10.1016/S0003-4975(97)00409-8

Hwang YK, Jeong U, Cho EC (2008) Production of Uniform-Sized Polymer Core–Shell Microcapsules by Coaxial Electrospraying. Langmuir 24 (6):2446-2451. doi:10.1021/la703546f

Ilić I, Dreu R, Burjak M, Homar M, Kerč J, Srčič S (2009) Microparticle size control and glimepiride microencapsulation using spray congealing technology. International Journal of Pharmaceutics 381 (2):176-183. doi:http://dx.doi.org/10.1016/j.ijpharm.2009.05.011

Ishikawa K, Ueyama Y, Mano T, Koyama T, Suzuki K, Matsumura T (1999) Self-setting barrier membrane for guided tissue regeneration method: Initial evaluation of alginate membrane made with sodium alginate and calcium chloride aqueous solutions. Journal of Biomedical Materials Research 47 (2):111-115.

Jain RA (2000) The manufacturing techniques of various drug loaded biodegradable poly(lactide-co-glycolide) (PLGA) devices. Biomaterials 21 (23):2475-2490. doi:http://dx.doi.org/10.1016/S0142-9612(00)00115-0

Jasuja AK (1982) Plain-jet airblast atomization of alternative liquid petroleum fuels under high ambient air pressure conditions. ASME 82-GT-32

Jeffreys H (1980) On the formation of water waves by wind. Proc Roy Soc Lond A 107:189

Kheirandish S, Gubaydullin I, Willenbacher N (2009) Shear and elongational flow behavior of acrylic thickener solutions. Part II: effect of gel content. Rheologica Acta 48 (4):397-407. doi:10.1007/s00397-008-0324-x

Kim B-S, Mooney DJ (1998) Development of biocompatible synthetic extracellular matrices for tissue engineering. Trends in Biotechnology 16 (5):224-230. doi:http://dx.doi.org/10.1016/S0167-7799(98)01191-3

Kim JY, Kim HW, Bae SJ, Joo DJ, Huh KH, Fang YH, Cho Y, Jeong JH, Kim YS, Lee JI (2012) Hybrid Cellular Spheroids From Hepatocellular Carcinoma and Insulin-Secreting Cell Lines. Transplantation Proceedings 44 (4):1095-1098. doi:http://dx.doi.org/10.1016/j.transproceed.2012.02.016

Kim S, Mewis J, Clasen C, Vermant J (2013) Superposition rheometry of a wormlike micellar fluid. Rheologica Acta:1-14. doi:10.1007/s00397-013-0718-2

Koch S, Schwinger C, Kressler J, Heinzen C, Rainov NG (2003) Alginate encapsulation of genetically engineered mammalian cells: Comparison of production devices,

methods and microcapsule characteristics. Journal of Microencapsulation: Micro and Nano Carriers 20 (3):303 - 316

Koo OM, Rubinstein I, Onyuksel H (2005) Role of nanotechnology in targeted drug delivery and imaging: a concise review. Nanomedicine: Nanotechnology, Biology and Medicine 1 (3):193-212. doi:http://dx.doi.org/10.1016/j.nano.2005.06.004

Kroesser FW, Middleman S (1969) Viscoelastic jet stability. AIChE Journal 15 (3):383-386. doi:10.1002/aic.690150316

Kulicke WM, Clasen C, Lohman C (2005) Characterization of Water-Soluble Cellulose Derivatives in Terms of the Molar Mass and Particle Size as well as Their Distribution. Macromolecular Symposia 223 (1):151-174. doi:10.1002/masy.200550511

Kurabayashi T (1959) Atomization of liquid by means of rotating nozzle. Trans Jpn Soc Mech Eng 25 (160):1266-1273

Kuzmin D (2010) A Guide to Numerical Methods for Transport Equations

Lanza RP, Chick WL (1997) Immunoisolation: at a turning point. Immunology Today 18 (3):135-139. doi:http://dx.doi.org/10.1016/S0167-5699(97)01008-6

Lee A, Sudau K, Ahn KH, Lee SJ, Willenbacher N (2012a) Optimization of Experimental Parameters to Suppress Nozzle Clogging in Inkjet Printing. Industrial & Engineering Chemistry Research 51 (40):13195-13204. doi:10.1021/ie301403g

Lee JI, Kim HW, Kim JY, Bae SJ, Joo DJ, Huh KH, Fang YH, Jeong JH, Kim MS, Kim YS (2012b) Microencapsulation of Pancreatic Islets With Canine Ear Cartilage for Immunoisolation. Transplantation Proceedings 44 (4):1091-1094. doi:http://dx.doi.org/10.1016/j.transproceed.2012.02.015

Lefebvre AH (ed) (1989) Atomization and Sprays. Hemisphere Publishing Corporation, New York

Leick S, Henning S, Degen P, Suter D, Rehage H (2010) Deformation of liquid-filled calcium alginate capsules in a spinning drop apparatus. Physical Chemistry Chemical Physics 12 (12):2950-2958. doi:10.1039/b921116k

Levic S, Djordjevic V, Rajic N, Milivojevic M, Bugarski B, Nedovic V (2013) Entrapment of ethyl vanillin in calcium alginate and calcium alginate/poly(vinyl alcohol) beads. Chem Pap 67 (2):221-228. doi:10.2478/s11696-012-0260-1

Lewis DH (1990) Controlled release of bioactive agents from lactide/glycolide polymers. Drugs Pharma Sci 45:1-41

Li J, Fontelos MA (2003) Drop dynamics on the beads-on-string structure for viscoelastic jets: A numerical study. Physics of Fluids 15 (4):922-937

Lim F, Sun AM (1980) Microencapsulated islets as bioartificial endocrine pancreas. Science 210:908-909

Lim G-P, Ong H-Y, Lee B-B, Ahmad MS, Singh H, Ravindra P (2013) Formation Of Chitosan-Alginate Capsules Using Extrusion-Dripping Method: Effect Of Stirring Speed And Biopolymers Types. Australian Journal of Basic and Applied Science 7 (5):84-90

Lin SP, Reitz RD (1998) Drop and spray formation from a liquid jet. Annual Review of Fluid Mechanics 30 (1):85-105. doi:10.1146/annurev.fluid.30.1.85

Liu Z, Liu Z (2006) Linear analysis of three-dimensional instability of non-Newtonian liquid jets. Journal of Fluid Mechanics 559:451-459. doi:10.1017/S0022112006000413

Löhner R (ed) (2008) Applied Computational Fluid Dynamics Techniques: An Introduction Based on Finite Element Methods. John Wiley & Sons, Ltd.

Lorenzetto GE, Lefebvre AH (1977) Measurements of drop size on a plain jet airblast atomizer. AIAA J 15:1006-1010

Macosko CW (ed) (1994) RHEOLOGY: Principles, Measurements and Applications.

Malkin AY (1994) Viscoelasticity. In: Rheology Fundamentals. ChemTec Publishing, Toronto, pp 245-307

Mancini M, Moresi M, Sappino F (1996) Rheological behaviour of aqueous dispersions of algal sodium alginates. Journal of Food Engineering 28 (3–4):283-295. doi:http://dx.doi.org/10.1016/0260-8774(95)00068-2

Mansour A, Chigier N (1995) Air-blast atomization of non-Newtonian liquids. Journal of Non-Newtonian Fluid Mechanics 58:161-194

Marani D, Hjelm J, Wandel M (2013) Use of Intrinsic Viscosity for Evaluation of Polymer-Solvent Affinity. Annual Transactions of the Nordic Rheology Society 21:255-262

Martín del Valle EM, Galán MA, Carbonell RG (2009) Drug Delivery Technologies: The Way Forward in the New Decade. Industrial & Engineering Chemistry Research 48 (5):2475-2486. doi:10.1021/ie800886m

Mayer E (1961). ARS J 31:1783-1785

McKinley GH (2005a) Dimensionless Groups For Understanding Free Surface Flows of Complex Fluids. Society of Rheology Bulletin 74 (2):6-10

McKinley GH (2005b) Visco-Elasto-Capillary Thinning and Break-Up of Complex Fluids. Hatsopoulos Microfluids Laboratory, Dept. of Mechanical Engineering, Massachusetts Institute of Technology, Cambridge, USA,

Meadows J, Williams PA, Kennedy JC (1995) Comparison of the extensional and shear viscosity characteristics of aqueous hydroxyethyl cellulose solutions. Macromolecules 28 (8):2683-2692. doi:10.1021/ma00112a013

Merrington AC, Richardson EG (1947) The break-up of liquid jets. Proceedings of the Physical Society 59 (1):1

Middleman S (1965) Stability of a viscoelastic jet. Chemical Engineering Science 20 (12):1037-1040. doi: 10.1016/0009-2509(65)80105-1

Miller E, Clasen C, Rothstein J (2009) The effect of step-stretch parameters on capillary breakup extensional rheology (CaBER) measurements. Rheologica Acta 48 (6):625-639. doi:10.1007/s00397-009-0357-9

Misthos P, Kakaris S, Sepsas E, Athanassiadi K, Skottis I (2006) Surgical Management of Late Postpneumonectomy Bronchopleural Fistula: The Transsternal, Transpericardial Route. Respiration 73 (4):525-528

Moghadam H, Samimi M, Samimi A, Khorram M (2008) Electro-spray of high viscous liquids for producing mono-sized spherical alginate beads. Particuology 6 (4):271-275. doi: 10.1016/j.partic.2008.04.005

Moghadam H, Samimi M, Samimi A, Khorram M (2009) Study of Parameters Affecting Size Distribution of Beads Produced from Electro-Spray of High Viscous Liquids. Iranian Journal of Chemical Engineering 6 (3 (Summer)):88-98

Mørch ÝA (2008) Novel Alginate Microcapsules for Cell Therapy. Norwegian University of Science and Technology, Trondheim

Mørch ÝA, Donati I, Strand BL (2006) Effect of Ca2+, Ba2+, and Sr2+ on Alginate Microbeads. Biomacromolecules 7 (5):1471-1480. doi:10.1021/bm060010d

Morris ER, Cutler AN, Ross-Murphy SB, Rees DA, Price J (1981) Concentration and shear rate dependence of viscosity in random coil polysaccharide solutions. Carbohydrate Polymers 1 (1):5-21. doi:http://dx.doi.org/10.1016/0144-8617(81)90011-4

Muller FL, Davidson JF (1994) Rheology of Shear Thinning Polymer Solutions. Industrial & Engineering Chemistry Research 33 (10):2364-2367. doi:10.1021/ie00034a016

Nazzaro F, Fratianni F, Coppola R (2012) Microtechnology and nanotechnology in food science. In: Boye JI, Arcand Y (eds) Green Technologies in Food Production and Processing. Food Engineering Series. Springer US, pp 471-494. doi:10.1007/978-1-4614-1587-9_17

Niedzwiedz K, Arnolds O, Willenbacher N, Brummer R (2009) How to characterize yield stress fluids with capillary breakup extensional rheometry (CaBER)? Applied Rheology 19 (4)

O'Donnell PB, McGinity JW (1997) Preparation of microspheres by the solvent evaporation technique. Advanced Drug Delivery Reviews 28 (1):25-42. doi:http://dx.doi.org/10.1016/S0169-409X(97)00049-5

Ohnesorge WV (1936) Die Bildung von Tropfen an Düsen und die Auflösung flüssiger Strahlen. ZAMM - Journal of Applied Mathematics and Mechanics / Zeitschrift für Angewandte Mathematik und Mechanik 16 (6):355-358. doi:10.1002/zamm.19360160611

Ortakci F, Sert S (2012) Stability of free and encapsulated Lactobacillus acidophilus ATCC 4356 in yogurt and in an artificial human gastric digestion system. Journal of Dairy Science 95 (12):6918-6925

Pan Y, Suga K (2006) A numerical study on the breakup process of laminar liquid jets into a gas. Physics of Fluids 18 (5):052101

Pearson JRA (1976) Instability in Non-Newtonian Flow. Annual Review of Fluid Mechanics 8 (1):163-181. doi:10.1146/annurev.fl.08.010176.001115

Peirone M, Ross CJD, Hortelano G, Brash JL, Chang PL (1998) Encapsulation of various recombinant mammalian cell types in different alginate microcapsules. Journal of Biomedical Materials Research 42 (4):587-596. doi:10.1002/(sici)1097-4636(19981215)42:4<587::aid-jbm15>3.0.co;2-x

Pfleger D, Becker S (2001) Modelling and simulation of the dynamic flow behaviour in a bubble column. Chemical Engineering Science 56 (4):1737-1747. doi:http://dx.doi.org/10.1016/S0009-2509(00)00403-6

Plateau J (ed) (1873) Statique expérimentale et théorique des liquides soumis aux seules forces moléculaires. Gauthier-Villars, Paris

Popplewell LM (2001) Evaluating encapsulation economics. Perfumer & Flavorist 26 (2):2-6

Prüsse U, Bruske F, Breford J, Vorlop KD (1998) Improvements to the jet cutting process for manufacturing spherical-particles from viscous polymer solutions. Chem Ing Tech 70:556-560

Rajagopalan R, Tien C (1973) Production of mono-dispersed drops by forced vibration of a liquid jet. The Canadian Journal of Chemical Engineering 51 (3):272-279. doi:10.1002/cjce.5450510302

Rathore S, Desai PM, Liew CV, Chan LW, Heng PWS (2013) Microencapsulation of microbial cells. Journal of Food Engineering 116 (2):369-381. doi:http://dx.doi.org/10.1016/j.jfoodeng.2012.12.022

Rayleigh L (1879) On the capillary phenomena of jets. Proc R Soc London 29

Rayleigh L (1892) XVI. On the instability of a cylinder of viscous liquid under capillary force. Philosophical Magazine Series 5 34 (207):145-154. doi:10.1080/14786449208620301

Reitz RD, Bracco FV (1986) Mechanisms of breakup of round liquids jets. In: Cheremisnoff N (ed) The encyclopedia of Fluid Mechanics. pp 233-249

Renggli-Zulliger N, Dudler J, Fujimuto N, Iwata K, So A (1999) Use of Encapsulated Cells Secreting Murine TIMP-2 Ameliorates Collagen-Induced Arthritis in Mice. Annals of the New York Academy of Sciences 878 (1):515-518. doi:10.1111/j.1749-6632.1999.tb07713.x

Reverchon E (1999) Supercritical antisolvent precipitation of micro- and nano-particles. The Journal of Supercritical Fluids 15 (1):1-21. doi:http://dx.doi.org/10.1016/S0896-8446(98)00129-6

Risk NK, Lefebvre AH (1984) Spray Characteristics of plain-jet airblast atomizers. Trans ASME J Eng Gas Turbines Power 106:639-644

Rodd LE, Scott TP, Cooper-White JJ, McKinley GH (2005) Capillary Break-up Rheometry of Low-Viscosity Elastic Fluids. Applied Rheology 15:12-27

Rodríguez-Rivero C, Del Valle EMM, Galán MA (2011) Development of a new technique to generate microcapsules from the breakup of non-Newtonian highly viscous fluid jets. AIChE Journal 57 (12):3436-3447. doi:10.1002/aic.12549

Rousseau I, Le Cerf D, Picton L, Argillier JF, Muller G (2004) Entrapment and release of sodium polystyrene sulfonate (SPS) from calcium alginate gel beads. European Polymer Journal 40 (12):2709-2715. doi:http://dx.doi.org/10.1016/j.eurpolymj.2004.07.022

Saihi D, Vroman I, Giraud S, Bourbigot S (2006) Microencapsulation of ammonium phosphate with a polyurethane shell. Part II. Interfacial polymerization technique. Reactive and Functional Polymers 66 (10):1118-1125. doi:http://dx.doi.org/10.1016/j.reactfunctpolym.2006.02.001

Salmons B, Gunzburg W (2010) Therapeutic Application of Cell Microencapsulation in Cancer. In: Pedraz J, Orive G (eds) Therapeutic Applications of Cell Microencapsulation, vol 670. Advances in Experimental Medicine and Biology. Springer New York, pp 92-103. doi:10.1007/978-1-4419-5786-3_9

Sant'Anna V, Malheiros PdS, Brandelli A (2011) Liposome encapsulation protects bacteriocin-like substance P34 against inhibition by Maillard reaction products. Food Research International 44 (1):326-330. doi:http://dx.doi.org/10.1016/j.foodres.2010.10.012

Sasaki E, Kurayama F, Ida J-i, Matsuyama T, Yamamoto H (2008) Preparation of microcapsules by electrostatic atomization. Journal of Electrostatics 66 (5–6):312-318. doi:http://dx.doi.org/10.1016/j.elstat.2008.02.001

Savart F (1833) Mémoire sur la constitution des veines liquides lancées par des orifices circulaires en mince paroi. Annali di Chimica 53:337-386

Schneider JM, Hendricks CD (1964) Source of Uniform-Sized Liquid Droplets. Review of Scientific Instruments 35 (10):1349-1350. doi:10.1063/1.1718742

Schrezenmeir J, Gero L, Laue C, Kirchgessner J, Muller A, Huls A, Passmann R, Hahn HJ, Kunz L, Mueller-Klieser W, Altman JJ (1992) The role of oxygen supply in islet transplantation. Transplantation Proceedings 24 (6):2925-2929

Schwinger C, Klemenz A, Busse K, Kressler J (2004) Encapsulation of living cells with polymeric systems. Macromolecular Symposia 210 (1):493-499. doi:10.1002/masy.200450655

Senuma Y, Lowe C, Zweifel Y, Hilborn JG, Marison I (2000) Alginate hydrogel microspheres and microcapsules prepared by spinning disk atomization. Biotechnology and Bioengineering 67 (5):616-622.

Serp D, Cantana E, Heinzen C, Von Stockar U, Marison IW (2000) Characterization of an encapsulation device for the production of monodisperse alginate beads for cell immobilization. Biotechnology and Bioengineering 70 (1):41-53.

Shiraishi S, Imai T, Otagiri M (1993) Controlled-release preparation of indomethacin using calcium alginate gel. Biol Pharm Bull 16 (11):1164-1168

Simeone M, Alfani A, Guido S (2004) Phase diagram, rheology and interfacial tension of aqueous mixtures of Na-caseinate and Na-alginate. Food Hydrocolloids 18 (3):463-470. doi:http://dx.doi.org/10.1016/j.foodhyd.2003.08.004

Smidsrød O (1970) Solution properties of alginate. Carbohydrate Research 13 (3):359-372. doi:http://dx.doi.org/10.1016/S0008-6215(00)80593-5

Solaro RC, F.; Battisti, A. (2010) Targeted Delivery of Protein Drugs by Nanocarriers. Materials 3:1928-1980

Southwest Research Institute S. http://www.swri.org/4org/d01/microenc/microen/release.htm.

Steffe JF (ed) (1992) Rheological Methods in Food Process Engineering. Freeman Press.

Stelter M, Brenn G, Yarin AL, Singh RP, Durst F (2000) Validation and application of a novel elongational device for polymer solutions. Journal of Rheology 44 (3):595-616

Sterling AM, Sleicher CA (1975) The instability of capillary jets. Journal of Fluid Mechanics 68 (03):477-495. doi:10.1017/S0022112075001772

Storz H, Zimmermann U, Zimmermann H, Kulicke W-M (2010) Viscoelastic properties of ultra-high viscosity alginates. Rheologica Acta 49 (2):155-167. doi:10.1007/s00397-009-0400-x

Sussman M, Puckett EG (2000) A Coupled Level Set and Volume-of-Fluid Method for Computing 3D and Axisymmetric Incompressible Two-Phase Flows. Journal of

Computational Physics 162 (2):301-337. doi:http://dx.doi.org/10.1006/jcph.2000.6537

Tanaka H, Irie S (1988) Preparation of stable alginate gel beads in electrolyte solutions using Ba2+ and Sr2+. Biotechnol Tech 2 (2):115-120. doi:10.1007/bf01876161

Tanner FX, Feigl KA, Althaus TO, Windhab EJ (2008) Modeling and Simulation of an Air-Assist Atomizer for Food Sprays. Paper presented at the ILASS Americas, 21 st Annual Conference on Liquid Atomization and Spray Systems, Orlando FL.

The National Cash Register C (1963) UK Patent: 907284.

Thu B, Bruheim P, Espevik T, Smidsrød O, Soon-Shiong P, Skjåk-Bræk G (1996) Alginate polycation microcapsules: II. Some functional properties. Biomaterials 17 (11):1069-1079. doi:http://dx.doi.org/10.1016/0142-9612(96)85907-2

Tirtaatmadja V, Sridhar T (1993) A filament stretching device for measurement of extensional viscosity. Journal of Rheology 37 (6):1081-1102

Tomotika S (1935) On the Instability of a Cylindrical Thread of a Viscous Liquid Sorrounded by Another Viscous Fluid. Proc R Soc Lond A:322-337

Tun T, Inoue K, Hayashi H, Aung T, Gu YJ, Doi R, Kaji H, Echigo Y, Wang WJ, Setoyama H, Imamura M, Maetani S, Morikawa N, Iwata H, Ikada Y (1996) A newly developed three-layer agarose microcapsule for a promising biohybrid artificial pancreas: Rat to mouse xenotransplantation. Cell Transplantation 5 (5, Supplement 1):S59-S63. doi:http://dx.doi.org/10.1016/0963-6897(96)00042-5

Umer H, Nigam H, Tamboli AM, Nainar MSM (2011) Microencapsulation: Process, Techniques and Applications. International Journal of Research in Pharmaceutical and Biomedical Sciences 2:474-481

Urbanska AM, Karagiannis ED, Guajardo G, Langer RS, Anderson DG (2012) Therapeutic effect of orally administered microencapsulated oxaliplatin for colorectal cancer. Biomaterials 33 (18):4752-4761. doi:http://dx.doi.org/10.1016/j.biomaterials.2012.03.023

Vadillo DC, Mathues W, Clasen C (2012) Microsecond relaxation processes in shear and extensional flows of weakly elastic polymer solutions. Rheologica Acta 51 (8):755-769

Vermant J, Walker L, Moldenaers P, Mewis J (1998) Orthogonal versus parallel superposition measurements. Journal of Non-Newtonian Fluid Mechanics 79 (2–3):173-189. doi:http://dx.doi.org/10.1016/S0377-0257(98)00105-0

Versteeg HK, Malalasekera W (eds) (2007) An Introduction to Computational Fluid Dynamics. The Finite Volume Method. Prentice Hall,

Voellmy C, Speiser P, Soliva M (1977) Microencapsulation of phenobarbital by spray polycondensation. Journal of Pharmaceutical Sciences 66 (5):631-634

Watanabe H, Matsuyama T, Yamamoto H (2003) Experimental study on electrostatic atomization of highly viscous liquids. Journal of Electrostatics 57 (2):183-197. doi: 10.1016/s0304-3886(02)00139-0

Webb PA (2000) A Primer on Particle Sizing by Static Laser Light Scattering. Technical Workshop Series: Introduction to the Latest ANSI/ISO Standard for Laser Particle Size Analysis.

Weber C (1931) Zum Zerfall eines Flüssigkeitsstrahls. Zeit für angewandte Mathematik und Mechanik. 11:136

Wissema JG, Davies GA (1969) The formation of uniformly sized drops by vibration-atomization. The Canadian Journal of Chemical Engineering 47 (6):530-535. doi:10.1002/cjce.5450470609

Wloka M, Rehage H, Flemming HC, Wingender J (2004) Rheological properties of viscoelastic biofilm extracellular polymeric substances and comparison to the behavior of calcium alginate gels. Colloid & Polymer Science 282 (10):1067-1076. doi:10.1007/s00396-003-1033-8

Xiao Q, Tong Q, Lim L-T (2012) Pullulan-sodium alginate based edible films: Rheological properties of film forming solutions. Carbohydrate Polymers 87 (2):1689-1695. doi:http://dx.doi.org/10.1016/j.carbpol.2011.09.077

Yarin AL (1993) Free Liquid Jets and Films: Hydrodynamics and Rheology. New York

Yeo S-D, Kiran E (2005) Formation of polymer particles with supercritical fluids: A review. The Journal of Supercritical Fluids 34 (3):287-308. doi:http://dx.doi.org/10.1016/j.supflu.2004.10.006

Zanin MP, Pettingill LN, Harvey AR, Emerich DF, Thanos CG, Shepherd RK (2012) The development of encapsulated cell technologies as therapies for neurological and

sensory diseases. Journal of Controlled Release 160 (1):3-13. doi:http://dx.doi.org/10.1016/j.jconrel.2012.01.021

Zhang WJ, Laue C, Hyder A, Schrezenmeir J (2001) Purity of alginate affects the viability and fibrotic overgrowth of encapsulated porcine islet xenografts. Transplantation Proceedings 33 (7–8):3517-3519. doi:http://dx.doi.org/10.1016/S0041-1345(01)02419-8

Zhang WJ, Marx SK, Laue C, Hyder A, Juergensen A, Bickel M, Schrezenmeir J (2000) Hoe 077 reduces fibrotic overgrowth around the barium alginate microcapsules. Transplantation Proceedings 32 (1):206-209. doi:http://dx.doi.org/10.1016/S0041-1345(99)00938-0

Zimmermann H, Ehrhart F, Zimmermann D, Müller K, Katsen-Globa A, Behringer M, Feilen PJ, Gessner P, Zimmermann G, Shirley SG, Weber MM, Metze J, Zimmermann U (2007) Hydrogel-based encapsulation of biological, functional tissue: fundamentals, technologies and applications. Appl Phys A 89 (4):909-922. doi:10.1007/s00339-007-4270-8

Zimmermann U, Cramer H, Jork A, Thürmer F, Zimmermann H, Fuhr G, Hasse C, Rothmund M (2008) Microencapsulation-Based Cell Therapy. In: Biotechnology. Wiley-VCH Verlag GmbH, pp 547-571. doi:10.1002/9783527620937.ch19